



HAL
open science

Commande robuste de générateurs électrochimiques hybrides

David Hernández-Torres

► **To cite this version:**

David Hernández-Torres. Commande robuste de générateurs électrochimiques hybrides. Autre. Université de Grenoble, 2011. Français. NNT : 2011GRENT075 . tel-00680983

HAL Id: tel-00680983

<https://theses.hal.science/tel-00680983>

Submitted on 20 Mar 2012

HAL is a multi-disciplinary open access archive for the deposit and dissemination of scientific research documents, whether they are published or not. The documents may come from teaching and research institutions in France or abroad, or from public or private research centers.

L'archive ouverte pluridisciplinaire **HAL**, est destinée au dépôt et à la diffusion de documents scientifiques de niveau recherche, publiés ou non, émanant des établissements d'enseignement et de recherche français ou étrangers, des laboratoires publics ou privés.

THÈSE

pour obtenir le grade de

DOCTEUR DE L'UNIVERSITÉ DE GRENOBLE

Spécialité: Génie Électrique

Arrêté ministériel : 7 août 2006

Présentée par

« **David HERNÁNDEZ-TORRES** »

Thèse dirigée par « **Pr. Olivier SENAME** »

et codirigée par « **Dr. Delphine RIU** »

préparée au sein du **Laboratoire de Génie Électrique de Grenoble (G2ELab)**
et du **Laboratoire de Grenoble Images Parole Signal Automatique (GIPSA-Lab)**
dans l'**École Doctorale: Électronique, Électrotechnique, Automatique et
Traitement du Signal (EEATS)**

**Commande Robuste de Générateurs
Électrochimiques Hybrides**

Thèse soutenue publiquement le **25 Octobre 2011**,
devant le jury composé de:

M., Mazen, ALAMIR

Directeur de Recherche CNRS au GIPSA-Lab à Grenoble, Président

Mme., Marie-cécile, PERA

Professeur au FEMTO-ST à Belfort, Rapporteur

M., Francesco, VASCA

Professeur de l'Université de Sannio (Italie), Rapporteur

M.,Loïc, BOUILLO

Ingénieur à PSA-Peugeot-Citroën, Examineur

M, Christophe, TURPIN

Chercheur CNRS au Laboratoire Laplace à Toulouse, Examineur

Mme., Florence, DRUART

Maître de Conférences au LEPMI-Lab à Grenoble, Examinatrice

M., Olivier, SENAME

Professeur au GIPSA-Lab à Grenoble, Directeur de thèse

Mme., Delphine, RIU

Maître de Conférences au G2ELab à Grenoble, Codirectrice



A mis padres y a mi esposa

Remerciements

Cette thèse a été financée par une allocation de recherche issue d'un projet Bonus Qualité de Recherche (BQR) avec l'Institut Polytechnique de Grenoble. J'ai eu l'opportunité de travailler dans deux laboratoires de recherche, le G2ELab et le Gipsa-Lab, au sein des équipes "Système et réseaux électriques" (SYREL) et "Systèmes linéaires et robustesse" respectivement.

Je voudrais tout d'abord remercier M. Olivier SENAME, Professeur au Gipsa-Lab, qui a été mon directeur de thèse. Merci pour m'avoir guidé pendant ces trois ans. En tant qu'ingénieur électrique spécialisé en "puissance", l'introduction au domaine de la commande a été un vrai défi pour moi. En commençant par mon projet M2R, et ensuite avec ma thèse, Olivier a su apporter son esprit, ses capacités, sa compréhension et ses connaissances dans son domaine.

Je voudrais aussi remercier à Mme. Delphine RIU, ma codirectrice de thèse et enseignante-chercheuse au G2ELab. Merci pour toutes les choses que t'as apporté à ce travail et pour tes idées toujours intéressantes. Merci pour ta capacité à m'orienter vers la direction correcte dans mes recherches, pour ton discernement et vision à l'analyse de mes résultats. Merci pour ton énergie et le temps consacré à ce projet, toujours là prête pour m'aider. J'ai beaucoup apprécié travailler avec vous, mes encadrants, merci encore une fois, je serais toujours reconnaissant.

Je tiens à remercier à M. Mazen ALAMIR, Directeur de Recherche CNRS au GIPSA-Lab, pour avoir accepté d'être le président de mon jury ainsi que à M. Francesco VASCA, Professeur de l'Université de Sannio (Italie), et Mme. Marie-Cécile PERA, Professeur au FEMTO-ST à Belfort, d'avoir accepté d'être rapporteur de mon mémoire. Je remercie également à M. Loïc BOUILLO, Ingénieur à PSA-Peugeot-Citroën, à M. Christophe TURPIN, Chercheur CNRS au Laboratoire Laplace à Toulouse, et à Mme. Florence DRUART, Maître de Conférences au LEPMI-Lab, d'avoir accepté de prendre part à mon jury. Je souhaite remercier l'ensemble des membres du jury pour l'énergie dédiée à la lecture et correction de mon mémoire de thèse. Vos corrections, remarques et commentaires ont été très appréciés.

Un remerciement spécial à M. Nicolas RETIERE, qui m'a donné l'opportunité et la motivation de venir en France, d'apprendre une nouvelle langue, de découvrir une nouvelle culture. J'ai bien aimé travailler avec toi en TP à l'UJF, pendant mon M2R, et merci pour tes commentaires pertinents pendant ma thèse. Estaré siempre muy agradecido.

Merci aux autres membres de l'équipe SYREL, à Seddik BACHA et Daniel ROYE, toujours là pour aider sans conditions, merci pour votre temps. Merci à Thierry CREUZET qui m'a beaucoup aidé lors des tests sur le banc d'essai. Egalement à Sandrine BAUDIN et à Florence pour toutes leurs aides concernant le banc d'essai PAC au LEPMI. Aux autres membres permanents des deux laboratoires, à E. WITRANT, G. MEUNIER, S. CATELLANI et A. LABONNE, merci à S. GARCIA et M. PELLISSIER du service bib-

liothécaire. Merci à tous les étudiants de master à l’UJF que j’ai pu rencontrer pendant les cours de TP et à mes stagiaires au G2ELab qui m’ont tous les jours appris des nouvelles choses. Merci à notre service info toujours efficace et prêt à résoudre les problèmes.

Je voudrais remercier tous mes collègues de l’équipe SYREL et de la salle Prodige “micro-réseaux”, ainsi que tous les doctorants et étudiants du laboratoire, au G2ELab et au Gipsa-Lab. Merci à tous mes amis et collègues, Matthieu, Didier, Bill, Arnaud, David, Damien, Phillipe, Haroun, merci à tout l’équipe œnologie pour ces soirées inoubliables, merci à la communauté roumaine du labo, Anca, Monica, Cristian, Iulien, Antoneta, Adrein, et bien d’autres. Merci aux membres de la seule équipe de baseball de Grenoble, Les Grizzlys, qui m’ont permis de continuer en France avec cette “passion”.

Agradezco eternamente a mis padres, Xiomara y Tibaldo. Este es el final de una etapa rica en aprendizajes que ustedes han sabido muy bien guiar, con amor, comprensión, y con ese cariño único que les caracteriza, los amo con todo mi corazón, y serán ustedes siempre mi guía y ejemplo a seguir en la vida. Gracias también a mi hermano Tibaldo por su apoyo a lo largo de todos estos años, sé que siempre podré contar contigo. Una mención especial a toda mi familia en Venezuela que, a pesar de la distancia, siempre los he tenido presentes. Gracias también a todos mis amigos venezolanos, donde sea que estén, por su apoyo incondicional, se les quiere.

Agradezco a la Universidad Simón Bolívar en Caracas, y a todo su cuerpo de profesores en Ingeniería Eléctrica, que me enseñaron las bases y fundamentos de esta hermosa carrera.

Finalment, en dernière dans ces phrases, mais en première dans mon cœur, je remercie ma femme Elodie. Merci pour partager ton temps et ta vie avec moi. Ces derniers mois pleins d’émotions resteront à jamais dans ma mémoire. Merci pour ta gentillesse, ton charme, ton énergie. Merci pour partager avec moi tes émotions, merci pour partager tout dans cette vie qui s’ouvre à nous avec plein de bonheur. Gracias por todo, gracias por estar junto a mí, y espero que el futuro nos depara muchas cosas bonitas.

Quiero terminar citando varias frases rindiendo honor a dos de los pensadores más notables de la historia latinoamericana, primero a nuestro libertador Simón Bolívar, y luego al desaparecido escritor argentino Ernesto Sábato.

“Dichoso el que, en lugar de un amigo, ha colocado en su pecho el amor, la inocencia y la virtud”.

“El gran poder existe en la fuerza irresistible del amor”.

“El que abandona todo por ser útil a su país, no pierde nada, y gana cuanto le consagra”.

Simón Bolívar

“Yo creo que la verdad es perfecta para las matemáticas, la química, la filosofía, pero no para la vida. En la vida, la ilusión, la imaginación, el deseo, la esperanza cuentan más”.

“Habrá siempre un hombre tal que, aunque su casa se derrumbe, estará preocupado por el Universo. Habrá siempre una mujer tal que, aunque el Universo se derrumbe, estará preocupada por su hogar”.

“La vida es tan corta y el oficio de vivir tan difícil, que cuando uno empieza a aprenderlo, ya hay que morirse”.

Ernesto Sábato

Contents

1	Résumé	1
1.1	Introduction	1
1.2	Outils de commande avancée	5
1.2.1	Outils d'identification	5
1.2.2	Outils de commande et analyse	7
1.2.2.1	La conception de la commande à l'aide des LMI	8
1.2.2.2	Le cas de la commande \mathcal{H}_∞	9
1.2.2.3	Les contrôleurs d'ordre réduit	10
1.2.2.4	Extension aux systèmes LPV	11
1.3	Modélisation des systèmes	12
1.3.1	Modèle du système électrique	13
1.3.1.1	Modèle du système double hacheur élévateur en parallèle	13
1.3.1.2	Modèle de l'onduleur de tension	15
1.3.2	Modèle de la PAC et du système Moteur-Compresseur	15
1.4	Commande et résultats	16
1.4.1	Synthèse des résultats obtenus dans la partie électrique	17
1.4.2	Synthèse des résultats obtenus dans la partie thermodynamique	18
1.5	Conclusions	20
2	General Introduction	23
3	Advanced Control Tools	31
3.1	Introduction	31
3.2	System identification tools	31
3.2.1	Some basic principles	31
3.2.2	Identification stages	32
3.2.2.1	Experiments and data acquisition	32
3.2.2.2	Data processing	33
3.2.2.3	Estimation procedure	34
3.2.2.4	Validation	36
3.2.3	A word on systems with feedback	36
3.3	Control design and analysis tools	36
3.3.1	Towards a generalized methodology	36
3.3.2	Linear matrix inequalities in control	37
3.3.2.1	Presentation	37
3.3.2.2	A classic motivation problem	38
3.3.2.3	Three LMI problems	39

3.3.2.4	Norms in control	39
3.3.2.5	Convexity and LMIs	41
3.3.2.6	Semi-definite programming (SDP)	42
3.3.2.7	The SDP problem of an \mathcal{H}_∞ controller	42
3.3.3	Control design using LMIs	43
3.3.3.1	Methodology of \mathcal{H}_∞ control	43
3.3.3.2	Formal presentation of the \mathcal{H}_∞ control problem using LMIs	48
3.3.3.3	Reduced order controllers	48
3.3.4	Extensions to LPV systems	55
3.3.4.1	Formulation of the LPV model	55
3.3.4.2	Full-order \mathcal{H}_∞ LPV control	58
3.3.4.3	Formal presentation of the \mathcal{H}_∞ control problem for LPV systems	59
3.3.4.4	Reduced order controllers	60
3.3.5	Analysis tools	66
3.3.5.1	Modeling uncertainties	66
3.3.5.2	μ -Analysis	67
3.4	Conclusion	72
4	Test-bench and Modeling	73
4.1	Introduction	73
4.2	Test-bench setups	73
4.2.1	Fuel cell test-bench	73
4.2.1.1	The GESI setup	76
4.2.1.2	Air pressure system	77
4.2.2	“Emulator” test-bench	77
4.3	Electrical equivalent circuits	79
4.3.1	Electrical equivalent source models	79
4.3.1.1	Fuel cell modeling	79
4.3.1.2	Super-capacitor model	80
4.3.2	Hybrid boost converters	82
4.3.2.1	Non-linear average model	82
4.3.2.2	Linear average state-space model	84
4.3.2.3	A basic sensitivity analysis of state-space matrix	87
4.3.3	Special case using a reversible converter	90
4.3.4	Voltage inverter for network connection	91
4.3.4.1	Inverter model	92
4.3.4.2	A new data set for the inverter system	94
4.3.4.3	Linear average state-space model	95
4.4	Fuel cell system	96
4.4.1	Fuel cell stack	97
4.4.2	A reduced order dynamic model of FC system	98
4.4.2.1	Dynamic equations of cathode pressures	99
4.4.2.2	Computing the static oxygen excess ratio	100
4.4.2.3	Dynamic equation of the supply manifold	101
4.4.2.4	Compressor model	103
4.4.2.5	Resuming a non-linear system of equations	105

4.4.3	Experimental identification and validation of FCS non-linear model	108
4.4.3.1	Model for sub-system χ	108
4.4.3.2	Model for sub-system (x_3, x_4)	110
4.4.3.3	Compressor models identification	113
4.4.4	Experimental identification and validation of FCS linear model	115
4.5	Conclusion	120
5	Control Applications	121
5.1	Introduction	121
5.2	Proposed control methodology	122
5.2.1	Problem objectives	122
5.3	Electrical sub-system	124
5.3.1	Hybrid boost converters	124
5.3.1.1	A classic control approach	124
5.3.1.2	Robust control approach	127
5.3.1.3	Robustness analysis	136
5.3.2	Hybrid boost system with reversible converter	144
5.3.3	Hybrid boost converters with voltage inverter	147
5.3.3.1	“Classic” control approach	149
5.3.3.2	Robust control approach	150
5.4	Air supply sub-system	157
5.4.1	Compressor system control	157
5.4.1.1	Classic control approach	158
5.4.1.2	Robust control approach	158
5.4.2	LPV speed control	166
5.4.2.1	Solution to the control of the non-linear compressor model	166
5.4.2.2	Model uncertainties problem solution	170
5.5	Complete system control	175
5.6	Conclusion	180
A	Matlab functions used for control	183
A.1	PI controller for an LTI system	183
A.1.1	The iLMI algorithm	183
A.1.2	Function for Static Output Feedback	186
A.1.3	Function to solve the generalized eigenvalue problem	187
A.2	PI controller for an LPV system	188
B	Open-loop state-space matrices	193
B.1	Hybrid boost converter system	193
B.1.1	Hybrid boost system with reversible converter	193
B.2	Voltage inverter system	194
B.3	Air supply system model	194
B.4	Complete system model	195
C	Some thermo-dynamical principles	197

List of Figures

1.1	Les étapes de l'identification de modèles.	6
1.2	General control configuration.	8
1.3	The (P, K) structure including weighting functions.	9
1.4	Equivalent topological model of the hybrid system studied.	14
1.5	Hybrid topology with voltage inverter.	15
1.6	Résultats expérimentaux pour une perturbation de 10% (courant et tension).	17
1.7	Résultats expérimentaux pour une perturbation de $\pm 20\%$, comparaison des commandes robuste et classique.	18
1.8	Analyse de robustesse en utilisant la μ -analysis.	18
1.9	Résultats de simulation, comparaison des contrôles \mathcal{H}_∞ d'ordre fixe et d'ordre complet avec la commande classique avec des PI.	19
1.10	Analyse de robustesse des systèmes en boucle fermée.	19
1.11	Diagramme de bloc du système complet.	20
1.12	Valeurs singulières de la boucle fermée.	20
1.13	Résultats de simulation, taux de consommation d'oxygène.	21
2.1	Power production from renewable energy sources.	25
3.1	The identification loop process.	33
3.2	Excitation signals example.	34
3.3	General control configuration.	44
3.4	The (P, K) structure including weighting functions.	45
3.5	Weighting function for $S(s)$	45
3.6	Weighting function for $KS(s)$	46
3.7	The gain scheduling approach [Bruzelius, 2004].	55
3.8	Controller polytopic reconstruction.	61
3.9	Modeling uncertainties.	66
3.10	LFT representation of uncertain plant $y = G_p u$	67
3.11	General control configurations of the perturbed system (a), configuration for robust performance analysis (b) and configuration for robust stability analysis (c).	68
3.12	Example detailed system for a robust performance analysis.	69
4.1	Experimental setup used for validation.	74
4.2	The Paxitech© fuel cell stack.	74
4.3	Characteristics of PEMFC from Paxitech©.	75
4.4	A PEM Fuel Cell System.	75
4.5	Experimental setup converter configuration.	76

4.6	GESI arrangement of power converters and super-capacitor.	78
4.7	Vairex© 24V air compressor characteristics.	78
4.8	“Emulator” test-bench setup configuration.	79
4.9	Fuel Cell dynamic model.	80
4.10	Measured and simulated FC dynamic.	81
4.11	The Ragone chart for several sources.	81
4.12	Equivalent topological model of the hybrid system studied.	82
4.13	PWM control for the boost power converters.	84
4.14	Validation of hybrid generator model (5.3.3.2) (open-loop).	84
4.15	Output DC bus voltage response to a 25% load step at $t = 2.5s$	85
4.16	Fuel cell current response to a 25% load step at $t = 2.5s$	85
4.17	Super-capacitor current response to a 25% load step at $t = 2.5s$	86
4.18	Bode plot of the open-loop MIMO linear system.	87
4.19	Root locus plot evolution for variations of $\pm 100\%$ in C	89
4.20	Root locus plot evolution for variations of $\pm 100\%$ in C_{sc}	90
4.21	Output DC bus voltage responses using a reversible converter for the SC.	91
4.22	Fuel cell current responses using a reversible converter for the SC.	92
4.23	Super-capacitor current responses using a reversible converter for the SC.	92
4.24	Hybrid topology with voltage inverter.	93
4.25	AC currents comparison using the topological model (dotted light-colored) and the non-linear average model (continuous dark lines).	95
4.26	Bode plot of the open-loop hybrid system with inverter.	97
4.27	A typical polarization curve with different fuel cell losses.	98
4.28	Manifold model block diagram proposed in [Pukrushpan et al., 2004a].	102
4.29	Compressor model block diagram [Pukrushpan et al., 2004a].	103
4.30	Compressor model diagram [Gasser, 2006].	105
4.31	Non-linear FCS model.	108
4.32	Voltage and pressure responses to a stack current ξ step.	109
4.33	Voltage and pressure responses to a p_{sm} pressure step.	110
4.34	Fourth and third-order model comparisons.	110
4.35	Closed-loop system considered for identification.	111
4.36	Compressor-motor speed dynamic identification with a PRBS input in the compressor-motor speed reference ω_{cp}^*	112
4.37	Compressor-motor speed dynamic identification with a PRBS input.	112
4.38	Compressor-motor speed dynamic identification with a chirp input.	113
4.39	Input signals, compressor flow W_{cp} and return manifold pressure p_{rm} , for the supply manifold pressure dynamic identification.	114
4.40	Supply manifold pressure p_{sm} dynamic identification with a PRBS input.	114
4.41	Compressor flow map (measured) and the non-linear regression model.	115
4.42	Compressor power contour map.	116
4.43	Validation of a linear dynamic model for $h_3(x_3, x_4) = W_{cp}$	116
4.44	Fuel cell pressure drop constant computation.	117
4.45	Inputs used to identify the model proposed by [Gasser, 2006].	117
4.46	Measured and simulated results for current and speed using the model proposed by [Gasser, 2006].	118
4.47	Measured and simulated results for mass flow and pressure using the model proposed by [Gasser, 2006].	118

5.1	Proposed methodology.	122
5.2	Approach for time-domain simulations.	123
5.3	Adaptation from the military aircraft norm <i>MIL-STD-704E</i> for: DC applications at 20-30V (left) and DC application for >200V systems (right).	123
5.4	Hybrid system control strategy proposed in Valero [2004].	124
5.5	Output voltage time response, method Valero [2004].	126
5.6	System currents time response, method Valero [2004].	126
5.7	Hybrid system control strategy proposed in Sailer [2008].	126
5.8	Output voltage time response, method Sailer [2008].	127
5.9	The first proposed control configuration.	128
5.10	Sensitivity function.	129
5.11	Complementary sensitivity function.	130
5.12	Simulation results using PI control (classic and robust).	130
5.13	Simulation results.	131
5.14	Simulation results, comparing several robust controllers.	132
5.15	Simulation results, comparing several robust controllers.	132
5.16	Sensitivity functions singular value plot for proposed robust PI controllers.	133
5.17	Simulation results of several proposed control structures.	133
5.18	Simulation results of several proposed control structures.	134
5.19	Simulation results.	134
5.20	Simulation results for the control inputs α_{fc} and α_{sc}	135
5.21	FC emulator model in MATLAB/SIMULINK.	135
5.22	FC emulator validation (0 – 10A step), open-loop.	136
5.23	FC emulator validation (0 – 35A step), open-loop.	137
5.24	Experimental results for 20% load step.	137
5.25	Experimental results for 5 and 20% load steps.	137
5.26	Experimental results for 10% load step (current and voltage).	138
5.27	Experimental results for $\pm 20\%$ load step, comparison between robust and classic PI controllers.	138
5.28	Experimental results comparison for 20% load step, output voltage.	139
5.29	Temperature of the power converters after 1h operation at rating load.	139
5.30	Weighting functions to model complex uncertainties	140
5.31	N-structure used to compute structured singular values plot.	141
5.32	Robustness analysis using μ -analysis.	142
5.33	Robustness analysis with μ -analysis using the iLMI PI controller.	142
5.34	Experimental results for several SOC_{sc} values.	143
5.35	Pareto curves for a proposed component design.	144
5.36	The proposed control configuration.	145
5.37	Singular values plots of the sensitivity functions $S(s)$	146
5.38	Singular values plots of the sensitivity functions for the full and reduced order controllers.	146
5.39	Simulation results using linear system (DC bus voltage).	147
5.40	Simulation results using non-linear system (DC bus voltage) with PI iLMI controller.	147
5.41	Simulation results for series of load current steps (DC bus voltage) with PI iLMI controller.	148

5.42	Simulation results for series of load current steps (DSystem currents) with PI iLMI controller.	148
5.43	Block diagram of the voltage inverter system.	149
5.44	Classic voltage inverter control strategy.	149
5.45	Simulation results using classic control.	151
5.46	Three-phase simulation results using classic control.	151
5.47	Control configuration in the P-K form for the inverter system.	152
5.48	Singular values plots of the sensitivity functions $S(s)$	152
5.49	Simulation results for several control structures.	153
5.50	Control configuration in the P-K form for the complete electrical system.	154
5.51	Singular values plot of the sensitivity function $S(s)$	154
5.52	Closed-loop singular values plot, comparison fixed order \mathcal{H}_∞ and classic control.	155
5.53	Simulation results, comparison of full and fixed order \mathcal{H}_∞ controllers with classic PI control.	155
5.54	Three-phase simulation results using fixed order \mathcal{H}_∞	156
5.55	Robustness analysis of the closed-loop systems.	156
5.56	Block diagram of the FC system with compressor-motor model.	158
5.57	Compressor proposed control strategy.	158
5.58	Oxygen excess ratio using linear model.	159
5.59	Oxygen excess ratio using linear model.	159
5.60	Control configuration in the P-K form for the compressor system.	160
5.61	Compressor system block diagram.	160
5.62	Closed-loop singular values plot.	161
5.63	Oxygen excess ratio simulation results.	162
5.64	Net power delivered by the FC.	162
5.65	Simulation results using linear model (reduced order controller in continuous line, full order controller in dashed line and classic PI controller in dotted line).	163
5.66	Polarization curve.	164
5.67	Compressor map.	164
5.68	Simulation results using non-linear model (reduced order controller in continuous line and classic PI control in dotted line).	165
5.69	Compressor LPV system block diagram.	169
5.70	Control configuration in the P-K form for the LPV system.	169
5.71	Singular values plot of the sensitivity function for \mathcal{H}_∞ polytopic controller.	170
5.72	Impulse response for \mathcal{H}_∞ polytopic controller at each vertex.	170
5.73	System response to a load step using gain scheduling approach.	171
5.74	System response to a speed reference step using gain scheduling approach.	171
5.75	Varying parameter trajectory.	171
5.76	Compressor LPV system block diagram.	172
5.77	Singular values plot of the sensitivity function for \mathcal{H}_∞ polytopic and PI LPV controllers.	173
5.78	System response to a load step using gain scheduling approach (\mathcal{H}_∞ polytopic controller in continuous line and PI LPV controller in dashed line).	174

5.79	System response to a speed reference step using gain scheduling approach (\mathcal{H}_∞ polytopic controller in continuous line and PI LPV controller in dashed line).	174
5.80	Varying parameter trajectory.	174
5.81	Complete system block diagram.	175
5.82	Control configuration in the P-K form for the complete system.	176
5.83	Closed-loop singular values plot.	176
5.84	Closed-loop singular values plot.	177
5.85	Simulation results, DC bus voltage.	177
5.86	Simulation results, oxygen excess ratio.	178
5.87	Simulation results, net power delivered to the load.	178
5.88	Simulation using linear system results and the reduced order \mathcal{H}_∞ controller for several complementary variables for a series steps in the load current. . .	179
C.1	Water saturation pressure calculation comparison.	200

List of Tables

- 3.1 Special structures for identification [Brely, 2003] 35
- 3.2 A review of useful MATLAB functions 70

- 4.1 FC model parameters 81
- 4.2 Participation factors matrix. 89
- 4.3 χ model parameters 109
- 4.4 x_3 model parameters 111
- 4.5 Identification results for the model proposed by [Gasser, 2006] 119

- 5.1 Control structures considered using the PI iLMI algorithm 132
- 5.2 Considered uncertainties levels 140
- 5.3 Maximum μ values for RS 142
- 5.4 Closed-loop system \mathcal{H}_∞ gain 145
- 5.5 Closed-loop \mathcal{H}_∞ gain 152
- 5.6 Closed-loop \mathcal{H}_∞ gain 161

- C.1 Water Saturation Pressure 199

Notations

A_{fc}	Fuel cell active area	[cm ²]
A_T	Valve opening area	[m ²]
C_D	Throttle discharge coefficient	-
C_p	Specific heat	[J.kg ⁻¹ °K]
D_w	Membrane diffusion coefficient	[cm ² /sec]
E	Fuel cell open circuit voltage	[V]
F	Faraday's number	[Coulombs]
I_{st}	Stack current	[A]
J	Rotational inertia	[kg.m ²]
M	Molecular Mass	[kg/mol]
P	Power	[Watt]
R	Gas constant or electrical resistance	[Ω]
T	Temperature	[°K]
V	Volume	[m ³]
W	Mass flow rate	[kg/sec]
a	Water activity	-
c	Water concentration	[mol/cm ³]
d_c	Compressor diameter	[m]
i	Current density	[A/cm ²]
m	Mass	[kg]
n	Number of cells or number of moles	-
n_d	Electro-osmotic drag coefficient	-
p	Pressure	[Pa]
t	Time	[s]
t_m	Membrane thickness	[cm]
u	System input	-
v	Voltage	[V]
x	Mass fraction or system state vector	-
y	Mole fraction or system measurements	-
γ	Ratio of the specific heats of air	-
η	Efficiency	-
λ	Excess ratio (Stoichiometric factor) or water content	-
ρ	Density	[kg/cm ³]
τ	Torque	[N.m]
ϕ	Relative humidity	-
ω	Rotational speed or humidity	[rad/s]

Subscripts

<i>a</i>	Armature of the DC machine
<i>act</i>	Activation losses
<i>an</i>	Anode
<i>atm</i>	Atmospheric
<i>ca</i>	Cathode
<i>cl</i>	Cooler
<i>cm</i>	Compressor-motor
<i>conc</i>	Concentration losses
<i>cp</i>	Compressor
<i>f</i>	Free energy or field of the DC machine
<i>fc</i>	Fuel Cell
<i>hm</i>	Humidifier
H_2	Hydrogen
H_2O	Water
<i>in</i>	Input
<i>inj</i>	Injected
<i>L</i>	Load
<i>m</i>	Membrane
<i>max</i>	Maximum
<i>membr</i>	Membrane
N_2	Nitrogen
<i>ohm</i>	Ohmic losses
<i>out</i>	Output
O_2	Oxygen
<i>rm</i>	Return manifold
<i>sc</i>	Super-capacitor
<i>sm</i>	Supply manifold
<i>v</i>	vapor
<i>w</i>	water

Note: As a standard notation, current and voltage values in lowercase denotes “exact” variables, while uppercase values denotes “average” variables.

Chapter 1

Résumé

1.1 Introduction

Contexte et motivations

(a) Développement des piles à combustible

Une pile à combustible (PAC) est un dispositif électrochimique qui peut convertir l'énergie chimique en énergie électrique à l'aide d'une paire d'électrodes, d'un électrolyte et d'un catalyseur. La source d'énergie de la PAC est issue d'un réservoir externe de combustible, comprenant généralement de l'hydrogène ou du gaz naturel. Le principe de fonctionnement d'une PAC est similaire à celui des batteries classiques, cependant un avantage important est qu'elle peut fonctionner en continu tant que du carburant est disponible pour la production d'énergie. Les PAC sont attrayantes car efficaces, flexibles avec leurs structures modulaires et écologiques avec pratiquement aucune émission. Les systèmes de production d'électricité basés sur les PAC peuvent jouer un rôle plus important dans l'avenir des applications de la génération distribuée (GD) d'énergie [Wang and Nehrir, Dec. 2007]. L'opération des PAC en tant que GD peut être conçue avec une connexion directe au réseau électrique ou comme un système autonome d'alimentation dans un site isolé [Han et al., 2007].

Le combustible entre dans la pile par l'anode, où il est oxydé en émettant des électrons qui vont voyager à travers un circuit externe. En même temps, grâce à l'équilibre énergétique, les ions passent à travers une membrane électrolytique perméable aux électrons. Enfin dans la cathode, l'oxydant est réduit, permettant la consommation d'électrons dans le circuit externe et l'établissement d'un courant électrique [Ellis et al., 2001]. Ceci est le principe essentiel de fonctionnement d'une PAC à membrane échangeuse de protons, aussi appelée membrane électrolyte polymérique ou PEM de l'anglais Proton Exchange Membrane ou Polymer Electrolyte Membrane. Les PAC PEM fonctionnent à $50 \sim 100^\circ$ avec une puissance allant de quelques kW jusqu'à 1 MW environ. Elles sont destinées à être un bon remplaçant du moteur à combustion interne et une source d'énergie importante pour l'avenir [Laughton, 2002, Cook, 2002, Sakhare et al., 2004]. La PEM, technologie des PAC la plus développée, est dédiée tant pour des applications de transport comme pour des applications de génération d'énergie portable. Les PAC sont généralement classées selon leur type d'électrolyte. D'autres technologies sont aussi considérées, comme: les piles à acide phosphorique (PAFC), les piles à carbonate fondu (MCFC) ou encore les piles à

oxydes solides (SOFC). Les SOFC utilisent un matériau céramique comme électrolyte et sont aussi bien développées que les PEMFC. Elles sont caractérisées par des températures de fonctionnement élevées ($> 500^{\circ}\text{C}$) et peuvent être une bonne option pour les applications de génération à grande puissance, en raison d'une efficacité assez élevée, obtenue lorsqu'elles sont associées avec des turbines à gaz ou à vapeur dans des cycles combinés [Ellis et al., 2001]. Concernant les PEMFC, elles sont composées par des électrodes de carbone liées à une membrane très mince de polymère. Ce système, connu sous le nom d'ensemble membrane-électrodes (MEA), est disposé entre deux plaques collectrices. Des canaux tracés au sein de ces plaques permettent la diffusion des gaz réactifs sur la surface de l'électrode. Des cellules individuelles composées par des plaques MEA sont assemblées pour former un "stack" pile à combustible.

Un autre avantage, et peut-être le plus important des PAC, est que il s'agit de sources *d'énergie propre*. Malgré l'invention du principe de fonctionnement de la pile il y a plus de 150 ans, il y a eu un important développement dans la technologie PAC dans les dernières décennies. En commençant par sa première utilisation commerciale lors du projet *Gemini* de la NASA en 1965 jusqu'à son état actuel de développement, qui a atteint une maturité très importante. Ce développement a été stimulé par la menace du réchauffement climatique et la nécessité d'une alternative aux combustibles fossiles à base d'hydrocarbures. Par ailleurs, ces dernières années, le prix de l'énergie, la propreté des sources d'énergie, l'épuisement des puits de pétrole (dépassement imminent du point "peak-oil"), et plusieurs autres conditions ont accéléré ce processus, non seulement avec la PAC, mais aussi avec d'autres types *d'énergies renouvelables*¹.

Le développement des PAC est désormais confronté à certains problèmes importants du point de vue du progrès technologique. Le fonctionnement de la cellule et son évolution ont donné place à l'utilisation du platine comme matériau catalyseur. En étant plus cher que l'or, le coût final de la pile augmente de manière exponentielle. Un autre problème courant est la disponibilité des PAC. En fait, les cellules individuelles ($\sim 1\text{V}$) sont connectées en série pour obtenir des tensions de fonctionnement plus élevées. Cela signifie qu'une défaillance sur l'une d'elle peut obliger la mise hors service de la pile. Un des plus grands défis dans le développement de la technologie PAC est d'améliorer la durabilité. D'après [Blunier, 2007], avant que la PAC devienne une technologie mature, la durée de vie d'une PAC qui se trouvait à environ 2000h en 2005, devrait être amélioré pour être comparé avec le moteur à combustion interne autour de 5000h² de durée de vie (cycles inclus). D'autres améliorations dans la densité de puissance (en W/kg), le coût, la masse et le volume de la technologie des compresseurs d'air sont également attendus dans un avenir proche.

Malgré les efforts de la communauté scientifique, et la recherche de nouveaux matériaux et polymères afin d'améliorer la performance de la PAC, le gouvernement des États-Unis a décidé d'arrêter le financement des recherches sur la PAC appliquées aux véhicules de transport³. La déclaration du Département d'Énergie de mai 2009 impose cependant que les ressources financières pour la recherche dans les applications *stationnaires* soient maintenues. Cette décision a eu une influence importante et a peut être entraîné un

¹Voir par exemple certains travaux de recherche récents au G2ELab dans les panneaux photovoltaïques [Stalter, 2009, Riffonneau, 2009, Picault, 2009], les éoliennes [Teninge, 2009], ou même la recherche très intéressante sur les architectures d'hydroliennes fluviales [Hauck, 2011]

²Ce qui correspond à environ 240.000 km

³Accédé le 04/2011: <http://www.nytimes.com/2009/05/08/science/earth/08energy.html>

retard de courte durée dans le développement de la PAC. En janvier 2011, une conférence sur ce développement a eu lieu à Grenoble⁴. Il y a eu un consensus qui indiquait que, même si le développement de nouveaux matériaux a été relativement lent ces dernières années, un nouvel élan est *en cours* et la communauté scientifique (au sein des PAC) a retrouvé sa dynamique. Les PAC restent encore une option intéressante pour le futur de la génération d'électricité.

Finalement, l'étude d'une technologie d'énergie *verte* apporte une forte motivation dans le milieu scientifique. Mis à part les problèmes technologiques relatifs au développement des PAC (coût, disponibilité et durabilité), un autre problème technique est toujours présent, le carburant. Aujourd'hui, il n'existe pas de capacité de production en masse d'hydrogène et l'infrastructure pour la distribution au consommateur final est inexistante (ou considérablement moins développée que celle du pétrole). Il faut considérer par exemple que, si l'hydrogène est produit à partir d'électrolyseurs, mais que l'énergie électrique est issue du réseau électrique qui est en même temps assurée par des postes de génération alimentés au charbon, alors la réduction des émissions de carbone est négligeable [Cook, 2002]. Un autre problème est que parfois la production d'hydrogène est associée à la production de pétrole. Par exemple, l'essence ou le méthanol peut être réformé pour produire de l'hydrogène, mais la réduction des émissions de carbone n'est pas exceptionnelle et l'efficacité globale est réduite. L'*idéal* pour les systèmes PAC serait l'utilisation des énergies renouvelables pour la production d'hydrogène. Ceci peut être considéré avec la production d'énergie à l'aide des éoliennes, des panneaux photovoltaïques ou des turbines micro hydroélectriques.

(b) Le *système* PAC

Une pile à combustible ne peut pas fonctionner seule. Lorsqu'on parle d'un *système* PAC, tous les systèmes auxiliaires, nécessaires pour son fonctionnement, sont inclus. Cela rend le système complexe avec une structure difficile à contrôler. Les éléments auxiliaires peuvent être divisés en deux groupes: sous-systèmes de gestion électrique et thermodynamique. Le premier assure la connexion en toute sécurité de la PAC à l'application électrique (charge) et le deuxième assure la gestion thermique du gaz, de l'eau et de l'air dans la PAC. Bien sûr, ces sous-systèmes sont très interdépendants, le débit de gaz dans la pile dépend directement de la demande de charge actuelle ou encore l'influence de la dynamique du débit d'air sur le sous-système électrique. En ce qui concerne l'efficacité, la pile aura une meilleure performance à des pressions de débit plus importantes, mais cela signifie aussi des taux de compression plus élevés, une plus forte consommation énergétique du compresseur, et une dégradation de l'efficacité globale du système. Etant donnée cette dépendance entre les sous-systèmes, une stratégie générale de commande du système complet semble être, *a priori*, une bonne solution. Un contrôle plus efficace est nécessaire pour garantir une gestion optimale de l'hydrogène et de l'air dans le système, en évitant la dégradation de la membrane de la pile (et la dégradation de la tension de sortie) pour un fonctionnement plus fiable et plus efficace. Une autre complexité est la nécessité d'une source auxiliaire. Comme il sera décrit plus tard dans cette thèse, la PAC doit être hybridée avec une source secondaire (souvent des batteries ou des super-condensateurs) afin de faire face aux transitoires de courant qui peuvent l'endommager. Cela signifie que les deux sources doivent être contrôlées pour garantir un bon fonctionnement de l'ensemble.

⁴Retrieved 05/2011: <http://fdfc2011.lepmi.grenoble-inp.fr/>

(c) Problèmes étudiés dans la thèse

Dans le contexte décrit précédemment, le besoin d'une approche de contrôle robuste multi-variables pour gérer à la fois les sous-systèmes électriques et thermodynamiques de la PAC est identifié. L'approche rejet de perturbations est largement abordée dans cette thèse, du fait qu'une hypothèse générale admettra que celle-ci aura une influence sur la durée de vie des cellules, rejetant les transitoires importants de courant. Les modèles présentés dans cette thèse font appel à la modélisation des paramètres thermodynamiques, tels que les flux des réactifs et de pressions. Il est à noter que les limitations sur la performance de la PAC sont dues non seulement aux caractéristiques des matériaux, mais aussi à l'optimisation des paramètres de fonctionnement thermodynamiques tel que le taux de débit de réactif [Gasser, 2006]. En fait, le contrôle du moteur du compresseur et le débit d'air d'alimentation sont considérés (dans cette thèse) comme étant des éléments centraux dans la dynamique de la PAC. Néanmoins, certaines hypothèses sont faites pour obtenir les modèles simplifiés adaptés au contrôle. Par exemple, le contrôle du débit de carburant, l'humidification de l'air ainsi que le contrôle de la température de la pile sont supposés parfaits. Un intérêt est également accordé à la commande robuste, visant à garantir la robustesse en stabilité et en performances des systèmes soumis à des incertitudes. D'autres problématiques comme la démonstration de l'avantage d'une approche multi-variables, en contraste avec les méthodologies classiques de contrôle découplé, ainsi que la validation d'une méthodologie généralisée avec une analyse complète de robustesse sont étudiées.

Objectifs de la thèse

Les contraintes de qualité d'énergie à respecter sont généralement fixées par des normes. Les systèmes doivent également être capables de s'adapter aux changements rapides de la charge ou des conditions d'opération. De ce fait, une modélisation orientée vers la commande et la stratégie de contrôle sont des aspects cruciaux. Dans une première approche, nous nous concentrerons sur la gestion du sous-système électrique de la PAC et sur le conditionnement de l'énergie. Plusieurs techniques de contrôle robuste linéaires sont conçues et comparées dans cette thèse, mais une plus grande importance est donnée aux contrôleurs d'ordre réduit (PI et commande \mathcal{H}_∞ d'ordre réduit) en raison de leur simplicité et praticité dans les applications industrielles. Pour inclure les spécifications de performance robuste dans la synthèse du contrôle PI, le problème de commande est écrit sous la forme d'un problème d'optimisation convexe en utilisant des LMI. Comme exposé plus loin dans le manuscrit, une méthode itérative avec des LMI (iLMI) est proposée dans He and Wang [2006] et est utilisée pour résoudre le problème de commande MIMO PI avec une certaine performance \mathcal{H}_∞ désirée. La méthodologie de commande est basée sur le contrôle des convertisseurs de puissance DC/DC (hacheurs parallèles) associés à une source hybride composée d'une PAC et d'une super-capacité (SC). La pile à combustible doit être associée à un dispositif de stockage d'énergie (super-condensateurs ou batteries) afin d'atténuer les effets nocifs des transitoires de courant et d'augmenter sa durée de vie. Classiquement, les composants du système de contrôle du système PAC sont conçus de manière indépendante les uns des autres. Cette approche permet de simplifier la stratégie de contrôle, mais n'est pas suffisante pour prendre en compte les différentes dynamiques du système et le couplage entre les variables thermodynamiques (pression, gaz) et électriques (courant continu ou tension). Par ailleurs, le temps dépensé pour la conception du système

peut devenir critique car il est souvent nécessaire de répéter et corriger le calcul des paramètres du contrôleur. Enfin, les fournisseurs d'équipement devraient être capables de concevoir leurs produits tout en sachant avec précision les paramètres de l'ensemble du système. Cependant, les performances des piles à combustible sont fortement liées à la température et à l'humidification de la membrane. Pour ce faire, des méthodes robustes et multi-variables semblent être particulièrement adaptées car elles sont capables de traiter des problèmes de contrôle pour les systèmes comprenant des incertitudes paramétriques.

Dans une deuxième approche, le contrôle robuste multi-variables du système d'alimentation d'air est analysé. Un résumé complet des différents types et technologies de compresseurs est présenté dans Blunier [2007]. Pour la modélisation du système moto-compresseur, nous avons concentré notre attention sur des modèles adaptés à la commande. Premièrement, nous avons considéré un modèle linéaire en espace d'état proposé par Gasser [2006]. Pour une deuxième topologie, nous avons considéré le modèle non-linéaire proposé dans les travaux de Suh [2006], qui correspond à une réduction d'ordre du modèle proposée par Pukrushpan et al. [2004a]. Plusieurs résultats encourageants sur la commande du système moto-compresseur sont proposés dans la littérature à fin d'optimiser la puissance nette délivrée par la pile et réduire ainsi la consommation d'énergie de l'ensemble. Des méthodologies d'optimisation avec des essais particuliers et avec l'approche "recherche du point extremum" sont présentées respectivement dans Tekin et al. [2006] et Chang and Moura [2009]. D'autres approches pour la commande du système d'alimentation en air peuvent inclure la commande non-linéaire, comme dans Talj et al. [2009] où la commande passive est utilisée dans le modèle non-linéaire d'ordre réduit proposé par Suh [2006]. Une analyse intéressante sur la performance des PAC à différentes conditions de fonctionnement et une contribution importante vers une stratégie pour déterminer le signal de référence en vitesse pour le compresseur sont présentées dans Thirumalai and White [2000].

En tout cas, il existe dans la littérature une absence sur les stratégies *robustes et multi-variables* de commande linéaire appliquée au système d'alimentation en air d'un générateur électrique autonome à PAC. Dans cette thèse une première approche à la commande robuste/multi-variables est présentée en utilisant des contrôleurs PI et \mathcal{H}_∞ d'ordre réduit. Une première méthodologie vers une commande robuste est également proposée pour le contrôle de la vitesse du moto-compresseur à l'aide des systèmes linéaires à paramètres variants (LPV) et le séquençement de gain (gain-scheduling).

1.2 Outils de commande avancée

Dans un premier temps, les outils de commande avancée sont présentés. Cette partie est divisée en deux sections: les outils pour l'identification des systèmes et les outils pour la commande. Commençons par décrire les principes de base de la méthodologie pour l'identification de systèmes.

1.2.1 Outils d'identification

Un résumé est présenté dans la thèse sur quelques principes de base pour l'identification de systèmes. Une présentation plus stricte et complète peut être trouvée dans les travaux de [Ljung, 1987] et [Landau, 1993].

Il faut savoir que, d'une façon générale, l'identification d'un système peut devenir un problème assez difficile, du point de vue de la méthodologie à utiliser mais aussi du point de vue du temps de calcul. Tout d'abord, quelques questions de base doivent être répondues. Par exemple, les entrées dans les essais expérimentaux contiennent-elles une information assez riche en harmoniques? La structure du modèle est elle connue? Est-elle linéaire ou non-linéaire? Si la structure du modèle est connue, les états du système peuvent être mesurés?

En tout cas, la méthodologie d'identification est divisée en deux parties:

- Définir le type de modèle pour l'identification, pour lequel deux options sont possibles: modèle paramétrisé ou non.
- Trouver les paramètres du modèle où la meilleure structure est adaptée aux mesures expérimentales.

Les différentes étapes de l'identification de modèles sont:

1. Les mesures expérimentales et l'acquisition des données.
2. Le traitement des données.
3. La procédure d'estimation.
4. La validation

Ceci est résumé dans la Figure 1.1.

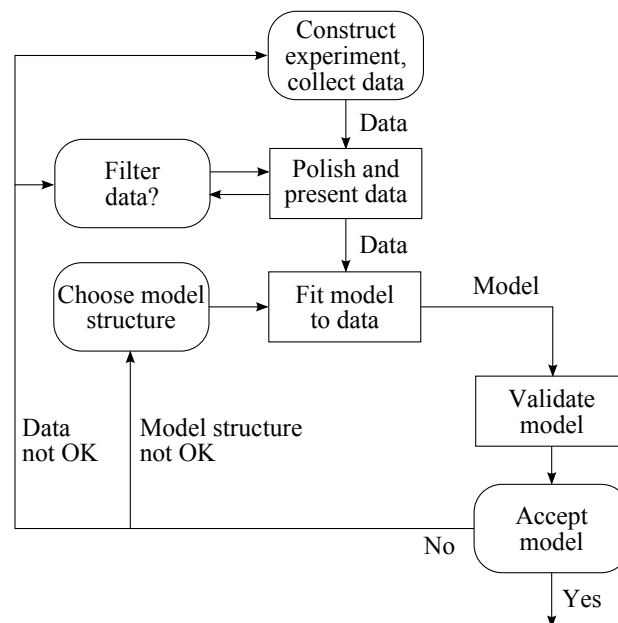


Figure 1.1: Les étapes de l'identification de modèles.

Pour les applications pratiques, une option intéressante est l'utilisation des outils proposés dans le *System Identification (SI) Toolbox* de MATLAB. Plus d'informations sur cet outil peut être trouvé dans [Ljung, 1988].

1.2.2 Outils de commande et analyse

Dans cette thèse l'outil des Inégalités Linéaires Matricielles (LMI) est fortement utilisé. Les principes de base des LMI et leur utilisation pour la solution au problème de commande \mathcal{H}_∞ sont présentés. D'une façon générale, le principe de sensibilité mixte est appliqué. Deux types de systèmes sont étudiés, les systèmes Linéaires Invariants dans le Temps (LTI) et les systèmes Linéaires à Paramètres Variants (LPV). Pour ces deux types de systèmes, des méthodologies de commande sont proposées pour l'obtention des contrôleurs d'ordre réduit. Notamment, on s'intéresse à la structure des contrôleurs PI, mais avec des performances \mathcal{H}_∞ .

Quelques principes de base très importants sont présentés. Comme le principe de convexité, qui permet de résoudre le problème de commande avec des algorithmes d'optimisation efficaces et robustes. Ou bien le principe du "Semi-definite Programming" (SDP), c'est-à-dire, la réalisation pratique des LMI en utilisant la programmation mathématique.

Ainsi, la programmation SDP d'un contrôleur \mathcal{H}_∞ est proposée comme suit.

Pour un système quelconque, deux fonctions mathématiques peuvent être définies:

- $V(x(t))$, est une fonction qui représente l'énergie stocké dans le système.
- $s(\omega(t), z(t))$, est une fonction qui définit le taux d'énergie entrant dans le système.

En conséquence, pour une fonction s dite *quadratique*, et un système LTI contrôlable, les énoncés suivants sont équivalents:

- Le système est entièrement dissipatif (s est complètement intégrable).
- Le système permet une fonction de stockage sous la forme: $V(x(t)) = x^T \mathcal{K} x$, avec $\mathcal{K} = \mathcal{K}^T \succ 0$.
- Il existe $\mathcal{K} = \mathcal{K}^T \succ 0$ telle que la LMI suivante à une solution:

$$\begin{aligned}
 F(\mathcal{K}) &= \begin{bmatrix} A^T \mathcal{K} + \mathcal{K} A & \mathcal{K} B \\ B^T \mathcal{K} & 0 \end{bmatrix} - \begin{bmatrix} 0 & I \\ C & D \end{bmatrix}^T \begin{bmatrix} Q & S \\ S^T & R \end{bmatrix} \begin{bmatrix} 0 & I \\ C & D \end{bmatrix} (\prec) \preceq 0 \\
 &= \begin{bmatrix} I & 0 \\ A & B \\ 0 & I \\ C & D \end{bmatrix}^T \left[\begin{array}{cc|cc} 0 & \mathcal{K} & 0 & 0 \\ \mathcal{K} & 0 & 0 & 0 \\ \hline 0 & 0 & -Q & -S \\ 0 & 0 & -S^T & -R \end{array} \right] \begin{bmatrix} I & 0 \\ A & B \\ 0 & I \\ C & D \end{bmatrix} (\prec) \preceq 0 \quad (1.1)
 \end{aligned}$$

La matrice P définie comme:

$$P = \begin{bmatrix} Q & S \\ S^T & R \end{bmatrix} \quad (1.2)$$

peut être utilisé pour définir l'énergie qui rentre dans le système. Avec cette matrice, plusieurs critères de performance peuvent être définies [Poussot-Vassal, 2008]: la performance \mathcal{H}_∞ , la performance \mathcal{H}_2 , les contraintes dans le domaine temporel (dépassement, temps de stabilisation,...), placement de pôles, etc.

La commande \mathcal{H}_∞ , présentée comme un problème d'optimisation avec des LMI, peut être définie en fixant la fonction quadratique $s(\omega, z) = \gamma_\infty^2 \omega^T \omega - z^T z$. Ainsi, la LMI qui dénote le problème \mathcal{H}_∞ , est donnée par:

$$\begin{bmatrix} I & 0 \\ A & B \\ \hline 0 & I \\ C & D \end{bmatrix}^T \begin{bmatrix} 0 & \mathcal{K} & | & 0 & 0 \\ \mathcal{K} & 0 & | & 0 & 0 \\ \hline 0 & 0 & | & -\gamma^2 I & 0 \\ 0 & 0 & | & 0 & I \end{bmatrix} \begin{bmatrix} I & 0 \\ A & B \\ \hline 0 & I \\ C & D \end{bmatrix} \prec 0 \quad (1.3)$$

$$= \begin{bmatrix} A^T \mathcal{K} + \mathcal{K} A & \mathcal{K} B & C^T \\ B^T \mathcal{K} & -\gamma^2 I & D^T \\ C & D & -I \end{bmatrix} \prec 0 \quad (1.4)$$

Des outils présentés dans la thèse permettent de trouver la solution de cette inégalité dans les cas des systèmes LTI ou LPV.

1.2.2.1 La conception de la commande à l'aide des LMI

Pour un système LTI donné par:

$$\begin{aligned} \dot{x} &= Ax(t) + B_1 \omega(t) + B_2 u(t) \\ z(t) &= C_1 x(t) + D_{11} \omega(t) + D_{12} u(t) \\ y(t) &= C_2 x(t) + D_{21} \omega(t) \end{aligned} \quad (1.5)$$

où $x(t) \in \mathbb{R}^n$ est le vecteur d'état, $\omega(t) \in \mathbb{R}^r$ sont les signaux d'entrées exogènes, $u(t) \in \mathbb{R}^m$ est l'entrée de commande, $z(t) \in \mathbb{R}^q$ est la sortie de performance et $y(t) \in \mathbb{R}^p$ est la sortie mesurée.

Ce système est présenté dans le diagramme de bloc de la Figure 1.2.

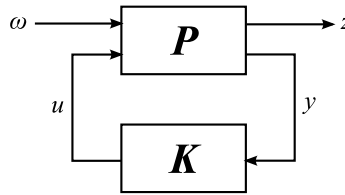


Figure 1.2: General control configuration.

où P est le système généralisé donné par:

$$P = \left[\begin{array}{c|cc} A & B_1 & B_2 \\ \hline C_1 & D_{11} & D_{12} \\ C_2 & D_{21} & D_{22} \end{array} \right] \quad (1.6)$$

La commande \mathcal{H}_∞ , est un problème de rejet de perturbation, le but est de minimiser le gain de la boucle fermée $T_{z\omega}$ entre les perturbations $\omega(t)$ et les sorties de performance $z(t)$, de façon à réduire l'influence des perturbations donnée sous la forme d'une contrainte \mathcal{H}_∞ comme:

$$\|T_{z\omega}(s)\|_{\infty} = \|\mathcal{F}_l(P(s), K(s))\|_{\infty} < \gamma_{\infty} \quad (1.7)$$

où \mathcal{F}_l est la représentation fractionnelle inférieure.

La performance souhaitée est ensuite représentée sous la forme des pondérations ou gabarits dans le domaine fréquentiel. Dans le cas du problème de sensibilité mixte S/KS , la pondération sur la fonction de sensibilité $S(s) = 1/(1 + K(s)G(s))$ est donnée par:

$$\frac{1}{W_e} = \frac{s + \omega_B A_{\epsilon}}{s/M + \omega_B} \quad (1.8)$$

où, un lien entre les différents paramètres (ω_B , M , et A_{ϵ}) et les spécifications de performances dans le domaine temporel (dépassement, temps de monté, etc) est possible.

La structure pour la conception de la commande dans le cas spécifique du problème de sensibilité mixte S/KS est présentée dans la Figure 1.3.

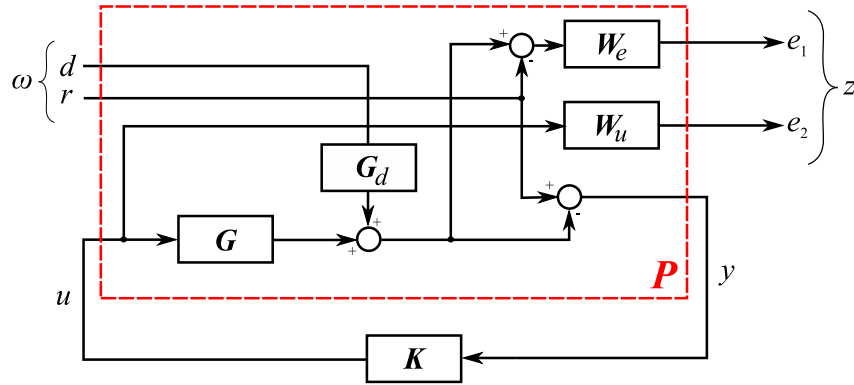


Figure 1.3: The (P, K) structure including weighting functions.

1.2.2.2 Le cas de la commande \mathcal{H}_{∞}

La commande \mathcal{H}_{∞} est un problème de rejet de perturbation. L'objectif est de minimiser le gain entre les perturbations et les sorties de performance.

Dans ce cas, la fonction de transfert en boucle fermée, déterminée par la représentation fractionnelle inférieure $\mathcal{F}_l(P, K)$ par rapport à K , est donnée par:

$$\mathcal{F}_l(P, K) = \mathcal{C}(sI - \mathcal{A})^{-1}\mathcal{B} + \mathcal{D} \quad (1.9)$$

où les matrices \mathcal{A} , \mathcal{B} , \mathcal{C} et \mathcal{D} , sont les matrices de la boucle fermée. Le contrôleur sous la forme généralisée est donnée par:

$$K(s) \left\{ \begin{bmatrix} \dot{x}_k \\ u \end{bmatrix} = \begin{bmatrix} A_k & B_k \\ C_k & D_k \end{bmatrix} \begin{bmatrix} x_k \\ y \end{bmatrix} \right. \quad (1.10)$$

avec $x_k \in \mathbb{R}^n$, $u \in \mathbb{R}^m$ et $y \in \mathbb{R}^p$. Les matrices de la boucle fermée deviennent:

$$\begin{aligned}
\mathcal{A} &= \begin{bmatrix} A + B_2(I - D_k D_{22})^{-1} D_k C_2 & B_2(I - D_k D_{22})^{-1} C_k \\ B_k(I - D_k D_{22})^{-1} C_2 & A_k + B_k(I - D_k D_{22})^{-1} D_{22} C_k \end{bmatrix} \\
\mathcal{B} &= \begin{bmatrix} B_1 + B_2(I - D_k D_{22})^{-1} D_k D_{21} \\ B_k(I - D_k D_{22})^{-1} D_{21} \end{bmatrix} \\
\mathcal{C} &= [C_1 + D_{12}(I - D_k D_{22})^{-1} D_k C_2 \quad D_{12}(I - D_k D_{22})^{-1} C_k] \\
\mathcal{D} &= D_{11} + D_{12}(I - D_k D_{22})^{-1} D_k D_{21}
\end{aligned} \tag{1.11}$$

Si le système P est strictement propre, c'est à dire, $D_{22} = 0$, les matrices de la boucle fermée peuvent être encore simplifiées comme:

$$\begin{aligned}
\mathcal{A} &= \begin{bmatrix} A + B_2 D_k C_2 & B_2 C_k \\ B_k C_2 & A_k \end{bmatrix} \\
\mathcal{B} &= \begin{bmatrix} B_1 + B_2 D_k D_{21} \\ B_k D_{21} \end{bmatrix} \\
\mathcal{C} &= [C_1 + D_{12} D_k C_2 \quad D_{12} C_k] \\
\mathcal{D} &= D_{11} + D_{12} D_k D_{21}
\end{aligned} \tag{1.12}$$

Comme avant, le système en boucle fermée est dit "stable" et respecte une performance \mathcal{H}_∞ , s'il existe un contrôleur $K(s)$ tel que:

$$\begin{bmatrix} \mathcal{A}^T \mathcal{K} + \mathcal{K} \mathcal{A} & \mathcal{K} \mathcal{B} & \mathcal{C}^T \\ \mathcal{B}^T \mathcal{K} & -\gamma^2 I & \mathcal{D}^T \\ \mathcal{C} & \mathcal{D} & -I \end{bmatrix} \prec 0 \tag{1.13}$$

Ce qui nous amène à la formulation du problème \mathcal{H}_∞ et la transformation de l'équation (1.13) dans une LMI. Cette formalité est présentée dans cette thèse dans le cadre des outils et algorithmes de commande avancée.

1.2.2.3 Les contrôleurs d'ordre réduit

On s'est intéressé, tout le long de la thèse, à la synthèse de contrôleurs d'ordre réduit. Ce type de contrôleurs, avec des structures simples, permettent une implémentation efficace et très intéressante du point de vue industriel.

Dans ce contexte, des contrôleurs PI avec performance \mathcal{H}_∞ sont considérés dans cette thèse. La stratégie proposée par He and Wang [2006], avec un algorithme itératif avec des LMI, est utilisée.

Pour le système (1.5), le problème de stabilisation du type retour de sortie statique (SOF), consiste à trouver un correcteur sous la forme:

$$u(t) = Fy(t) \tag{1.14}$$

L'objectif de la synthèse d'un contrôleur PI avec performance \mathcal{H}_∞ est de trouver un correcteur sous la forme:

$$u(t) = F_1 y(t) + F_2 \int_0^t y(\theta) d\theta \quad (1.15)$$

Avec la formulation du problème \mathcal{H}_∞ présentée dans l'équation (1.13), l'algorithme proposé par He and Wang [2006] est utilisé pour la solution du problème de commande d'un PI avec performance \mathcal{H}_∞ .

Avec la structure du contrôleur sous la forme (1.15), un changement de variables est proposé.

$$\bar{x} = \begin{bmatrix} x(t) \\ \int_0^t y(\theta) d\theta \end{bmatrix} \text{ and } \bar{y} = \begin{bmatrix} C_2 x(t) \\ \int_0^t y(\theta) d\theta \end{bmatrix} \quad (1.16)$$

Si l'on impose $D_{21} = 0$, en gardant la généralité, le système (1.5) devient:

$$\begin{aligned} \dot{\bar{x}} &= \bar{A}\bar{x}(t) + \bar{B}_1\omega(t) + \bar{B}_2u(t) \\ z(t) &= \bar{C}_1\bar{x}(t) + \bar{D}_{11}\omega(t) + \bar{D}_{12}u(t) \\ \bar{y}(t) &= \bar{C}_2\bar{x}(t) \end{aligned} \quad (1.17)$$

avec:

$$\begin{aligned} \bar{A} &= \begin{bmatrix} A & 0 \\ C_2 & 0 \end{bmatrix}, \bar{B}_1 = \begin{bmatrix} B_1 \\ 0 \end{bmatrix}, \bar{B}_2 = \begin{bmatrix} B_2 \\ 0 \end{bmatrix} \\ \bar{C}_2 &= \begin{bmatrix} C_2 & 0 \\ 0 & I \end{bmatrix}, \bar{C}_1 = [C_1 \quad 0] \\ \bar{D}_{11} &= D_{11}, \bar{D}_{12} = D_{12} \end{aligned}$$

L'algorithme proposé par He and Wang [2006] est divisé en deux parties. Dans un premier temps, une variable de décision initiale P_i est calculée avec une méthodologie itérative. Dans une deuxième approche, une procédure itérative similaire est utilisée pour trouver la solution du problème \mathcal{H}_∞ et le contrôleur désiré.

L'implémentation de cette algorithme sous MATLAB a été résolue dans cette thèse. Cette implémentation est présentée en Annexe. D'autres contrôleurs d'ordre réduit sont aussi considérés. Comme les contrôleurs d'ordre fixe et la réduction de l'ordre après la synthèse. Ces stratégies sont détaillées plus tard dans le mémoire.

1.2.2.4 Extension aux systèmes LPV

Le problème de commande \mathcal{H}_∞ pour un système LPV est une extension du cas LTI. L'inégalité (1.13) doit être transformée dans une LMI pour un système LPV. Pour ceci on utilise la notation polytopique.

Le contrôleur LPV $K(\rho)$ peut être défini comme:

$$\begin{bmatrix} \dot{x}_k \\ u \end{bmatrix} = \begin{bmatrix} A_k(\rho) & B_k(\rho) \\ C_k(\rho) & D_k(\rho) \end{bmatrix} \begin{bmatrix} x_k \\ y \end{bmatrix} \quad (1.18)$$

avec le paramètre ρ_i défini comme:

$$\rho_i \in [\underline{\rho}_i \quad \bar{\rho}_i], \forall i = 1, \dots, l \quad (1.19)$$

Finalement la boucle fermée du système est donnée par:

$$\begin{bmatrix} \dot{\xi} \\ z \end{bmatrix} = \begin{bmatrix} \mathcal{A}(\rho) & \mathcal{B}(\rho) \\ \mathcal{C}(\rho) & \mathcal{D}(\rho) \end{bmatrix} \begin{bmatrix} \xi \\ \omega \end{bmatrix} \quad (1.20)$$

où ξ sont les variables dynamiques de la boucle fermée et les matrices d'état sont encore une fois:

$$\begin{aligned} \mathcal{A}(\rho) &= \begin{bmatrix} \varphi_{11}(\rho) & B_2(\rho)C_k(\rho) \\ B_k(\rho)C_2(\rho) & \varphi_{22}(\rho) \end{bmatrix} \\ \mathcal{B}(\rho) &= \begin{bmatrix} B_1(\rho) + B_2(\rho)D_k(\rho)D_{21}(\rho) \\ B_k(\rho)D_{21}(\rho) \end{bmatrix} \\ \mathcal{C}(\rho) &= [C_1(\rho) + D_{12}(\rho)D_k(\rho)C_2(\rho) \quad D_{12}(\rho)C_k(\rho)] \\ \mathcal{D}(\rho) &= D_{11}(\rho) + D_{12}(\rho)D_k(\rho)D_{21}(\rho) \end{aligned} \quad (1.21)$$

avec les variables $\varphi_{11}(\rho) = A(\rho) + B_2(\rho)D_k(\rho)C_2(\rho)$ et $\varphi_{22}(\rho) = A_k(\rho) + B_k(\rho)D_{22}(\rho)C_k(\rho)$.

Avec ces définitions, la commande LPV \mathcal{H}_∞ se réduit à la formulation présentée dans Poussot-Vassal [2008] pour trouver la solution au problème LMI et obtenir ainsi les matrices du contrôleur $A_k(\rho)$, $B_k(\rho)$, $C_k(\rho)$ et $D_k(\rho)$.

L'étape finale dans cette méthodologie est la reconstruction polytopique de la commande \mathcal{H}_∞ .

Ceci est donné comme:

$$K(\rho) = \sum_{i=1}^N \alpha_i(\rho) \left[\begin{array}{c|c} A_{k_i} & B_{k_i} \\ \hline C_{k_i} & D_{k_i} \end{array} \right] \quad (1.22)$$

avec:

$$\alpha_i(\rho) := \frac{\prod_{k=1}^l |\rho_k - \mathcal{C}(\omega_i)_k|}{\prod_{k=1}^l (\bar{\rho}_k - \underline{\rho}_k)}, i = 1, \dots, N \quad (1.23)$$

$$\alpha_i(\rho) \geq 0 \text{ and } \sum_{i=1}^N \alpha_i(\rho) = 1 \quad (1.24)$$

1.3 Modélisation des systèmes

Dans une deuxième partie de la thèse des différents modèles sont étudiés. Les bancs d'essai dédiés à l'identification des modèles et validation de la commande sont détaillés. Un banc d'essai, avec une pile PEM de 1kW, était disponible pour des mesures expérimentales. Un autre banc d'essai, avec un émulateur de la dynamique de la pile, était conçu pour la validation expérimentale des lois de commande sur la partie électrique du système.

Dans cette deuxième section, les modèles et les paramètres des systèmes sont donnés. La modélisation moyenne, linéaire et non-linéaire est utilisée pour modéliser les convertisseurs de puissance, y compris la configuration des hacheurs élévateurs en parallèle et l'onduleur de tension. Ces modèles sont validés par comparaison avec les modèles topologiques échantillonnés.

Plusieurs modèles sont détaillés. Deux modèles importants sont retenus dans la suite pour l'application des stratégies de commande pour le système d'alimentation en air. Le premier, c'est une réduction à un troisième ordre d'un modèle proposé par Pukrushpan et al. [2004a]. Le deuxième est un modèle linéaire du système de gestion d'air proposé par Gasser [2006].

1.3.1 Modèle du système électrique

Les modèles proposés dans cette partie sont issues d'une méthodologie utilisant des modèles électriques équivalents. Ainsi les modèles de la PAC et de la super-capacité (SC) sont des modèles équivalents électriques dans des versions simplifiées.

La PAC est modélisée par un modèle simplifié adapté à la commande. Ce modèle est connu avec le nom de modèle de capacités de double couche, qui représente la dynamique capacitive de la couche de charge entre les électrodes et la membrane électrolytique.

Le modèle statique de la pile est donné par :

$$\begin{aligned} v_{fc} &= E - v_{act} - v_{ohm} - v_{conc} \\ &= E - [v_0 + v_a (1 - e^{-c_1 i})] - [i R_{ohm}] - \left[i \left(c_2 \frac{i}{i_{max}} \right)^{c_3} \right] \end{aligned} \quad (1.25)$$

où les paramètres de l'équation peuvent être trouvés avec une régression non-linéaire à partir des données expérimentales.

La SC est caractérisée avec un modèle simple composé par une impédance capacitive en série. Ce modèle simple est, comme dans le cas de la PAC, adapté à la commande. Les paramètres du modèle peuvent être retrouvés dans le travail de Sailler [2008] pour des différentes conditions d'opération.

Dans les sections suivantes les modèles des convertisseurs de puissance sont présentés.

1.3.1.1 Modèle du système double hacheur élévateur en parallèle

Les convertisseurs de puissance sont modélisés en utilisant la modélisation moyenne. Les modèles moyens peuvent être linéaires ou non-linéaires suivant la dynamique du convertisseur.

Dans le premier cas étudié, le modèle du système hybride composé par deux hacheurs élévateurs connectés en parallèle est présenté. Ce modèle est présenté dans la Figure 1.4. Le convertisseur flyback n'est pas modélisé et une structure simplifiée est obtenue. La justification et la validité de ce choix est présentée ultérieurement dans le mémoire.

Le modèle moyen non-linéaire de cette topologie hybride est donné par :

$$\begin{aligned} \frac{dV_{C_c}}{dt} &= \frac{1}{C_c} \left[I_{fc} - \frac{V_{C_c}}{R_{tc}} \right], \quad \frac{dV_{C_a}}{dt} = \frac{1}{C_a} \left[I_{fc} - \frac{V_{C_a}}{R_{ta}} \right] \\ \frac{dI_{fc}}{dt} &= \frac{1}{L_{fc}} [E_0 - V_{C_a} - V_{C_c} - (R_m + R_L)I_{fc} - (1 - \alpha_{fc})V_C] \\ \frac{dI_{sc}}{dt} &= \frac{1}{L_{sc}} [V_{sc} - R_{sc}I_{sc} - (1 - \alpha_{sc})V_C], \quad \frac{dV_{sc}}{dt} = \frac{1}{C_{sc}} I_{sc} \\ \frac{dV_C}{dt} &= \frac{1}{C} [(1 - \alpha_{fc})I_{fc} + (1 - \alpha_{sc})I_{sc} - I_{load}] \end{aligned} \quad (1.26)$$

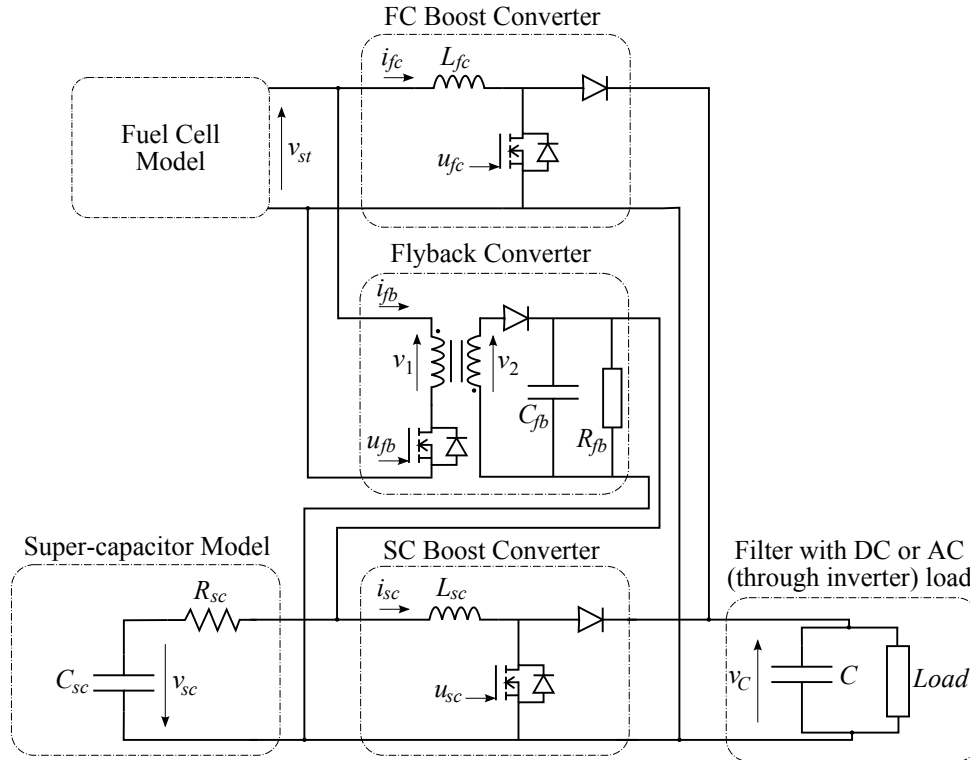


Figure 1.4: Equivalent topological model of the hybrid system studied.

Le modèle moyen est utilisé dans la suite pour obtenir le modèle adapté à la commande désirée (voir par exemple Bacha et al. [1994] pour plus de détails dans la modélisation moyenne adaptée aux convertisseurs de puissance). On considère seulement l'utilisation de modèles moyens de premier ordre. Les variables d'état de ce modèle sont: V_{C_c} et V_{C_a} les capacités de double couche dans la cathode et l'anode respectivement, I_{fc} le courant de sortie de la PAC, I_{sc} le courant de sortie de la super-capacité et V_C la tension du bus continu et aux bornes de la capacité du filtre de sortie. Les entrées sont les rapports cycliques des convertisseurs α_{fc} et α_{sc} , et le courant de la charge I_{load} comme entrée de perturbation.

Le modèle linéaire du système est obtenu avec la linéarisation autour d'un point de fonctionnement. Les conditions d'opération ont été choisies pour une tension du bus continu $V_C = 24V$ et un courant dans la PAC de $I_{fc} = 35,2A$. Une analyse de sensibilité et des facteurs de participation, permet d'étudier l'influence des paramètres physiques sur les modes du système.

1.3.1.2 Modèle de l'onduleur de tension

Pour garantir une connexion à une application AC, un onduleur de tension est considéré. La topologie complète, avec un deuxième hacheur réversible pour la source secondaire est présentée dans la Figure 1.5. Pour plus de simplicité, seulement le cas d'une application isolée est considérée.

Encore une fois, le modèle moyen obtenu à partir de la topologie du système est utilisé.

Le modèle du système de l'onduleur dans les repères de Park est donnée par:

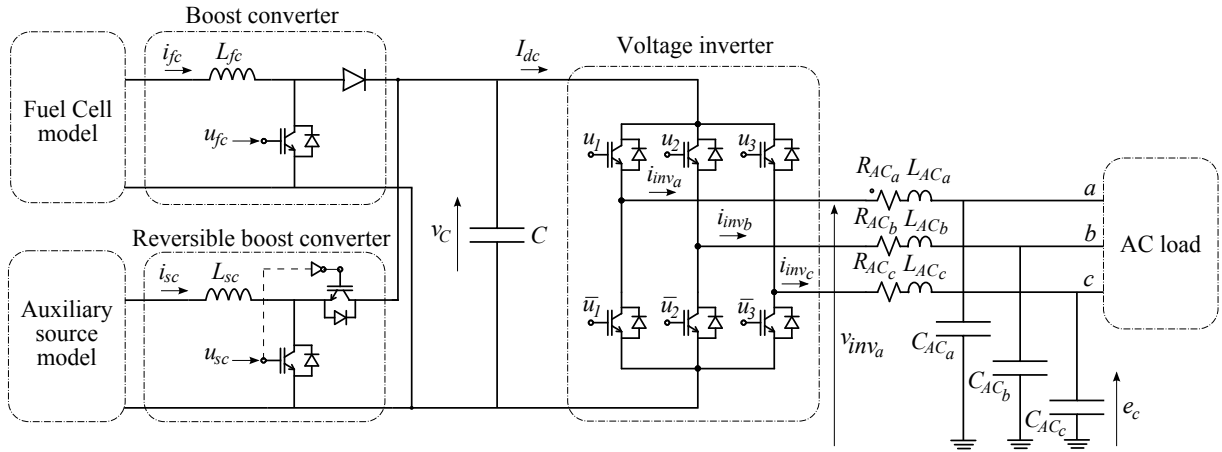


Figure 1.5: Hybrid topology with voltage inverter.

$$\begin{aligned}
 \frac{dI_{inv_d}}{dt} &= -\frac{R_{AC}}{L_{AC}} I_{inv_d} - \frac{1}{L_{AC}} E_d + \frac{1}{L_{AC}} \frac{V_C}{2} \beta_d + I_{inv_q} \omega_{net} \\
 \frac{dI_{inv_q}}{dt} &= -\frac{R_{AC}}{L_{AC}} I_{inv_q} - \frac{1}{L_{AC}} E_q + \frac{1}{L_{AC}} \frac{V_C}{2} \beta_q - I_{inv_d} \omega_{net} \\
 \frac{dE_d}{dt} &= \frac{1}{C_{AC}} I_{inv_d} - \frac{1}{C_{AC}} I_{load_d} + E_q \omega_{net} \\
 \frac{dE_q}{dt} &= \frac{1}{C_{AC}} I_{inv_q} - \frac{1}{C_{AC}} I_{load_q} - E_d \omega_{net}
 \end{aligned} \tag{1.27}$$

où les variables d'état sont $I_{inv_{d,q}}$ les courants en sortie de l'onduleur et $E_{d,q}$ les tensions aux bornes de la capacité du filtre de sortie C_{AC} . Les entrées sont $\beta_{d,q}$ la valeur moyenne des signaux de commande de l'onduleur. La perturbation est le courant de la charge $I_{load_{d,q}}$. Avec ω_{net} la fréquence AC du réseau.

1.3.2 Modèle de la PAC et du système Moteur-Compresseur

Dans une dernière section de modélisation, le modèle complet de la PAC est présenté. Le modèle complet inclus les interactions thermodynamiques dans la PAC, contenus dans le débit de réactants (hydrogène et oxygène), les échanges de chaleur/température, la dynamique du vapeur d'eau, et la gestion de puissance électrique. Deux modèles sont proposés dans cette thèse. D'abord un modèle non-linéaire, d'ordre quatre, proposé par Suh [2006], comme une réduction d'ordre du modèle complet proposée par Pukrushpan et al. [2004a]. Ensuite, un modèle linéaire adapté à la commande et proposé par Gasser [2006] est présenté.

La notation utilisée pour représenter le modèle non-linéaire est issue des travaux de Talj et al. [2009]. Si l'on considère cette notation et une réduction d'ordre additionnelle, suite à la définition de la pression d'air dans la cathode ($p_{air,ca} = p_{O_2} + p_{H_2} + p_{sat}$), alors le modèle non-linéaire devient :

$$\begin{aligned}
\dot{\chi} &= -\mu_1\chi + \mu_2x_4 + \mu_3 - \mu_4\xi \\
\dot{x}_3 &= -c_9x_3 - \frac{c_{10}}{x_3} \left[\left(\frac{x_4}{c_{11}} \right)^{c_{12}} - 1 \right] h_3(x_3, x_4) + c_{13}u \\
\dot{x}_4 &= c_{14} \left[1 + c_{15} \left[\left(\frac{x_4}{c_{11}} \right)^{c_{12}} - 1 \right] \right] [h_3(x_3, x_4) - c_{16}(-\chi + x_4)]
\end{aligned} \tag{1.28}$$

où les variables d'état sont χ la pression d'air dans la cathode, x_3 la vitesse du moto-compresseur et x_4 la pression dans la chambre de sortie de la pile. Les constantes μ_i et c_j (avec $i \in [1, 4]$ et $j \in [9, 16]$) sont définies dans Talj et al. [2009] et elles sont dépendantes des paramètres physiques du système.

Les résultats obtenus pour l'identification des modèles sont aussi présentés dans cette section. Un effort a été fait pour l'identification des modèles linéaire et non-linéaire, ainsi que pour les caractéristiques statiques de la PAC et du moto-compresseur. Une solution est proposée au problème d'identification d'un système contenant une boucle fermée de commande, tel est le cas de la commande en vitesse du compresseur.

1.4 Commande et résultats

Les résultats obtenus avec les outils de commande proposés sont présentés dans cette dernière section. Plusieurs cas d'étude sont analysés. L'analyse de la boucle fermée est complétée avec les modèles en boucle ouvert présentés dans la section de modélisation du système. Dans un premier temps, la méthodologie pour la commande est décrite. Ensuite, les résultats obtenus sont séparés dans deux parties: sous-système électrique et sous-système d'alimentation en air.

Dans le sous-système électrique plusieurs topologies sont analysées. Les résultats sont obtenus pour des topologies avec le système hybride de hacheurs élévateurs, avec un deuxième hacheur élévateur réversible en courant, et avec l'inclusion d'un onduleur de tension pour des applications alternatives. Pour le sous-système d'alimentation en air, un premier problème est présenté pour la commande en vitesse du moto-compresseur. Le problème de la commande LPV est présenté par la suite, avec une formulation spéciale en prenant en compte des incertitudes paramétriques sur le modèle. Finalement, une première approche à une commande robuste est présentée pour le système complet d'équations.

Un algorithme avec une version simplifiée de la méthode proposée par He and Wang [2006] a été développé dans cette thèse. La programmation de cet algorithme est faite sous MATLAB avec l'aide des outils d'optimisation *Yalmip* (interfaçage) et *Sedumi*, *Sdpt3* (routines de solution du problème d'optimisation sous la forme d'une LMI).

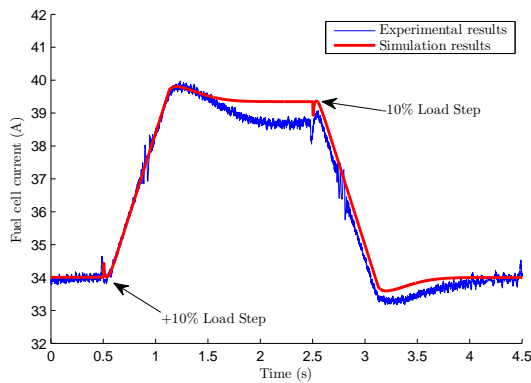
Quelques résultats remarquables sont présentés à continuation à titre illustratif.

1.4.1 Synthèse des résultats obtenus dans la partie électrique

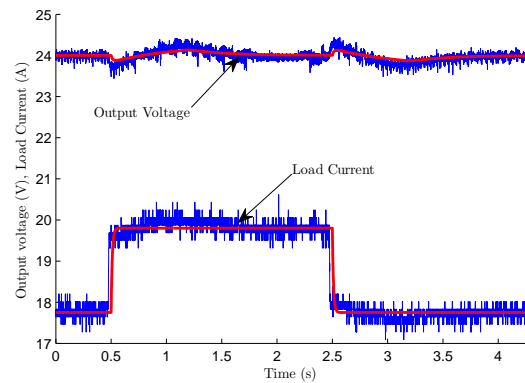
La méthodologie proposée dans la thèse est utilisée pour obtenir un contrôleur d'ordre réduit (PI) pour le système hybride de convertisseurs de puissance. En utilisant des fonctions de pondération appropriées, l'obtention d'un contrôleur PI multivariable est possible. La méthodologie de commande proposée est détaillée dans le chapitre ? de la thèse.

Après validation des résultats obtenus dans la boucle fermée à l'aide des simulations temporelles, une validation expérimentale a été mise en place. Un banc d'essai dédié a été conçu pour évaluer l'efficacité de la méthode de commande.

La Figure 1.6 montre les résultats obtenus dans l'expérience avec la méthode proposée et la comparaison avec les résultats en simulation. Ces résultats sont obtenus pour une perturbation de 10% dans le courant de la charge du système. Une bonne concordance des résultats est constatée.



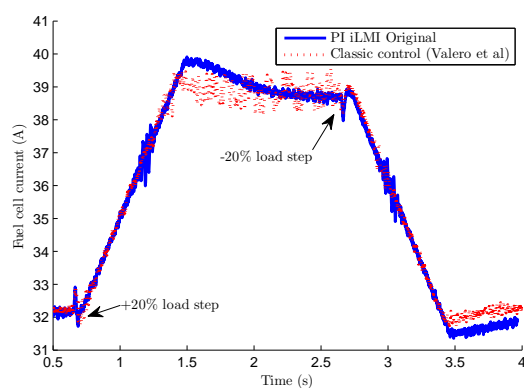
(a) Perturbation de 10% (Courant PAC)



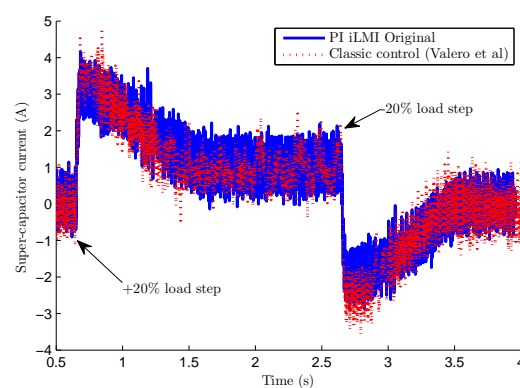
(b) Perturbation de 10% (Tension bus DC)

Figure 1.6: Résultats expérimentaux pour une perturbation de 10% (courant et tension).

Dans la Figure 1.7, la réponse temporelle obtenue dans l'expérience est comparée avec la dynamique d'une méthodologie de commande classique à base des PI. Dans les deux cas, la tension du bus DC est régulée efficacement. Le PI classique a une réponse temporelle plus rapide, cependant des ondulations apparaissent dans le courant de la pile, contrairement aux résultats obtenus avec la commande robuste.



(a) Perturbation de 20% (Courant PAC)



(b) Perturbation de 20% (Courant SC)

Figure 1.7: Résultats expérimentaux pour une perturbation de $\pm 20\%$, comparaison des commandes robuste et classique.

Une analyse de robustesse est présentée avec des variations paramétriques. L'outil de la μ -analyse est utilisé pour évaluer la robustesse des contrôleurs. Des variations

paramétriques sont définies dans les composants physiques du système (résistances, inductances, capacités). La Figure 1.8 présente les résultats de la μ -analyse. Le contrôleur \mathcal{H}_∞ d'ordre complet est utilisé comme référence. Les résultats montrent la robustesse des contrôleurs ($\mu < 1$) devant les incertitudes dans le cas de la robustesse en stabilité et robustesse en performance.

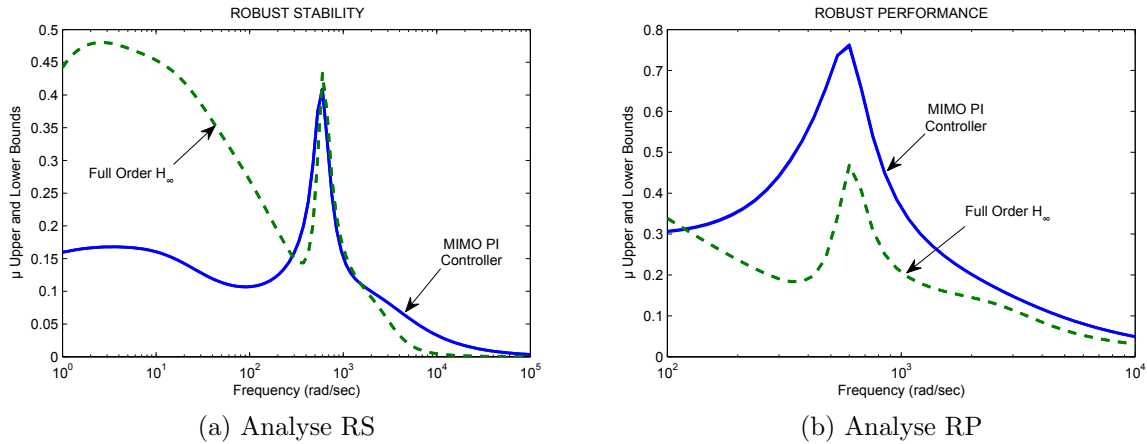


Figure 1.8: Analyse de robustesse en utilisant la μ -analysis.

Le cas d'un système hybride avec un onduleur de tension pour de application AC a été aussi étudié. Avec un modèle de l'onduleur dans le référentiel de Park, le choix des paramètres des fonctions de pondérations est fait pour garantir une réponse rapide face à des perturbations.

Comme dans le cas précédent, les résultats obtenus avec les méthodes robustes sont comparés avec la méthode classique de commande. Cette fois-ci, le contrôleur d'ordre réduit est donné par une commande \mathcal{H}_∞ d'ordre fixé. Les réponses temporelles obtenues avec les différentes méthodologies sont comparées dans la Figure 1.9 pour une perturbation de 10% dans le courant de la charge. Un rejet de perturbation efficace est obtenu dans toutes les méthodologies étudiées. L'apport en robustesse est en contraste supérieur pour les contrôleurs robustes. La Figure 1.10 montre le tracé des valeurs singulières de la boucle fermée pour des variations paramétriques de $\pm 10\%$ dans les composants du filtre AC. La méthode proposée présente une amélioration considérable de la robustesse.

1.4.2 Synthèse des résultats obtenus dans la partie thermodynamique

Dans cette dernière partie, des résultats sont présentés pour la commande du système moto-compresseur et pour le système complet, c'est à dire, la commande des systèmes de gestion électrique et système de gestion d'air.

Une commande classique est présentée pour comparaison avec les méthodes proposées. Cette commande est composée par deux boucles de contrôle: le contrôle de vitesse du moto-compresseur et le contrôle du taux de consommation d'oxygène λ_{O_2} . Le paramètre a une influence directe sur la performance de la PAC et sur la puissance efficace fournie à la charge.

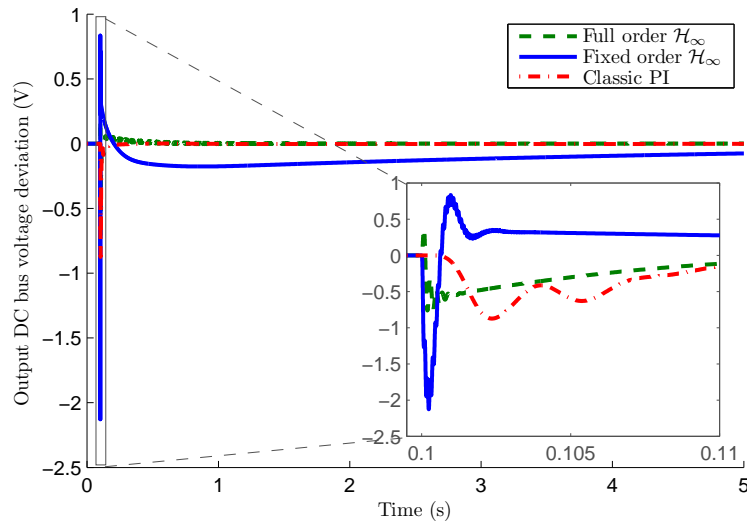


Figure 1.9: Résultats de simulation, comparaison des contrôles \mathcal{H}_∞ d'ordre fixe et d'ordre complet avec la commande classique avec des PI.

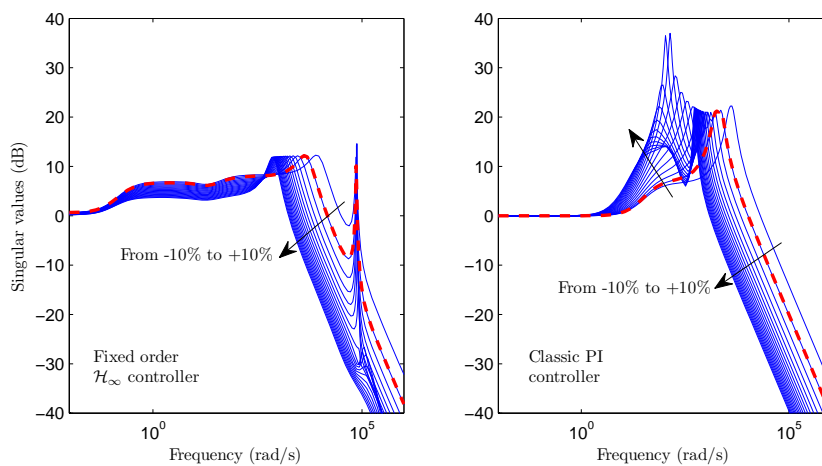


Figure 1.10: Analyse de robustesse des systèmes en boucle fermée.

Un premier contrôle est proposé pour la commande en vitesse du compresseur. Des résultats intéressants sont obtenus, notamment pour le contrôleur \mathcal{H}_∞ obtenu avec la réduction d'ordre. Ensuite, une méthodologie de commande LPV est proposée pour le système de gestion d'air. Plusieurs possibilités de modèles affins LPV sont proposées et deux types de problèmes sont résolus: le problème de commande non-linéaire et le problème de commande robuste d'un système soumis à des incertitudes. Des résultats prometteurs sont obtenus avec des simulations temporelles en utilisant la technique de programmation de gain. Enfin, quelques résultats sont présentés pour une première proposition d'une méthodologie de commande pour le système complet.

Le diagramme de bloc du système complet est présenté dans la Figure 1.11. Les entrées de commande sont les rapports cycliques des convertisseurs de puissance et la vitesse de référence du compresseur. Les fonctions de pondération sont choisies pour garantir une bonne performance dans la tension du bus continu et du taux de consommation d'oxygène.

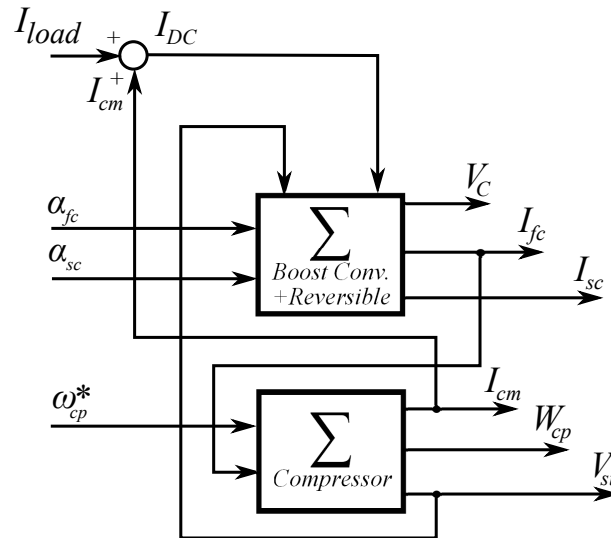


Figure 1.11: Diagramme de bloc du système complet.

Les résultats obtenus sont présentés dans les Figures 1.12 et 1.13. La régulation obtenue avec la méthodologie proposée est satisfaisante avec la commande \mathcal{H}_∞ d'ordre réduit. L'amélioration dans la régulation de λ_{O_2} a une influence directe sur l'augmentation de la puissance nette délivrée à la charge.

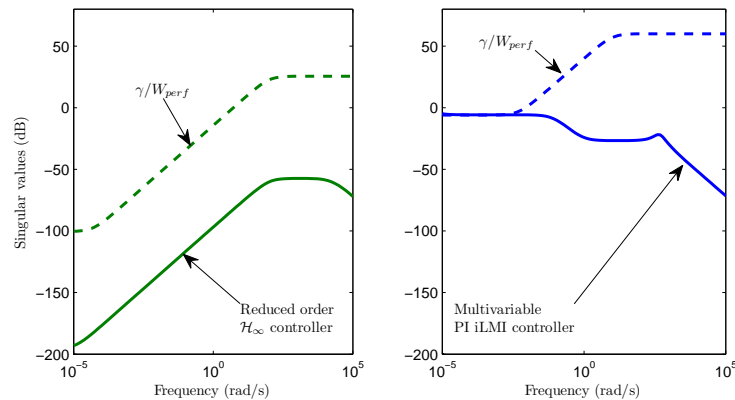


Figure 1.12: Valeurs singulières de la boucle fermée.

1.5 Conclusions

Dans cette thèse une méthodologie de commande pour un système hybride pile à combustible a été proposée. Deux caractéristiques remarquables sont: la méthode *multivariable* et la *robustesse*. Les comparaisons faites avec les méthodes classiques de commande montrent que des améliorations importantes peuvent être accomplies avec la méthodologie proposée, notamment en ce qui concerne la robustesse. On s'est intéressé à l'analyse des contrôleurs d'ordre réduit, vue leur simplicité d'implémentation. Un cas particulier a été l'analyse d'un contrôleur PI multivariable, obtenu dans le cadre de la commande \mathcal{H}_∞ et l'application des outils LMI. Des résultats très prometteurs ont été obtenus, cependant

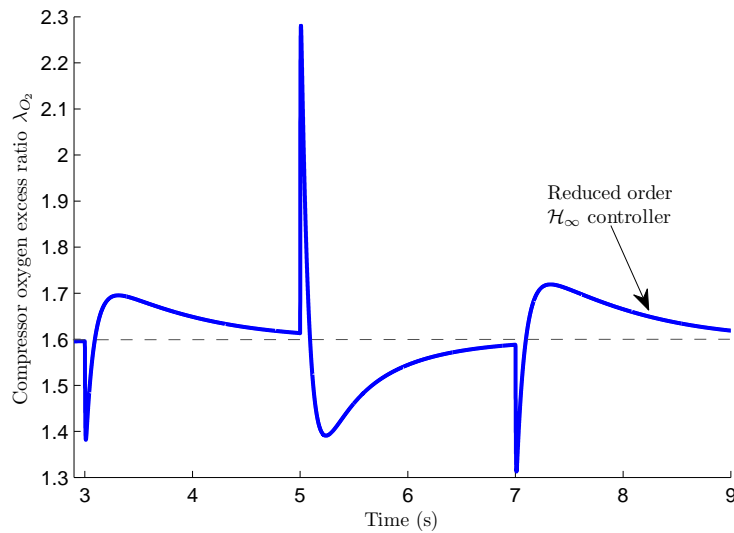


Figure 1.13: Résultats de simulation, taux de consommation d'oxygène.

quelques limitations dans les algorithmes étudiés sont aussi présentées.

La méthodologie multivariable a été conçue comme un premier pas vers l'implémentation d'une stratégie généralisée de commande, ayant comme objectif d'aider à l'intégration des aspects robustesse dans la conception de la commande.

Chapter 2

General Introduction

Context and motivations

(a) Fuel cell developments

A fuel cell (FC) is an electro-chemical device converting chemical energy into electrical energy by means of an electrode pair, an electrolyte and a catalyzer. The energy source for the FC comes from an external reservoir of fuel, commonly hydrogen or natural gas to be reformed into hydrogen. The operating principle of a FC is similar as in conventional batteries, however an important advantage is that the FC can be continuously operating as long as the fuel is available for power production. FC's are attractive because they are efficient, flexible in the modular structure they can adopt and environmentally friendly with practically no emissions. Power generation systems based on FC's are expected to play a more important role in the future of Distributed Generation (DG) applications [Wang and Nehrir, Dec. 2007]. FC's operating as DG can be connected to the utility grid or can be operated as a stand-alone power supply system in a remote area [Han et al., 2007].

The fuel enters the FC by the anode, where it is oxidized emitting electrons that will travel through an external circuit. At the same time, due to energy balance, ions pass through an electrolyte membrane permeable to electrons. Finally in the cathode, the oxidant is reduced, allowing the consumption of electrons in the external circuit and establishing an electrical current [Ellis et al., 2001]. This is the essential operating principle for a Proton Exchange Membrane FC, also called Polymer Electrolyte Membrane FC (PEMFC). PEMFC operates at $50 \sim 100^\circ$ with power ranging from a few kW to 1MW approximately. PEMFC are intended to be a good replacement of the internal combustion engine and an important energy source for the future [Laughton, 2002, Cook, 2002, Sakhare et al., 2004]. As it has been the FC technology the more developed, this type of FC is set to be used both transport and portable power applications. FC are generally classified according to the electrolyte type. Other FC technology includes: Phosphoric Acid FC (PAFC), Molten Carbonate FC (MCFC) and Solid Oxide FC (SOFC). SOFC uses a ceramic material as the electrolyte and are the technology is also well developed as the PEMFC. SOFC are characterized by high operating temperatures ($>500^\circ$) and its has been considered as good option for large utility-scale power applications, due to the high efficiency obtained when combined with gas turbines or steam cycles [Ellis et al., 2001]. Concerning the PEMFC, they are composed by carbon electrodes attached to a

very thin polymer membrane. This set, known as Membrane Electrode Assembly (MEA) is sandwiched between two collector plates. Channels traced within these plates allow the diffusion of the reactive gases on the electrode surface. Individual cells composed by MEA plates are assembled to form the FC “stack”.

Another advantage, and may be the most important one, of FC, is that they are proper *green energy*. Despite being discovered more than 150 years ago, there has been an important development in FC technology in the last decades. Beginning with its first commercial use during NASA’s *Gemini* project in 1965 to its actual state of development, which has achieved a very important maturity. Certainly this development has been boosted by the global warming threat and the need of an alternative to the fossil-hydrocarbon based energy. Moreover in recent years, the energy prices and the cleanliness of actual energy sources, the depletion of oil wells, the imminent reach of the peak-oil point, and several other conditions have accelerated this process, not only with FC but with other types of *renewable energy*¹.

The FC development has come however with some important technological issues. The cell operation and its evolution, yielded to the use of platinum as catalyzer material. Being more expensive than gold, the final cost of the stack rises exponentially. Another common problem is the FC availability. Actually, individual cells ($\sim 1V$) are connected in series to obtain higher operational voltages. This means that a failure on a single cell means that the whole stack has to be put out of service. One of the greatest challenges in FC technology is to improve durability. According to [Blunier, 2007], before the FC becomes a mature technology, the life-span of a FC that stood at 2000h approximately in 2005, should be improved to be compared with the combustion engine for 5000h² of life-span including cycles. Other improvements in the FC power density (in W/Kg), the cost, mass and volume of the air compressor technology are also expected in the near future.

Despite the effort of the scientific community, and the research on new materials and polymers to improve FC performance, the US government decided to drop research funds on FC for cars³. The Energy Department statement of May 2009 dictates however that pay for research into *stationary* fuel cells will be maintained. This decision had an important influence and may be resulted on a short stagnation on FC development. In 2011 a FC conference was held in Grenoble⁴ and it was stated that even though the development of new materials was relatively slow in recent years, a new impulse in the field is *in process* and a new momentum was regained. The FC remains then a very interesting option for the future of energy production.

Finally, the strong motivation of a *green energy* technology is highly valued. Besides the technological problems involved on FC development (cost, availability and durability), an other technical problem is always present, the fuel. Today, there is no hydrogen mass-production capability, and the infrastructure for its distribution to final consumers is inexistent (or at least vastly less developed than oil & gas infrastructure). It should be considered for example that, if hydrogen is produced from electrolyzers, if the electrical

¹See for example some of the recent research works at G2ELab on photovoltaics [Stalter, 2009, Riffonneau, 2009, Picault, 2009], wind power [Teninge, 2009], or even an interesting research on micro-hydro cross-flow water-turbine power generation [Hauck, 2011].

²Corresponding to roughly 240,000km

³Retrieved 04/2011: <http://www.nytimes.com/2009/05/08/science/earth/08energy.html>

⁴Retrieved 05/2011: <http://fdfc2011.lepmi.grenoble-inp.fr/>

energy is taken from the grid and the grid energy is ensured by coal burning power stations, then the reduction on carbon emissions is negligible [Cook, 2002]. Another problem is that sometimes hydrogen production is associated with oil production. For example, gasoline or methanol can be reformed to produce hydrogen, however the reduction of carbon emissions is not exceptional and the overall efficiency is reduced. Still economically feasible solutions with high impact on carbon emissions are: the use of natural gas from conventional gas outlets to produce hydrogen and the use of the hydrogen produced from natural gas made at large refineries, nevertheless both solutions are still bounded to the oil industry. The **dream** for the FC system is to use only renewable energy sources for hydrogen production. This can be considered with the use of wind turbines, photovoltaics or micro-hydraulic turbines. This set-up is presented in Figure 2.1.

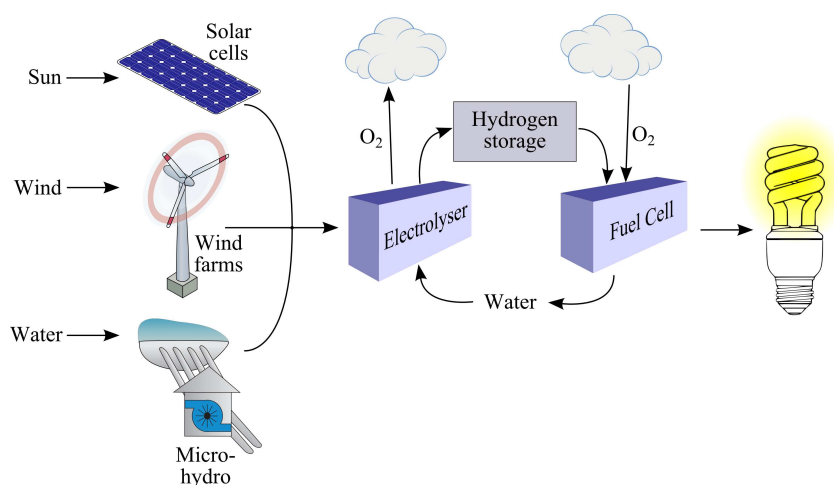


Figure 2.1: Power production from renewable energy sources.

(b) The FC system

A fuel cell may not operate alone. When referring to a FC *system*, all the auxiliary systems, needed for operation, are included. This makes the complete system a rather complex structure to control. The auxiliary elements can be divided into two groups: electrical and thermo-dynamical management sub-systems. The first ensures the safe connection of the FC to the electrical application (load) and the second sub-system ensures the gas, water, air and thermal management of the FC. Of course, these sub-systems are both highly dependent, as the gas flow in the stack directly depends on the load current demand, then the electrical sub-system is influenced by the flow dynamics. In terms of the FC efficiency, the stack will have a better performance at higher flow pressures, but this means higher compression ratios and higher energy consumption of the compressor-motor sub-system, an a degraded overall system efficiency. Given these interactions between both systems, a general control strategy for the complete FC system seems to be, *a priori*, a good solution. A more efficient control is necessary to guarantee an optimal management of hydrogen and air in the system, avoiding stack membrane degradation (and output voltage degradation) for a more reliable and efficient operation. Another complexity is the need of an auxiliary source. As it will be described later in the dissertation, the FC source needs to be hybridized with a secondary source (commonly batteries or super-capacitors)

in order to cope with harmful current transients. This means that both sources are also to be managed for proper operation.

(c) Problems involved in the thesis

Within the context described before, a need is identified for a robust multivariable control approach to manage both the electrical and thermo-dynamical sub-systems on the FC. The disturbance rejection approach is extensively adopted in this thesis, since, as a general proposition, this will have an influence on the cells life-span, avoiding non-desired high energy transients. The models presented in this dissertation involve thermo-dynamical parameter modeling, such as reactant flows and pressures. It should be noted that limitations on the FC performance are due not only to material characteristics, but also on the optimization of the thermo-dynamical operating parameters as, for example, the flow rate of reactant streams [Gasser, 2006]. In fact, as a central part of the FC dynamic behavior, the control of the compressor-motor and the supply air flow are considered in this dissertation. Nevertheless, some assumptions are made to obtain simplified control-oriented models. For example, the fuel flow control, the air humidification and the stack temperature controls are assumed to be perfect. An interest is also given to robust control, aiming to achieve robust stability and performance for systems subject to uncertainties. Other problems include demonstrating the advantage of a multivariable approach over the classical decoupled control methodologies and the validation of a generalized methodology with complete robustness analysis.

State-of-the-art

A complete review of FC models proposed in literature, is presented in Hissel and Turpin [2008]. A summary of the recent trends on more complex and precise electro-chemistry models is presented in the work of Shah et al. [2011]. The energy conditioning using several power converter control configurations and FC system considerations are presented in Pera et al. [2007], Barragán [2009] and Suh and Stefanopoulou [2005]. Notably in Suh and Stefanopoulou [2005], an interesting approach on co-ordinated (centralized) controllers is presented. The advantage of a *centralized controller* is shown to optimally manage the FC current and the air input flow. However, no robustness results are presented and the hybrid source problem is not addressed. Multivariable Multiple Input-Multiple Output (MIMO) robust control in these type of system has already been studied in literature, as in Gadoura et al. [2002] and Rafiei et al. [2003], where robust \mathcal{H}_∞ is proposed. However, application to the real model and order reduction is not addressed. Full order controllers are also computed using state and output feedback, as in Takegami et al. [2004], with the use of 2-degree-of-freedom structure. In Petrovic and Rakic [2005], or even Alvarez-Ramirez et al. [2001], in addition to full order \mathcal{H}_∞ control, simple Proportional-Integral (PI) control is proposed, however robust performance criteria in the PI control synthesis and the MIMO case are not considered. A multivariable \mathcal{H}_∞ controller is proposed in Sedghisigarchi and Feliachi [2004] for SOFC systems, but the control input is directly applied to fuel consumption control and no auxiliary system (air supply) is considered. In Kazmi and Bhatti [2009] a robust \mathcal{H}_∞ controller using Linear Matrix Inequalities (LMI) is proposed for a polytopic set of systems under several loading conditions. Once again,

robustness is not deeply analyzed and the proposed controller is limited to the SISO case. An attractive approach for multivariable \mathcal{H}_∞ control is presented in Wang et al. [2008], with interesting model identification and control design results. The hybrid system and the power converter control problems are not solved, since control inputs are directly the fuel and air flows. This work was later extended for a multivariable robust PI controller in Wang and Ko [2010]. In the work of Li et al. [2010] a robust \mathcal{H}_∞ (full-order) controller using LMI is proposed and the robustness is analyzed using μ -analysis.

Other effective control strategies can also be found in the literature. See for example the use and experimental validation of adaptive controllers in Jiang et al. [2007], the use of advanced controller with fuzzy logic in Sakhare et al. [2004], or the use of optimal control with linear quadratic (LQ) control in Domenico et al. [2010] and Suh and Stefanopoulou [2005].

A high number of power converter control designs are based on Pulse-width-modulation (PWM) control. PWM of DC-DC boost converters is generally divided in two approaches: voltage-mode and current-mode control. Boost power converters dynamics includes right-hand-side (RHS) zero. To provide more damping to the system, in the current-mode control an additional stabilizing current loop is used. The control then becomes a multi-loop feedback problem, see Middlebrook [1987] and Alvarez-Ramirez et al. [2001]. The problem becomes more complex when multivariable control is needed for several parallel connected converters, as is the case of hybrid power generation systems. It should be noticed that, in this work, the optimization of the control references is not addressed. However a rich literature can be found on this subject, control strategies can be based on imposed reference signals related to the FC dynamic, using for example a Maximum Power Point Tracker (MPPT) algorithm or a tracking on the FC efficiency curve. See for example the works of Han et al. [2007], Thounthong et al. [2009], Thounthong and Rael [2009], Suh and Stefanopoulou [2005], Candusso [2002] or even Valero et al. [2006] for several examples on primary level control methodologies. See also the works of Zhi-dan et al. [2008], for an adaptive approach using MPPT algorithm for FC inner-loop current control, and Becherif and Hissel [2010] for an MPPT algorithm considering the FC net power and the power consumption from the compressor-motor and the air supply system.

In this thesis the discrete control problem solution for real-time implementation is not addressed. It is considered that the switching frequency of the power converters is considerably superior when compared to the sampling frequency of the controller board used for real-time implementation. But discrete-time control could be easily designed following the same methodology. For a synthesis on discrete-domain controller implementation see for example the work of Valero [2004]. In this dissertation we also considered that harmonics are perfectly filtered, this will not (obviously) be the case on real-world implementations. An interesting analysis on harmonics effects on FC stacks is presented in Fontes et al. [2007].

Objectives of the thesis

Energy quality constraints to be respected are commonly fixed by norms. These systems should also be able to adapt to fast changes in load or in the operating conditions. Then, appropriate control-oriented modeling and the control strategy itself are critical issues. In a first approach we will focus on the control of the electrical sub-system of the FC and the

power management. Several linear robust control techniques are designed and compared in this dissertation, but more importance is given to small order controllers (PI and Reduced order \mathcal{H}_∞ control) due to their simplicity in practical industrial application. To include robust performance specifications in the PI control synthesis, the control problem is written as an LMI convex optimization problem. As seen later, the iterative LMI (iLMI) method proposed in He and Wang [2006] is used to solve the MIMO PI control problem for given desired \mathcal{H}_∞ performance. The methodology will focus on the control of DC/DC boost power converters associated to the hybrid source composed by a FC and a Super-Capacitor (SC). The fuel cell has to be associated with a storage device (super-capacitors or batteries) in order to mitigate harmful current transients and to increase its lifespan. Classically, each component of the hybrid fuel cell control system is designed independently of each other. This approach allows simplifying the control strategy, but is not sufficient to take into account the various dynamics of the system and the coupling between thermodynamical (gas pressure) and electrical (DC current or voltage) variables. Besides, time spent for the design of the system can become critical since it is often necessary to iterate for the calculation of controller parameters. Finally, equipment suppliers should be able to design their products while knowing accurately the parameters of the whole system. However, fuel cell performances are closely linked to temperature and membrane humidification. For that purpose, robust and multivariable methods seem to be particularly adapted since they are able to deal with control issues for uncertain systems.

In a second approach, the multivariable robust control of the air supply system is analyzed in this dissertation. A complete resume of compressor types and technologies is presented in Blunier [2007]. For the compressor-motor system modeling, we have focused our attention on control-oriented models. First we have considered a linear control-oriented model proposed by Gasser [2006]. For a second topology we have considered the non-linear model proposed by Suh [2006], which is a reduced order version of the non-linear model proposed by the now well known work of Pukrushpan et al. [2004a]. Several elegant results on FC and compressor-motor group control have been proposed in the literature to optimize the net power and reduce the energy consumption of the whole group. Optimization techniques for FC generators including compressor-motor group using particle swarm optimization and extremum seeking approach have been presented in Tekin et al. [2006] and Chang and Moura [2009] respectively. Other approaches for the FC air supply control system may include non-linear control, as in the work of Talj et al. [2009] where passivity control is used on the reduced order non-linear model proposed by Suh [2006]. An interesting analysis on FC performance at different loading conditions and a valuable contribution on a strategy for determine the compressor speed reference signal may be found in the work of Thirumalai and White [2000].

In any case, the literature lacks *robust multivariable* linear control strategies applied to the air supply control system of an autonomous FC power generator. In this dissertation a first proposition is presented for robust/multivariable control using PI and Reduced order \mathcal{H}_∞ control. A glance of a robust controller is also proposed for compressor-motor speed control using Linear Parameter Varying (LPV) systems and gain-scheduling.

Structure of the thesis

In accordance with the previous general introduction the thesis structure is presented as follows. The thesis is basically divided in three chapters: a chapter with the control tools applied for robust control, a chapter describing the models structures, and a final chapter with control design and results.

In *chapter 3* the control tools used during the thesis are presented. This chapter is divided into three sections: tools for model identification, tools for control design and synthesis, and tools for robustness analysis. In the first section the methodology for identification measurements and data processing is presented. Then, the tools for model identification using the MATLAB's *System Identification Toolbox* are described. In the second section, the control tools applied during the thesis are introduced. In a first part robust control tools are presented for LTI systems. These tools include both full-order \mathcal{H}_∞ and reduced order controllers, with the introduction of a MIMO PID robust control using LMI tools. In a second part, robust control methods are presented for LPV systems. Controllers include the full-order \mathcal{H}_∞ and a simplified PID methodology for LPV systems, again exploiting the LMI tools. In a final part for this chapter, the μ -analysis methodology for robustness analysis is described. Examples on a simple system of equations are given for illustration purposes of the control methodologies.

In *chapter 4* the models used for control applications are presented. In a first part, the test-bench dedicated to model identification and control experimental validation are described. Then, the system models are presented and divided into two sections: electrical and thermo-dynamical sub-systems. The electrical sub-system model description comprises the parallel hybrid boost power converter models using average modeling and, in a second approach, the introduction of the voltage inverter model for alternative power applications. The validations of these models from the topological systems equations (exact model) are presented. The thermo-dynamical sub-system description is divided into a model description of the FC stack and both non-linear and linear equation systems including the air compressor dynamics. The models described in this section are devoted for control-oriented applications. These models are validated from measurements and identification from the real test-bench set-ups, including a special set-up, described earlier in the chapter, for the air compressor model identification.

Finally in *chapter 5* control applications are introduced. The structure of this application chapter is presented in similitude with the time-line of the work realized during the thesis. The chapter is divided into three sections: control design of the electrical sub-system, control design for the air supply sub-system and finally a control structure for the complete system of equations. The control methodology and the results obtained for each section are presented. Simulation and *experimental* results for control validation of the electrical sub-system are given. An approach to LPV control, including a proposition for an LPV speed controller for the air motor-compressor system are described.

Contributions

This thesis provide an effective application of **multivariable robust** control for the FC **hybrid** generator *system*, including the power management of a secondary source. The methodology involved in the control strategy aims to provide a *generic* approach, where

control design is straightforward. An emphasis is given for reduced order and simplified PI control. The main contributions are then concerned with:

- MIMO robust control of hybrid boost power converter system with experimental validation.
- MIMO robust control of complete FC system: electrical and thermo-dynamical subsystems.
- An LPV control approach for compressor speed control.

List of publications during the thesis

Journal papers

- ◇ Hernandez-Torres, D.; Riu, D.; Sename, O. and Druart, F. A robust multivariable approach for hybrid fuel cell supercapacitor power generation system. *European Physical Journal of Applied Physics*, **2011**, 54.

Conference papers

- ◇ Hernandez-Torres, D.; Riu, D.; Sename, O. and Druart, F. Robust Control Analysis using Real-Time Implementation of a Hybrid Fuel Cell Power Generation System. *Fundamentals and Developments of Fuel Cells Conference - FDFC*, 2011, **2011**.
- ◇ Hernandez-Torres, D.; Riu, D.; Sename, O. and Druart, F. Robust optimal control strategies for a hybrid fuel cell power management system. *36th Annual Conference on IEEE Industrial Electronics Society - IECON*, **2010**, 698-703.
- ◇ Hernandez-Torres, D.; Riu, D.; Sename, O. and Druart, F. On the Robust Control of DC-DC Converters: Application to a Hybrid Power Generation System. *4th IFAC Symposium on system, structure and control*, **2010**.
- ◇ Hernandez-Torres, D.; Riu, D. and Sename, O. Design and Experimental Validation of a Robust Control Method for a Hybrid Fuel Cell Power Generation System. *IEEE Energy Conversion Congress & Expo - ECCE*, **2010**, 4482-4489.
- ◇ Hernandez-Torres, D.; Sautreuil; Retiere, N.; Riu, D. and Sename, O. A new methodology for aircraft HVDC power systems design. *IEEE International Conference on Industrial Technology - ICIT*, **2009**, 166-171.

Chapter 3

Advanced Control Tools

3.1 Introduction

In this chapter the methodologies used for model identification, control design and analysis are presented. The theoretical aspects described here on system identification are not exhaustive, a review of specialized references on this topic is however presented. First, a brief background on identification is introduced in section 3.2, which will be considered as a part of the methodology proposed in our application framework.

This chapter also includes a description of some of the advanced control design tools used within the thesis framework. These tools are presented in section 3.3. Most of the tools used in this thesis are a part of the control design methodologies for multivariable robust control. Several application examples are given in this section to allow the reader an easy and practical comprehension of the proposed tools.

3.2 System identification tools

3.2.1 Some basic principles

This section is not meant to be a reference on system identification, but a recall on some of the most important features of the methodologies presented in the literature. An extensive theory on this topic can be found for example in [Ljung, 1987] and [Landau, 1993]. For practical applications, an interesting option is the use of the functions and graphical user interfaces developed in the *System Identification (SI) Toolbox* in MATLAB. More details on that toolbox are available in [Ljung, 1988].

It should be noticed that a system identification can be a difficult and time consuming problem to deal with. First, several important questions should be posed. For example, are the system experimental excitation inputs rich enough in harmonics for identification? Is the model structure known? Is it linear or non-linear? If the model structure is known what are the state measures available for identification?

Several scenarios are possible when trying to identify a real system. However the most common situation is a trade-off between a system that is easily described by physical equations and systems that can be efficiently identified from sufficient experimental data. In that case, the system can be, maybe partially, described by some physical equations and a set of experimental data is available to find the system parameters. When using

experimental data, a special care should be taken when choosing test-cases and excitation input signals. When selected properly, these specifications could lead to an easily solvable identification problem.

In any case, the identification process can be divided in two steps [Laroche, 2007]:

- Define the model type of identification, for which there are two options: parametric or non-parametric.
- Find the model parameters or the best adapted structure.

Identification problems can be classified according to different criteria. The first is the linear or non-linear properties of the system and model. The second is a classification based on the known structure of the model. If the analytical equations of a model are unknown, then a *black box* model can be used along with a set of experimental data to find a model that adequately represent the dynamic behavior of the system. If the physical equations of the system are known, then an Ordinary Differential Equations (ODEs) parameter estimation model is used for identification, this is the so-called *grey box* identification problem. A possibly final classification can be realized for dynamical or static system. However, in terms of the identification methodology, a static identification problem can be treated as a grey box problem with no dynamical states. The use of the *Surface Fitting Tool* will be more straightforward, where custom user defined equations are possible. A final option for static curve fitting is the on-line tool `zun-zun`¹, where a “function finder” capability could be useful. A review on several MATLAB functions useful for identification is presented at the end of this chapter in Table 3.2.

In this thesis, both static and dynamical identification problems are considered for linear systems. The grey box problem is used for the dynamical identification. The following sections are focused in this type of problems. Let us now describe several parts of an identification problem.

3.2.2 Identification stages

With a set of acquired experimental data, the division of the identification process in several stages is possible. The complete identification loop, presented in Ljung [1995], is described in Figure 3.1. The different stages in the identification loop are described hereafter.

3.2.2.1 Experiments and data acquisition

In order to achieve an efficient identification, the input signals to the real system should contain as much information as possible. The ideal signal to do this is a white noise, however the common practice in real applications is to use a *Pseudo Random Binary Sequence* (PRBS) [Brely, 2003].

The PRBS autocorrelation function² given by:

$$C(v) = \sum_{j=0}^{N-1} a_j a_{j+v} \quad (3.1)$$

¹See (retrieved on April 2011) : <http://zunzun.com/>

²The cross-correlation of a signal with itself

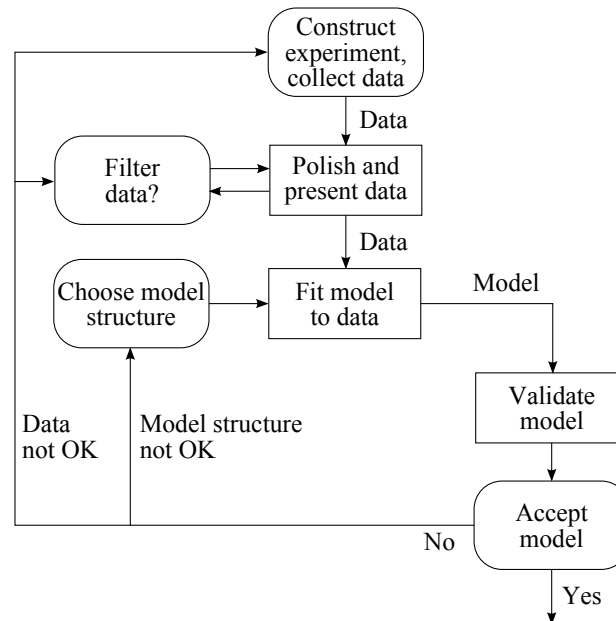


Figure 3.1: The identification loop process.

can only take two values:

$$C(v) = \begin{cases} m & \text{if } v \equiv 0 \\ h = mc & \text{if } v \neq 0 \end{cases} \quad (3.2)$$

with N the number of bits of the binary sequence (BS) a_j with $j = 0, 1, \dots, N - 1$, composed by m ones and $N - m$ zeros, c denotes the duty cycle of the PRBS given by $c = \frac{m-1}{N-1}$.

Finally the PRBS amplitude can be fixed according to the physical meaning of each excitation signal. Other options used sometimes for model identification or validation are the multi-sine signal and the frequency-based methods, these options are useful to fix the excitation signal bandwidth. See the work of Van den Hof and Schram [1995] for a survey on identification and control techniques using frequency-based methods. In Figure 3.2 an example of the PRBS and the chirp signal excitation inputs are presented.

3.2.2.2 Data processing

At this point of the identification process, the measured data should be treated. An initial analysis of the measured data is recommended. The variations of the different system states with respect to the excitation signals should be studied. From this point the use of the MATLAB *SI Toolbox Graphical User Interface (GUI)* could be time saving³. Of course that alternatively, the individual functions in the toolbox can also be applied directly from the Command Window.

Normally measured data is corrupted with some measurement noise. So a second step could be to filter the data. Subsequently steps could include the selection of data

³Even when you are not considering using the GUI, it could be useful for data processing that can be directly exported to the MATLAB workspace.

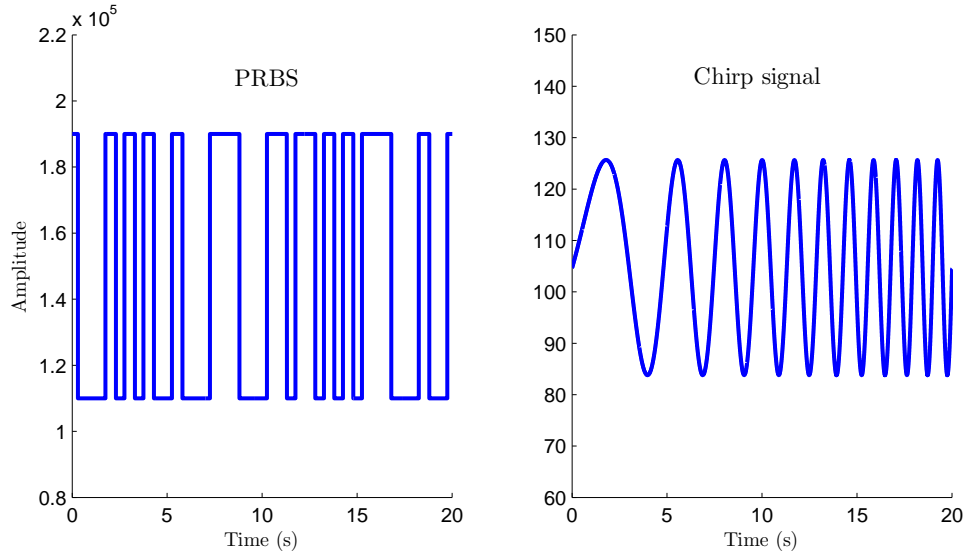


Figure 3.2: Excitation signals example.

subsets, handling offsets and data trends, resampling data or transforming between time and frequency domains.

3.2.2.3 Estimation procedure

This process can be divided in two parts: choosing the model structure and the parameter estimation itself.

Concerning the model structure (usually defined by the desired model usage), there are generally two different options: a model for simulation and analysis or obtaining a control-oriented model. In the first case, a complete and detailed high order model describing the system dynamics is usually obtained. In the second case a simplified model is looked for, then advanced or classical control techniques are easier to be realized.

For linear systems, the generalized system behavior is defined by [Brely, 2003]:

$$y(t) = G(q^{-1})u(t - n_k) + H(q^{-1})d(t) \quad (3.3)$$

where $y(t)$, $u(t)$ and $d(t)$ are the system output, input and disturbance respectively. $G(q^{-1})$ and $H(q^{-1})$ are the system and the disturbance transfer functions respectively, n_k is the input-output delay and q is the forward shift operator.

The functions $G(q^{-1})$ and $H(q^{-1})$ can be described as:

$$G(q^{-1}) = \frac{B(q^{-1})}{A(q^{-1}) \times F(q^{-1})} \quad (3.4)$$

$$H(q^{-1}) = \frac{C(q^{-1})}{A(q^{-1}) \times D(q^{-1})} \quad (3.5)$$

where A , B , C , D and F are polynomials:

Table 3.1: Special structures for identification [Brely, 2003]

Used polynomials	Structure
B	FIR (<i>Finite Impulse Response</i>)
$A B$	ARX
$A B C$	$ARMAX$
$A C$	$ARMA$
$A B D$	$ARARX$
$A B C D$	$ARARMAX$
$B F$	OE (<i>Output error</i>)
$B F C D$	BJ (<i>Box-Jenkins</i>)

$$\begin{aligned}
 A(q^{-1}) &= 1 + a_1 q^{-1} + \dots + a_{n_A} q^{-n_A} \\
 B(q^{-1}) &= b_1 + b_2 q^{-1} + \dots + b_{n_B} q^{-n_B+1} \\
 C(q^{-1}) &= 1 + c_1 q^{-1} + \dots + c_{n_C} q^{-n_C} \\
 D(q^{-1}) &= 1 + d_1 q^{-1} + \dots + d_{n_D} q^{-n_D} \\
 F(q^{-1}) &= 1 + f_1 q^{-1} + \dots + f_{n_F} q^{-n_F}
 \end{aligned} \tag{3.6}$$

$$\tag{3.7}$$

The identification objective now translates into finding the polynomial parameters a_j , b_j , c_j , d_j and f_j . Several special structures for identification can then be defined. The most common is the **Auto Regressive Moving Average with eXternal inputs** or ARMAX structure, because of its trade off between simplicity and system description. In this structure there are three polynomials to be determined: $A(q^{-1})$, $B(q^{-1})$ and $C(q^{-1})$ ($F(q^{-1}) = D(q^{-1}) = 1$).

The system representation is then given by:

$$A(q^{-1})y(t) = B(q^{-1})u(t - n_k) + C(q^{-1})d(t) \tag{3.8}$$

The other used structures are summarized in Table 3.1.

For non-linear models using the *SI Toolbox*, three options are possible: non-linear ARX models, Hammerstein-Wiener models and nonlinear state-space models. Non-linear ARX models are black box structures extended from the linear case. These models are build using the function `idnlarx`. The non-linear ARX structure is given by [Ljung, 1988]:

$$y(t) = f(y(t-1), \dots, y(t-n_a), u(t-n_k), \dots, u(t-n_k-n_b+1)) \tag{3.9}$$

with n_a the number of past output terms used to predict the current output, n_b the number of past input terms used to predict the current output, n_k the time delay from input to output as in the linear case, and the function f is a flexible nonlinearity estimator.

Hammerstein-Wiener models are used for combined linear systems with some static non-linear structure that can be used to describe non-linear behavior on linear systems as saturations, dead zones, etc.

Finally the nonlinear state-space models are an option where the physical meaning of the equations is important. The system should be presented as a set of n first order Ordinary Differential Equations (ODE), where n is the number of states.

To find the final estimated parameters different methods are proposed: gradient method, least-squares method, recursive methods, etc. The choice will depend on the model structure and the properties of the measured data.

In this thesis, some identification problems using ARX models and non-linear ODE models are solved, as seen in chapter 4.

3.2.2.4 Validation

The quality of the model obtained after identification can be evaluated in various ways. A first step is to compare the simulation results of the identified models with some validation data, in order to evaluate the accuracy of a model. A loss function evaluating the prediction error can also be useful to validate the model results. The model validation is achieved using a different measure set from that used for identification (the validation data). If after validation the model obtained is not accepted, then some modification could be considered on the data set or the model structure, following the identification loop described in Figure 3.1.

3.2.3 A word on systems with feedback

There are some situations where experimental measures are obtained on systems with feedback, for example in the case of a real-time running industrial process where the normal operation requires feedback control. In this case only output error methods could give reliable results. The works developed by Hansen et al. [1989] evolved into a solution to the closed-loop identification using fractional representations. In [Landau and Karimi, 1997], the general methodology of the Closed-Loop Output Error (CLOE) algorithm is presented, along with other recursive closed-loop algorithms. However, these methods are defined only for linear system identification. Despite this, the work of Hansen et al. [1989] was extended to the non-linear case in [Dasgupta and Anderson, 1996]. A closed-loop identification analysis is also presented in [Van den Hof and Schram, 1995].

In this thesis the identification problem of a system with feedback was tackled using a simplified version of the non-linear dynamic. This will be presented later in chapter 4.

3.3 Control design and analysis tools

3.3.1 Towards a generalized methodology

In this section a general presentation of the robust and optimal control theory used in this thesis is proposed. The basic principles of the Linear Matrix Inequalities (LMI) tools and the \mathcal{H}_∞ robust control theory are developed. The mixed sensitivity methodology is studied. Attention is given to the output-feedback systems, which are of interest since on industrial applications full access to system states is virtually impossible. Solution to the \mathcal{H}_∞ control problem using traditional Riccati equation as well as advanced tools (LMI) are presented. The work of Scherer et al. [1997] describes the use of LMI tools for output-feedback systems. The advanced tools section is developed using the Yalmip[Löfberg, 2004] interface, along with known solvers Sedumi, Sdpt3⁴.

⁴Sedumi website (retrieved on april 2011): <http://sedumi.ie.lehigh.edu/>
Sdpt3 website (retrieved on april 2011):

Several results on reduced and fixed order control can be found in the literature. The reader could refer to the works of Apkarian and Noll [2006], Hol et al. [2003] or even Le [2010] for detailed surveys on this type of controllers. A special focus in this work is given to reduced and fixed order robust controllers with the use of LMI tools. Specially the case of Proportional-Integral-Derivative (PID) controllers are of interest for their simplicity in practical applications, in particular in the benchmark thesis context. A special case using an iterative LMI methodology to solve the PID control design problem is presented in this section. Then some extensions of these problems to Linear Parameter Varying (LPV) systems are proposed.

The control design tools presented in this section are part of an effort towards a generalized robust control methodology. For this reason, the proposed tools are displayed in a didactic format, making it easy for the reader to apply and adapt the control design methodology to their own needs. Some numerical examples are presented throughout this section to illustrate the advantages of the developed tools. Let us now introduce the LMI tools.

3.3.2 Linear matrix inequalities in control

3.3.2.1 Presentation

A summary of the most important events on LMIs history is given below [Boyd et al., 1994]:

- 1890: The first LMI is proposed, an analytical solution to the Lyapunov LMI using the Lyapunov equation.
- 1940's: Application of Lyapunov methods to real control problems. Small size LMI's are solved manually.
- 1960's: It is known that LMI appearing in the positive-real (PR) lemma can be solved using a certain algebraic Riccati equation (ARE).
- 1980's: Recognition of the "convex programming" for computer solution to LMI's.

An LMI is written in the form:

$$A(x) = A_0 + A_1 x_1 + \dots + A_N x_N \prec 0 \quad (3.10)$$

where x is the vector of "decision" or "optimization" variables, A_i are symmetric matrices and \prec is read as negative definite. The solution of an LMI means solving a convex optimization problem, i.e., a problem where a solution is guaranteed given the structure of the equations. This is important since, even if the problem has no analytical solution, convexity assures at least a numerical solution to the problem in control synthesis [Gahinet et al., 1995].

LMIs are considered as a very powerful tool in robust control optimization theory. LMIs are a mathematical formulation allowing to solve an optimization problem by means

of efficient algorithms of convex optimization. These tools are then often used to define a formal methodology for control problems.

A wide range of problem specifications and constraints can be written as LMI's [Gahinet et al., 1995]. The usual approach using LMIs consists first in reformulating the control problem in the form of a convex optimization problem, using some relaxations and change of variables. Then, one of the main advantages of these tools is the efficient numerical solution, given the availability of advanced and powerful algorithms developed to solve this kind of optimization problem. Finally the solution to the original problem can be reconstructed from the optimization result. In the following sections the basic theory for understanding LMIs is presented. Again, this section on LMIs is intended to be a brief recall on the basic principles leading to the control procedure proposed in this thesis. A complete review on LMI theory can be found in [Poussot-Vassal, 2008], [Scherer and Weiland, 2005] or [Boyd et al., 1994].

3.3.2.2 A classic motivation problem

Consider an unstable linear system described by the following state-space system:

$$\dot{x} = Ax(t) + Bu(t) \quad (3.11)$$

$$y = Cx(t) + Du(t) \quad (3.12)$$

The considered problem is to find a controller that stabilizes this system by means of a state-feedback (State-Feedback Stabilization). The control law is then given by:

$$u(t) = Kx(t) \quad (3.13)$$

According to the definition of stability in the sense of Lyapunov, the following quadratic Lyapunov function can be defined [Poussot-Vassal, 2008]:

$$v(x(t)) = x^T(t)\mathbf{P}^{-1}x(t) \quad (3.14)$$

with $P \succ 0$.

So, the stability condition for the closed-loop system can be expressed as follows [He and Wang, 2006]:

$$(A + BK)\mathbf{P} + \mathbf{P}(A + BK)^T \prec 0 \quad (3.15)$$

In that form the problem to be solved is not linear, due to the coupling between the unknown variables K and \mathbf{P} . The change of variables $\mathbf{L} = K\mathbf{P}$ can be used to linearize equation (3.15) as:

$$A\mathbf{P} + \mathbf{P}A^T + B\mathbf{L} + \mathbf{L}B^T \prec 0 \quad (3.16)$$

with $\mathbf{P} \succ 0$ and any given \mathbf{L} .

This is an LMI and the solution to this equation gives the controller expression $K = \mathbf{L}\mathbf{P}^{-1}$ that stabilizes the system in (3.11).

3.3.2.3 Three LMI problems

In the literature, common LMI problems are classified in three categories [Gahinet et al., 1995]:

- **(i) Feasibility problem:** this problem consists in finding the solution x that satisfies the equation:

$$A(x) \prec 0 \quad (3.17)$$

with A defined as the equation (3.10).

- **(ii) Minimization of a linear objective function:** in this case, a convex objective subject to LMI constraints is minimized. For a convex objective, this problem can be written as:

$$\text{Minimize } c^T x \text{ subject to } A(x) \succ 0.$$

where c^T is the linear convex objective.

- **(iii) Generalized eigenvalue problem:** this case is similar to the previous problems, but with the following structure:

$$\text{Minimize } \lambda \text{ subject to } \begin{cases} A(x) \prec \lambda B(x) \\ B(x) \succ 0 \\ C(x) \prec 0 \end{cases} \quad (3.18)$$

The optimization problems solved in this thesis are based on the minimization of a linear objective function, i.e., problem (i).

3.3.2.4 Norms in control

Before the presentation of the control synthesis methodologies based on LMI tools, some basic definitions are given for better understanding the mathematical implications of the control procedure. These definitions are summarized in the work of Poussot-Vassal [2008] and they are more detailed in the classic book by Zhou et al. [1996].

Definition 1 *Dynamic LTI system*

Given matrices $A \in \mathbb{R}^{n \times n}$, $B \in \mathbb{R}^{n \times r}$, $C \in \mathbb{R}^{q \times n}$ and $D \in \mathbb{R}^{q \times r}$, a linear time invariant (LTI) system is described by:

$$\Sigma_{LTI} : \begin{cases} \dot{x} = Ax(t) + B\omega(t) \\ z = Cx(t) + D\omega(t) \end{cases} \quad (3.19)$$

where $x(t)$ is the state vector taking values in the state-space $X \in \mathbb{R}^n$, $\omega(t)$ is the input to the system with values in the input space $W \in \mathbb{R}^r$ and $z(t)$ is the output vector with values in the output space $Z \in \mathbb{R}^q$.

Definition 2 Generalized definition of norm

If X is a vector space, the function $\|x\|_p$ defined on X is the p -norm of x and its generalized definition is given by:

$$\|x\|_p = \left(\sum_{i=1}^n |x_i|^p \right)^{1/p}, \text{ for } 1 \leq p \leq \infty \quad (3.20)$$

Using the generalized definition of a norm, the particular cases of 1, 2 and ∞ norms can be found defining $p = 1, 2, \infty$. From this it follows:

$$\|x\|_1 = \sum_{i=1}^n |x_i| \quad (3.21)$$

$$\|x\|_2 = \sqrt{\sum_{i=1}^n |x_i|^2} \quad (3.22)$$

$$\|x\|_\infty = \max_{1 \leq i \leq n} |x_i| \quad (3.23)$$

Definition 3 Norms \mathcal{L}_1 , \mathcal{L}_2 and \mathcal{L}_∞

◇ The norm 1 of a function $x(t)$ is given by:

$$\|x(t)\|_1 = \int_0^{+\infty} |x(t)| dt \quad (3.24)$$

◇ The norm 2 of a function $x(t)$ is given by:

$$\|x(t)\|_2 = \sqrt{\int_0^{+\infty} x^*(t) x(t) dt} = \sqrt{\frac{1}{2\pi} \int_{-\infty}^{+\infty} X^*(j\omega) X(j\omega) d\omega} \quad (3.25)$$

This norm corresponds to the energy of signal $x(t)$.

◇ The ∞ norm is given by:

$$\|x(t)\|_\infty = \sup_t |x(t)| \Rightarrow \|X\|_\infty = \sup_\omega \|X(j\omega)\| \quad (3.26)$$

Definition 4 \mathcal{H}_∞ norm

The \mathcal{H}_∞ norm of a dynamic LTI system (3.19) from input $\omega(t)$ to output $z(t)$, is the energy-to-energy gain defined by:

$$\|G(j\omega)\|_\infty = \sup_{\omega \in \mathbb{R}} \bar{\sigma}(G(j\omega)) = \max_{\omega(t) \in \mathcal{L}_2} \frac{\|z\|_2}{\|\omega\|_2} \quad (3.27)$$

For a MIMO system this norm represents the maximum value in the singular value plot of $G(j\omega)$. This means that it is the largest gain of the system fed by a harmonic input signal [Poussot-Vassal, 2008].

3.3.2.5 Convexity and LMIs

Convexity is a very important property in optimization. One of the main advantages is to simplify the complexity of the problem by guaranteeing convergence to a global optimum in polynomial time. A complete presentation on convex optimization is given in the work of Scherer and Weiland [2005].

As stated in [Poussot-Vassal, 2008]:

The convexity provides a framework where optimization results are now well established and where efficient and robust tools are available.

Actually, the tools and algorithms developed for convex optimization are very powerful and easy to implement in the structure of a now well established control methodology. Moreover, an important number of these tools are freely available and fully compatible for use with MATLAB (See `Yalmip` interface and `Sedumi` solver for example).

Let us now define a convex function and a special case of a convex function: the LMI.

Definition 5 *A convex function*

A function $f : \mathbb{R}^p \rightarrow \mathbb{R}$ is convex if and only if $\forall x, y \in \mathbb{R}^p$ and $\lambda \in [0, 1]$,

$$f(\lambda x + (1 - \lambda)y) \leq \lambda f(x) + (1 - \lambda)f(y) \quad (3.28)$$

A special case of a convex function is given by the strict LMI constraint, defined by:

Definition 6 *The LMI constraint*

An LMI constraint in a vector $x \in \mathbb{R}^p$ is defined as:

$$F(x) = F_0 + \sum_{i=1}^m F_i x_i \succeq 0 (\succ 0) \quad (3.29)$$

A classic example of an LMI constraint is the Lyapunov inequality for an autonomous system $\dot{x} = Ax$. The stability LMI associated with this system is [Poussot-Vassal, 2008]:

$$\begin{aligned} x^T \mathcal{K} x &\succ 0 \\ x^T (A^T \mathcal{K} + \mathcal{K} A) x &\prec 0 \end{aligned} \quad (3.30)$$

that can be rearranged as:

$$F(\mathcal{K}) = \begin{bmatrix} -\mathcal{K} & 0 \\ 0 & A^T \mathcal{K} + \mathcal{K} A \end{bmatrix} \prec 0 \quad (3.31)$$

In this case $\mathcal{K} = \mathcal{K}^T$ is the decision variable and $F(\mathcal{K}) \prec 0$ is linear in \mathcal{K} .

3.3.2.6 Semi-definite programming (SDP)

Semi-definite programming problems are the practical and mathematical programming realization of LMIs. LMI programming is a generalization of Linear Programming, which is the optimization problem where the cost function is linear and the set of feasible constraints is defined by *affine* inequalities [Scherer and Weiland, 2005]. The SDP problem can be defined as:

Definition 7 SDP problem

Assuming that constraint functions G_1, \dots, G_m map \mathcal{X} into a set of symmetric matrices, the general semi-definite program can be defined as:

$$\text{minimize} \quad f(x) \quad (3.32)$$

$$\text{subject to} \quad x \in \mathcal{X}, G_1(x) \preceq 0, \dots, G_m(x) \preceq 0 \quad (3.33)$$

From this definition, two important considerations are now exposed:

- The SDP problem is called *convex* if f and G_1, \dots, G_m are *convex*.
- This problem is called **linear matrix inequality optimization problem** if f and G_1, \dots, G_m are *affine* in x .

Using these definitions and other important results described later, the SDP problem for an \mathcal{H}_∞ controller is now presented.

3.3.2.7 The SDP problem of an \mathcal{H}_∞ controller

For any given system, two mathematical functions are now defined:

- $V(x(t))$, is a storage function that represents the energy stored in the system.
- $s(\omega(t), z(t))$, is a function that defines the rate of energy entering into the system.

So a given function s under the *quadratic* form, i.e.:

$$s(\omega(t), z(t)) = \begin{bmatrix} \omega \\ z \end{bmatrix}^T \begin{bmatrix} Q & S \\ S^T & R \end{bmatrix} \begin{bmatrix} \omega \\ z \end{bmatrix} = \omega^T Q \omega + \omega^T S z + z^T S^T \omega + z^T R z \quad (3.34)$$

and a controllable LTI system in the form of (3.19), the following statements are equivalent:

- The system is strictly dissipative (s is completely integrable).
- The system allows a storage function under the form: $V(x(t)) = x^T \mathcal{K} x$, with $\mathcal{K} = \mathcal{K}^T \succ 0$.

- There exists $\mathcal{K} = \mathcal{K}^T \succ 0$ such that the following LMI is feasible:

$$\begin{aligned}
F(\mathcal{K}) &= \begin{bmatrix} A^T\mathcal{K} + \mathcal{K}A & \mathcal{K}B \\ B^T\mathcal{K} & 0 \end{bmatrix} - \begin{bmatrix} 0 & I \\ C & D \end{bmatrix}^T \begin{bmatrix} Q & S \\ S^T & R \end{bmatrix} \begin{bmatrix} 0 & I \\ C & D \end{bmatrix} (\prec) \preceq 0 \\
&= \begin{bmatrix} I & 0 \\ A & B \\ 0 & I \\ C & D \end{bmatrix}^T \left[\begin{array}{cc|cc} 0 & \mathcal{K} & 0 & 0 \\ \mathcal{K} & 0 & 0 & 0 \\ \hline 0 & 0 & -Q & -S \\ 0 & 0 & -S^T & -R \end{array} \right] \begin{bmatrix} I & 0 \\ A & B \\ 0 & I \\ C & D \end{bmatrix} (\prec) \preceq 0 \quad (3.35)
\end{aligned}$$

The matrix P that is defined as:

$$P = \begin{bmatrix} Q & S \\ S^T & R \end{bmatrix} \quad (3.36)$$

can be used to define how the energy enters the system. With this matrix several performance criteria can now be defined [Poussot-Vassal, 2008]: the \mathcal{H}_∞ performance, the \mathcal{H}_2 performance, time domain constraints (overshoot, stabilization time,...), pole placement, etc.

For example, the \mathcal{H}_∞ control problem presented as an LMI optimization problem, can be obtained defining the quadratic function $s(\omega, z) = \gamma_\infty^2 \omega^T \omega - z^T z$. The LMI to be solved is given by:

$$\begin{bmatrix} I & 0 \\ A & B \\ 0 & I \\ C & D \end{bmatrix}^T \left[\begin{array}{cc|cc} 0 & \mathcal{K} & 0 & 0 \\ \mathcal{K} & 0 & 0 & 0 \\ \hline 0 & 0 & -\gamma^2 I & 0 \\ 0 & 0 & 0 & I \end{array} \right] \begin{bmatrix} I & 0 \\ A & B \\ 0 & I \\ C & D \end{bmatrix} \prec 0 \quad (3.37)$$

$$= \begin{bmatrix} A^T\mathcal{K} + \mathcal{K}A & \mathcal{K}B & C^T \\ B^T\mathcal{K} & -\gamma^2 I & D^T \\ C & D & -I \end{bmatrix} \prec 0 \quad (3.38)$$

However we will see that this not an LMI, but a Bilinear Matrix Inequality (BMI), because matrices A , B , C and D are the closed-loop state-space matrices and therefore intrinsically include the controller to be synthesized. This is described in more details in the following section 3.3.3 where these closed-loop matrices will be defined in details. The transformation of this BMI into an LMI and the generalized control methodology using LMIs are presented henceforth.

3.3.3 Control design using LMIs

3.3.3.1 Methodology of \mathcal{H}_∞ control

(a) General control configuration

The basic principles of the \mathcal{H}_∞ control theory and the subsequently representation as an LMI optimization problem are presented in this section.

Given the following system:

$$\begin{aligned} \dot{x} &= Ax(t) + B_1\omega(t) + B_2u(t) \\ z(t) &= C_1x(t) + D_{11}\omega(t) + D_{12}u(t) \\ y(t) &= C_2x(t) + D_{21}\omega(t) \end{aligned} \quad (3.39)$$

where $x(t) \in \mathbb{R}^n$ is the state space vector, $\omega(t) \in \mathbb{R}^r$ is the exogenous input signal, $u(t) \in \mathbb{R}^m$ is the control input, $z(t) \in \mathbb{R}^q$ is the performance output and $y(t) \in \mathbb{R}^p$ is the measured output.

This system is represented by the block diagram in Figure 3.3.

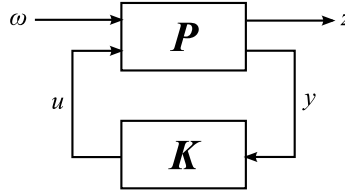


Figure 3.3: General control configuration.

where P is referred to as the generalized system given by:

$$P = \left[\begin{array}{c|cc} A & B_1 & B_2 \\ \hline C_1 & D_{11} & D_{12} \\ C_2 & D_{21} & D_{22} \end{array} \right] \quad (3.40)$$

The \mathcal{H}_∞ control is a disturbance attenuation problem, the goal of which is to minimize the gain of the closed-loop system $T_{z\omega}$ from disturbance $\omega(t)$ to output $z(t)$, so that the impact of the disturbances is minimized in the sense of the \mathcal{H}_∞ norm constraint:

$$\|T_{z\omega}(s)\|_\infty = \|\mathcal{F}_l(P(s), K(s))\|_\infty < \gamma_\infty \quad (3.41)$$

where \mathcal{F}_l is the “lower” linear-fractional representation.

It is however difficult (numerically) to find the optimal solution (global minimum for $\|T_{z\omega}(s)\|_\infty$) [Zhou et al., 1996], [Skogestad and Postlethwaite, 1996]. Normally a sub-optimal controller is found by defining the limitation in the minimal value of γ_∞ as a percentage of the global minimum γ value. In that case γ_∞ in equation (3.41) is the minimum bound of the sub-optimal \mathcal{H}_∞ control problem.

(b) Performance specifications

Before describing the control methodology using LMIs, some introductory principles on defining the desired performance specifications are presented. The desired performance specifications are introduced in the form of some weighting functions (frequency filters) on the sensitivity transfer characteristics [Skogestad and Postlethwaite, 1996]. The system P in (3.40) then includes the original open-loop system and the specified weighting functions. This structure is presented in more details in Figure 3.4, which corresponds

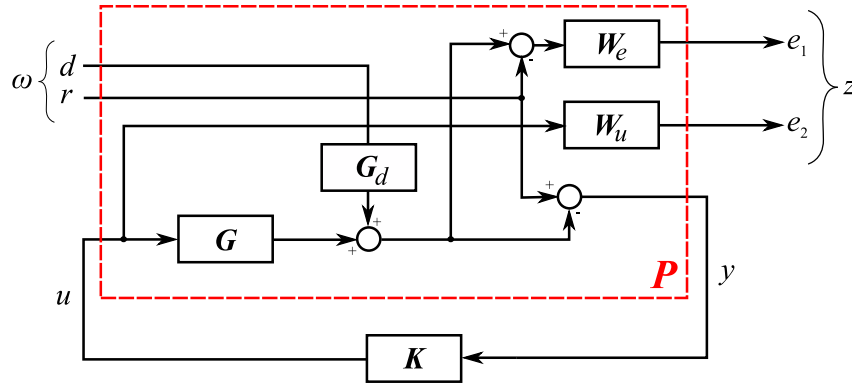


Figure 3.4: The (P, K) structure including weighting functions.

(if $G_d = 0$) to the S/KS mixed sensitivity problem. However, these results can be easily extended to the general case.

The functions with robustness and performance requirements are given with the following structure:

- Weighting function on the sensitivity function $S(s) = 1/(1 + K(s)G(s))$:

$$\frac{1}{W_e} = \frac{s + \omega_B A_\epsilon}{s/M + \omega_B} \quad (3.42)$$

Normally A_ϵ is chosen to be small enough, $M < 2$ (6dB) for a sufficient module

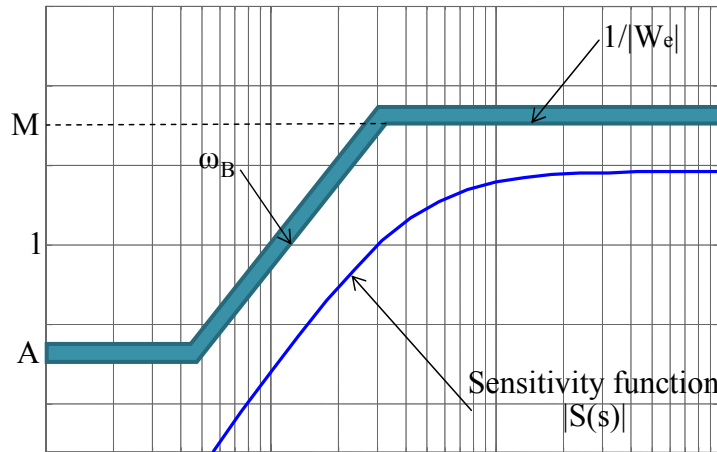
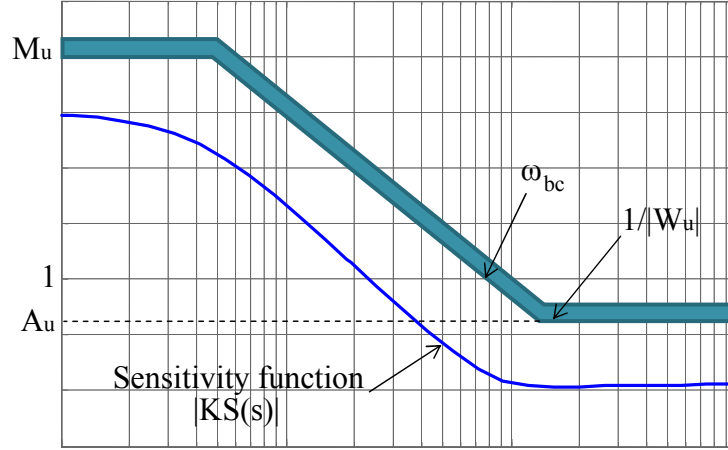


Figure 3.5: Weighting function for $S(s)$.

margin and ω_B has an influence on the closed-loop bandwidth and the system time response. The function $1/W_e(s)$ can be representative of time-domain response specifications, where M has an influence on the system overshoot, A_ϵ is the steady-state error and ω_B is representative of the response time.

- Weighting function on the sensitivity function $KS(s) = K(s)/(1 + K(s)G(s))$:

$$\frac{1}{W_u} = \frac{A_u s + \omega_{bc}}{s + \omega_{bc}/M_u} \quad (3.43)$$

Figure 3.6: Weighting function for $KS(s)$.

For this weighting function M_u is chosen to match system behavior at low frequencies and is normally used to include some limitation on the control input (for limitations on system actuators for example). In this case ω_{bc} has an influence on the system robustness and can be chosen accordingly for good robust performance.

On the system illustration in Figure 3.4, G is the plant model and G_d is the disturbance model. If the previously presented weighting functions are represented by the state space systems (A_e, B_e, C_e, D_e) and (A_u, B_u, C_u, D_u) , and if we take $G_d = 1$ without loss of consistency, then the extended model including weighting functions is given by:

$$\begin{aligned}\hat{x} &= \hat{A}\hat{x}(t) + \hat{B}_1\omega(t) + \hat{B}_2u(t) \\ z(t) &= \hat{C}_1\hat{x}(t) + \hat{D}_{11}\omega(t) + \hat{D}_{12}u(t) \\ y(t) &= \hat{C}_2\hat{x}(t) + \hat{D}_{21}\omega(t)\end{aligned}\quad (3.44)$$

with state, input and output vector given by:

$$\begin{aligned}\hat{x} &= [x \quad x_e \quad x_u]^T \\ \omega &= [d \quad r]^T \\ z &= [e_1 \quad e_2]^T\end{aligned}$$

and state space matrices:

$$\begin{aligned}\hat{A} &= \begin{bmatrix} A & 0 & 0 \\ -B_e C_1 & A_e & 0 \\ 0 & 0 & A_u \end{bmatrix} & \hat{B}_1 &= \begin{bmatrix} B_1 & 0 \\ -B_e & B_e \\ 0 & 0 \end{bmatrix} & \hat{B}_2 &= \begin{bmatrix} B_2 \\ 0 \\ B_u \end{bmatrix} \\ \hat{C}_1 &= \begin{bmatrix} -D_e C_1 & C_e & 0 \\ 0 & 0 & C_u \end{bmatrix} & \hat{C}_2 &= [C_2 \quad 0 \quad 0] & \hat{D}_{11} &= \begin{bmatrix} -D_e & d_e \\ 0 & 0 \end{bmatrix} \\ \hat{D}_{12} &= \begin{bmatrix} 0 \\ D_u \end{bmatrix} & \hat{D}_{21} &= [1 \quad 0]\end{aligned}$$

(c) Full order \mathcal{H}_∞ control

In this section the synthesis of an \mathcal{H}_∞ controller is proposed that solves equation (3.41). In this case, the closed-loop system is given by $\mathcal{F}_l(P, K)$, the lower linear fractional representation (LFR) with respect to K , is given by:

$$\mathcal{F}_l(P, K) = \mathcal{C}(sI - \mathcal{A})^{-1}\mathcal{B} + \mathcal{D} \quad (3.45)$$

where matrices \mathcal{A} , \mathcal{B} , \mathcal{C} and \mathcal{D} are the closed-loop state space system matrices. With the generalized controller system form given as:

$$K(s) \left\{ \begin{bmatrix} \dot{x}_k \\ u \end{bmatrix} = \begin{bmatrix} A_k & B_k \\ C_k & D_k \end{bmatrix} \begin{bmatrix} x_k \\ y \end{bmatrix} \right. \quad (3.46)$$

with $x_k \in \mathbb{R}^n$, $u \in \mathbb{R}^m$ and $y \in \mathbb{R}^p$, then the closed-loop matrices are given by:

$$\begin{aligned} \mathcal{A} &= \begin{bmatrix} A + B_2(I - D_k D_{22})^{-1} D_k C_2 & B_2(I - D_k D_{22})^{-1} C_k \\ B_k(I - D_k D_{22})^{-1} C_2 & A_k + B_k(I - D_k D_{22})^{-1} D_{22} C_k \end{bmatrix} \\ \mathcal{B} &= \begin{bmatrix} B_1 + B_2(I - D_k D_{22})^{-1} D_k D_{21} \\ B_k(I - D_k D_{22})^{-1} D_{21} \end{bmatrix} \\ \mathcal{C} &= [C_1 + D_{12}(I - D_k D_{22})^{-1} D_k C_2 \quad D_{12}(I - D_k D_{22})^{-1} C_k] \\ \mathcal{D} &= D_{11} + D_{12}(I - D_k D_{22})^{-1} D_k D_{21} \end{aligned} \quad (3.47)$$

If the system P is strictly proper, i.e. $D_{22} = 0$, then the closed-loop matrices can be further simplified as:

$$\begin{aligned} \mathcal{A} &= \begin{bmatrix} A + B_2 D_k C_2 & B_2 C_k \\ B_k C_2 & A_k \end{bmatrix} \\ \mathcal{B} &= \begin{bmatrix} B_1 + B_2 D_k D_{21} \\ B_k D_{21} \end{bmatrix} \\ \mathcal{C} &= [C_1 + D_{12} D_k C_2 \quad D_{12} C_k] \\ \mathcal{D} &= D_{11} + D_{12} D_k D_{21} \end{aligned} \quad (3.48)$$

Then as presented before, the closed-loop system is said to be stable and to meet \mathcal{H}_∞ performance if there exists a controller $K(s)$ such that:

$$\begin{bmatrix} \mathcal{A}^T \mathcal{K} + \mathcal{K} \mathcal{A} & \mathcal{K} \mathcal{B} & \mathcal{C}^T \\ \mathcal{B}^T \mathcal{K} & -\gamma^2 I & \mathcal{D}^T \\ \mathcal{C} & \mathcal{D} & -I \end{bmatrix} \prec 0 \quad (3.49)$$

Now the formal solution of this problem and the transformation of inequality (3.49) into an LMI can be presented.

3.3.3.2 Formal presentation of the \mathcal{H}_∞ control problem using LMIs

This section presents the formal solution for an \mathcal{H}_∞ controller for LTI systems as presented by Scherer et al. [1997] and developed by Pousot-Vassal [2008].

Solution 1 *LTI/ \mathcal{H}_∞ solution as an LMI*

The dynamic output-feedback controller K , with the structure shown in (3.46), that solves the \mathcal{H}_∞ control problem using LMIs from inequality (3.49) is given by:

minimize γ_∞ subject to the following LMIs in \mathbf{X} , \mathbf{Y} , $\tilde{\mathbf{A}}$, $\tilde{\mathbf{B}}$, $\tilde{\mathbf{C}}$ and $\tilde{\mathbf{D}}$:

$$\begin{bmatrix} M_{11} & *^T & *^T & *^T \\ M_{21} & M_{22} & *^T & *^T \\ M_{31} & M_{32} & M_{33} & *^T \\ M_{41} & M_{42} & M_{43} & M_{44} \end{bmatrix} \prec 0 \quad (3.50)$$

$$\begin{bmatrix} \mathbf{X} & I_n \\ I_n & \mathbf{Y} \end{bmatrix} \succ 0$$

with:

$$\begin{aligned} M_{11} &= \mathbf{A}\mathbf{X} + \mathbf{X}\mathbf{A}^T + B_2\tilde{\mathbf{C}} + \tilde{\mathbf{C}}^T B_2^T \\ M_{21} &= \tilde{\mathbf{A}} + \mathbf{A}^T + C_2^T \tilde{\mathbf{D}}^T B_2^T \\ M_{22} &= \mathbf{Y}\mathbf{A} + \mathbf{A}^T \mathbf{Y} + \tilde{\mathbf{B}}C_2 + C_2^T \tilde{\mathbf{B}}^T \\ M_{31} &= B_1^T + D_{21}^T \tilde{\mathbf{D}}^T B_2^T \\ M_{32} &= B_1^T \mathbf{Y} + D_{21}^T \tilde{\mathbf{B}}^T \\ M_{33} &= -\gamma_\infty I_m \\ M_{41} &= C_1 \mathbf{X} + D_{12} \tilde{\mathbf{C}} \\ M_{42} &= C_1 + D_{12} \tilde{\mathbf{D}} C_2 \\ M_{43} &= D_{11} + D_{12} \tilde{\mathbf{D}} D_{21} \\ M_{44} &= -\gamma_\infty I_p \end{aligned} \quad (3.51)$$

The Controller K can be reconstructed using the following transformation:

$$\begin{aligned} A_k &= N^{-1}(\tilde{\mathbf{A}} - \mathbf{Y}\mathbf{A}\mathbf{X} - \mathbf{Y}B_2 D_k C_2 \mathbf{X} - N B_k C_2 \mathbf{X} - \mathbf{Y}B_2 C_k M^T)M^{-T} \\ B_k &= N^{-1}(\tilde{\mathbf{B}} - \mathbf{Y}B_2 D_k) \\ C_k &= (\tilde{\mathbf{C}} - D_k C_2 \mathbf{X})M^{-T} \\ D_k &= \tilde{\mathbf{D}} \end{aligned} \quad (3.52)$$

where M and N can be found defining $MN^T = I_n - \mathbf{X}\mathbf{Y}$. §

3.3.3.3 Reduced order controllers

A special interest is given in this thesis to reduced order controllers. Indeed, the order of the \mathcal{H}_∞ controller designed in 3.3.3.2 equals the extended system one. This is a problem for high order systems but also for control methodologies where several weighting functions

are used. A classical solution is the (post-synthesis) order reduction of the controller K , a posteriori. However, from an industrial application point of view, effectiveness and simplicity of lower order controllers, remains as the paradigm to respect when choosing a control strategy [Hol et al., 2003, Boivin et al., 2003]. For these reasons two fixed order controller strategies are considered: simple Proportional plus Integral (PI) control and lower order \mathcal{H}_∞ controller synthesis. We will focus now on these two fixed order control methodologies.

(a) Multivariable PID control with \mathcal{H}_∞ performance

In this thesis a multivariable PID controller design with \mathcal{H}_∞ performance is considered. A PID controller is of interest given its simplicity on practical application to real world problems. However, as will be shown later, PID design with \mathcal{H}_∞ performance using LMIs will fall into the a hard class optimization problem. According to the properties of the systems considered in this thesis, only PI control is considered (no derivative action needed).

The proposed control strategy to design a multivariable PI controller used in this thesis, is based on solving some imposed LMI constraints to the system (3.39) and using the iterative LMI (iLMI) algorithm method proposed by He and Wang [2006]. The first step of this algorithm relies on a model transformation so that the PI controller design on the original model becomes an Static Output-Feedback (SOF) design upon a new representation. The SOF control problem, given some \mathcal{H}_∞ performance criteria, is solved using the iLMI algorithm. The problem formulation of a PID controller into the SOF form is proposed by Zheng et al. [2002]. The implementation of this algorithm in MATLAB is presented in appendix A. For system (3.39) the problem formulation in the SOF form consists in finding a controller on the form:

$$u(t) = Ky(t) \quad (3.53)$$

where $K \in \mathbb{R}^{m \times p}$ is such that the closed loop of the system satisfies certain desired performances.

For a multivariable PI controller, u is given by:

$$u(t) = K_1 y(t) + K_2 \int_0^t y(\theta) d\theta \quad (3.54)$$

where:

$$K = [K_1 \quad K_2] \quad (3.55)$$

Below the design of a PID controller satisfying some \mathcal{H}_∞ performance criteria, is presented in the framework of the mixed sensitivity problem, i.e. from the generalized system (3.44).

In order to transform the PID design into an SOF one, let us consider the following state and output vectors:

$$\bar{x} = \begin{bmatrix} x(t) \\ \int_0^t y(\theta) d\theta \end{bmatrix} \quad \text{and} \quad \bar{y} = \begin{bmatrix} \widehat{C}_2 x(t) \\ \int_0^t y(\theta) d\theta \end{bmatrix} \quad (3.56)$$

Then, the system composed by (3.44) and (3.56), setting $D_{21} = 0$ without loss of generality, can be written as:

$$\begin{aligned}\dot{\bar{x}} &= \bar{A}\bar{x}(t) + \bar{B}_1\omega(t) + \bar{B}_2u(t) \\ z(t) &= \bar{C}_1\bar{x}(t) + \bar{D}_{11}\omega(t) + \bar{D}_{12}u(t) \\ \bar{y}(t) &= \bar{C}_2\bar{x}(t)\end{aligned}\quad (3.57)$$

with:

$$\begin{aligned}\bar{A} &= \begin{bmatrix} \hat{A} & 0 \\ \hat{C}_2 & 0 \end{bmatrix} & \bar{B}_1 &= \begin{bmatrix} \hat{B}_1 \\ 0 \end{bmatrix} & \bar{B}_2 &= \begin{bmatrix} \hat{B}_2 \\ 0 \end{bmatrix} \\ \bar{C}_2 &= \begin{bmatrix} \hat{C}_2 & 0 \\ 0 & I \end{bmatrix} & \bar{C}_1 &= \begin{bmatrix} \hat{C}_1 & 0 \end{bmatrix} & \bar{D}_{11} &= \hat{D}_{11} & \bar{D}_{12} &= \hat{D}_{12}\end{aligned}$$

The algorithm proposed by He and Wang [2006] is divided in two parts. In the first part an initial decision matrix P is found through an iterative process. This is presented now as solution 2.

Solution 2 PI/\mathcal{H}_∞ controller using iterative LMI algorithm

The iteration procedure is used to solve the problem in equation (3.57) using the following set of linearizing variables:

$$\mathbf{L} = \mathbf{P}^{-1}, \quad \mathbf{V}_1 = \mathbf{P}\bar{\mathbf{B}}_2\mathbf{K}, \quad \mathbf{V}_2 = \mathbf{K}\bar{\mathbf{C}}_2\mathbf{L}$$

Variables \mathbf{P} , \mathbf{L} , \mathbf{V}_1 and \mathbf{V}_2 are used to compute the initial decision matrix \mathbf{P}_i according to the following simplified algorithm proposed by He and Wang [2006]:

Step 1) Define $i = 1$, $\mathbf{P} = \mathbf{P}_i = I$ and $\mathbf{L} = \mathbf{L}_i = I$.

Step 2) Find \mathbf{P}_i and \mathbf{L}_i , subject to the LMI set (3.58) and minimizing trace $(\mathbf{P}_i\mathbf{L}_{i-1} + \mathbf{L}_i\mathbf{P}_{i-1})$:

$$\begin{aligned}& \begin{bmatrix} \mathbf{P}_i & I \\ I & \mathbf{L}_i \end{bmatrix} \succeq 0 \\ & \begin{bmatrix} \psi_{11} & \mathbf{P}_i\bar{\mathbf{B}}_1 & \bar{\mathbf{C}}_1^T + \bar{\mathbf{C}}_2^T\mathbf{K}^T\bar{\mathbf{D}}_{12}^T \\ * & -\gamma I & \bar{\mathbf{D}}_{11}^T \\ * & * & -\gamma I \end{bmatrix} \prec 0 \\ & \begin{bmatrix} \xi_{11} & \bar{\mathbf{B}}_1 & \mathbf{L}_i\bar{\mathbf{C}}_1^T + \mathbf{V}_2^T\bar{\mathbf{D}}_{12}^T \\ * & -\gamma I & \bar{\mathbf{D}}_{11}^T \\ * & * & -\gamma I \end{bmatrix} \prec 0\end{aligned}\quad (3.58)$$

with:

$$\psi_{11} = \mathbf{P}_i\bar{\mathbf{A}} + \bar{\mathbf{A}}^T\mathbf{P}_i + \mathbf{V}_1\bar{\mathbf{C}}_2 + \bar{\mathbf{C}}_2^T\mathbf{V}_1^T \quad (3.59)$$

$$\xi_{11} = \bar{\mathbf{A}}\mathbf{L}_i + \mathbf{L}_i\bar{\mathbf{A}}^T + \bar{\mathbf{B}}_2\mathbf{V}_2 + \mathbf{V}_2^T\bar{\mathbf{B}}_2^T \quad (3.60)$$

Step 3) If trace $(\mathbf{P}_i \times \mathbf{L}_i) - n < \epsilon_1$, with ϵ_1 a given tolerance, then an initial $\mathbf{P} = \mathbf{P}_i$ is found.

Step 4) An initial $\mathbf{P} = \mathbf{P}_i$ can not be found if between two iterations trace $(\mathbf{P}_i \mathbf{L}_i) - \text{trace}(\mathbf{P}_{i-1} \mathbf{L}_{i-1}) < \epsilon_2$, with ϵ_2 a given tolerance.

Step 5) Define $i = i + 1$ and go to step 2.

The second part of the algorithm computes the multivariable controller \mathbf{K} .

Step 1) Define $k = 1$ and $\mathbf{P} = \mathbf{P}_k = \mathbf{P}_i$, the initial decision matrix.

Step 2) Find \mathbf{K} given \mathbf{P}_k . This is, minimize α_k subject to the following LMI:

$$\begin{bmatrix} \phi_{11} & \mathbf{P}_k \bar{\mathbf{B}}_1 & \bar{\mathbf{C}}_1^T + \bar{\mathbf{C}}_2^T \mathbf{K}^T \bar{\mathbf{D}}_{12}^T \\ * & -\gamma I & \bar{\mathbf{D}}_{11}^T \\ * & * & -\gamma I \end{bmatrix} \prec 0 \quad (3.61)$$

with:

$$\phi_{11} = \mathbf{P}_k \bar{\mathbf{A}} + \bar{\mathbf{A}}^T \mathbf{P}_k + \mathbf{P}_k \bar{\mathbf{B}}_2 \mathbf{K} \bar{\mathbf{C}}_2 + \bar{\mathbf{C}}_2^T \mathbf{K}^T \bar{\mathbf{B}}_2^T \mathbf{P}_k - \alpha \mathbf{P}_k$$

Step 3) If $\alpha_k \leq 0$, \mathbf{K} controller for γ is found, STOP!

Step 4) Define $k = k + 1$. Find \mathbf{P}_k given \mathbf{K} . This is, minimize α_k subject to the LMI (3.61).

Step 5) If $\alpha_k \leq 0$, \mathbf{K} controller for γ is found, STOP!

Step 6) Find \mathbf{P}_k given \mathbf{K} and α_k . This is, minimize trace (\mathbf{P}_k) subject to the LMI (3.61).

Step 7) If $\|\mathbf{P}_k - \mathbf{P}_{k-1}\| / \|\mathbf{P}_k\| < \delta$, then go to **Step 8)**. Otherwise define $k = k + 1$ and $\mathbf{P} = \mathbf{P}_{k-1}$, and go to **Step 2)**. δ is a defined tolerance in the iteration process.

Step 8) The controller can not be found with this algorithm. §

Note: It should be noted that this algorithm has been extensively tested in this thesis with good results. In the work of He and Wang [2006] good results using this algorithm are presented for simple illustrative examples. During this thesis it has been observed that the first part of the algorithm (finding an initial \mathbf{P}_i) has a lower convergence speed and normally a higher number of iterations than the second part (finding the controller \mathbf{K}). A trade-off should be made between the numerical precision of \mathbf{P}_i and the algorithm convergence tolerance ϵ_1 . Concerning sub-optimal value of γ , it can be computed using the numerical implementation developed and described in the work of Poussot-Vassal [2008]. A numerical value of $\gamma \leq 1$ means that all performance specifications are respected, otherwise no formal conclusion is possible. For numerical implementation, and better algorithm convergence, scaling the system input/output gain should be considered. A detailed description on system scaling is presented in Skogestad and Postlethwaite [1996]. More details on the iLMI algorithm performance are presented later in chapter 5.

(b) Fixed Order \mathcal{H}_∞ Performance Controller

Fixed order \mathcal{H}_∞ controllers are also considered in this thesis. As for the PI control, this type of controller is interesting because lower-order controller could be important for real implementation. It should be noticed that, fixing the \mathcal{H}_∞ controller order is difficult since the LMI constraints that describe the control problem formulation usually lead

to a non-smooth optimization problem. To compute this controller, a MATLAB Toolbox called `hifoo`⁵ has been developed by Gumussoy et al. [2009]. Using `hifoo`, will yield to the computation of a controller K that stabilizes plant P and that minimizes the maximum \mathcal{H}_∞ gain of the closed-loop system. One of the drawbacks of this function is the time-consuming computations involved, given the non-smooth/non-convex functions associated.

Another option is to use the function `hinfstruct` from the *Robust Control Toolbox*, however this function is available only from MATLAB's release version R2011a⁶. Using this function, the controller structure and order can be fixed before the synthesis. The function minimizes the \mathcal{H}_∞ norm of the closed-loop. The function inputs allow for simple gain controllers, fixed state-space or transfer functions and even PID controllers. However the controller should be in a decentralized form. Again this falls into the non-smooth/non-convex optimization problem. Good results have been shown in the literature using `hinfstruct` and the reader could refer to the work of Apkarian and Noll [2006] for more information regarding this type of optimization problem.

Let us now present a first example using the control tools described until now.

Example 1 *Application examples: Full order \mathcal{H}_∞ and PI iLMI controllers for a boost converter*

In this example both the full order \mathcal{H}_∞ and the PI iLMI control problems are solved for simple system. The system is given by a single boost converter connected to a resistive load.

The system equations are given by:

$$\begin{cases} L \frac{di_L}{dt} = E - v_C (1 - \alpha_{dc}) \\ C \frac{dv_C}{dt} = (1 - \alpha_{dc}) i_L - i_{load} \end{cases}$$

where the state variables are i_L and v_C , the inductance current and the output capacitor filter voltage respectively. The system inputs are the load current i_{load} , the input source voltage E and the converter PWM duty cycle α_{dc} .

The LTI state-space representation (3.19) of this system after linearization is given as:

$$\begin{aligned} \frac{d}{dt} \begin{bmatrix} i_L \\ v_C \end{bmatrix} &= \begin{bmatrix} 0 & -(1 - \alpha_{dc_e})/L \\ (1 - \alpha_{dc_e})/C & 0 \end{bmatrix} \begin{bmatrix} i_L \\ v_C \end{bmatrix} + \dots \\ &\dots + \begin{bmatrix} 0 & 1/L & v_{C_e}/C \\ -1/C & 0 & i_{L_e} \end{bmatrix} \begin{bmatrix} i_{load} \\ E \\ \alpha_{dc} \end{bmatrix} \end{aligned}$$

If the load is modeled as a constant resistance, then the A state-space matrix becomes:

⁵Available at (retrieved on april 2011): <http://www.cs.nyu.edu/overton/software/hifoo/>

⁶(Retrieved on April 2011):

<http://www.mathworks.com/help/toolbox/robust/ref/hinfstruct.html>

$$A = \begin{bmatrix} 0 & -(1 - \alpha_{dc_e})/L \\ (1 - \alpha_{dc_e})/C & -1/(R_{load}C) \end{bmatrix}$$

Measured outputs of this system are i_L and v_C . The system parameters are: $E = 13.4V$, $v_{C_e} = 24V$, $L = 50\mu H$ and $C = 18.8mF$. The system is linearized around an operating point corresponding to $i_{load} = 20A$. A special property of this system is that if the load is modeled using a constant current source, then the linear model becomes critically stable (complex conjugated poles with no real part). This is classically solved using a multi-loop feedback strategy, as explained later in the dissertation. The extended system is obtained by defining some weighting filters on the sensitivity functions $S(s)$ and $KS(s)$. The weights are designed for a closed-loop rise time of $t_r = 1 - 2s$ approximately and a limitation of the system gain to $M < 2$ at a cross-over frequency of $\omega_B = 1 \text{ rad/s}$. The chosen weighting functions are given by:

$$W_{perf} = \frac{0.5s + 1}{s + 0.001} \text{ and } W_u = \frac{s + 15.71}{0.01s + 15.71}$$

Using these design performance settings, and the control structure shown in Figure 3.4 with $G_d = 1$, the algorithm in Solution 1 for the full order \mathcal{H}_∞ yields a stable solution with a performance index $\gamma_\infty = 0.5$. In the other hand the PI iLMI algorithm in Solution 2 yields a stable result at the cost of a high performance index $\gamma_{PI} = 1000$ where all design specifications may be not respected. Indeed, it is not possible to stabilize the boost converter system while guaranteeing at the same time all performance specifications, this is however different for the full order \mathcal{H}_∞ controller as the performance index obtained is $\gamma_\infty < 1$.

The \mathcal{H}_∞ 4th order controller obtained is in the form:

$$\begin{bmatrix} \dot{x}_k \\ u \end{bmatrix} = \begin{bmatrix} A_k & B_k \\ C_k & D_k \end{bmatrix} \begin{bmatrix} x_k \\ y \end{bmatrix}$$

However a reduced order controller can be easily obtained from the full order controller (4th order) using the functions `balreal` and `modred` in MATLAB, identifying the weakly coupled states in the full order system. Then the reduced order controller state-space matrices are given by:

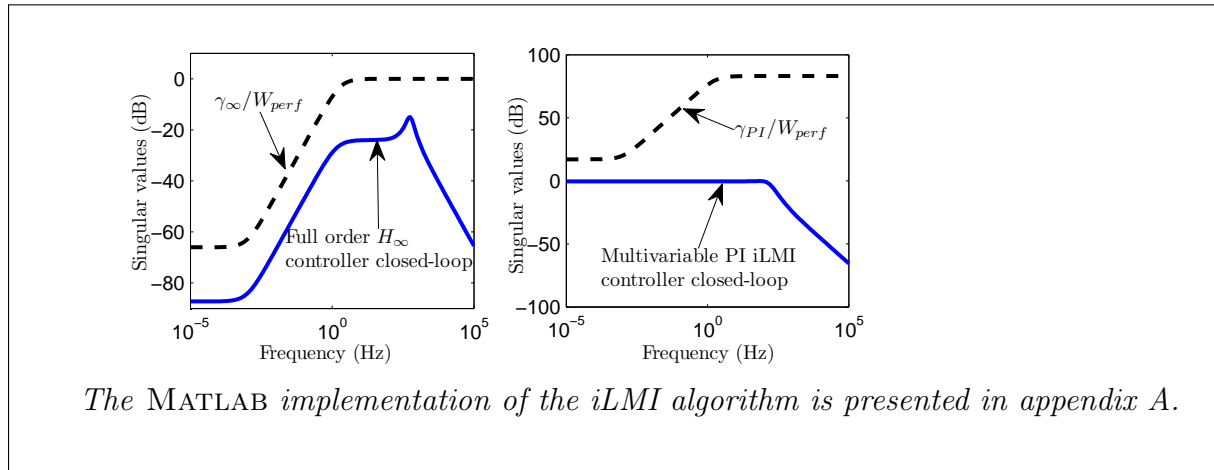
$$A_k = -0.001004, B_k = [3.059 \times 10^{-8} \quad -0.1975], \\ C_k = -0.1975, D_k = [0.0009472 \quad -0.005132]$$

this is obtained considering an open-loop system with $u = [i_{load} \quad \alpha_{dc}]^T$.

The PI controller gains obtained are given by:

$$K_p = [0.0010 \quad 0.0109] \text{ and } K_i = [0.5514 \quad 0.2159]$$

The results obtained are shown in the following Figure where the singular values plots of the closed-loop systems are presented for the full order \mathcal{H}_∞ and the PI iLMI controllers respectively:



The MATLAB implementation of the *iLMI* algorithm is presented in appendix A.

3.3.4 Extensions to LPV systems

Important attention has been given to gain scheduling control theory for several years. The use of Linear Parameter Varying (LPV) systems is a way to tackle the control problem of a non-linear process through a transformation into “linear” systems. The linear control system theory can then be used to obtain non-local controllers and solve the “non-linear” control problem.

Control problem formulations using LMIs can be extended to the LPV case. See [Scherer and Weiland, 2005] or [Bruzelius, 2004] for complete reviews on LPV systems theory. Refer to [Briat, 2008] for a the same problem considering time delayed systems.

The idea of gain scheduling is the parametrization of a linear system with a fixed structure. This approach is presented in Figure 3.7. Note that the measured outputs going to the “Gain scheduled” block can be different from the controlled measured outputs.

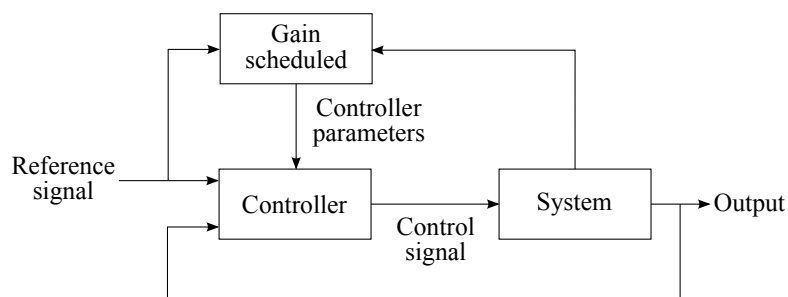


Figure 3.7: The gain scheduling approach [Bruzelius, 2004].

The gain scheduling approach for LPV systems can be commonly divided in three stages:

1. Formulation of the LPV model.
2. Synthesis of the LPV controller.
3. Controller reconstruction.

3.3.4.1 Formulation of the LPV model

(a) Some basic definitions

An LPV system is a system whose state matrices are parameter dependent. In some particular cases, these models can be interpreted as the linearization of the non-linear model of the process along the trajectory of the varying parameter ρ . To understand this, it is important to define in consequence what is an LPV system and the representation structure on these systems. Two types of system representation are used in this thesis: affine or polytopic representations. Refer to [Scherer and Weiland, 2005, Zin, 2005] for an insight on these types of systems. Let us now define an LPV system.

Definition 8 *Dynamic LPV system*

Given linear matrix functions $A \in \mathbb{R}^{n \times n}$, $B \in \mathbb{R}^{n \times r}$, $C \in \mathbb{R}^{q \times n}$ and $D \in \mathbb{R}^{q \times r}$, a linear

parameter varying (LPV) system is described by:

$$\Sigma_{LPV} : \begin{cases} \dot{x} = A(\rho(\cdot))x(t) + B(\rho(\cdot))\omega(t) \\ z = C(\rho(\cdot))x(t) + D(\rho(\cdot))\omega(t) \end{cases} \quad (3.62)$$

where $x(t)$ is the state vector taking values in the state-space $X \in \mathbb{R}^n$, $\omega(t)$ is the input to the system with values in the input space $W \in \mathbb{R}^r$ and $z(t)$ is the output vector with values in the output space $Z \in \mathbb{R}^q$.

Then with $\rho(\cdot)$ a varying parameter vector, the following system definitions can be enunciated [Poussot-Vassal, 2008]:

- $\rho(\cdot) = \rho$ a constant, then system (3.62) is an LTI (Linear Time-invariant) system,
- $\rho(\cdot) = \rho(t)$, then system (3.62) is an LTV (Linear Time-variant) system with known parameter variation,
- $\rho(\cdot) = \rho(x(t))$, then system (3.62) is a quasi-LPV system,
- $\rho(\cdot) = \rho(t)$, an external parameter, then system (3.62) is an LPV system.

Two common LPV system representations are possible: affine or polytopic representation. Let us now define these types of systems.

(b) Affine and polytopic representations

Definition 9 Affine systems

Given a dynamic LPV system as (3.62), the system is said to be affine if matrices $A(\cdot)$, $B(\cdot)$, $C(\cdot)$ and $D(\cdot)$ are fixed affine functions of some real varying parameter vector $\rho = (\rho_1, \dots, \rho_l)$, i.e.:

$$\underbrace{\begin{bmatrix} A(\rho) & B(\rho) \\ C(\rho) & D(\rho) \end{bmatrix}}_{S(\rho)} = \underbrace{\begin{bmatrix} A_0 & B_0 \\ C_0 & D_0 \end{bmatrix}}_{S_0} + \rho_1 \underbrace{\begin{bmatrix} A_1 & B_1 \\ C_1 & D_1 \end{bmatrix}}_{S_1} + \dots + \rho_l \underbrace{\begin{bmatrix} A_l & B_l \\ C_l & D_l \end{bmatrix}}_{S_l}$$

$$S(\rho) = S_0 + \rho_1 S_1 + \dots + \rho_l S_l \quad (3.63)$$

where matrices S_0, S_1, \dots, S_l are the affine matrix representations of the LPV system.

Using the MATLAB *Robust Control Toolbox*⁷ this type of system can be defined using the function `psys` with the following syntax (for a system with $l = 2$):

$$\text{affs} = \text{psys}(\text{pv}, [\text{s0}, \text{s1}, \text{s2}])$$

where parameter vector `pv` is defined using the function `pvec` with the following valid syntax:

$$\text{pv} = \text{pvec}(\text{'box'}, \text{range}, \text{rates})$$

⁷See Table 3.2 at the end of this chapter for a review on some useful functions from the MATLAB *Robust Control Toolbox*.

Definition 10 Polytopic systems

An LPV system is said to be polytopic if it can be written as:

$$\begin{aligned} \left[\begin{array}{c|c} A(\rho) & B(\rho) \\ \hline C(\rho) & D(\rho) \end{array} \right] &= \sum_{i=1}^N \alpha_i(\rho) \left[\begin{array}{c|c} A(\omega_i) & B(\omega_i) \\ \hline C(\omega_i) & D(\omega_i) \end{array} \right] \\ &\in \text{Co} \left\{ \left[\begin{array}{c|c} A_1 & B_1 \\ \hline C_1 & D_1 \end{array} \right], \dots, \left[\begin{array}{c|c} A_N & B_N \\ \hline C_N & D_N \end{array} \right] \right\} \end{aligned} \quad (3.64)$$

where ω_i are the extremities of the polytope formed by the extreme values of parameter vector ρ , Co denotes the “convex hull”, and $\alpha_i(\rho)$ is defined as:

$$\alpha_i(\rho) := \frac{\prod_{k=1}^l |\rho_k - \mathcal{C}(\omega_i)_k|}{\prod_{k=1}^l (\bar{\rho}_k - \underline{\rho}_k)}, i = 1, \dots, N \quad (3.65)$$

$$\alpha_i(\rho) \geq 0 \text{ and } \sum_{i=1}^N \alpha_i(\rho) = 1 \quad (3.66)$$

with $\mathcal{C}(\omega_i)_k$ the k^{th} component of vector $\mathcal{C}(\omega_i)$ defined as:

$$\mathcal{C}(\omega_i)_k = \left\{ \rho_k \mid \rho_k = \bar{\rho}_k \text{ if } (\omega_i)_k = \underline{\rho}_k \text{ or } \rho_k = \underline{\rho}_k \text{ otherwise} \right\} \quad (3.67)$$

with $N = 2^l$ the number of vertices of the polytope. Matrices A_i , B_i , C_i and D_i , are known matrices obtained at each vertex ω_i of the polytope.

Using MATLAB, an LPV system in the polytopic form will be defined as ($l = 2$):

```
pols = psys([s1,s2,s3,s4])
```

Likewise, the vertices of the varying parameter vector can be defined as:

```
pv = pvec('pol',vertices)
```

As an example we will consider now a polytopic system representation for a process with two varying parameters, this is an illustration also presented in [Poussot-Vassal, 2008].

Example 2 Polytopic system with two varying parameters

Considering a system with two varying parameters ($l = 2$, $N = 4$), the system vertices ω_i and vector $\mathcal{C}(\omega)$ will be given by:

$$\omega = \begin{bmatrix} \omega_1 \\ \omega_2 \\ \omega_3 \\ \omega_4 \end{bmatrix} = \begin{bmatrix} \underline{\rho}_1 & \underline{\rho}_2 \\ \underline{\rho}_1 & \bar{\rho}_2 \\ \bar{\rho}_1 & \underline{\rho}_2 \\ \bar{\rho}_1 & \bar{\rho}_2 \end{bmatrix} \text{ and } \mathcal{C}(\omega) = \begin{bmatrix} \bar{\rho}_1 & \bar{\rho}_2 \\ \bar{\rho}_1 & \underline{\rho}_2 \\ \underline{\rho}_1 & \bar{\rho}_2 \\ \underline{\rho}_1 & \underline{\rho}_2 \end{bmatrix} \quad (3.68)$$

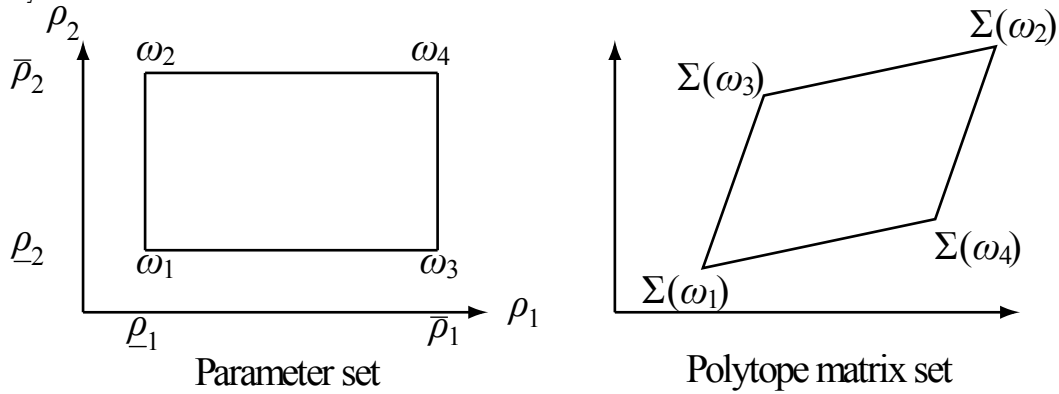
The polytopic system will be defined as:

$$\begin{aligned} \left[\begin{array}{c|c} A(\rho) & B(\rho) \\ \hline C(\rho) & D(\rho) \end{array} \right] &= \alpha_1(\rho) \left[\begin{array}{c|c} A(\omega_1) & B(\omega_1) \\ \hline C(\omega_1) & D(\omega_1) \end{array} \right] + \alpha_2(\rho) \left[\begin{array}{c|c} A(\omega_2) & B(\omega_2) \\ \hline C(\omega_2) & D(\omega_2) \end{array} \right] + \dots \\ \dots + \alpha_3(\rho) \left[\begin{array}{c|c} A(\omega_3) & B(\omega_3) \\ \hline C(\omega_3) & D(\omega_3) \end{array} \right] &+ \alpha_4(\rho) \left[\begin{array}{c|c} A(\omega_4) & B(\omega_4) \\ \hline C(\omega_4) & D(\omega_4) \end{array} \right] \end{aligned} \quad (3.69)$$

with $\alpha_i(\rho)$ defined as the following using equation (3.65):

$$\begin{aligned} \alpha_1(\rho) &= \frac{|\rho_1 - \bar{\rho}_1| |\rho_2 - \bar{\rho}_2|}{(\bar{\rho}_1 - \underline{\rho}_1)(\bar{\rho}_2 - \underline{\rho}_2)}, & \alpha_2(\rho) &= \frac{|\rho_1 - \underline{\rho}_1| |\rho_2 - \bar{\rho}_2|}{(\bar{\rho}_1 - \underline{\rho}_1)(\bar{\rho}_2 - \underline{\rho}_2)} \\ \alpha_3(\rho) &= \frac{|\rho_1 - \bar{\rho}_1| |\rho_2 - \underline{\rho}_2|}{(\bar{\rho}_1 - \underline{\rho}_1)(\bar{\rho}_2 - \underline{\rho}_2)}, & \alpha_4(\rho) &= \frac{|\rho_1 - \underline{\rho}_1| |\rho_2 - \underline{\rho}_2|}{(\bar{\rho}_1 - \underline{\rho}_1)(\bar{\rho}_2 - \underline{\rho}_2)} \end{aligned} \quad (3.70)$$

Graphically, these polytopic coordinates can be represented as [Poussot-Vassal, 2008]:



Using MATLAB with the polytopic system and the parameter vectors defined before, the system vertex ω_i and the convex decompositions $\alpha_i(\rho)$ can be obtained with the following syntax:

```
[alpha,vertx] = polydec(pv,pols)
```

3.3.4.2 Full-order \mathcal{H}_∞ LPV control

The \mathcal{H}_∞ control for LPV systems is an extension of the LTI case. The goal again is to transform inequality (3.49) into an LMI but now for an LPV system. We will retain hereafter the polytopic notation.

As in the LTI case, the controller $K(\rho)$ can be defined as:

$$\begin{bmatrix} \dot{x}_k \\ u \end{bmatrix} = \begin{bmatrix} A_k(\rho) & B_k(\rho) \\ C_k(\rho) & D_k(\rho) \end{bmatrix} \begin{bmatrix} x_k \\ y \end{bmatrix} \quad (3.71)$$

with parameter ρ_i defined as:

$$\rho_i \in [\underline{\rho}_i \quad \bar{\rho}_i], \forall i = 1, \dots, l \quad (3.72)$$

Finally the closed-loop system is given by:

$$\begin{bmatrix} \dot{\xi} \\ z \end{bmatrix} = \begin{bmatrix} \mathcal{A}(\rho) & \mathcal{B}(\rho) \\ \mathcal{C}(\rho) & \mathcal{D}(\rho) \end{bmatrix} \begin{bmatrix} \xi \\ \omega \end{bmatrix} \quad (3.73)$$

where ξ are the closed-loop dynamic variables and state matrices are again:

$$\begin{aligned} \mathcal{A}(\rho) &= \begin{bmatrix} A(\rho) + B_2(\rho)D_k(\rho)C_2(\rho) & B_2(\rho)C_k(\rho) \\ B_k(\rho)C_2(\rho) & A_k(\rho) + B_k(\rho)D_{22}(\rho)C_k(\rho) \end{bmatrix} \\ \mathcal{B}(\rho) &= \begin{bmatrix} B_1(\rho) + B_2(\rho)D_k(\rho)D_{21}(\rho) \\ B_k(\rho)D_{21}(\rho) \end{bmatrix} \\ \mathcal{C}(\rho) &= [C_1(\rho) + D_{12}(\rho)D_k(\rho)C_2(\rho) \quad D_{12}(\rho)C_k(\rho)] \\ \mathcal{D}(\rho) &= D_{11}(\rho) + D_{12}(\rho)D_k(\rho)D_{21}(\rho) \end{aligned} \quad (3.74)$$

With these definitions the formal \mathcal{H}_∞ control problem for an LPV system can now be presented.

3.3.4.3 Formal presentation of the \mathcal{H}_∞ control problem for LPV systems

Solution 3 LPV/ \mathcal{H}_∞ solution as an LMI

The dynamic output-feedback controller $K(\rho)$, with the structure shown in (3.71), that solves the \mathcal{H}_∞ control problem using LMIs for an LPV system is given by:

minimize γ_∞ subject to the following LMIs in \mathbf{X} , \mathbf{Y} , $\tilde{\mathbf{A}}$, $\tilde{\mathbf{B}}$, $\tilde{\mathbf{C}}$ and $\tilde{\mathbf{D}}$:

$$\begin{bmatrix} M_{11} & *^T & *^T & *^T \\ M_{21} & M_{22} & *^T & *^T \\ M_{31} & M_{32} & M_{33} & *^T \\ M_{41} & M_{42} & M_{43} & M_{44} \end{bmatrix} \prec 0 \quad (3.75)$$

$$\begin{bmatrix} \mathbf{X}(\rho) & I_n \\ I_n & \mathbf{Y}(\rho) \end{bmatrix} \succ 0$$

with:

$$\begin{aligned} M_{11} &= A(\rho)\mathbf{X}(\rho) + \mathbf{X}(\rho)A(\rho)^T + \frac{\partial \mathbf{X}(\rho)}{\partial \rho} \dot{\rho} + B_2 \tilde{\mathbf{C}}(\rho) + \tilde{\mathbf{C}}(\rho)^T B_2^T \\ M_{21} &= \tilde{\mathbf{A}}(\rho) + A(\rho)^T + C_2^T \tilde{\mathbf{D}}(\rho)^T B_2^T \\ M_{22} &= \mathbf{Y}(\rho)A(\rho) + A(\rho)^T \mathbf{Y}(\rho) + \frac{\partial \mathbf{Y}(\rho)}{\partial \rho} \dot{\rho} + \tilde{\mathbf{B}}(\rho)C_2 + C_2^T \tilde{\mathbf{B}}(\rho)^T \\ M_{31} &= B_1(\rho)^T + D_{21}^T \tilde{\mathbf{D}}(\rho)^T B_2 \\ M_{32} &= B_1(\rho)^T \mathbf{Y}(\rho) + D_{21}^T \tilde{\mathbf{B}}(\rho)^T \\ M_{33} &= -\gamma_\infty I_m \\ M_{41} &= C_1(\rho)\mathbf{X}(\rho) + D_{12} \tilde{\mathbf{C}}(\rho) \\ M_{42} &= C_1(\rho) + D_{12} \tilde{\mathbf{D}}(\rho)C_2 \\ M_{43} &= D_{11}(\rho) + D_{12} \tilde{\mathbf{D}}(\rho)D_{21} \\ M_{44} &= -\gamma_\infty I_p \end{aligned} \quad (3.76)$$

Controller $K(\rho)$ can be reconstructed using the following transformation:

$$\begin{aligned}
A_k(\rho) &= N(\rho)^{-1}(\tilde{\mathbf{A}}(\rho) - \mathbf{Y}(\rho)A(\rho)\mathbf{X}(\rho) - \mathbf{Y}(\rho)B_2D_k(\rho)C_2\mathbf{X}(\rho) \\
&\quad - N(\rho)B_k(\rho)C_2\mathbf{X}(\rho) - \mathbf{Y}(\rho)B_2C_k(\rho)M(\rho)^T)M(\rho)^{-T} \\
B_k(\rho) &= N(\rho)^{-1}(\tilde{\mathbf{B}}(\rho) - \mathbf{Y}(\rho)B_2D_k(\rho)) \\
C_k(\rho) &= (\tilde{\mathbf{B}}(\rho) - D_k(\rho)C_2\mathbf{X}(\rho))M(\rho)^{-T} \\
D_k(\rho) &= \tilde{\mathbf{D}}(\rho)
\end{aligned} \tag{3.77}$$

where $M(\rho)$ and $N(\rho)$ can be found with a feasible solution to the equation $M(\rho)N(\rho)^T = I_n - \mathbf{X}(\rho)\mathbf{Y}(\rho)$. §

Actually, from this definition, two important requirements are inferred:

- The open-loop system should be strictly proper, i.e. $D_{22}(\rho) = 0$.
- The LPV open-loop system should be parameter-independent on input and output matrices, i.e.:

$$M(\rho) = \begin{bmatrix} \dot{x} \\ z \\ y \end{bmatrix} = \left[\begin{array}{c|cc} A(\rho) & B_1(\rho) & B_2 \\ \hline C_1(\rho) & D_{11}(\rho) & D_{12} \\ C_2 & D_{21} & 0 \end{array} \right] \begin{bmatrix} x \\ \omega \\ u \end{bmatrix} \tag{3.78}$$

In the special conditions where this second requirement is not meet, then a classical solution consists in using proper transfer functions to filter the open-loop system input/output. See [Poussot-Vassal, 2008] for more details, in particular on how to choose the filter parameters.

The final step in this methodology is the polytopic reconstruction of the \mathcal{H}_∞ controller. This will be given as:

$$K(\rho) = \sum_{i=1}^N \alpha_i(\rho) \left[\begin{array}{c|c} A_{k_i} & B_{k_i} \\ \hline C_{k_i} & D_{k_i} \end{array} \right] \tag{3.79}$$

with:

$$\alpha_i(\rho) := \frac{\prod_{k=1}^l |\rho_k - \mathcal{C}(\omega_i)_k|}{\prod_{k=1}^l (\bar{\rho}_k - \underline{\rho}_k)}, i = 1, \dots, N \tag{3.80}$$

$$\alpha_i(\rho) \geq 0 \text{ and } \sum_{i=1}^N \alpha_i(\rho) = 1 \tag{3.81}$$

This is represented graphically in Figure 3.8 [Poussot-Vassal, 2008].

3.3.4.4 Reduced order controllers

Applying the same reasoning used with the LTI control problems, interest is now given to reduced order controllers. Reduced order controllers for LPV systems are directly presented in this thesis in the form of simple multivariable PI(D) controllers.

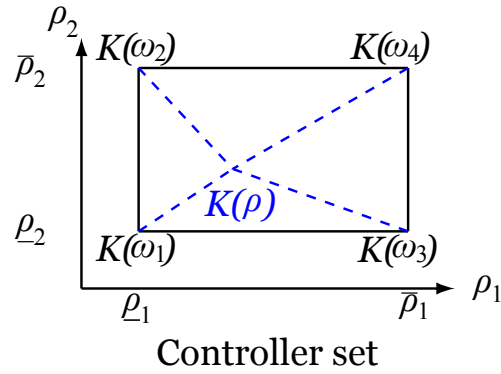


Figure 3.8: Controller polytopic reconstruction.

Multivariable PI control with \mathcal{H}_∞ performance for LPV systems The simplified multivariable PI control strategy presented here was proposed by Mattei [2001]. Let us focus on the second problem proposed in [Mattei, 2001], the “generalized” case, where the restriction of an LPV system strictly proper in y is removed, i.e. $D_{21}(\rho)$ and $D_{22}(\rho)$ are **not** null matrices $\forall \rho \in \Pi \subset \mathbb{R}^{n_p}$, with Π the compact hyper-rectangle of varying parameters.

The LPV system is now defined as:

$$\begin{bmatrix} \dot{x} \\ z \\ y \end{bmatrix} = \begin{bmatrix} A(\rho) & B_1(\rho) & B_2(\rho) \\ C_1(\rho) & D_{11}(\rho) & D_{12}(\rho) \\ C_2(\rho) & D_{21}(\rho) & D_{22}(\rho) \end{bmatrix} \begin{bmatrix} x \\ \omega \\ u \end{bmatrix} \quad (3.82)$$

For this system the goal now is to define a robust multivariable PI controller. The controller state-space structure is then given as:

$$\begin{cases} \dot{x}_I = G_I y \\ u = K_I(\rho)x_I + K_p(\rho)y \end{cases} \quad (3.83)$$

where $x_I \in \mathbb{R}^{n_c}$ is the integrator state of the PI controller and G_I is a constant matrix indicating which measured output y will account for integral action⁸.

From Mattei [2001], for the LPV system (3.82), there exists a multivariable PI controller in the form of (3.83) that guarantees quadratic stability for a given rate of convergence β and that minimizes the \mathcal{H}_∞ norm of the closed-loop to a lower bound γ_b , if there exists a positive definite symmetric matrix \mathbf{P} and a given gain matrix $\mathbf{K}_y = [K_1 \ K_2]$ with $K_1 \in \mathbb{R}^{m \times p}$ and $K_2 \in \mathbb{R}^{m \times n_c}$, such that:

$$\begin{bmatrix} \varphi_{11} & *^T & *^T \\ (\tilde{B}_1(\rho) + \tilde{B}_2(\rho)\mathbf{K}_y\tilde{D}_{21}(\rho))^T \mathbf{P} & -I & *^T \\ \gamma_b^{-1}(\tilde{C}_1(\rho) + D_{12}(\rho)\mathbf{K}_y\tilde{C}_2(\rho)) & \gamma_b^{-1}D_{11}(\rho) & -I \end{bmatrix} \prec 0 \quad (3.84)$$

with:

$$\varphi_{11} = (\hat{A}(\rho) + \tilde{B}_2(\rho)\mathbf{K}_y\tilde{C}_2(\rho))^T \mathbf{P} + \mathbf{P}(\hat{A}(\rho) + \tilde{B}_2(\rho)\mathbf{K}_y\tilde{C}_2(\rho)) \quad (3.85)$$

where $\hat{A}(\rho) = \tilde{A}(\rho) + \beta I$ and:

⁸See the application example 3 for an illustration in the use of this matrix G_I .

$$\begin{aligned}\tilde{A}(\rho) &= \begin{bmatrix} A(\rho) & 0 \\ G_I C_2(\rho) & 0 \end{bmatrix} & \tilde{B}_1(\rho) &= \begin{bmatrix} B_1(\rho) \\ G_I D_{21}(\rho) \end{bmatrix} & \tilde{B}_2(\rho) &= \begin{bmatrix} B_2(\rho) \\ G_I D_{22}(\rho) \end{bmatrix} \\ \tilde{C}_1(\rho) &= [C_1(\rho) \quad 0] & \tilde{C}_2(\rho) &= \begin{bmatrix} C_2(\rho) & 0 \\ 0 & I \end{bmatrix} & \tilde{D}_{21}(\rho) &= \begin{bmatrix} D_{21}(\rho) \\ 0 \end{bmatrix}\end{aligned}$$

The controller gains that are (possibly) gain-scheduled, assuming that matrix $(I + D_{22}(\rho)K_1)$ is invertible, are obtained with:

$$\begin{bmatrix} K_p(\rho) \\ K_I(\rho) \end{bmatrix} = \begin{bmatrix} K_1(I + D_{22}(\rho)K_1)^{-1} \\ (I - K_1(I + D_{22}(\rho)K_1)^{-1}D_{22}(\rho))K_2 \end{bmatrix} \quad (3.86)$$

It is clear however that the inequality (3.84) is not an LMI. Two solutions are proposed in [Mattei, 2001] to achieve transformation into solvable LMIs. These solutions are now enunciated for two special cases: a system with D_{12} null and with matrix B_2 parameter-independent (*Problem #1*) or a system with D_{12} and D_{21} null matrices and C_2 parameter-independent (*Problem #2*).

Solution 4 Gain-scheduled PI controller (*Problem #1*)

Consider the LPV system (3.82) with matrix D_{12} null and with matrix B_2 parameter-independent. For this system there exists a multivariable PI controller in the form of (3.83) that guarantees quadratic stability for a given rate of convergence β and that minimizes the \mathcal{H}_∞ norm of the closed-loop to a lower bound γ_b , if there exists two positive definite symmetric matrices $P_1 \in \mathbb{R}^m$ and $P_2 \in \mathbb{R}^{n-m}$ and a given gain matrix $\mathbf{W}_y \in \mathbb{R}^{m \times p}$, such that:

$$\begin{bmatrix} \bar{A}(\rho)^T \mathbf{P} + \mathbf{P} \bar{A}(\rho) + \widehat{\mathbf{W}}_y \widehat{C}_2(\rho) + \widehat{C}_2(\rho)^T \widehat{\mathbf{W}}_y^T & *^T & *^T \\ \widehat{B}_1(\rho)^T \mathbf{P} + \widehat{D}_{21}(\rho)^T \widehat{\mathbf{W}}_y^T & -I & *^T \\ \gamma_b^{-1} \widehat{C}_1(\rho) & \gamma_b^{-1} D_{11}(\rho) & -I \end{bmatrix} \prec 0 \quad (3.87)$$

with:

$$\begin{aligned}\widehat{\mathbf{W}}_y &= \begin{bmatrix} \mathbf{W}_y \\ 0 \end{bmatrix} & \bar{A}(\rho) &= T^{-1}(\widehat{A}(\rho))T & \widehat{B}_1(\rho) &= T^{-1}(\tilde{B}_1(\rho)) \\ \widehat{C}_1(\rho) &= (\tilde{C}_1(\rho))T & \widehat{C}_2(\rho) &= (\tilde{C}_2(\rho))T & \mathbf{P} &= \begin{bmatrix} P_1 & 0 \\ 0 & P_2 \end{bmatrix}\end{aligned}$$

where T is a non-singular transformation such that $T^{-1}\tilde{B}_2 = [I \quad 0]^T$. A possible value for the controller output-feedback gain matrix $K_y \in \mathbb{R}^{m \times p}$ is:

$$K_y = [K_1 \quad K_2] = P_1^{-1}W_y \quad \S \quad (3.88)$$

Now *Problem #2* is presented.

Solution 5 Gain-scheduled PI controller (Problem #2)

Consider the LPV system (3.82) with matrices D_{12} and D_{21} null and with matrix C_2 parameter-independent. For this system there exists a multivariable PI controller in the form of (3.83) that guarantees quadratic stability for a given rate of convergence β and that minimizes the \mathcal{H}_∞ norm of the closed-loop to a lower bound γ_b , if there exists two positive definite symmetric matrix $Q_1 \in \mathbb{R}^p$ and $Q_2 \in \mathbb{R}^{n-p}$ and a given gain matrix $W_y \in \mathbb{R}^{m \times p}$, such that:

$$\begin{bmatrix} \overline{A}(\rho)^T \mathbf{Q} + \mathbf{Q} \overline{A}(\rho) + \widehat{W}_y \widehat{B}_2(\rho)^T + \widehat{B}_2(\rho) \widehat{W}_y^T & *^T & *^T \\ \widehat{B}_1(\rho)^T & -I & *^T \\ \gamma_b^{-1} \widehat{C}_1(\rho) \mathbf{Q} & \gamma_b^{-1} D_{11}(\rho) & -I \end{bmatrix} \prec 0 \quad (3.89)$$

with:

$$\begin{aligned} \widehat{W}_y &= \begin{bmatrix} W_y^T \\ 0 \end{bmatrix} & \overline{A}(\rho) &= T^{-1}(\widehat{A}(\rho))T & \widehat{B}_1(\rho) &= T^{-1}(\widetilde{B}_1(\rho)) \\ \widehat{B}_2(\rho) &= T^{-1}(\widetilde{B}_2(\rho)) & \widehat{C}_1(\rho) &= (\widetilde{C}_1(\rho))T & \mathbf{Q} &= \begin{bmatrix} Q_1 & 0 \\ 0 & Q_2 \end{bmatrix} \end{aligned}$$

where T is a non-singular transformation such that $\widetilde{C}_2 T = [I \ 0]$. A possible value for the controller output-feedback gain matrix $K_y \in \mathbb{R}^{m \times p}$ is:

$$K_y = [K_1 \ K_2] = W_y Q_1^{-1} \quad \S \quad (3.90)$$

The implementation of these problems in MATLAB, as functions to obtain an LPV PI controller, is presented in appendix A. Coming back to Example 1, let us now present a new numerical example for the LPV control strategies previously presented.

Example 3 *Application examples: Full order \mathcal{H}_∞ and multivariable PI controllers for an LPV system, the boost converter case*

In this example, a continuation of Example 1, the full order \mathcal{H}_∞ and the multivariable PI control problems are solved for a simple LPV system. The system is the same as in Example 1, a single boost converter, but now considering a resistance modeled load with uncertain but bounded values.

The uncertain state-space matrix is given by:

$$A(\rho) = \begin{bmatrix} 0 & -(1 - \alpha_{dc_e})/L \\ (1 - \alpha_{dc_e})/C & -\rho \end{bmatrix}$$

with:

$$\rho = \frac{1}{R_{load}C}$$

Variations of $\pm 10\%$ in the load current are considered to obtain the bound values of ρ .

The previous design specifications are kept except for a lower limitation in the high frequency gain to $M < 0.25$ and a higher steady-state error for better numerical convergence, $A_\epsilon = 0.1$. With these specifications, the performance weighting function becomes:

$$W_{perf} = \frac{4s + 1}{s + 0.1}$$

Weight W_u on the sensitivity function $KS(s)$ is kept unchanged. Since we want to introduce integral action to both measured outputs, matrix G_I is defined as:

$$G_I = \begin{bmatrix} 1 & 0 \\ 0 & 1 \end{bmatrix}$$

With these specifications, algorithm in Solution 3 is used to solve the full order \mathcal{H}_∞ control problem. The algorithm yields a possible solution with a performance index $\gamma_\infty = 10.82$. The gain-scheduled controller obtained is in the form:

$$\begin{bmatrix} \dot{x}_k \\ u \end{bmatrix} = \begin{bmatrix} A_k(\rho) & B_k(\rho) \\ C_k(\rho) & D_k(\rho) \end{bmatrix} \begin{bmatrix} x_k \\ y \end{bmatrix}$$

with:

$$K(\rho) = \alpha_1(\rho) \left[\begin{array}{c|c} A_k(\omega_1) & B_k(\omega_1) \\ \hline C_k(\omega_1) & D_k(\omega_1) \end{array} \right] + \alpha_2(\rho) \left[\begin{array}{c|c} A_k(\omega_2) & B_k(\omega_2) \\ \hline C_k(\omega_2) & D_k(\omega_2) \end{array} \right]$$

where:

$$\begin{aligned} \omega_1 &= \underline{\rho} \\ \omega_2 &= \bar{\rho} \end{aligned}$$

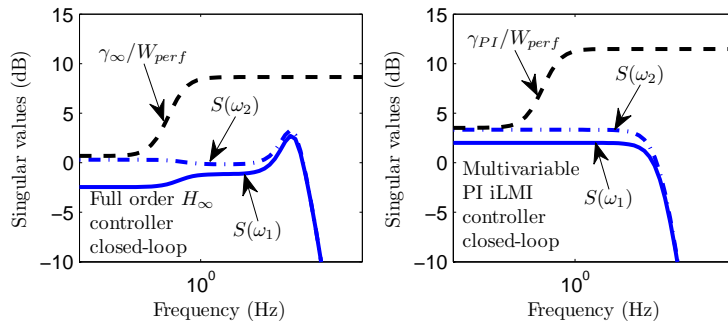
Polytopic coordinates $\alpha_1(\rho)$ and $\alpha_2(\rho)$ can be easily computed using the function `polydec`.

Finally the algorithm presented in Solution 5 is used to solve the LPV PI control problem. A controller is found with a performance index $\gamma_{PI} = 14.99$. The multi-variable PI controller is however not gain-scheduled in this case, since matrix D_{22} is parameter independent, see equation (3.86). This is a **robust** design of a multivariable PI controller.

The PI controller gains obtained are given by:

$$K_p = [0.6459 \quad 5.7802] \quad \text{and} \quad K_i = [-302.6470 \quad 303.4072]$$

Comparison of both controllers are presented in the following figure with the closed-loop singular values plots:



3.3.5 Analysis tools

In this dissertation, domain analysis of closed-loop systems is based on both time and frequency responses. However, robustness is a key feature on the proposed control methodologies. A complete review on robustness analysis, for both SISO and MIMO systems, can be found in the work of Skogestad and Postlethwaite [1996].

A control system is said to be *robust* if it is insensitive to a model subject to uncertainties. These uncertainties on the model/plant could be representative of the “unknown” or “unmodeled” dynamics of the system. The goal of the robust analysis is to determine if the controller satisfies both stability conditions and desired performances for a system subject to modeling uncertainties.

The approach proposed in Skogestad and Postlethwaite [1996] consists in:

1. Find a proper mathematical model of system uncertainties.
2. Check the robust stability conditions of the closed-loop.
3. Check the robust performance conditions of the closed-loop.

3.3.5.1 Modeling uncertainties

In this thesis, in chapter 5, uncertainties are modeled with the unstructured input-multiplicative form and are represented by the uncertainties weights. This configuration is presented in Figure 3.9. See [Skogestad and Postlethwaite, 1996] for other types of model uncertainty representation. In this representation the model uncertainties are lumped in a single weighting function w_I . The weighting functions for uncertainties modeling can be computed using the `ucover` function in the MATLAB *Control System Toolbox*.

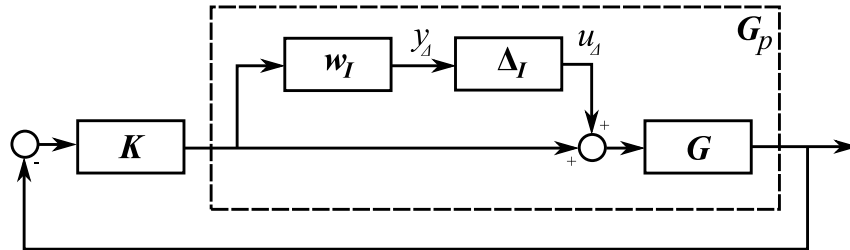


Figure 3.9: Modeling uncertainties.

The perturbed system becomes:

$$\Pi : G_p(s) = G(s)(1 + w_I(s)\Delta_I(s)) \quad (3.91)$$

with Δ_I s.t. $\|\Delta_I\|_\infty < 1$.

To obtain this weighting function the nominal model $G(s)$ is chosen. Then, for each frequency ω , the smallest radius $l_I(\omega)$ that includes all the possible families of models is obtained, i.e.:

$$l_I(\omega) = \max_{G_p \in \Pi} \left| \frac{G_p(j\omega) - G(j\omega)}{G(j\omega)} \right| \quad (3.92)$$

with an uncertain weighting function given by:

$$|w_I(j\omega)| \geq l_I(j\omega), \forall \omega \quad (3.93)$$

Uncertainty representation in Figure 3.9 is also called an *unstructured* uncertainty if the perturbation matrix Δ_I is a “full” complex matrix.

On the other hand, a somehow fairly general form used to represent an uncertain model is the Linear Fractional Transformation (LFT). An uncertain plant represented using LFT is shown in Figure 3.10. In this system the perturbed plant is given by:

$$G_p = F_u \left(\begin{bmatrix} F_{11} & F_{12} \\ F_{21} & F_{22} \end{bmatrix}, \Delta_I \right) = F_{22} + F_{21} \Delta_I (I - F_{11} \Delta_I)^{-1} F_{12} \quad (3.94)$$

where the nominal plant is given by $G = F_{22}$.

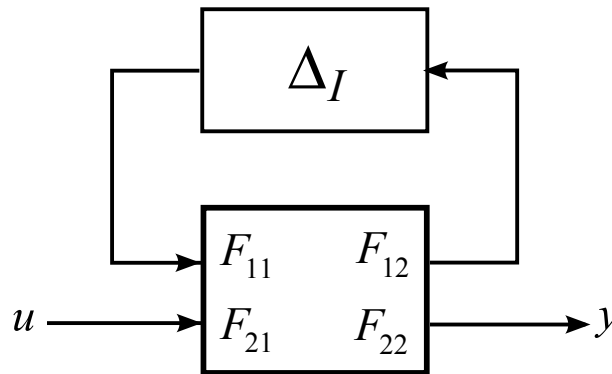


Figure 3.10: LFT representation of uncertain plant $y = G_p u$.

3.3.5.2 μ -Analysis

The robustness analysis in the presence of model uncertainties is carried out using μ -analysis. These techniques are detailed in [Skogestad and Postlethwaite, 1996] and [Zhou et al., 1996], and are applied to practical problems in [Gadoura et al., 2002] and [Sename and Dugard, 2003] for example. Let us now define the structured singular value μ .

(a) Structured singular value μ

The structured singular value is normally noted as μ . The obtention of this value represents an analysis tool used to estimate the stability margins of a multivariable system subject to uncertainties. However, now the perturbation matrix is written using the structured form, i.e., $\Delta = \text{diag} \{ \Delta_i \}$, a block-diagonal matrix. Each block Δ_i can be either a scalar or a matrix, taking real or complex values (according to the uncertainty type).

The general control configurations for the perturbed system, for the robust performance and for the robust stability analysis are presented in Figure 3.11.

In the general case, the structured singular value $\mu(M)$, defined for the $M-\Delta$ structure is defined by

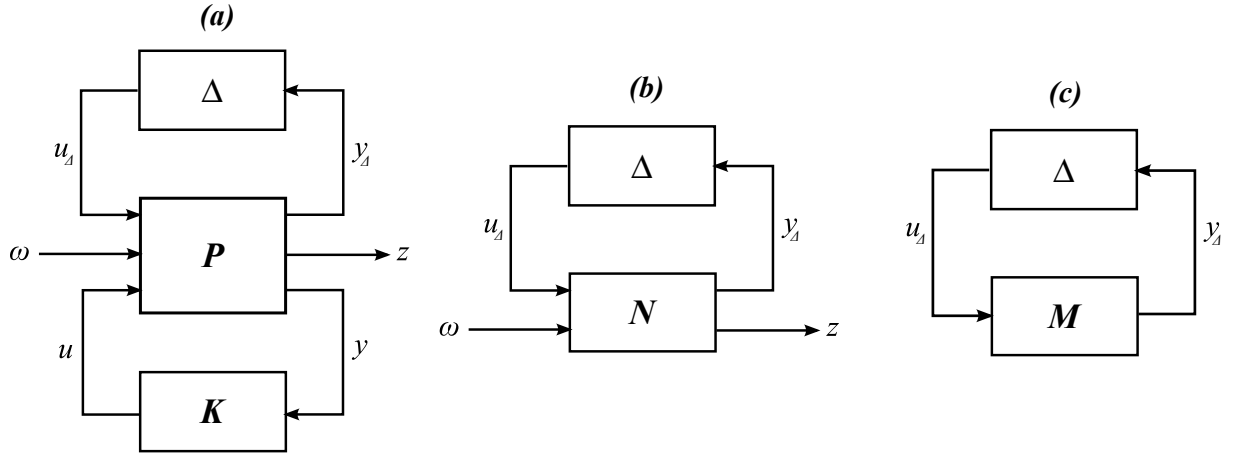


Figure 3.11: General control configurations of the perturbed system (a), configuration for robust performance analysis (b) and configuration for robust stability analysis (c).

$$\mu(M) = \left(\min_{\Delta \in \Delta_f} \{ \bar{\sigma}(\Delta) \mid \det(I - M\Delta) = 0 \} \right)^{-1} \quad (3.95)$$

with matrix Δ defined as a perturbation structure Δ_f defined as:

$$\Delta_f = \begin{bmatrix} \Delta_1 & 0 & 0 & 0 \\ 0 & \Delta_2 & 0 & 0 \\ 0 & 0 & \ddots & 0 \\ 0 & 0 & 0 & \Delta_f \end{bmatrix} \quad (3.96)$$

In practice, due to numerical solution issues, the maximum and minimum bounds of the value of μ are computed. Using the Nyquist theorem, it can be shown that the stability limit is reached at $\det(I - M(s)\Delta(s)) = 0$. The value of $\mu(M)^{-1}$ appears as the measure of the smallest perturbation $\Delta \in \Delta_f$ that drives the system to the unstable region. This value represents a certain “distance” of the system to reach instability. The value of μ can be computed using the `mussv` function in the MATLAB *Control System Toolbox*.

(b) μ -Conditions for RS and RP

According to the different closed-loop configurations presented in Figure 3.11, μ -conditions for robust stability (RS) and robust performance (RP) are now resumed [Skogestad and Postlethwaite, 1996]:

- Nominal stability (NS)** $\Leftrightarrow N$ is internally stable.
- Robust stability (RS)** $\Leftrightarrow \forall \omega, \mu_{\Delta_i}(N_{11}(j\omega)) < 1$ and NS.
- Nominal performance (NP)** $\Leftrightarrow \forall \omega, \mu_{\Delta_f}(N_{22}(j\omega)) < 1$ and NS.
- Robust performance (RP)** $\Leftrightarrow \forall \omega, \mu_{\hat{\Delta}}(N(j\omega)) < 1$ and NS.

where:

$$N = \begin{bmatrix} N_{11} & N_{12} \\ N_{21} & N_{22} \end{bmatrix} \quad (3.97)$$

For the RP case, μ is computed with respect to the following perturbation structure:

$$\hat{\Delta} = \begin{bmatrix} \Delta & 0 \\ 0 & \Delta_P \end{bmatrix} \tag{3.98}$$

where Δ_P is a full complex perturbation matrix.

In the case of a RS, the following interpretation is accurate. If the value of μ at a given frequency is different from 1, then at this frequency the closed loop system remains stable with larger uncertainties of $1/\mu$ times the uncertainty level used to compute μ . If the value of μ is plotted through some frequency range, the effect of uncertainty on the stability and performance of the closed-loop system can be estimated. This is the concept of μ -analysis.

A detailed example, showing a proposed configuration for μ -analysis on a multivariable system, is shown in Figure 3.12.

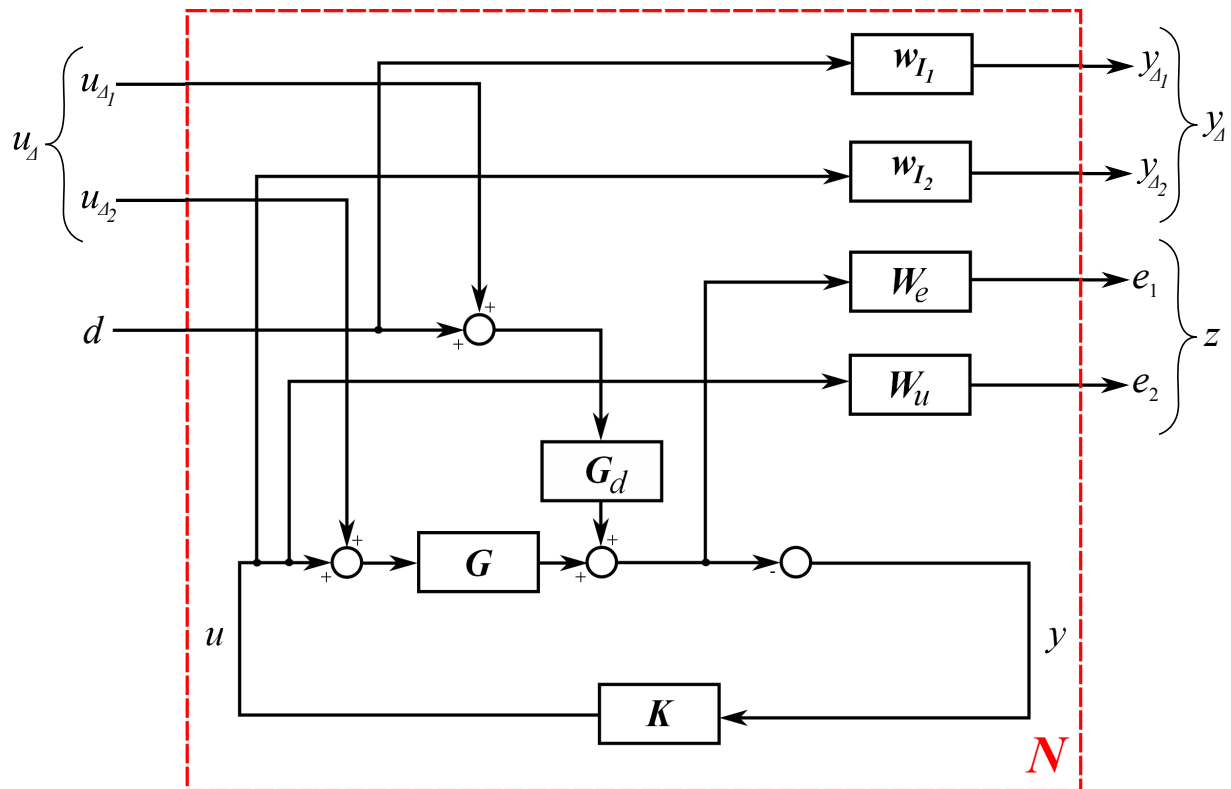


Figure 3.12: Example detailed system for a robust performance analysis.

Table 3.2: A review of useful MATLAB functions

<i>Functions for identification purposes</i>	
Function	Description
<code>idgrey</code>	Define a <i>grey box</i> model to solve an identification problem.
<code>idnlgrey</code>	An extension of the precedent function for non-linear equations systems.
<code>iddata</code>	Measured data can be loaded as an identification data object using this function.
<code>advise</code>	This command gives a general (useful) analysis on the measured data. It could give you some hints on the choice of a suitable method for identification.
<code>idfilt</code>	Function used to filter the measured data.
<code>detrend</code>	Function used for handling offsets and data trends in the measured data.
<code>resample</code>	Function used for resampling measured data, this could be useful for faster identification algorithm compilation, but resampling factor should be chosen carefully.
<code>pem</code>	Function used to solve the identification problem using the iterative prediction-error minimization method
<i>Functions for control design and analysis purposes</i>	
<code>hinfsyn</code>	Used to compute an \mathcal{H}_∞ controller for an LTI system.
<code>hifoo</code>	Compute a reducer order \mathcal{H}_∞ controller, use the simple syntax <code>K=hifoo(P, order)</code>
<code>hinfstruct</code>	Compute a fixed-order controller that minimizes the closed-loop \mathcal{H}_∞ norm, PID control structures are accepted as input (only available from MATLAB's release R2011a).
<code>psys</code>	Define polytopic or parameter-dependent linear systems. Use syntax <code>affs = psys(pv, [s0,s1,s2])</code> with <code>pv</code> defined by function <code>pvec</code> .
<code>pvec</code>	Define parameter vector for time-varying parameters specifying range and rate of variation. Use syntax <code>pv = pvec('box',range,rates)</code> .

Table 3.2 (Continued)

Function	Description
<code>polydec</code>	Compute polytopic coordinates with respect to box corners, use syntax <code>[alpha,vertx] = polydec(pv,pols)</code> .
<code>ucover</code>	Function used to compute an uncertain weight for uncertainty representation.
<code>mussv</code>	Computation of the structured singular value of a closed-loop system subject to uncertainties.

3.4 Conclusion

A variety of robust control methodologies were presented in this chapter. The robust strategies make intensive use of the LMI methods. A glimpse was presented in this chapter on the generalized methodology, however a complete description of the robust generalized methodology, applied to the FC system will be presented later in the Control Applications chapter.

A robust methodology for multivariable PI control design has been proposed where time/frequency and robust performance is adjusted using weighting functions. This is very important in real-time applications given the simplicity of the control structure.

As it will become clearer later in this dissertation, a critical step in our proposed methodology is to check the controller robustness. A complete methodology for robustness analysis using μ -analysis was proposed.

An introduction to a system identification procedure was also presented in this chapter. These identification methods are directly applied in the following chapter where models of the studied systems are presented.

Chapter 4

Test-bench and Modeling

4.1 Introduction

In this chapter the modeling aspects of the fuel cell (FC) system are exposed. The Fuel Cell *System* (FCS) refers to the fuel cell stack itself and to all the auxiliary sub-systems associated. In this thesis a focus was given on the electrical sub-systems and the air pressure system to the FC with the modeling of the air compressor and the supply manifold dynamic. These systems were studied through real test-bench setups. The electrical subsystem model and control was validated on a setup of power converters for a two-source hybrid system using an emulator of the FC dynamic. The second series of model validations was performed on a real FC test-bench with an air compressor dedicated and designed for FCS. The test-bench systems used for validation are presented first in section 4.2. Then the different models equations are exposed divided in two sections: the electrical in section 4.3 and the thermo-dynamic systems for FCS in section 4.4. Validation results for these models are then presented.

Let us now introduce the test-bench used for model/control validation.

4.2 Test-bench setups

4.2.1 Fuel cell test-bench

The fuel cell setup test-bench is located at LEPMI¹ Laboratory in the Grenoble campus. The test-bench is composed by different elements that allow to efficiently control, operate and visualize several parameters of the FCS such as: fluid dynamics (pressure, gas flow rates, reactant stoichiometric values, etc.), thermo-dynamic parameters (stack temperature, humidification rates, etc.), or even electrical parameters (single cell voltage, stack current and power). The test-bench also has an automatic control system to independently manage the electrical and thermo-dynamical variables, as well as a thermostat/cryostat analog control for thermal management. It is also equipped with the security elements necessary to ensure safe operation of the FCS, as: stack malfunction detectors, voltage and pressure limiters, hydrogen leak detection, a security system for test-bench neutralization with nitrogen injection is also available.

The test-bench used for validation with the real FCS is presented in Figure 4.1.

¹From French: “Laboratoire d’Électrochimie et de Physicochimie des Matériaux et des Interfaces”



Figure 4.1: Experimental setup used for validation.

The stack considered in this thesis is a PEMFC from French company Paxitech© and mounted on a UBzM© frame with a nominal power of 475W. A picture of this stack is shown in Figure 4.2. The arrangement is composed by a 16-cell/100 cm² effective area stack. The typical characteristic of a single cell is normally given in a polarization curve, a plot of the cell voltage versus the current density. The difference between the ideal voltage (constant $\sim 1V$) and the actual voltage in the polarization curve, represents the different losses in the cell. The polarization and power curves of the stack considered can be shown in Figure 4.3. As it can be seen in these figures, even though the nominal power of the PEMFC is 475W it can reach a maximal power capacity of 1kW under special conditions.

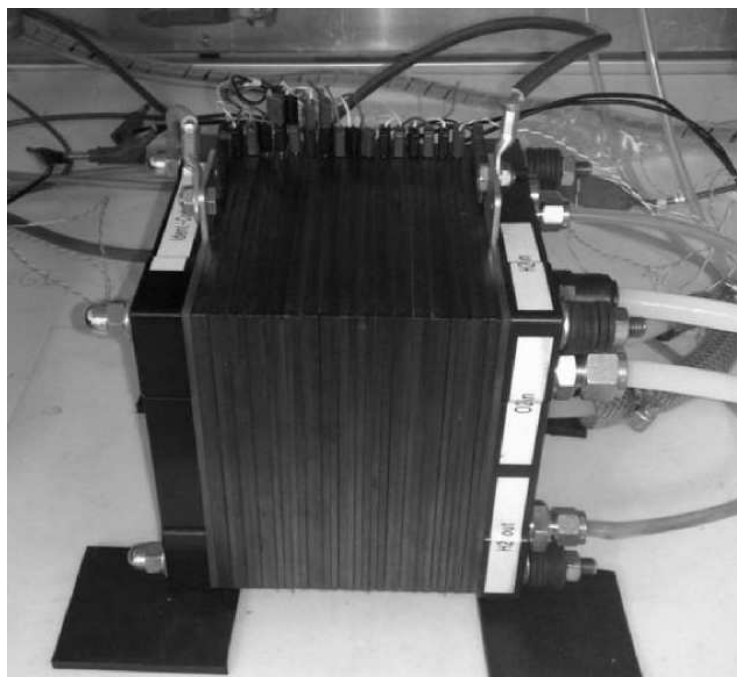


Figure 4.2: The Paxitech© fuel cell stack.

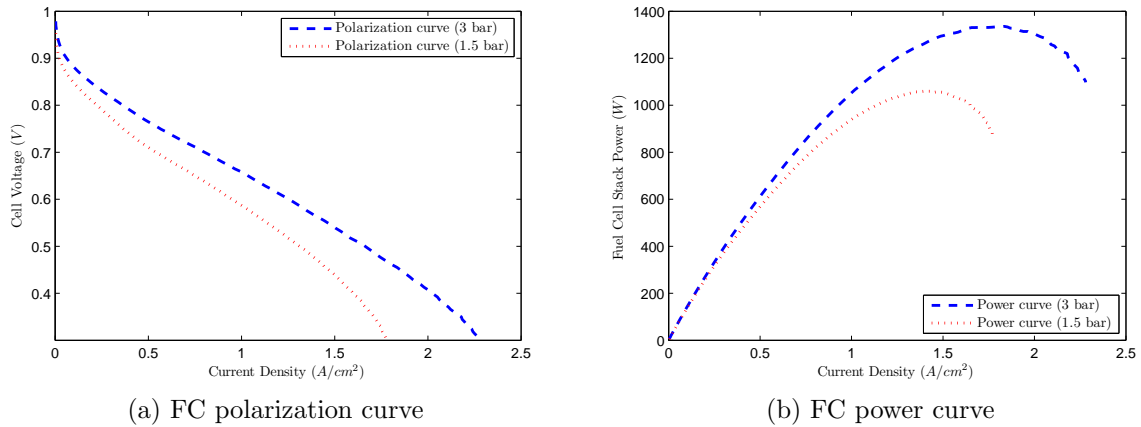


Figure 4.3: Characteristics of PEMFC from Paxitech©.

A scheme of the FCS with the auxiliary components installed at LEPMI is presented in Figure 4.4, this is similar to the “classical” FCS including auxiliary equipments as presented in [Pukrushpan et al., 2004a].

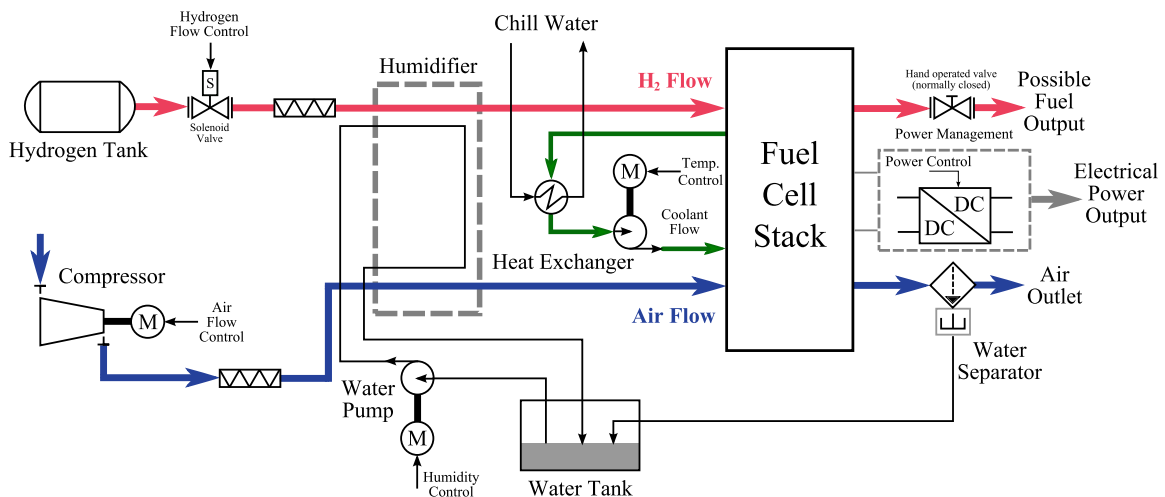


Figure 4.4: A PEM Fuel Cell System.

The air channel entering at the FC stack input is controlled by air flow and pressure regulators. For air flow control the setup is equipped with *Smart series 5800S* models from *Brooks Instruments*©, with reading/regulation capabilities using 0 – 5V control signals. For pressure reading purposes the test-bench is provided by series 21 *Keller*© piezoresistive transmitters. For the pressure reading/regulation option, a *VP50* proportional control valve from *Norgren*© was installed for air back-pressure control.

Even though this setup was available for tests, there were several problems encountered during this thesis in order to properly exploit the stack operation. Notably one major problem was due to the extinction of the company originally charged to develop the stack mounting and the security and associated operation equipment. This problem and several minor changes in the setup configuration, as well as operation for research purposes with different stack (with different characteristics), makes clear that at the end of this thesis the setup will have to suffer a complete makeover to ensure safe operation for both the

FCS and the operators. It is expected now to change and renew the whole mounting by the end of 2011. For these reasons, there was an important limitation in this thesis for obtaining results with the real FC stack. Despite this problem, using this setup it was possible to identify the static (polarization) and dynamic model of the FC stack. Also, installing the air compressor on this system, but using an air volume instead of the real stack, it was possible to identify the compressor and the supply manifold models. This will be presented later in this work.

However, due to limitations explained before, it was not possible to use this test-bench to further validate the control strategies proposed in this thesis for the complete FCS, which will be part of future works. Also, for security reasons, validation of the control strategies for the electrical power management sub-system was possible after substituting the FC stack by an emulator of the dynamics recorded on the real FC. Again, this is presented later in this chapter.

4.2.1.1 The GESI setup

In the work of [Frati, 2006] several components of the GESI demonstrator (from French “Générateur Electrochimique et Stockage Isolé”, Electrochemical Generator and Isolated Storage) were practically developed. In that work a test-bench was designed for a 500W nominal power with the PEMFC stack present at LEPMI. The principles of these power converter interface for FCS are presented in more details in [Dang, 2006], especially the case of the Interleaved Double Dual boost (IDD boost) converter, which is notably used here to reduce losses in the converter transformation stage. Later in the work of [Sailler, 2008] a basic control strategy for the GESI demonstrator was proposed.

The general layout of the test-bench is presented in Figure 4.5.

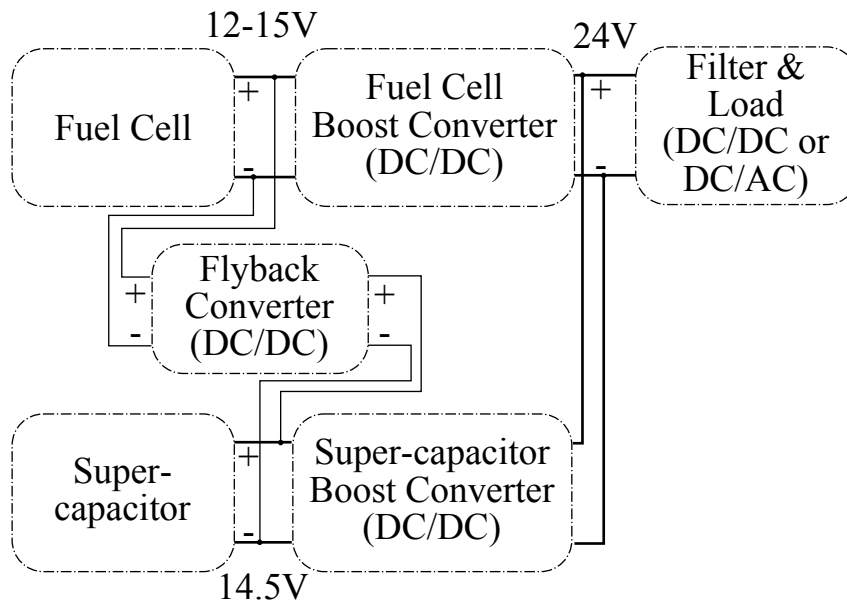


Figure 4.5: Experimental setup converter configuration.

Figure 4.5 presents the hybrid feature of the GESI system. The auxiliary source should be capable to supply sufficient instant power to guarantee normal operation in the presence of important energy transients without any deterioration of the FC. The technology behind high-current super-capacitors has been designed for this purpose. The

studied system is then composed by a hybrid FC/Super-capacitor power generator. The two sources and their respective boost converters are connected in parallel and a DC filter connects the output with the supplied DC load. A 58F Maxwell[®] super-capacitor (SC) was selected in the previous works when developing the GESI setup. The power converters were designed for a 500W nominal power and a 24V rated DC bus output voltage. The SC converter in the GESI test-bench is not reversible, this means that the SC recharge from FC current is assured by a third converter, a flyback converter. The flyback however, is controlled independently from the boost converters. Under normal loading conditions, at approximately 475W, the flyback converter will operate at 0.4A to keep the SC charge at a nominal voltage of 14.5V in the SC. A small auxiliary 12V battery is used to power the control boards for the boost converters, generating the necessary PWM signals. The PWM is fixed at 50kHz. A DS1104 dSPACE[®] real-time control board is used to capture the system currents and voltage and to send the 0 – 5V control signal for the PWM (duty cycle). All the parameters associated with this system are presented later in this chapter for system modeling. A picture of the GESI arrangement is presented in Figure 4.6.

4.2.1.2 Air pressure system

This thesis is devoted to the control of the FCS and the special case of the electrical and the thermo-dynamic sub-systems. In order to obtain a control-oriented model of the FCS it was decided to consider the air supply system only. For this reason the choice of an air compressor was critical in this thesis.

According to the requirements of the FCS at LEPMI, an air compressor was chosen to guarantee at least an air flow of 60 slpm² and a pressure range of 1 – 2 bars (absolute). With these characteristics and allowing an oversizing factor for future stack expansion at LEPMI, the Vairex[®] *VV-0520.08 INT* model dry fixed vane air compressor was chosen. The compressor has an operating range of 24 – 40V and nominal power of 900 – 1200W. The air flow ranges from 0.2 – 10g/s at compression pressures of 1.1 – 2 bars (abs). The compressor layout and the compressor map as given by manufacturer are given in Figure 4.7.

4.2.2 “Emulator” test-bench

As it will be presented later in this chapter, the FC model used for control purposes combines the dynamic performance, by means of a simplified electrical equivalent circuit modeling, with the static polarization curve characteristic. For the real-time experimentation, an emulation (Hardware-in-the-loop simulation) of the FC dynamic was implemented to avoid damage on the real FC during tests. The model used for the emulator represents the static and dynamic characteristics of the PEMFC, sending a 0-10V control signal to a voltage-controlled DC source. A Xantrex[®] 100-60 DC programmable source and a Simulink/dSPACE real-time environment was used to emulate the FC dynamics. This setup was located at G2ELab in the Grenoble campus. A similar work on fuel cell emulation using the same procedure was previously presented in [Tritschler, 2007].

The test-bench configuration is presented in Figure 4.8.

²Standard liters per minute

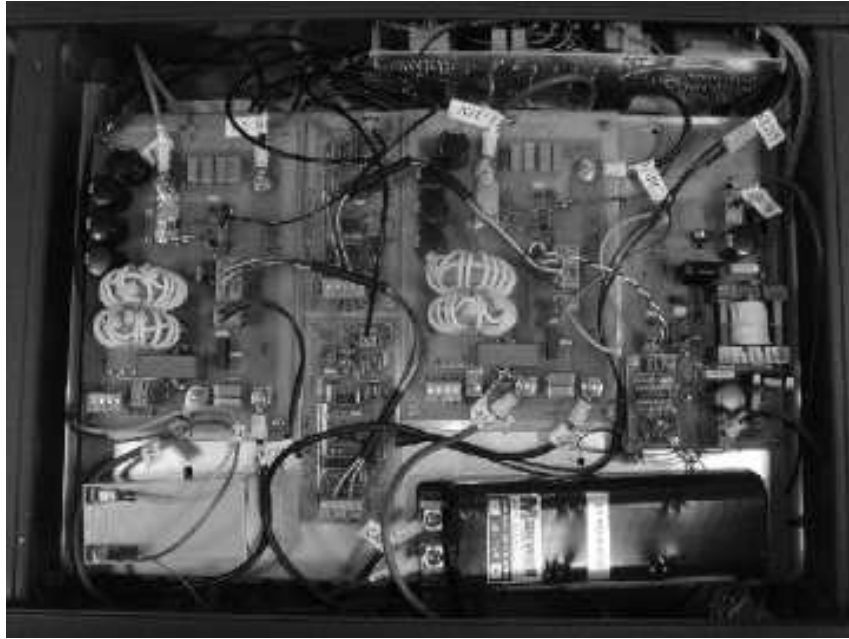
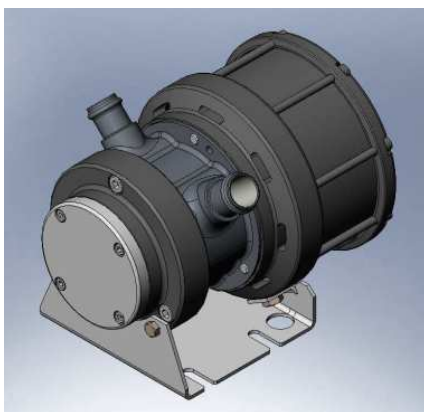
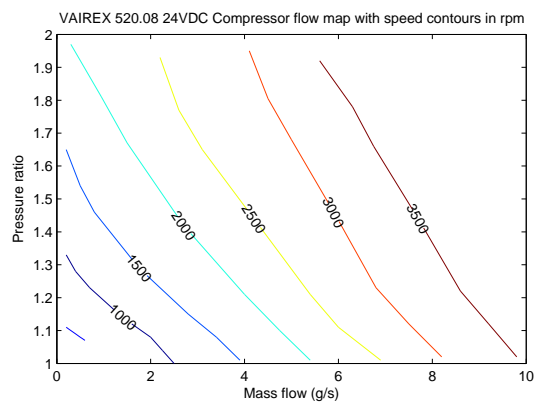


Figure 4.6: GEI arrangement of power converters and super-capacitor.



(a) Compressor layout



(b) Compressor map

Figure 4.7: Vairex© 24V air compressor characteristics.

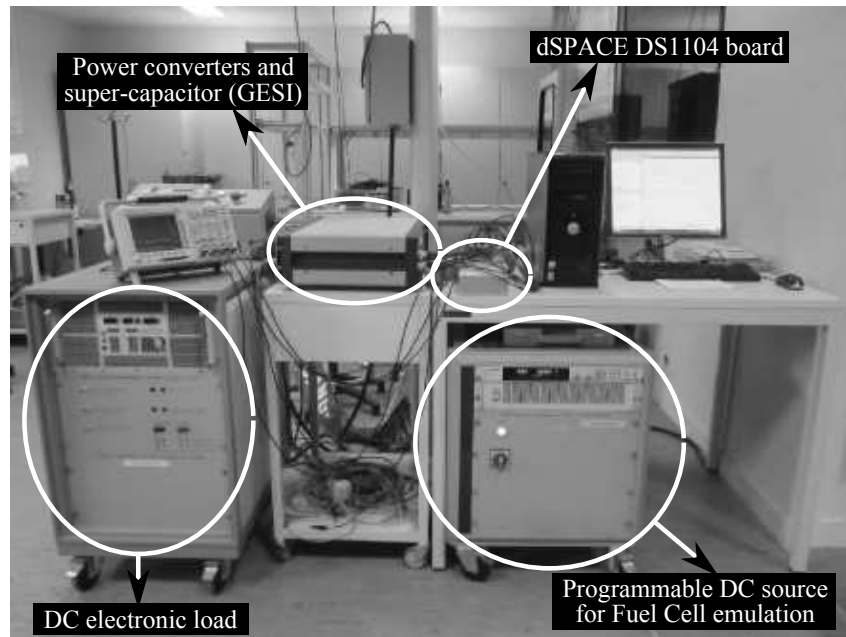


Figure 4.8: “Emulator” test-bench setup configuration.

4.3 Electrical equivalent circuits

In this section the electrical sub-system model of the FCS is presented. The basic structure considered for the electrical power management is the GESI structure, in order to more easily exploit results on the test-bench presented before. However other structures are also considered, as the use of a reversible power converter for the secondary source and a voltage inverter for network connection or isolated three-phase operation.

Even if the complete model of the FC stack will be presented later, in this section the electrical equivalent models of the FC and the SC are also given. These simplified models represent the approximated dynamic of the real system, at the cost of a reduction on the system detailed representation, a control-oriented model can then be obtained. For numerical implementations, a complete review of the open-loop models presented here is given in appendix B.

Let us now introduce these simplified models for the FC and SC systems.

4.3.1 Electrical equivalent source models

4.3.1.1 Fuel cell modeling

A FC stack is composed by a series connexion of individual cells. A single FC is composed by a membrane sandwiched between two electrodes, the cathode and the anode. The combination of oxygen and hydrogen within this membrane, along with a catalyzer element distributed in the cathode and anode surface (normally platinum), produces a chemical reaction with electron liberation (electrical current), heat and water as sub-products. The three components, cathode, anode and electrolyte are arranged together to form a single Membrane Electrolyte Assembly (MEA).

A FC also has a dynamic behavior normally represented in terms of variations of the cell current and the air (oxygen) pressure. Different modeling options are possible. Then

a complete and detailed review on fuel cell modeling methodologies is presented in [Hissel and Turpin, 2008].

For a simplified control-oriented model, the electrical equivalent representation is a good option. This model represents the so-called “double layer” charge, which is the capacitive behavior of the layer of charge near the electrode/electrolyte membrane [Pukrushpan et al., 2004a]. Even when this model can be used to model the FC dynamic, there is a claim in [Pukrushpan et al., 2004a] that literature values of the RC time constant represents a extremely fast dynamic and thus a poor correspondence with the real cell dynamic. Despite this, in [Sailler, 2008] a good review of measures on the Paxitech© FC stack considered in this thesis is presented using the method of electrochemical impedance spectroscopy. Moreover, in [Hissel and Turpin, 2008] and [Wang et al., 2005], models based on electrode impedance and equivalent electrical circuits seems to precisely represent the FC dynamic. The electrical equivalent model is presented in Figure 4.9.

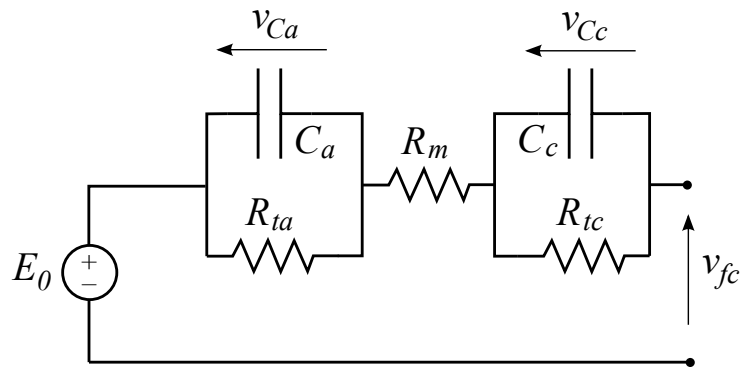


Figure 4.9: Fuel Cell dynamic model.

In this model E_0 is the open-loop voltage in V, R_m is the FC membrane resistance in Ω , R_{ta} and R_{tc} are the anode and cathode transfer resistances in Ω and C_a and C_c are the anode and cathode double layer capacitances in F. The values of these parameters were taken from [Sailler, 2008] for an operating condition of the FC stack at 30° and 20A. The membrane resistance was recalculated from measures on the real fuel cell operating with air at an excess ratio of 1.5. The model parameters are given in Table 4.1. A comparison between the model simulation and the measured data is presented in figure 4.10. Even though the estimated response is not completely representative of the measured dynamic, this model is considered valuable for control-oriented purposes due to its simplicity. To tackle this weakness, important for a special control strategy proposed later in this work, a more complete model with efficient account on the FC dynamic will be presented afterwards.

4.3.1.2 Super-capacitor model

The FC has several limitations for power delivery, its dynamic is relatively slow, with this a low capacity to absorb large energy transients. Most importantly, these large energy transients could have an adverse effect on the cells life expectancy (aging) due to fuel or oxygen starvation [Thounthong and Rael, 2009]. To cope with these problems hybridization is commonly proposed as a solution. Super-capacitor are used here to manage the unbalance between power and energy in the hybrid source, with the FC providing the base energy and the SC providing the instant power when needed. The choice of the SC is kept

Table 4.1: FC model parameters

Parameter	Value	Units
E_0	13.4	Volts
R_m	7.63×10^{-2}	Ω
R_{tc}	2.04×10^{-3}	Ω
R_{ta}	4.72×10^{-4}	Ω
$C_a = C_c$	2.12	F

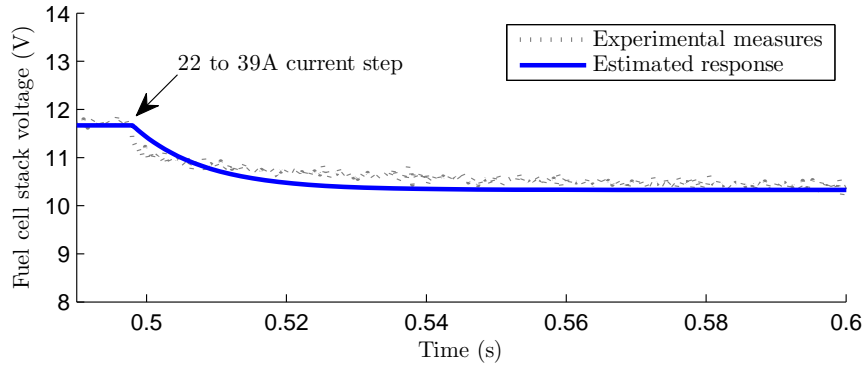


Figure 4.10: Measured and simulated FC dynamic.

in this thesis for compatibility with the GESI test-bench. The choice of different source types will depend on the specific application (stationary power production, automobile, etc) and the Ragone chart (Figure 4.11³) will help for a better choice considering the power/energy trade-off.

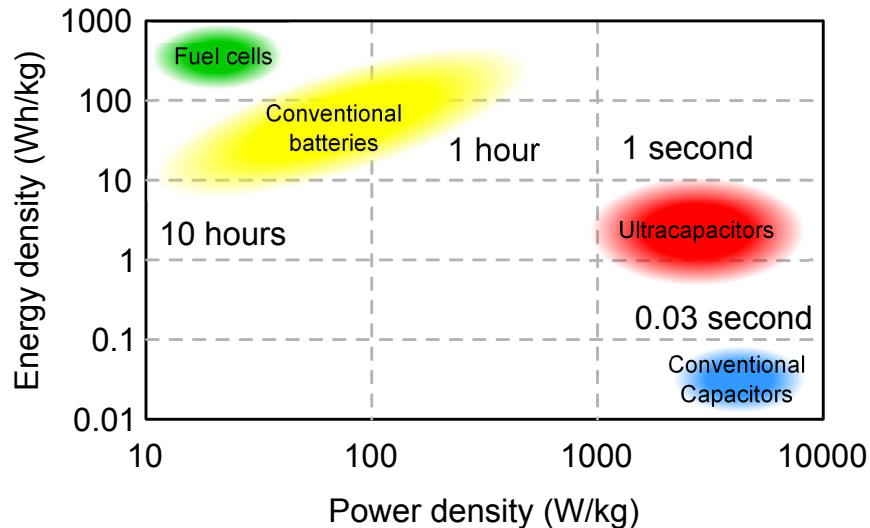


Figure 4.11: The Ragone chart for several sources.

In the case of the GESI test-bench, the model of the 58F Maxwell[©] super-capacitor was established in [Sailler, 2008] from impedance spectrum measures. These results showed

³From Maxwell Technologies: <http://www.maxwell.com>

that a simple equivalent series resistance and capacitance model was sufficient to represent the SC dynamic in a wide frequency range. This simplified model of the SC dynamic was found to be suitable for control-oriented modeling. More complex and detailed models can be found in the literature on SC modeling, see [Buller et al., 2002] for example. The parameter values for this model are $C_{sc} = 58\text{F}$ and $R_{sc} = 0.019\Omega$ taken from the manufacturer data-sheet. The super-capacitor model was not identified and should be noted that such parameters are strongly influenced by temperature and SC voltage.

4.3.2 Hybrid boost converters

4.3.2.1 Non-linear average model

The studied system is then composed by a hybrid FC/SC power generator. The two sources and their respective boost converters are connected in parallel and a DC filter connects the output with the supplied DC load. This configuration is presented in Figure 4.12. However, for the sake of simplicity in the system model, it is considered that the SC is not under charging condition, so the flyback converter is not considered.

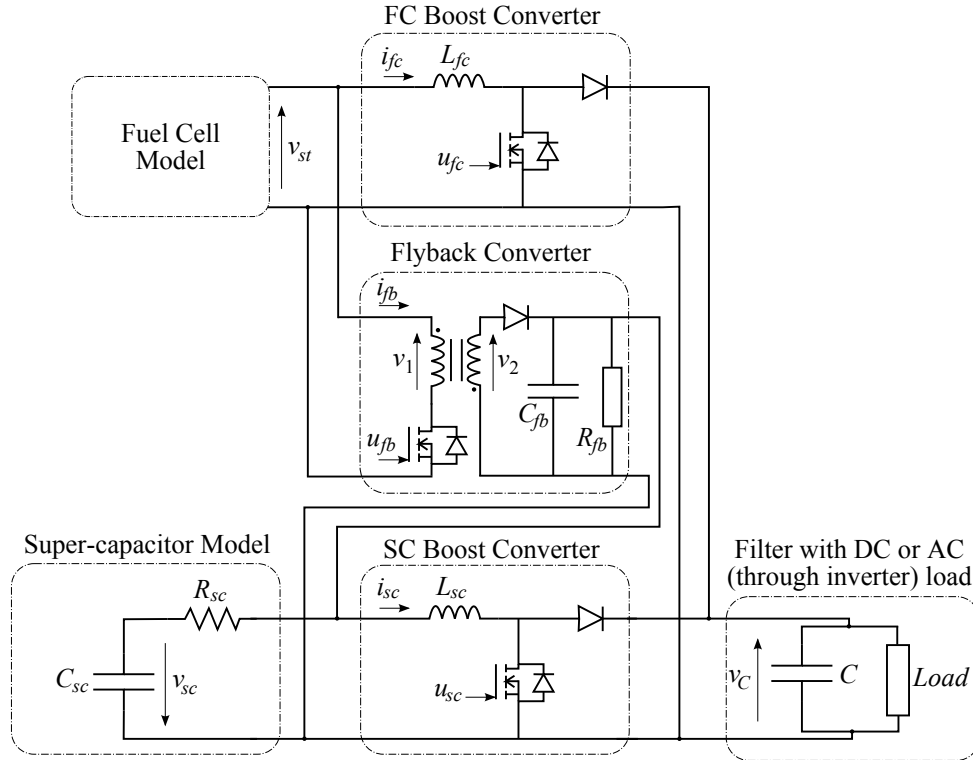


Figure 4.12: Equivalent topological model of the hybrid system studied.

The model equations for a single boost converter are given by:

$$\begin{cases} L \frac{di_L}{dt} = E - v_C (1 - u_{dc}) \\ C \frac{dv_C}{dt} = (1 - u_{dc}) i_L - i_{load} \end{cases} \quad (4.1)$$

with state variables i_L and v_C , the inductance current and the output capacitor filter voltage respectively, and with inputs given by the load current i_{load} , the input source voltage E .

Now for the hybrid system in Figure 4.12 (taking off the flyback converter), the model equations becomes:

$$\begin{aligned}
\frac{dV_{C_c}}{dt} &= \frac{1}{C_c} \left[I_{fc} - \frac{V_{C_c}}{R_{tc}} \right], \quad \frac{dV_{C_a}}{dt} = \frac{1}{C_a} \left[I_{fc} - \frac{V_{C_a}}{R_{ta}} \right] \\
\frac{dI_{fc}}{dt} &= \frac{1}{L_{fc}} [E_0 - V_{C_a} - V_{C_c} - (R_m + R_L)I_{fc} - (1 - \alpha_{fc})V_C] \\
\frac{dI_{sc}}{dt} &= \frac{1}{L_{sc}} [V_{sc} - R_{sc}I_{sc} - (1 - \alpha_{sc})V_C], \quad \frac{dV_{sc}}{dt} = \frac{1}{C_{sc}} I_{sc} \\
\frac{dV_C}{dt} &= \frac{1}{C} [(1 - \alpha_{fc})I_{fc} + (1 - \alpha_{sc})I_{sc} - I_{load}]
\end{aligned} \tag{4.2}$$

The average model is used here to subsequently obtain the desired control-oriented model (see [Bacha et al., 1994] for more details on average modeling). We only consider *first order* average models. The state variables are: V_{C_c} the double layer capacitor in the FC cathode, V_{C_a} the double layer capacitor in the FC anode, I_{fc} the FC output current, I_{sc} the super-capacitor output current, V_{sc} the super-capacitor voltage and V_C the output filter capacitor voltage. The control inputs to the system are α_{fc} and α_{sc} (converter PWM duty cycles), the average values of u_{fc} and u_{sc} , the switching functions of the FC and super-capacitor power converters respectively. I_{load} is the disturbance input.

The model parameters were obtained from [Fрати, 2006]. The smoothing inductances for each boost converter were designed to allow a maximum current ripple of 10%. A powder core with permeability $\mu = 125$ was chosen. A total inductance of $50\mu\text{H}$ was obtained for each power converter with 32 turns of 12 AWG cooper wire. An additional resistance of $R_L = 0.024\Omega$ can be associated with the inductance resistance. The output filter capacitance was designed to filter high frequencies with 4 paper-technology capacitors of $4.7\mu\text{F}$ and 4 chemical capacitors of $4.700\mu\text{F}$, that for each power converter output. It is worth noting that the frequency for the PWM was fixed to 50kHz. An oscilloscope screen-capture of the PWM signal is presented in Figure 4.13. The PWM control modulation signal (0 – 5V) is amplified to a 0 – 8V triangle signal for better precision. The control input in the Figure 4.13 corresponds to a 4.2V signal.

With this topological and non-linear average modeling description of the hybrid converter system, several measures were used to validate the given model. The measures were taken from the real running fuel cell stack, for a load resistance of 4Ω . Figure 4.14 show the validation results for a load step of 100% (4Ω to 2Ω step). The validation results show a good agreement between measured data and simulations results with the non-linear average model. A small overshoot can be seen in the measured output current, this is preumed to be due to the unknow dynamic introduced by the electronic source used to emulate the current step. The average model itself is validated when compared to the topological model results. The topological model refers here to the complete model of the hybrid converter system considering the switching functions of the PWM as control inputs. MATLAB/SIMULINK is used to simulate the switching functions considering ideal components. Sampling time stands at 200msec. For these simulations, the duty cycles are fixed at their steady-state values corresponding to a FC current of 35.2A, i.e., $\alpha_{fc_e} = 0.5925$ and $\alpha_{sc_e} = 0.3875$. The comparison of topological and average modeling for a +50% load step at $t = 0\text{s}$ and -50% load step at $t = 0.05\text{s}$ are presented in figures 4.15, 4.16 and 4.17 for the output DC bus voltage, the FC and the SC currents respectively. These simulation results were obtained for the first cycles of the load step response and

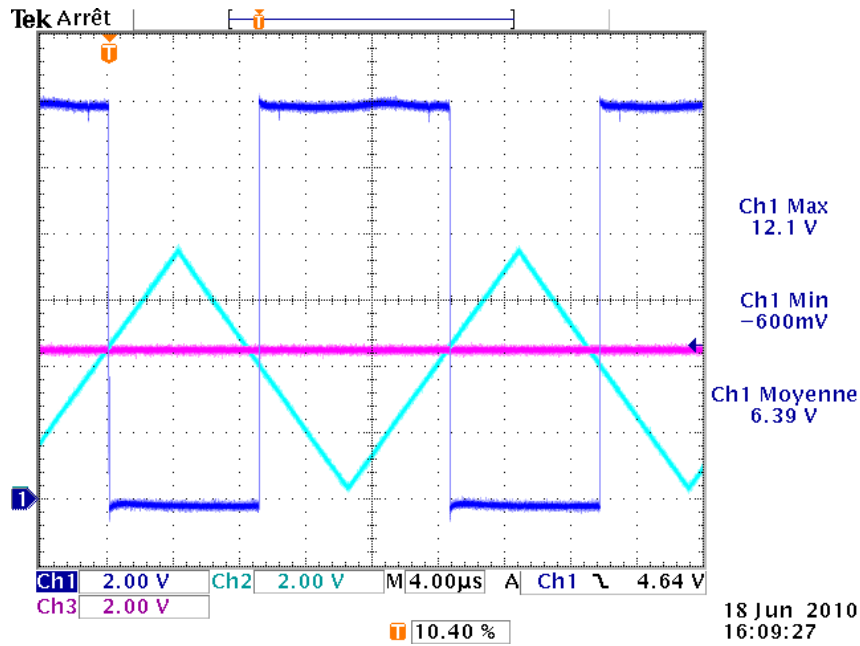


Figure 4.13: PWM control for the boost power converters.

with the SC contribution to the instantaneous current requirement to the load. Note that the flyback converter can only support a maximum 5A charging current to the SC.

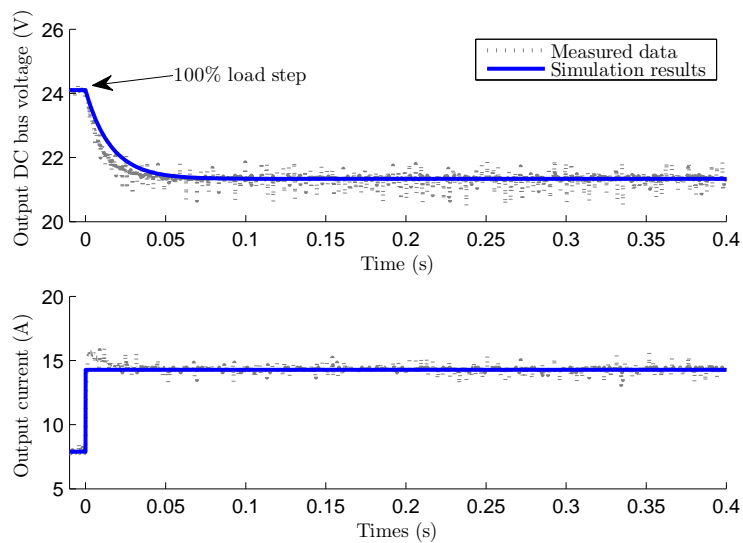


Figure 4.14: Validation of hybrid generator model (5.3.3.2) (open-loop).

The results presented in these figures show a good concordance with both of these models. But for linear control purposes, obtaining a linear model is of interest. The linear model obtained from the previous non-linear average model is now presented.

4.3.2.2 Linear average state-space model

With the non-linear model described in the previous section, a linear model can be easily obtained linearizing at a given operation point. The steady-state equilibrium point can be

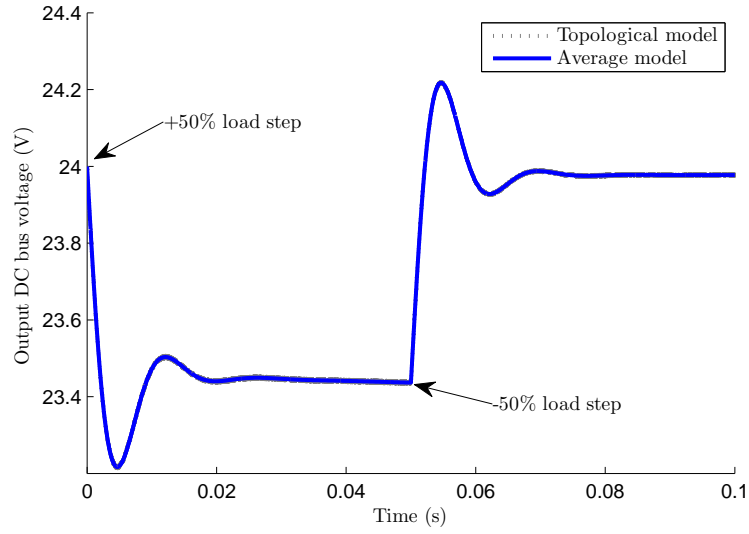


Figure 4.15: Output DC bus voltage response to a 25% load step at $t = 2.5$ s.

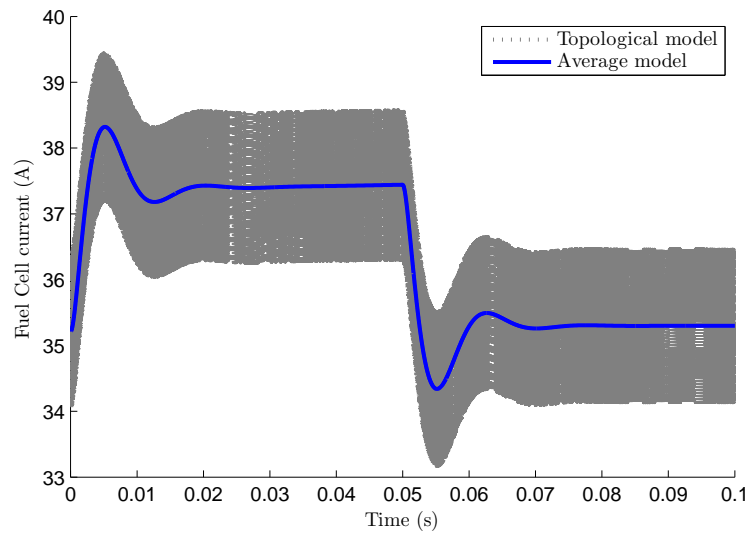


Figure 4.16: Fuel cell current response to a 25% load step at $t = 2.5$ s.

found imposing $d/dt = 0$ and solving the non-linear equation system in (5.3.3.2). MATLAB function `fsolve` can also be used for this goal.

The following linear state-space description can now be defined as:

$$\begin{aligned}
 \Delta \dot{x} &= A \Delta x + B_1 \Delta \omega + B_2 \Delta u \\
 \Delta x &= [\Delta V_{C_c} \quad \Delta V_{C_a} \quad \Delta I_{f_c} \quad \Delta I_{s_c} \quad \Delta V_{s_c} \quad \Delta V_C]^T \\
 \Delta u &= [\Delta \alpha_{f_c} \quad \Delta \alpha_{s_c}]^T, \quad \Delta \omega = \Delta i_{load}
 \end{aligned} \tag{4.3}$$

with:

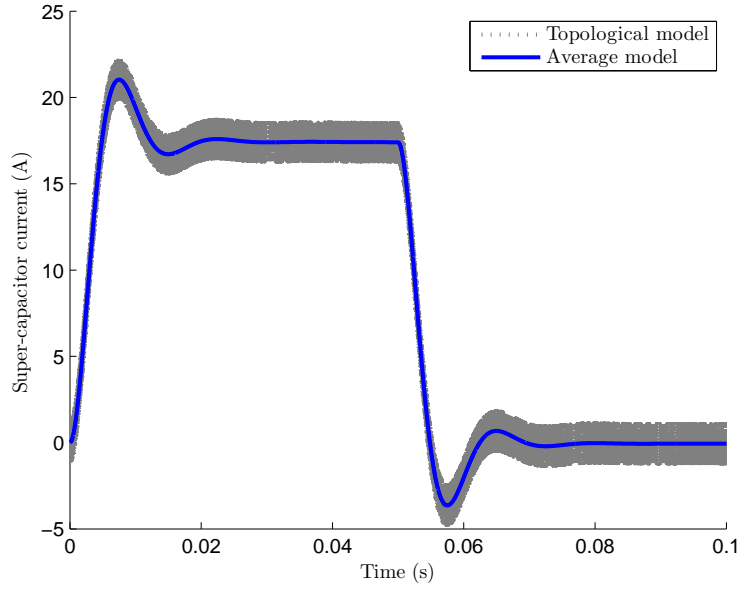


Figure 4.17: Super-capacitor current response to a 25% load step at $t = 2.5$ s.

$$A = \begin{bmatrix} -\frac{1}{R_{tc}C_c} & 0 & \frac{1}{C_c} & 0 & 0 & 0 \\ 0 & -\frac{1}{R_{ta}C_a} & \frac{1}{C_a} & 0 & 0 & 0 \\ -\frac{1}{L_{fc}} & -\frac{1}{L_{fc}} & -\frac{R_m+R_L}{L_{fc}} & 0 & 0 & -\frac{(1-\alpha_{fce})}{L_{fc}} \\ 0 & 0 & 0 & -\frac{R_{sc}}{L_{sc}} & \frac{1}{L_{sc}} & -\frac{(1-\alpha_{sce})}{L_{sc}} \\ 0 & 0 & 0 & \frac{1}{C_{sc}} & 0 & 0 \\ 0 & 0 & \frac{(1-\alpha_{fce})}{C} & \frac{(1-\alpha_{sce})}{C} & 0 & 0 \end{bmatrix}$$

$$B_1 = \left[0 \ 0 \ 0 \ 0 \ 0 \ -\frac{1}{C}\right]^T, \quad B_2 = \begin{bmatrix} 0 & 0 & \frac{V_{C_e}}{L_{fc}} & 0 & 0 & -\frac{I_{fce}}{C} \\ 0 & 0 & 0 & \frac{V_{C_e}}{L_{sc}} & 0 & -\frac{I_{sce}}{C} \end{bmatrix}^T$$

Suffix e stands for a steady-state variable. The prefix Δ denotes a linearized variable $\Delta x = x - x_e$, this notation will be dropped henceforth for the sake of simplicity in the presentation.

For the multivariable linear model of the hybrid system computed at a fixed operating condition with $I_{fc} = 35.2$ A and a DC bus voltage of $V_C = 24$ V, the Bode plot is computed and presented in Figure 4.18. A first interesting property when analyzing this system is the fact of a natural rejection of variations in the load current given the reduced gain of the i_{load} to V_C transfer function. The complete open-loop state-space matrices for this system are presented in appendix B. The linear system has the following poles:

$$\begin{aligned}
 p_1 &= -990.7972 \\
 p_{2,3} &= -116.1616 \pm 580.6203i \\
 p_{4,5} &= -217.1241 \pm 68.0373i \\
 p_6 &= -0.7266
 \end{aligned}$$

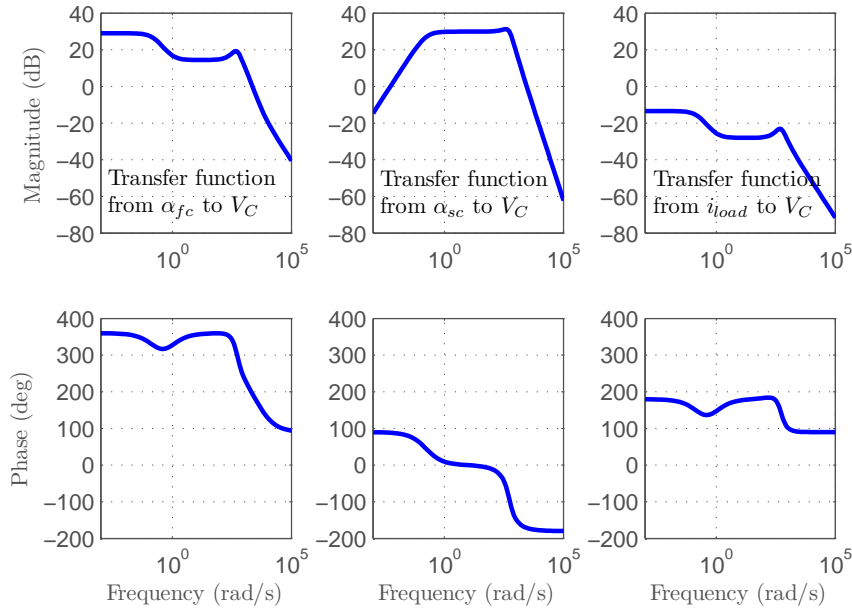


Figure 4.18: Bode plot of the open-loop MIMO linear system.

4.3.2.3 A basic sensitivity analysis of state-space matrix

A brief sensitivity and participation factor analysis is now presented. The sensitivity analysis will give the eigenvalue λ_i sensitivity to variations in the diagonal element a_{kk} in the state-space matrix A . In the other hand, the participation factor analysis will indicate the amount of participation of certain respective state in a certain corresponding mode. A review on this theory can be found in [Kundur, 1993].

The *eigenvalues* of A are the values for which there is a non-trivial solution to the equation:

$$A\Phi = \lambda\Phi \quad (4.4)$$

Most notably a non-trivial solution is given by the known *characteristic equation* of the state-space system:

$$\det(A - \lambda I) = 0 \quad (4.5)$$

For a given eigenvalue λ_i , the value of vector Φ_i that satisfies equation (4.4) is called a *right eigenvector* of state-space matrix A , with size $n \times 1$. In a similar manner, the

n-row vector Ψ_i is called the *left eigenvector* for a given eigenvalue λ_i and is defined by the following equation:

$$\Psi A = \lambda \Psi \quad (4.6)$$

After some considerations, and the solution of the first-order differential equation, the free motion dynamic time response of the state-space system can be described by [Kundur, 1993]:

$$\Delta x(t) = \sum_{i=1}^n \Phi_i \Psi_i \Delta x(0) e^{\lambda_i t} \quad (4.7)$$

With this meaning that the time-domain response for the i th state is given by:

$$\begin{aligned} \Delta x_i(t) = & \Phi_{i1} \Psi_{i1} \Delta x(0) e^{\lambda_1 t} + \Phi_{i2} \Psi_{i2} \Delta x(0) e^{\lambda_2 t} + \dots \\ & \dots + \Phi_{in} \Psi_{in} \Delta x(0) e^{\lambda_n t} \end{aligned} \quad (4.8)$$

From these expressions, the sensitivity of an eigenvalue λ_i with respect to element a_{kj} of the state-space matrix A will be given by the scalar product of the left eigenvalue element Ψ_{ik} and the right eigenvector element Φ_{ji} , i.e.:

$$\frac{\partial \lambda_i}{\partial a_{kj}} = \Psi_{ik} \Phi_{ji} \quad (4.9)$$

Finally the participation factors matrix is defined as:

$$P = [p_1 \quad p_2 \quad \dots \quad p_n] \quad (4.10)$$

with:

$$p_i = \begin{bmatrix} p_{1i} \\ p_{2i} \\ \vdots \\ p_{ni} \end{bmatrix} = \begin{bmatrix} \Phi_{1i} \Psi_{i1} \\ \Phi_{2i} \Psi_{i2} \\ \vdots \\ \Phi_{ni} \Psi_{in} \end{bmatrix} \quad (4.11)$$

where Φ_{ki} and Ψ_{ik} are the k th entry of the right Φ_i and left Ψ_i eigenvector respectively.

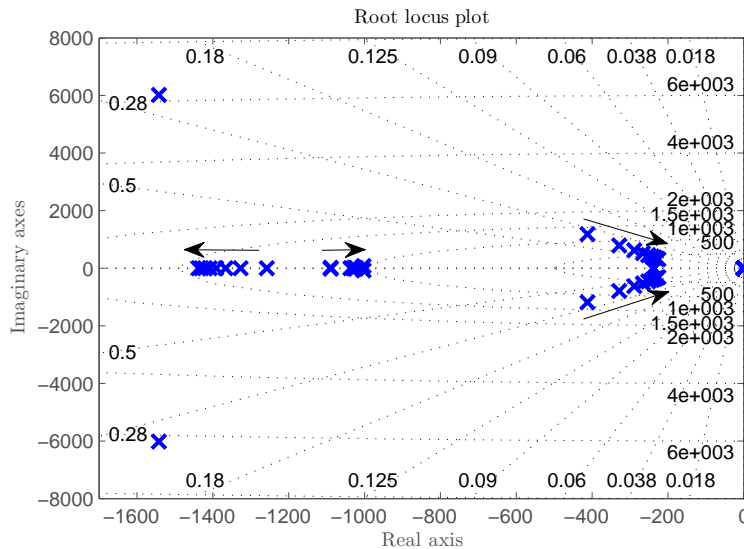
There are 4 modes associated to the hybrid FC/SC converter system. Mode 1 is related to pole p_1 , mode 2 is related to the complex conjugated poles p_2, p_3 , mode 3 to poles p_4, p_5 and mode 4 to single real pole p_6 . Applying the previous sensitivity definition, several conclusions are proposed. The participation factors matrix for this system is given in Table 4.2. Absolute values are used to compute this participation factors matrix. Modes 1 and 2 are influenced by the double layer capacitances C_a and C_c and by the DC bus filter capacitor C . The mode 4 is affected by the SC value C_{sc} . The first conclusion is that the whole system dynamic is highly dominated by the value of capacitance C . The

Table 4.2: Participation factors matrix.

Variable	Mode 1	Mode 2	Mode 3	Mode 4		
V_{C_c}	0.0001	0.0074	0.0074	0.5059	0.5059	0.0003
V_{C_a}	1.0074	0.0023	0.0023	0.0040	0.0040	0.0000
I_{f_c}	0.0078	0.2737	0.2737	0.2589	0.2589	0.0019
I_{s_c}	0.0004	0.2759	0.2759	0.2967	0.2967	0.0015
V_{s_c}	0.0000	0.0003	0.0003	0.0020	0.0020	1.0030
V_C	0.0007	0.5396	0.5396	0.0438	0.0438	0.0001

second conclusion is on the importance of the C_{sc} value, since it affects the mode 4, a real eigenvalue close to the imaginary axis and then associated to the entire system stability.

From this matrix it can be concluded that mode 1 will have an influence on the double layer capacitance voltage in the FC anode V_{C_a} . Modes 2-3 affect mainly the dynamics of the output DC bus voltage V_C . Modes 4-5 are influent on voltage V_{C_c} in the FC cathode and mode 6 acts on the SC dynamic voltage V_{s_c} . Finally modes 2-3 and 4-5 have a similar influence on currents I_{f_c} and I_{s_c} . Conclusions obtained with this analysis are confirmed with an “initial”⁴ the root locus plot of system poles subject to variations in the identified critical parameters. Figures 4.19 and 4.20 show the roots evolution for a variation of $\pm 100\%$ in the filter capacitor C and in the SC value C_{sc} . Notably Figure 4.20 shows how this real pole becomes close to the imaginary axis when increasing the SC value. This analysis could play an important role for system component design, for a robustness analysis as it will be done later in this dissertation, or even for control purposes.

Figure 4.19: Root locus plot evolution for variations of $\pm 100\%$ in C .

⁴The root locus analysis is not exhaustive and is presented here only as an illustration. A more realistic analysis may consider the variations in the operating values of α_{f_c} and α_{s_c} which in our case, as a simplification, were kept constant.

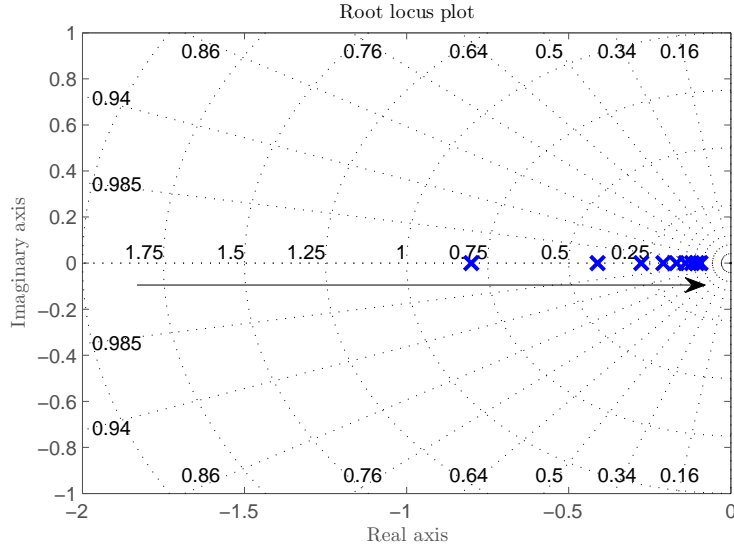


Figure 4.20: Root locus plot evolution for variations of $\pm 100\%$ in C_{sc} .

4.3.3 Special case using a reversible converter

Even when it was decided to keep the power converter configuration shown in Figure 4.12, it should be noted that a more common solution is to consider a reversible converter for the secondary source, in this case the SC.

The equation of a single reversible boost converter is given by:

$$\begin{cases} L \frac{di_L}{dt} = (E - v_C \alpha_{dc}) k \\ C \frac{dv_C}{dt} = i_L \alpha_{dc} - i_{load} \end{cases} \quad (4.12)$$

with:

$$\begin{cases} \alpha_{sc} = 1 - \alpha_{dc} \text{ and } k = 1 & \text{if } i_{sc} > 0 \\ \alpha_{sc} = \alpha_{dc} \text{ and } k = -1 & \text{if } i_{sc} < 0 \end{cases}$$

where α_{dc} is the equivalent value of the duty cycle and k defines the flow direction of current i_{sc} .

Using this definition, for the hybrid parallel connection to a non-reversible boost converter (for the FC), the equations of the non-linear average model (given in equations (5.3.3.2)) for I_{sc} and V_C are modified as follows:

$$\begin{aligned} \frac{dI_{sc}}{dt} &= \frac{1}{L_{sc}} [V_{sc} - R_{sc} I_{sc} - \alpha_{sc} V_C] \\ \frac{dV_C}{dt} &= \frac{1}{C} [(1 - \alpha_{fc}) I_{fc} + \alpha_{sc} I_{sc} - i_{load}] \end{aligned} \quad (4.13)$$

The new linearized state-space model for this system is similar to model in (4.3) but with the following state-space matrices:

$$A = \begin{bmatrix} -\frac{1}{R_{tc}C_c} & 0 & \frac{1}{C_c} & 0 & 0 & 0 \\ 0 & -\frac{1}{R_{ta}C_a} & \frac{1}{C_a} & 0 & 0 & 0 \\ -\frac{1}{L_{fc}} & -\frac{1}{L_{fc}} & -\frac{R_m+R_L}{L_{fc}} & 0 & 0 & -\frac{(1-\alpha_{fce})}{L_{fc}} \\ 0 & 0 & 0 & -\frac{R_{sc}}{L_{sc}} & \frac{1}{L_{sc}} & -\frac{\alpha_{scee}}{L_{sc}} \\ 0 & 0 & 0 & \frac{1}{C_{sc}} & 0 & 0 \\ 0 & 0 & \frac{(1-\alpha_{fce})}{C} & \frac{\alpha_{scee}}{C} & 0 & 0 \end{bmatrix}$$

$$B_1 = \left[0 \ 0 \ 0 \ 0 \ 0 \ -\frac{1}{C}\right]^T, \quad B_2 = \begin{bmatrix} 0 & 0 & \frac{V_{Ce}}{L_{fc}} & 0 & 0 & -\frac{I_{fce}}{C} \\ 0 & 0 & 0 & -\frac{V_{Ce}}{L_{sc}} & 0 & -\frac{I_{scee}}{C} \end{bmatrix}^T$$

The validation of this model with the reversible converter for the auxiliary source through simulations and comparisons with the switched topological model is presented in Figures 4.21, 4.22 and 4.23 for the output DC bus voltage and the FC and SC currents respectively. In these simulation load steps of +50%, -100% and +50% are subsequently applied at times $t = 0s$, $t = 0.05s$ and $t = 0.15s$. Only the first seconds of the dynamic response are presented. As in the previous case, the average model perfectly represents the dynamics of the hybrid system.

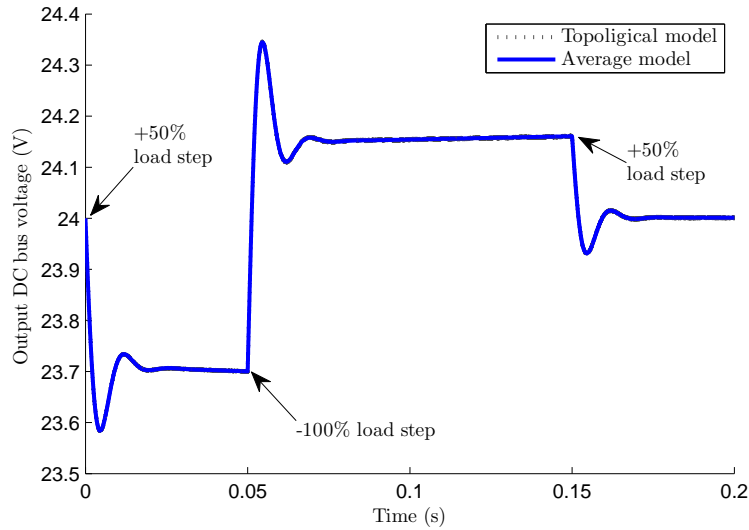


Figure 4.21: Output DC bus voltage responses using a reversible converter for the SC.

4.3.4 Voltage inverter for network connection

To achieve connection of the hybrid generator to an AC network, a power inverter is now considered. The complete topology considered with a voltage inverter and a reversible boost converter for the auxiliary source is presented in Figure 4.24. The topology shown has an AC filter, composed by a series resistance/inductance and a shunt capacitor, connected to an AC isolated load. However, connection to the network is possible and the

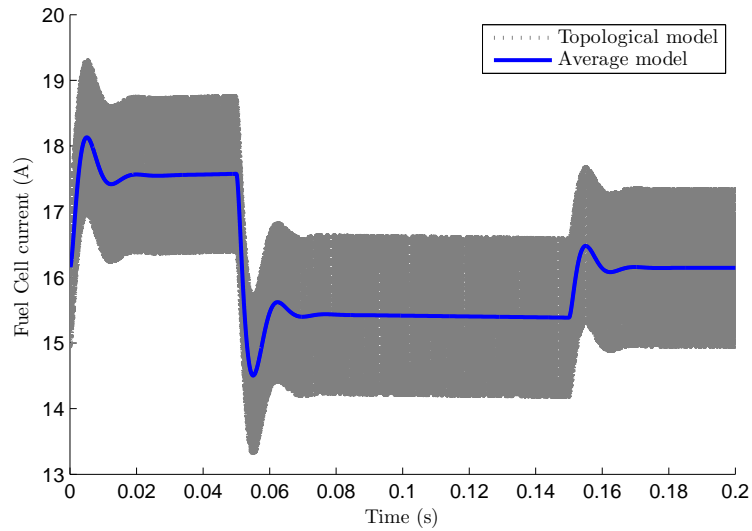


Figure 4.22: Fuel cell current responses using a reversible converter for the SC.

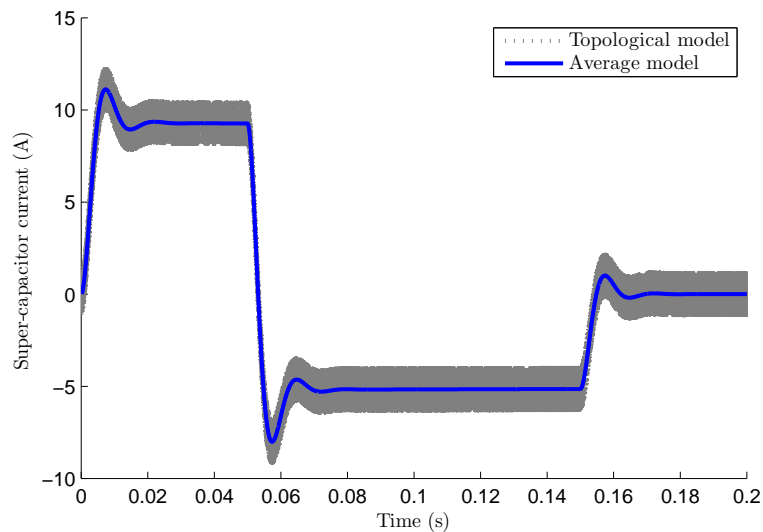


Figure 4.23: Super-capacitor current responses using a reversible converter for the SC.

AC filter can be modified to correspond with the desired application. For simplicity, only the hybrid generator operating with an isolated load is studied, this case is considered sufficient here for illustrating the control strategies proposed. For a detailed review on integration structures of power generators using several structures of power converters see [Gaztañaga, 2006].

4.3.4.1 Inverter model

Again the non-linear average model is used and obtained from the topological model of the voltage inverter. A detailed exposition of inverter equations using average modeling is presented in [Gombert, 2005]. The topological model consider the switching functions of the converter that in this case is composed by signals u_1 , u_2 and u_3 with values between

+1 and -1. The state $u_1 = 1$ indicates a closed switch position, at this time the complementary signal will be $\bar{u}_1 = -1$, indicating an open position. The relationship between the switching functions, DC and AC voltages is given by equation (4.14).

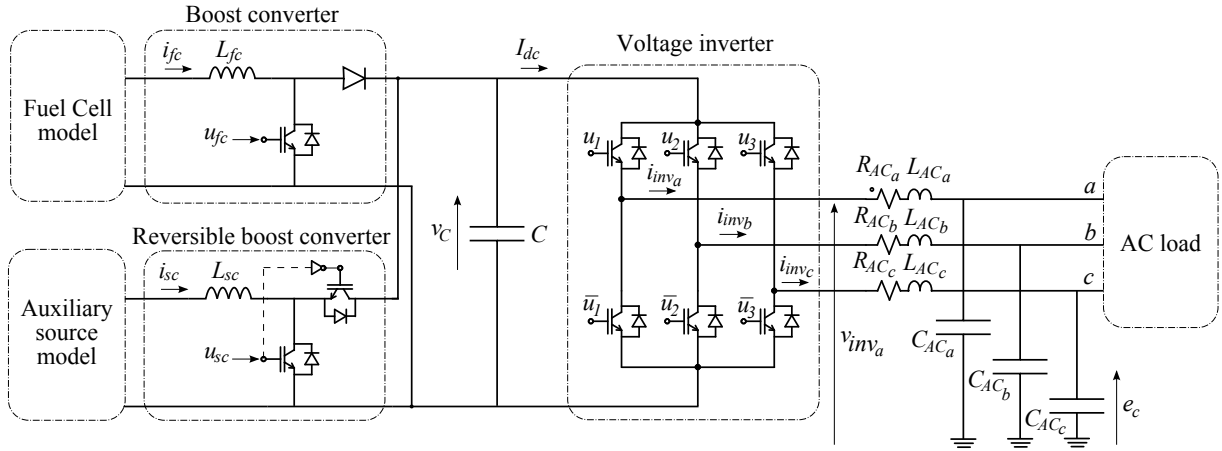


Figure 4.24: Hybrid topology with voltage inverter.

$$\begin{bmatrix} v_{inv_a} \\ v_{inv_b} \\ v_{inv_c} \end{bmatrix} = \frac{1}{6} \begin{bmatrix} 2u_1 - u_2 - u_3 \\ -u_1 + 2u_2 - u_3 \\ -u_1 - u_2 + 2u_3 \end{bmatrix} V_C \quad (4.14)$$

The relationship between the three-phase currents and the DC current I_{dc} is given by equation (4.15). This equation considers that the zero component of the current is null.

$$I_{dc} = \frac{1}{2} \begin{bmatrix} u_1 & u_2 & u_3 \end{bmatrix} \begin{bmatrix} \dot{i}_{inv_a} \\ \dot{i}_{inv_b} \\ \dot{i}_{inv_c} \end{bmatrix} \quad (4.15)$$

Applying the Park coordinates transformation to these equation and considering average values of system variables, equations (4.14) and (4.15) gives the desired model of the voltage inverter:

$$\begin{cases} \begin{bmatrix} V_{inv_d} \\ V_{inv_q} \end{bmatrix} = \frac{1}{2} \begin{bmatrix} \beta_d \\ \beta_q \end{bmatrix} V_C \\ I_{dc} = \frac{3}{4} \begin{bmatrix} \beta_d & \beta_q \end{bmatrix} \begin{bmatrix} I_{inv_d} \\ I_{inv_q} \end{bmatrix} \end{cases} \quad (4.16)$$

where uppercases represents average-valued variables and β_i is the average value of switching function u_i .

Let us now describe the equations associated with the AC filter presented in Figure 4.24. The dynamic equation system is composed by equations of active components L_{AC} and C_{AC} . The system is given equations (4.17).

$$\begin{aligned}\frac{d\mathbf{i}_{inv_{abc}}}{dt} &= -\frac{R_{AC}}{L_{AC}}\mathbf{i}_{inv_{abc}} - \frac{1}{L_{AC}}\mathbf{e}_{abc} + \frac{1}{L_{AC}}\mathbf{v}_{inv_{abc}} \\ \frac{d\mathbf{e}_{abc}}{dt} &= \frac{1}{C_{AC}}\mathbf{i}_{inv_{abc}} - \frac{1}{C_{AC}}\mathbf{i}_{load_{abc}}\end{aligned}\quad (4.17)$$

with \mathbf{e}_{abc} the voltage vector at the terminals of capacitors $C_{AC_{abc}}$ and where:

$$\mathbf{i}_{inv_{abc}} = [I_{inv_a} \quad I_{inv_b} \quad I_{inv_c}]^T \quad (4.18)$$

$$\mathbf{v}_{inv_{abc}} = [V_{inv_a} \quad V_{inv_b} \quad V_{inv_c}]^T \quad (4.19)$$

$$\mathbf{e}_{abc} = [E_a \quad E_b \quad E_c]^T \quad (4.20)$$

As before, using the Park transformation of coordinates in a rotating reference frame, the complete inverter non-linear average model becomes:

$$\begin{aligned}\frac{dI_{inv_d}}{dt} &= -\frac{R_{AC}}{L_{AC}}I_{inv_d} - \frac{1}{L_{AC}}E_d + \frac{1}{L_{AC}}\frac{V_C}{2}\beta_d + I_{inv_q}\omega_{net} \\ \frac{dI_{inv_q}}{dt} &= -\frac{R_{AC}}{L_{AC}}I_{inv_q} - \frac{1}{L_{AC}}E_q + \frac{1}{L_{AC}}\frac{V_C}{2}\beta_q - I_{inv_d}\omega_{net} \\ \frac{dE_d}{dt} &= \frac{1}{C_{AC}}I_{inv_d} - \frac{1}{C_{AC}}I_{load_d} + E_q\omega_{net} \\ \frac{dE_q}{dt} &= \frac{1}{C_{AC}}I_{inv_q} - \frac{1}{C_{AC}}I_{load_q} - E_d\omega_{net}\end{aligned}\quad (4.21)$$

where ω_{net} is the AC system frequency.

4.3.4.2 A new data set for the inverter system

There is an important limitation for the voltage inverter and the maximum power that it can supply to the AC application. Actually, given a voltage drop on the AC filter, there is a limitation on the DC bus voltage according to the following equation [Valero, 2004] :

$$\frac{2V_C}{3} \geq \sqrt{(V_{net_{max}} + L_{AC}\omega_{net}I_{inv_{max}} \sin(\varphi))^2 + (L_{AC}\omega_{net}I_{inv_{max}} \cos(\varphi))^2} \quad (4.22)$$

where $V_{net_{max}}$ is the peak network voltage, φ is the loading angle, ω_{net} is the network frequency and $I_{inv_{max}}$ the maximum possible current at the inverter arms.

This means that with the generator system provided before with a 24V nominal DC bus voltage, it is not possible to achieve a conversion to typical AC low voltage values. To comply with a network voltage operating at 230V, it was decided to consider a second data set for the entire hybrid generation system. The new data used corresponds to the system parameters of a setup located at G2ELab in Grenoble called the “*universal*” test-bench. The inverter data is presented in [Valero, 2004] and [Tritschler, 2010], and the boost converters data can be found in the test-bench data-sheet. The system topology is exactly the same as in Figure 4.24.

The DC bus of the new data system is fixed at 400V to comply with equation (4.22) and with the bus converter voltage limitations.

The new data system is described as follows:

- **Fuel cell data:** The FC data is taken from [Pukrushpan et al., 2004a] and corresponds to a PEMFC with a nominal power of 10kW and 312 cells. Given the current limitation on the boost converter at 50A, the cell active area is fixed at 75cm². A simple electrical equivalent model of the FC is used with a single double layer capacitance $C_{dl} = 5\text{mF}$, a parallel resistance (representing activation and concentration losses) $R_t = 0.1415\Omega$ and a membrane resistance $R_m = 0.8490\Omega$. The open-circuit voltage is given by $E_0 = 245\text{V}$.
- **Auxiliary source:** For the auxiliary source a capacitor with the exact characteristics of the 58F Maxwell© capacitor is considered. However, from voltage limitations, a series-connected 10-cell capacitor pack is studied.
- **Boost converter data:** The boost converter inductance for the FC is given by $L_{fc} = 6\text{mH}$. The complementary reversible boost converter has an inductance $L_{sc} = 0.82\text{mH}$. Finally, the DC bus capacitor filter is fixed as $C = 2200\mu\text{F}$.
- **Inverter and AC filter data:** The inverter switch configuration is realized from a 6 IGBT arrangement (50A, 1200V and 10kHz). The AC filter parameters are: $R_{AC} = 0.0286\Omega$, $L_{AC} = 3\text{mH}$ and $C_{AC} = 100\mu\text{F}$ per-phase.

With these parameters the topological and non-linear average models of the voltage inverter were simulated. The Figure 4.25 compares the output AC currents of both models for an operating point of 5.25kW with the FC supplying 40A. A +25% load step at $t = 30.02\text{s}$ is simulated. An good model correspondance is obtained.

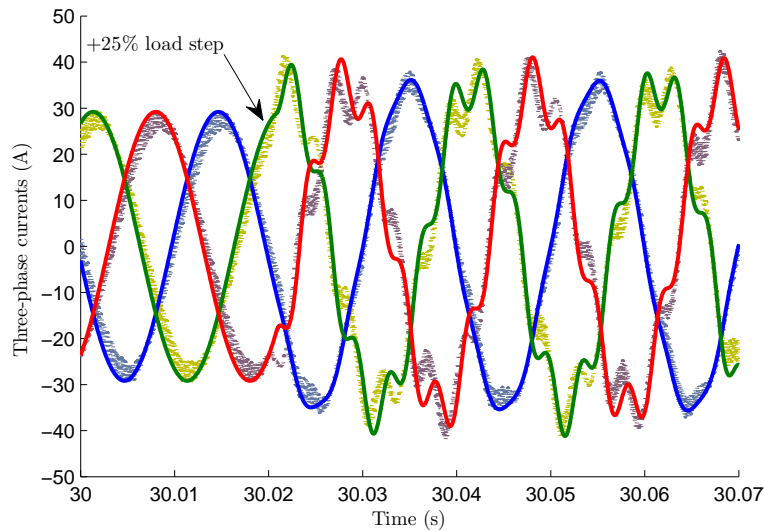


Figure 4.25: AC currents comparison using the topological model (dotted light-colored) and the non-linear average model (continuous dark lines).

4.3.4.3 Linear average state-space model

With the fixed operating conditions described before, the model is now linearized for control purposes.

The linear state-space description is defined by:

$$\begin{aligned}\Delta\dot{x} &= A\Delta x + B_1\Delta\omega + B_2\Delta u \\ \Delta x &= [\Delta I_{inv_d} \quad \Delta I_{inv_q} \quad \Delta E_d \quad \Delta E_q]^T \\ \Delta u &= [\Delta\beta_d \quad \Delta\beta_q \quad \Delta V_C]^T, \Delta\omega = \Delta I_{load_q}\end{aligned}\tag{4.23}$$

with:

$$A = \begin{bmatrix} -\frac{R_{AC}}{L_{AC}} & \omega_{net} & -\frac{1}{L_{AC}} & 0 \\ -\omega_{net} & -\frac{R_{AC}}{L_{AC}} & 0 & -\frac{1}{L_{AC}} \\ \frac{1}{C_{AC}} & 0 & 0 & \omega_{net} \\ 0 & \frac{1}{C_{AC}} & -\omega_{net} & 0 \end{bmatrix}$$

$$B_1 = \begin{bmatrix} 0 & 0 & -\frac{1}{C_{AC}} & 0 \end{bmatrix}^T, B_2 = \begin{bmatrix} \frac{V_{C_e}}{2L_{AC}} & 0 & 0 & 0 \\ 0 & \frac{V_{C_e}}{2L_{AC}} & 0 & 0 \\ \frac{\beta_d}{2L_{AC}} & \frac{\beta_q}{2L_{AC}} & 0 & 0 \end{bmatrix}^T$$

In this system the convention of fixed $E_{de} = 0$ and $I_{inv_{de}} = 0$ is used. The operating conditions are computed with $E_{qe} = \sqrt{3}v_{net}$ and $I_{inv_{qe}} = \sqrt{3}i_{load}$, where v_{net} is the network RMS line-to-line voltage and current i_{load} is given by:

$$i_{load} = \frac{P_{load}}{\sqrt{3}v_{net} \cos \varphi}\tag{4.24}$$

where $\cos \varphi$ is the power factor of the load and P_{load} is the three-phase active load in W.

For the given system parameters and a three-phase loading condition of 5.25kW at $\cos \varphi = 0.9$ inductive, the bode plot of transfer functions of V_C from β_d , β_q and i_{load_q} is presented in Figure 4.26. In these plots it can be seen that, in contrast with the bode plot of the hybrid system without reversible converter (Figure 4.18), the hybrid system with inverter does not has a “natural” disturbance rejection due to high gain values at lower frequencies in the transfer function of V_C from i_{load_q} .

4.4 Fuel cell system

We are now interested in the whole FC system modeling for centralized control strategies that will be presented in chapter 5. Then a reduced 4th order model of the Polymer Electrolyte Membrane or Proton Exchange Membrane (PEM) Fuel Cell (FC) system is presented. Previously a simplified electric equivalent circuit model for the FC stack was considered, but now a control-oriented dynamic non-linear model is presented. The complete model of the FC system includes the thermodynamical system interactions of the FC that contains the reactant (hydrogen and oxygen) flow, heat/temperature, water and power management subsystems. This complete model of the FC system is presented

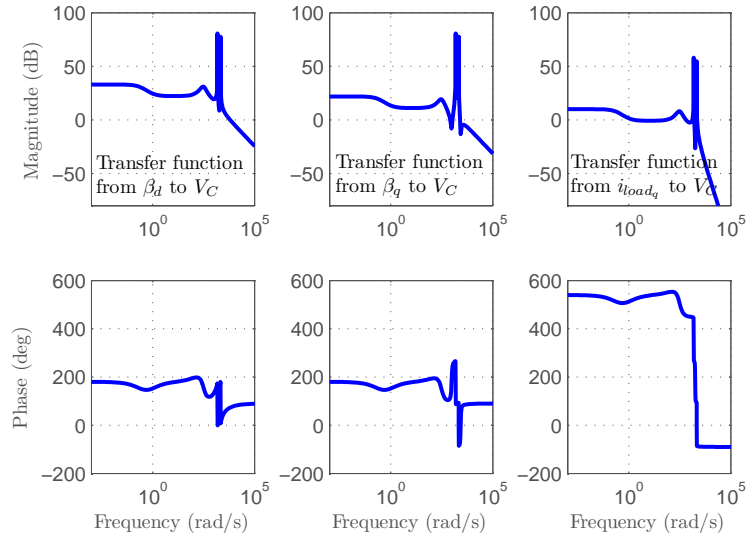


Figure 4.26: Bode plot of the open-loop hybrid system with inverter.

by [Pukrushpan et al., 2004a]. In that work a non-linear model of the PEMFC is proposed for modeling an automotive fuel cell propulsion system. The subsequent works of [Suh, 2006] and [Talj et al., 2009] are considered for a control-oriented model of the FC system, which is a reduced order version of the model proposed by [Pukrushpan et al., 2004a].

In any case, if the PEMFC system is to be used as stationary power source (distributed generation) or as a mobile or vehicle transportation technology, the system should adapt to fast changes in load demand, so modeling and control over varying operating conditions is a critical issue. The reduced order model presented in this section involves thermodynamic parameter modeling, such as reactant flows and pressures.

The PEMFC system includes the Stack Voltage dynamic itself as well as the auxiliary FC dynamics, i.e. compressor and manifold dynamics. In this section the same division is used to present the whole FC system, first the stack voltage model is presented followed by the FC reduced order dynamic equation system. As it will be presented in this section, the core of the auxiliary system model is the air supply model. The FC dynamic is highly coupled with the air pressure dynamic, for this reason a focus is given here on the model of the key component of the air supply system, the compressor-motor dynamic. Static and dynamic models of the compressor-motor system are presented. Finally the reduced order model is completely validated through real test-bench measures. The results for model validation and identification are presented.

4.4.1 Fuel cell stack

As described before, a FC stack is composed by a series connexion of individual cells. When an electrical current is drawn from the stack a voltage drop occurs due to *Polarization*. In the static V-I polarization characteristic of the FC stack, the voltage decreases most importantly due to three factors: activation losses, ohmic losses and transportation losses. Figure 4.27 show the polarization curve of the FC stack of 475W indicating the different associated losses.

The polarization curve is presented in terms of the cell voltage and the current density,

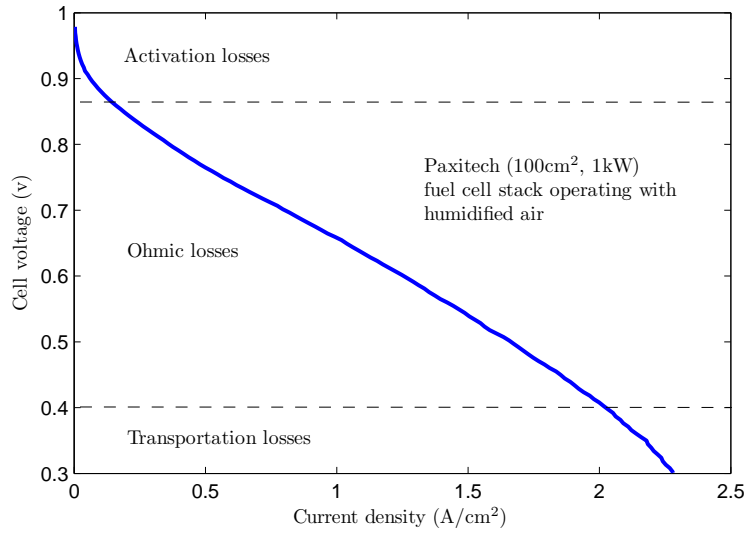


Figure 4.27: A typical polarization curve with different fuel cell losses.

which is given by:

$$i = \frac{I_{st}}{A_{fc}} \quad (4.25)$$

where the stack electrical current I_{st} in Ampères, the per cell active area A_{fc} in cm^2 .

The stack model used in this thesis is presented in the work of [Pukrushpan et al., 2004a]. This static model is given in the form:

$$\begin{aligned} v_{fc} &= E - v_{act} - v_{ohm} - v_{conc} \\ &= E - [v_0 + v_a (1 - e^{-c_1 i})] - [i R_{ohm}] - \left[i \left(c_2 \frac{i}{i_{max}} \right)^{c_3} \right] \end{aligned} \quad (4.26)$$

where the equation parameters can be found through a non-linear regression from measured data on the real FC stack.

Let us now introduce the dynamic system of equations.

4.4.2 A reduced order dynamic model of FC system

In the FC system, parameters as the stack and anode/cathode temperature, the supply oxidant pressures, or the membrane hydration are critical to proper operation of the FC and to avoid cell degradation. Only the water content (humidity) could directly affect FC performance, efficiency and durability. Problems on the stability analysis of water accumulation or the oxygen starvation are presented in [McCain et al., 2008] and [Pukrushpan et al., 2004b] respectively, remarking the importance of a proper modeling of these parameters dynamics. Even though these parameters are not considered as *dynamic* variables in the reduced order model presented in this thesis, their steady-state values are used to compute the reduced order model parameters. To better understand the dynamical models presented in this section, a summary of some thermo-dynamical principles is presented in Appendix C.

As presented before, the reduced 4th order control-oriented model described here was developed in [Suh, 2006] and [Talj et al., 2009], as a manipulation of the complete 9th order model presented in [Pukrushpan et al., 2004a].

In this reduced order model it is assumed that:

- All gases respect the ideal gas law.
- The stack temperature and the reactant humidification are perfectly externally-controlled.
- The hydrogen pressure is perfectly controlled.
- The water content in the gas diffusion layer is neglected.

4.4.2.1 Dynamic equations of cathode pressures

From these assumptions and respecting the mass conservation principle, the rate of change in oxygen and nitrogen species mass in the FC cathode can be computed with:

$$\frac{dm_{O_2,ca}}{dt} = W_{O_2,ca,in} - W_{O_2,ca,out} - W_{O_2,reacted} \quad (4.27)$$

$$\frac{dm_{N_2,ca}}{dt} = W_{N_2,ca,in} - W_{N_2,ca,out} \quad (4.28)$$

In these equations:

$W_{O_2,ca,in}$ is the input oxygen mass flow rate.

$W_{O_2,ca,out}$ is the output oxygen mass flow rate.

$W_{O_2,reacted}$ is the amount of oxygen mass flow rate used in the reaction.

$W_{N_2,ca,in}$ is the input nitrogen mass flow rate.

$W_{N_2,ca,out}$ is the output nitrogen mass flow rate.

We now compute partial pressures using:

$$p_{O_2,ca} = \frac{m_{O_2,ca} \mathcal{R} T_{st}}{V_{ca}} \quad (4.29)$$

$$p_{N_2,ca} = \frac{m_{N_2,ca} \mathcal{R} T_{st}}{V_{ca}} \quad (4.30)$$

Then, the dry air pressure in the cathode is given by:

$$p_{a,ca} = p_{O_2,ca} + p_{N_2,ca} \quad (4.31)$$

With these equations and keeping the same notation as in [Suh, 2006], the dynamic state variables of the cathode dynamics are p_{O_2} and p_{N_2} . With these assumptions, equations (4.27) and (4.28) become:

$$\frac{dp_{O_2}}{dt} = \frac{\mathcal{R}T_{st}}{\mathcal{M}_{O_2}V_{ca}}(W_{O_2,ca,in} - W_{O_2,ca,out} - W_{O_2,reacted}) \quad (4.32)$$

$$\frac{dp_{N_2}}{dt} = \frac{\mathcal{R}T_{st}}{\mathcal{M}_{N_2}V_{ca}}(W_{N_2,ca,in} - W_{N_2,ca,out}) \quad (4.33)$$

where \mathcal{R} is the universal gas constant, T_{st} is the stack temperature, \mathcal{M}_{O_2} and \mathcal{M}_{N_2} are the molar mass of oxygen/nitrogen and V_{ca} is the cathode volume.

4.4.2.2 Computing the static oxygen excess ratio

With the dynamic values of partial pressures p_{O_2} and p_{N_2} , the oxygen excess ratio can be computed using several non-linear static relationships. The utility of computing the oxygen excess ratio for control purposes will be presented later in the next chapter.

We compute now the inlet flow properties $W_{O_2,ca,in}$ and $W_{N_2,ca,in}$. The air partial pressure is assumed equivalent to the cathode pressure (perfect humidification control), i.e. Pukrushpan et al. [2004a]:

$$p_{a,ca,in} = p_{ca,in} \quad (4.34)$$

The vapor pressure is computed by:

$$p_{v,ca} = \phi_{atm}p_{sat}(T_{st}) \quad (4.35)$$

where $\phi_{atm} = 0.5$ is the relative atmospheric humidity

And the air molar mass:

$$\mathcal{M}_{a,ca,in} = y_{0_2,atm} \times \mathcal{M}_{O_2} + (1 - y_{0_2,atm}) \times \mathcal{M}_{N_2} \quad (4.36)$$

where $y_{0_2,atm} = 0.21$ is the oxygen molar ratio. Finally the inlet flows are calculated.

The humidity ratio is defined as:

$$w_{ca} = \frac{\mathcal{M}_v}{\mathcal{M}_{a,ca,in}} \frac{p_{v,ca}}{p_{a,ca}} \quad (4.37)$$

The different gases flow rates are computed as:

- Air input flow:

$$W_{a,ca,in} = \frac{1}{1 + w_{ca}} W_{ca,in} \quad (4.38)$$

- Oxygen input flow:

$$W_{O_2,ca,in} = x_{O_2,atm} W_{a,ca,in} \quad (4.39)$$

- Nitrogen input flow:

$$W_{N_2,ca,in} = (1 - x_{O_2,atm})W_{a,ca,in} \quad (4.40)$$

where:

$$x_{O_2,atm} = \frac{y_{O_2,atm} \times \mathcal{M}_{O_2}}{y_{O_2,atm} \times \mathcal{M}_{O_2} + (1 - y_{O_2,atm}) \times \mathcal{M}_{N_2}} \quad (4.41)$$

At the end, using electro-chemistry principles, and given the stack electrical current I_{st} as an input, we compute the oxygen mass flow rate used in the reaction and the vapor mass flow rate generated in the reaction:

$$W_{O_2,reacted} = \mathcal{M}_{O_2} \times \frac{nI_{st}}{4F} \quad (4.42)$$

In these equations n is the number of cells in the stack and F is the Faraday number ($F = 96,485$ Coulombs).

With these definitions, computation of air pressure and flow is possible. Finally an important performance parameter, the oxygen excess ratio λ_{O_2} , can be defined:

$$\lambda_{O_2} = \frac{W_{O_2,ca,in}}{W_{O_2,reacted}} \quad (4.43)$$

4.4.2.3 Dynamic equation of the supply manifold

The manifold model represents the dynamics associated with the pipes and connections between devices in the fuel cell system. The manifold dynamic model is presented as a block diagram in Figure 4.28. The pressure dynamics models of the supply manifold is presented in detail in both [Pukrushpan et al., 2004a] and [Gasser, 2006].

As before, the mass conservation principle holds:

$$\frac{dm}{dt} = W_{in} - W_{out} \quad (4.44)$$

Then, using the ideal gas equation:

$$\frac{dp_{sm}}{dt} = \frac{\mathcal{R}_a T_{cp}}{V_{sm}} (W_{cp} - W_{ca,in}) \quad (4.45)$$

where W_{cp} is the compressor air flow in kg/s, V_{sm} is the supply manifold volume in m³ and T_{cp} the temperature from the air compressor which will be defined hereafter.

We now define the air flow at the cathode output which is described using the nozzle flow equation, represented by the upstream pressure p_{ca} , the upstream temperature T_{cp} and the downstream pressure p_{atm} . There are two regions in the nozzle flow characteristic, divided by:

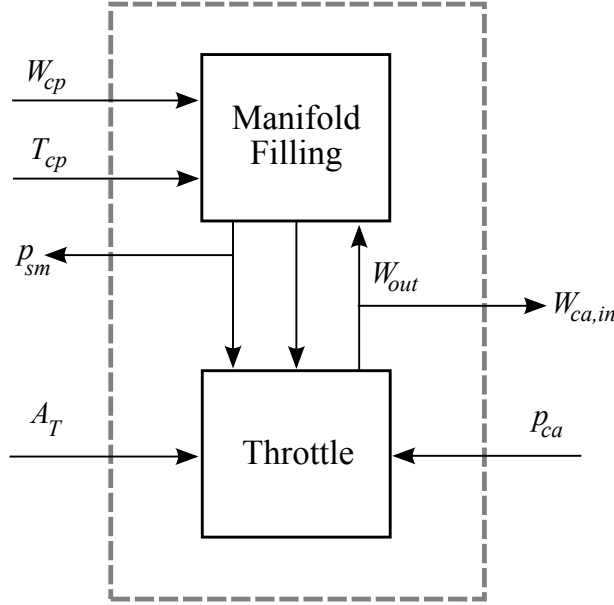


Figure 4.28: Manifold model block diagram proposed in [Pukrushpan et al., 2004a].

$$\left(\frac{p_{atm}}{p_{ca}} \right)_{crit} = \left(\frac{2}{\gamma + 1} \right)^{\frac{\gamma}{\gamma - 1}} \quad (4.46)$$

This critical value divides the characteristic nozzle flow region in critical region and sub-critical region.

For the sub-critical region where $(p_{atm}/p_{ca}) > (p_{atm}/p_{ca})_{crit}$, the flow is defined by:

$$W_{ca,in} = \frac{C_D A_T p_{ca}}{\sqrt{\mathcal{R} T_{st}}} \left(\frac{p_{atm}}{p_{ca}} \right)^{1/\gamma} \left\{ \frac{2\gamma}{\gamma - 1} \left[1 - \left(\frac{p_{atm}}{p_{ca}} \right)^{\frac{\gamma-1}{\gamma}} \right] \right\}^{1/2} \quad (4.47)$$

with C_D the discharging coefficient, A_T the opening area of the nozzle in m^2 , γ the ratio of specific heats of the gas at constant pressure C_p/C_v (equal to 1.4 for air), p_{atm} the atmospheric pressure and T_{st} the stack temperature in $^{\circ}K$.

For the critical region where $(p_{atm}/p_{ca}) \leq (p_{atm}/p_{ca})_{crit}$, the flow is defined by:

$$W_{ca,in} = \frac{C_D A_T p_{ca}}{\sqrt{\mathcal{R} T_{st}}} \gamma^{1/2} \left(\frac{2}{\gamma + 1} \right)^{\frac{\gamma+1}{2(\gamma-1)}} \quad (4.48)$$

However, if the pressure difference is small and **always** fall within the sub-critical region, then a linear approximation is possible, as it is the case with the air flow entering the cathode from the supply manifold:

$$W_{ca,in} = k_{ca,in} (p_{sm} - p_{ca}) \quad (4.49)$$

4.4.2.4 Compressor model

Compressor modeling is somehow considered as the core of the fuel cell model. Two proposed models are presented in the following sections. First, the non-linear model proposed by [Pukrushpan et al., 2004a], and secondly, a linear model is proposed by [Gasser, 2006].

(a) Compressor model proposed by [Pukrushpan et al., 2004a]

The compressor model presented here is a non-linear compressor model proposed by [Pukrushpan et al., 2004a]. The block diagram representation of this model is shown in Figure 4.29.

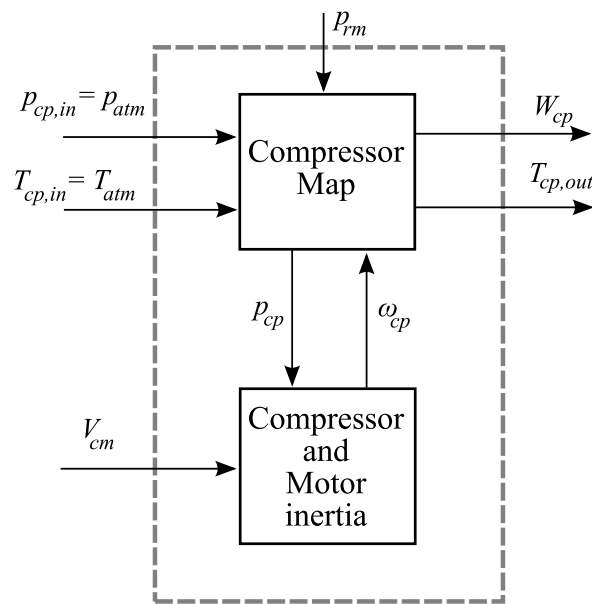


Figure 4.29: Compressor model block diagram [Pukrushpan et al., 2004a].

The compressor model is composed by a static compressor map, used to determinate the air flow rate through the compressor, and by a dynamic model of the system inertia, which determines the compressor speed used to find the air flow rate. The state in the model is the compressor speed ω_{cp} . The inputs to the model are the air pressure p_{atm} and temperature T_{atm} (atmospheric), the supply manifold pressure p_{sm} (downstream pressure) and the voltage command of the compressor voltage v_{cm} .

The compressor flow map can be normally found in the device manufacturer data-sheet. In [Pukrushpan et al., 2004a] the Jensen & Kristensen map regression method is presented to compute the compressor air flow rate, avoiding the use of look-up tables (not suitable for simulations). This method is presented with details in [Pukrushpan et al., 2004a] and the air flow rate W_{cp} is computed using a regression algorithm on the compressor map and the compressor diameter d_c in m, the air density ρ_a in kg/m^3 , and the air gas constant \mathcal{R}_a .

A look-up table is used to obtain the compressor efficiency η_{cp} . Then the temperature of the air leaving the compressor is then computed by:

$$T_{cp} = T_{atm} + \frac{T_{atm}}{\eta_{cp}} \left[\left(\frac{p_{sm}}{p_{atm}} \right)^{\frac{\gamma-1}{\gamma}} - 1 \right] \quad (4.50)$$

Then the torque required to drive the compressor, is given by:

$$\tau_{cp} = \frac{C_p}{\omega_{cp}} \frac{T_{atm}}{\eta_{cp}} \left[\left(\frac{p_{sm}}{p_{atm}} \right)^{\frac{\gamma-1}{\gamma}} - 1 \right] W_{cp} \quad (4.51)$$

where the torque τ_{cp} is in N.m and C_p is the specific heat capacity of the air equals $1004 \text{ J.kg}^{-1}.\text{°K}^{-1}$. Both the temperature equation (4.50) and the torque equation (4.51) of the compressor are derived from turbine literature. The dynamic speed-inertia equation is given by:

$$J_{cp} \frac{d\omega_{cp}}{dt} = (\tau_{cm} - \tau_{cp}) \quad (4.52)$$

with J_{cp} the combined compressor and motor inertia in kg.m^2 , ω_{cp} the compressor speed in rad/sec, and τ_{cm} the compressor motor torque input.

Substituting equation (4.50) into equation (4.45) yields to the final expression for the supply manifold dynamic.

Today the use of permanent magnet DC motor is attractive due to efficiency and performance. In that case the voltage equation for the DC machine is:

$$v_{cm} = i_{cm} R_{cm} + v_{cm,ind} \quad (4.53)$$

The induced voltage and torque τ_{cm} are given by:

$$v_{cm,ind} = k_v \omega_{cp} \quad (4.54)$$

$$\tau_{cm} = k_t i_{cm} \quad (4.55)$$

(b) Compressor model proposed by [Gasser, 2006]

The compressor model presented in this section is a linear compressor model proposed in [Gasser, 2006]. The diagram representation of this model is shown in Figure 4.30.

The voltage equation of the circuit is given by:

$$v_{cm} = L_{cm} \frac{di_{cm}}{dt} + R_{cm} i_{cm} + k_m \omega_{cp} \quad (4.56)$$

The torque equation of the system is given by equation (4.52) and the DC machine torque equation is given by equation (4.55), as the DC machine of the compressor-motor proposed in [Gasser, 2006] is also a permanent magnet DC motor.

The torque of the compressor is obtained by:

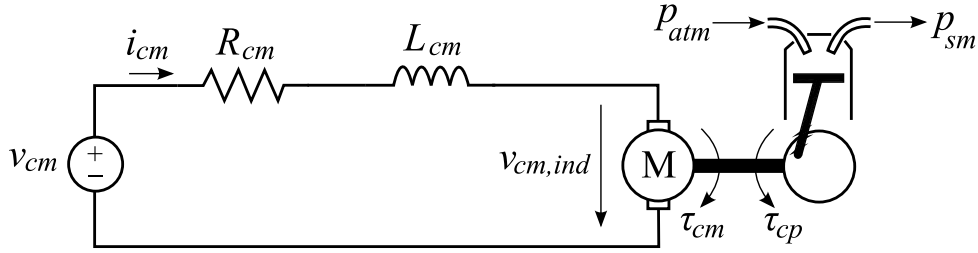


Figure 4.30: Compressor model diagram [Gasser, 2006].

$$\tau_{cp} = k_p(p_{atm} - p_{sm}) \quad (4.57)$$

For the compressor characteristic, the relationship between the output mass flow rate W_{cp} and the compressor speed ω_{cp} is assumed to be linear by a factor $k_{m,cp}$. A friction torque $\tau_{fric} = k_f\omega_{cp}$ is also considered in the equations. The complete linear model for the compressor-motor system is given by:

$$\begin{bmatrix} \frac{di_{cm}}{dt} \\ \frac{d\omega_{cp}}{dt} \\ \frac{dp_{sm}}{dt} \end{bmatrix} = \begin{bmatrix} -\frac{R_{cm}}{L_{cm}} & -\frac{k_e}{L_{cm}} & 0 \\ \frac{k_t}{J_{cp}} & -\frac{k_d}{J_{cp}} & -\frac{k_p}{J_{cp}} \\ 0 & \frac{\mathcal{R}T k_{m,cp}}{V_{sm}\mathcal{M}_{air}} & -\frac{\mathcal{R}T}{V_{sm}\mathcal{M}_{air}k_h} \end{bmatrix} \begin{bmatrix} i_{cm} \\ \omega_{cp} \\ p_{sm} \end{bmatrix} \quad (4.58)$$

$$+ \begin{bmatrix} \frac{1}{L_{cm}} & 0 \\ 0 & \frac{k_p}{J_{cp}} \\ 0 & \frac{\mathcal{R}T}{V_{sm}\mathcal{M}_{air}k_h} \end{bmatrix} \begin{bmatrix} v_{cm} \\ p_{atm} \end{bmatrix}$$

The system output is:

$$\begin{bmatrix} W_{cp} \\ p_{sm} \end{bmatrix} = \begin{bmatrix} 0 & k_{m,cp} & 0 \\ 0 & 0 & 1 \end{bmatrix} \begin{bmatrix} i_{cm} \\ \omega_{cp} \\ p_{sm} \end{bmatrix} \quad (4.59)$$

4.4.2.5 Resuming a non-linear system of equations

The system equations are now resumed using exactly the same system notation as in [Talj et al., 2009], which is a more simplistic presentation designed for control purposes. The non-linear system of equations is composed by the re-arrangement of equations 4.32, 4.33, 4.45 and 4.52.

With the new notation the system is given in the form:

$$\dot{x} = f(x) + g_u u + g_\xi \xi \quad (4.60)$$

where the state vector is given by:

$$x = [x_1 \ x_2 \ x_3 \ x_4]^T = [p_{O_2} \ p_{N_2} \ \omega_{cp} \ p_{sm}]^T \quad (4.61)$$

and corresponding inputs are, u the compressor-motor voltage v_{cm} and ξ the fuel cell stack current.

Note that the dynamic variable for i_{cm} is not considered in this non-linear representation. The resumed system equations are given by:

$$\begin{aligned} \dot{x}_1 &= c_1(-x_1 - x_2 + x_4 - c_2) - \frac{c_3 x_1 \psi(x_1, x_2)}{c_4 x_1 + c_5 x_2 + c_6} - c_7 \xi \\ \dot{x}_2 &= c_8(-x_1 - x_2 + x_4 - c_2) - \frac{c_3 x_2 \psi(x_1, x_2)}{c_4 x_1 + c_5 x_2 + c_6} \\ \dot{x}_3 &= -c_9 x_3 - \frac{c_{10}}{x_3} \left[\left(\frac{x_4}{c_{11}} \right)^{c_{12}} - 1 \right] h_3(x_3, x_4) + c_{13} u \\ \dot{x}_4 &= c_{14} \left[1 + c_{15} \left[\left(\frac{x_4}{c_{11}} \right)^{c_{12}} - 1 \right] \right] [h_3(x_3, x_4) - c_{16} (-x_1 - x_2 + x_4 - c_2)] \end{aligned} \quad (4.62)$$

with:

$$\begin{aligned} \psi(x_1, x_2) &= \begin{cases} c_{17}(x_1 + x_2 + c_2) \left(\frac{c_{11}}{x_1 + x_2 + c_2} \right)^{c_{18}} \sqrt{1 - \left(\frac{c_{11}}{x_1 + x_2 + c_2} \right)^{c_{12}}} & \text{for } \zeta > c_{19} \\ c_{20}(x_1 + x_2 + c_2) & \text{for } \zeta \leq c_{19} \end{cases} \\ \zeta &= \frac{c_{11}}{x_1 + x_2 + c_2} \end{aligned}$$

The performance output z for this system is given by:

$$z = \begin{bmatrix} y_1 \xi - c_{21} u (u - c_{22} x_3) \\ \frac{c_{23}}{c_{24} \xi} (x_4 - x_1 - x_2 - c_2) \end{bmatrix} \quad (4.63)$$

Finally the measured output y is defined by:

$$y = \begin{bmatrix} h_1(x_1, x_2) \\ x_4 \\ h_3(x_3, x_4) \end{bmatrix} \quad (4.64)$$

with $h_1(x, x_2)$ the fuel cell stack voltage and $h_3(x_3, x_4)$ the compressor air flow map.

The system constants c_i for $i = 1$ to 24 are given by:

$$\begin{aligned}
c_1 &= \frac{\mathcal{R}T_{st}k_{ca,in}}{\mathcal{M}_{O_2}V_{ca}} \left(\frac{x_{O_2,atm}}{1+w_{atm}} \right), \quad c_2 = p_{sat}, \quad c_3 = \frac{\mathcal{R}T_{st}}{V_{ca}}, \quad c_4 = \mathcal{M}_{O_2}, \quad c_5 = \mathcal{M}_{N_2} \\
c_6 &= \mathcal{M}_v p_{sat}, \quad c_7 = \frac{\mathcal{R}T_{st}n}{4V_{ca}F}, \quad c_8 = \frac{\mathcal{R}T_{st}k_{ca,in}}{V_{ca}\mathcal{M}_{N_2}} \left(\frac{1-x_{O_2,atm}}{1+w_{atm}} \right) \\
c_9 &= \frac{\eta_{cm}k_t k_v}{J_{cp}R_{cm}}, \quad c_{10} = \frac{C_p T_{atm}}{J_{cp}\eta_{cp}}, \quad c_{11} = p_{atm}, \quad c_{12} = \frac{\gamma-1}{\gamma} \\
c_{13} &= \frac{\eta_{cm}k_t}{J_{cp}R_{cm}}, \quad c_{14} = \frac{\mathcal{R}T_{atm}}{V_{sm}\mathcal{M}_{a,atm}}, \quad c_{15} = \frac{1}{\eta_{cp}}, \quad c_{16} = k_{ca,in} \\
c_{17} &= \frac{C_D A_T}{\sqrt{\mathcal{R}T_{st}}} \sqrt{\frac{2\gamma}{\gamma-1}}, \quad c_{18} = \frac{1}{\gamma}, \quad c_{19} = \left(\frac{2}{\gamma+1} \right)^{\frac{\gamma}{\gamma-1}} \\
c_{20} &= \frac{C_D A_T}{\sqrt{\mathcal{R}T_{st}}} \gamma^{1/2} \left(\frac{2}{\gamma+1} \right)^{\frac{\gamma+1}{2(\gamma-1)}}, \quad c_{21} = \frac{1}{R_{cm}}, \quad c_{22} = k_v \\
c_{23} &= k_{ca,in} \frac{x_{O_2,atm}}{1+w_{atm}}, \quad c_{24} = \frac{n\mathcal{M}_{O_2}}{4F}
\end{aligned}$$

A further model reduction

Again from the interesting work of [Talj et al., 2009], a further model reduction is proposed. Besides the simplification from the somewhat complex system equations (4.62), given the non-linearity on function $\psi(x_1, x_2)$, the change of coordinates proposed in [Talj et al., 2009] has an important physical meaning for our system, since a new dynamic variable, the cathode air pressure $\chi = p_{air,ca}$ is defined. This has an actual advantage because in our test-bench the air pressure is directly measured.

The change of coordinates is defined by:

$$\chi = x_1 + x_2 + c_2 \quad (4.65)$$

Assuming that the approximation $c_4 x_1 + c_5 x_2 + c_6 = \kappa(x_1 + x_2 + c_2)$ holds for a given constant κ and that the function $\psi(\chi)$ is a linear function of χ in the form $\psi(\chi) = c_{20}\chi$ (see [Talj et al., 2009] for detailed demonstration), then the following third-order model is obtained:

$$\begin{aligned}
\dot{\chi} &= -\mu_1 \chi + \mu_2 x_4 + \mu_3 - \mu_4 \xi \\
\dot{x}_3 &= -c_9 x_3 - \frac{c_{10}}{x_3} \left[\left(\frac{x_4}{c_{11}} \right)^{c_{12}} - 1 \right] h_3(x_3, x_4) + c_{13} u \\
\dot{x}_4 &= c_{14} \left[1 + c_{15} \left[\left(\frac{x_4}{c_{11}} \right)^{c_{12}} - 1 \right] \right] [h_3(x_3, x_4) - c_{16}(-\chi + x_4)]
\end{aligned} \quad (4.66)$$

with:

$$\mu_1 = c_1 + c_8 + \frac{c_3 c_{20}}{\kappa}, \quad \mu_2 = c_1 + c_8, \quad \mu_3 = \frac{c_2 c_3 c_{20}}{\kappa}, \quad \mu_4 = c_7$$

4.4.3 Experimental identification and validation of FCS non-linear model

In this section the experimental validation of the models described before is presented. The experimental results were obtained on the test-bench setups described earlier in this chapter.

In a first section the dynamic third-order system $\Sigma(\chi, x_3, x_4)$ in (4.66) is identified. Then the identification of the static and dynamic models of the motor-compressor system are presented.

The non-linear model (4.66) is identified dividing the system in separate sub-systems. The complete model, composed by the sub-systems $\Sigma(\chi)$, $\Sigma(x_3)$ and $\Sigma(x_4)$, is represented graphically in Figure 4.31.

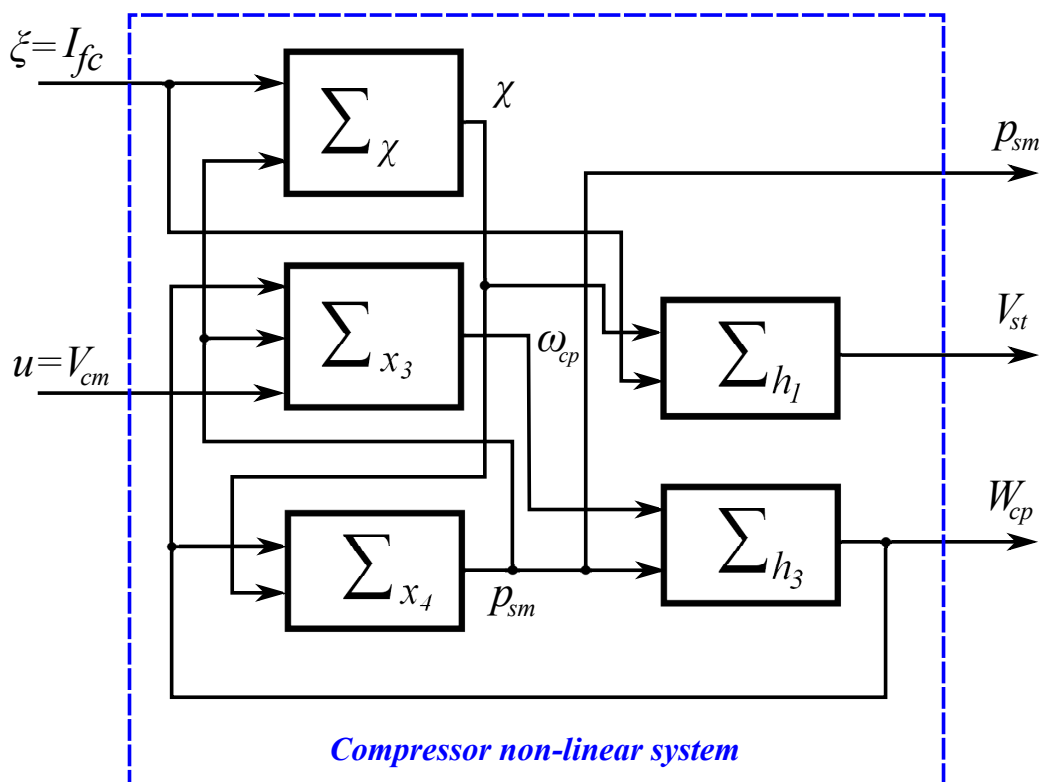


Figure 4.31: Non-linear FCS model.

4.4.3.1 Model for sub-system χ

This sub-system is composed by the first equation of system (4.66). Identification of this model was obtained from measured data on the real fuel cell stack. The 16-cell/100 cm² Paxitech© stack was used with operation under non-humidified air. The cathode air pressure was established at 1.5bar. The air stoichiometric factor was fixed to 1.6. However for these tests there was no possible back-pressure control on the stack, the output pressure is then the atmospheric pressure. Also for this reason, it was not possible to directly identify the pressure response of sub-system χ . Despite this limitation, the pressure dynamic was approximated using the stack voltage measure and the known physical parameters of the

stack. This model is identified from measures of the FC output voltage and assuming an equivalent pressure drop obtained from static measurements on the FC stack.

The model responses to current steps ξ and to pressure steps $x_4 = p_{sm}$ are presented in Figures 4.32 and 4.33. The voltage drop gives a good correlation with the measured response. The pressure dynamic is fairly similar to the stack voltage dynamic in terms of the system time constant. This is in agreement with pressure dynamics obtained in [Pukrushpan et al., 2004a].

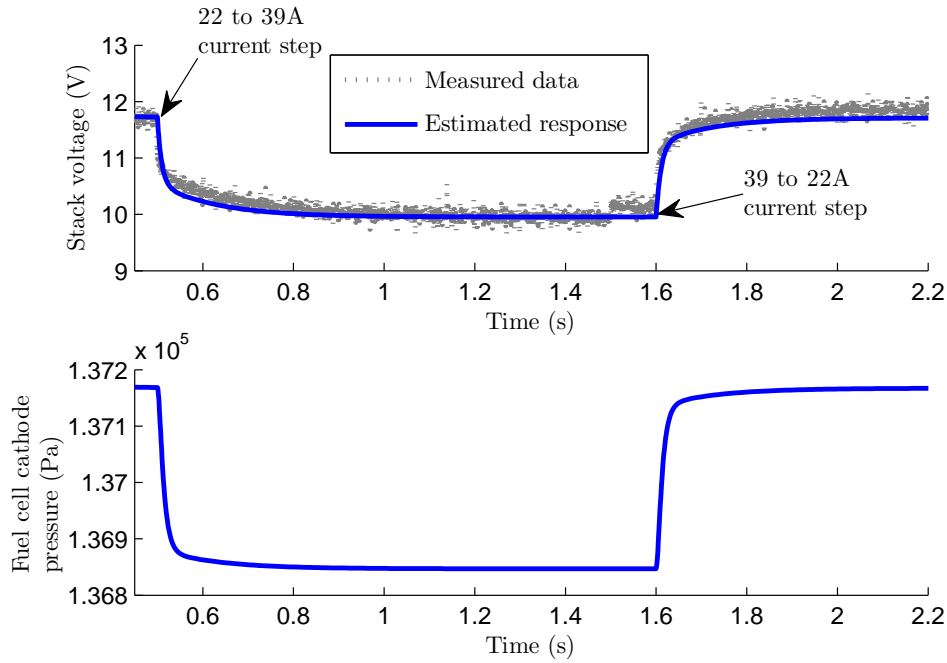


Figure 4.32: Voltage and pressure responses to a stack current ξ step.

To validate the model reduction of the equation on χ in the third-order system, Figure 4.34 show the comparison between the non-linear model (x_1, x_2) and the linear model χ , the first equation of system (4.66). The simulation of the non-linear model (x_1, x_2) was obtained using the parameters found with the identification of sub-system (x_3, x_4) , that are presented in the following section. The obtained model parameters are presented in Table 4.3.

Table 4.3: χ model parameters

Parameter	Value
μ_1	-399.3
μ_2	391.2
μ_3	350
μ_4	-7718.8

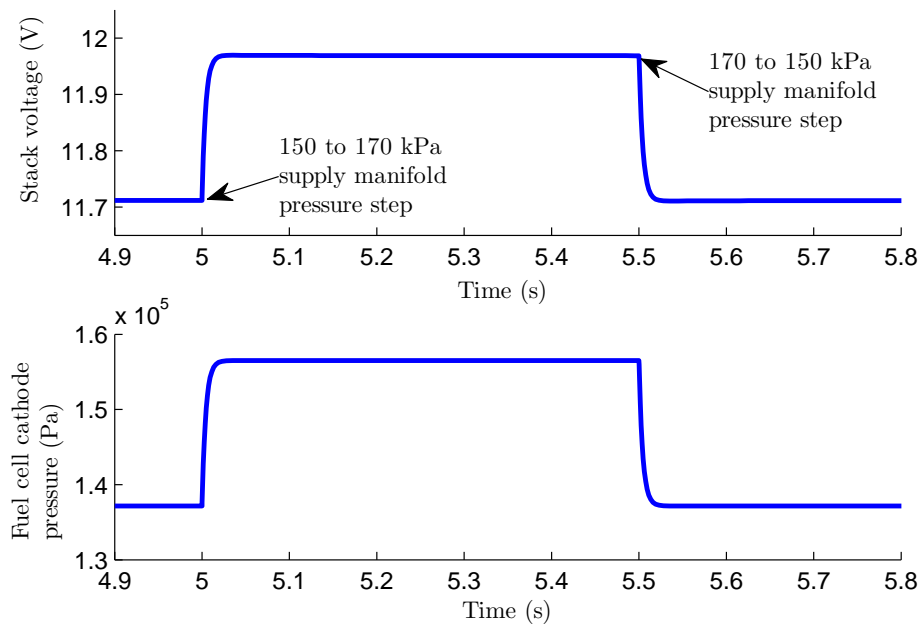


Figure 4.33: Voltage and pressure responses to a p_{sm} pressure step.

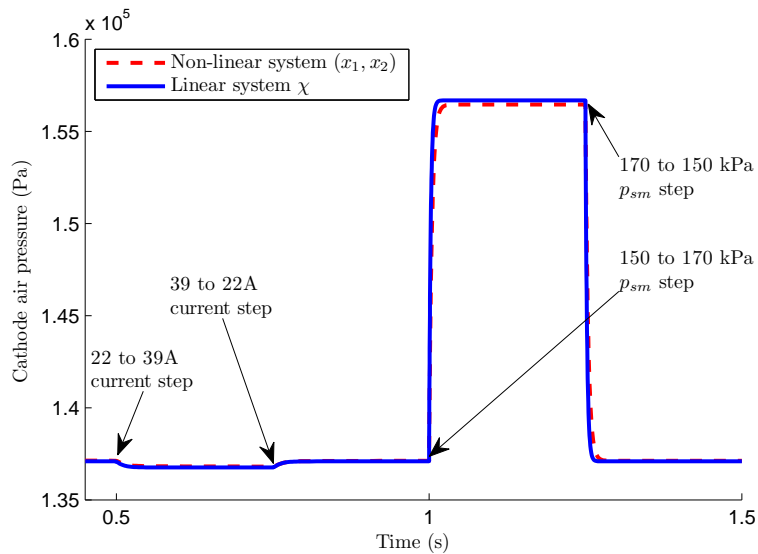


Figure 4.34: Fourth and third-order model comparisons.

4.4.3.2 Model for sub-system (x_3, x_4)

Model parameter identification for the sub-system (x_3, x_4) is not an easy task. Two important limitations were significantly influential in the identification procedure results. First, the existence of a closed-loop for compressor-motor speed control. Second, the influence of pipe-installation problems in the supply-manifold.

Actually, the problem of the closed-loop in the control speed was solved using multiple identification algorithm executions. A linear PI controller was assumed for the speed control loop. After several attempts, no information concerning the compressor control

data was obtained from Vairex© and opening the motor controller integrated unit would have invalidate the equipment warranty. The identification algorithm was first executed to find a feasible set of PI controller parameters. Then with these parameters fixed, the system parameters for equation in x_3 were computed with known parameter boundaries. In conclusion we used the identification approach for systems with feedback with known controller $K(s)$ and reconstruction of control input u (cf. to Figure 4.35).

The PI parameters obtained are given by $k_p = 3$ and $k_i = 9.5$. The identified parameters for system in x_3 are presented in Table 4.4. The PRBS input signal used for identification is presented in Figure 4.36. Identification results on the compressor-motor speed system are presented in Figures 4.37 and 4.38 for PRBS and chirp signal inputs respectively. The `idnlgrey` function for non-linear “grey-box” model was used to find the unknown system parameters.

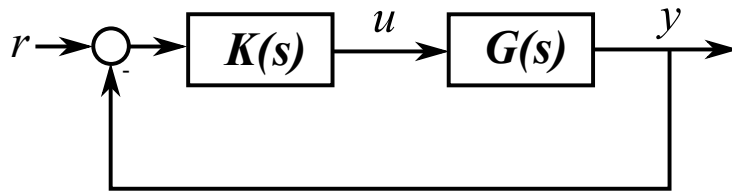


Figure 4.35: Closed-loop system considered for identification.

Table 4.4: x_3 model parameters

Parameter	Value
c_9	2300
c_{10}	774.7
c_{13}	1069.5

Two important problems were detected in the test-bench used for model identification: a somehow high pressure drop in the supply manifold, and secondly, the oversize of the chosen compressor-motor. Indeed, the compressor-motor was chosen with an oversize factor to comply with future expansions in the FC test-bench at LEPMI. The compressor maximum power consumption stands at 1200W with a maximum mass flow of 10g/s. This compressor has an air output orifice of 26.67mm in diameter, however for the nominal operating point of the 16-cell stack a 13.72mm pipe diameter was enough. This will create a bottleneck for high mass flow rates. For this reason the sub-system of dynamic equation in x_4 was not properly identified for the compressor-motor mounting realized at LEMPI. This is a pending problem that should be solved in future works with proper compressor-motor mounting. To cope with this limitation, a linear generic state-space system was identified for the dynamic of x_4 from compressor measures. This model was found using the MATLAB *Identification Toolbox* and an ARX linear model and then transforming the result into a continuous state-space system. It is important to note that for security reasons, as proposed in [Gasser, 2006], these tests were not performed using the real FC stack connected to the compressor-motor system at the same time. A dead volume, using a one-cell empty stack was used to simulate the hydraulic flow resistance of the real FC stack.

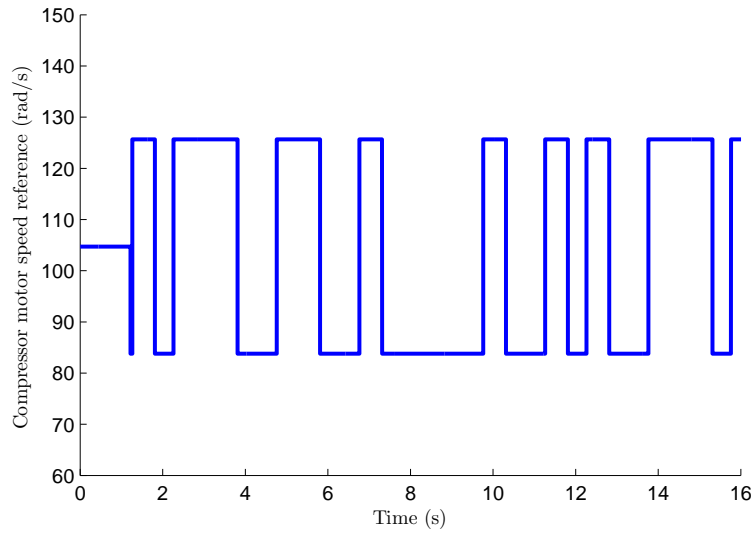


Figure 4.36: Compressor-motor speed dynamic identification with a PRBS input in the compressor-motor speed reference ω_{cp}^* .

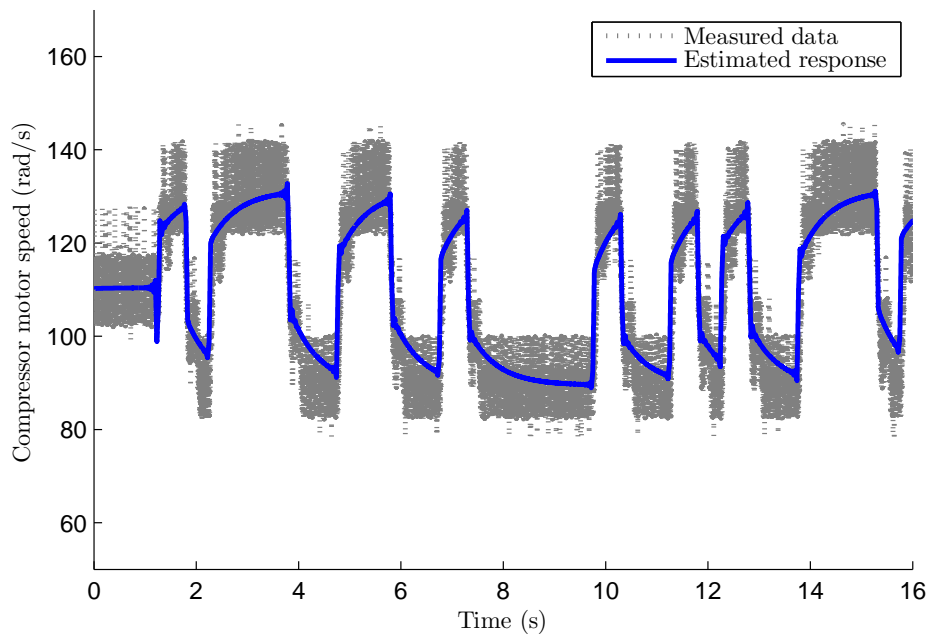


Figure 4.37: Compressor-motor speed dynamic identification with a PRBS input.

The actual cathode hydraulic flow resistance was computed from steady-state measurement on the real FC, this will be shown later for identification of the compressor model from [Gasser, 2006].

The obtained model for the system dynamic of x_4 is given in the form:

$$\begin{aligned} \dot{x} &= Ax + Bu \\ y &= Cx + Du \end{aligned}$$

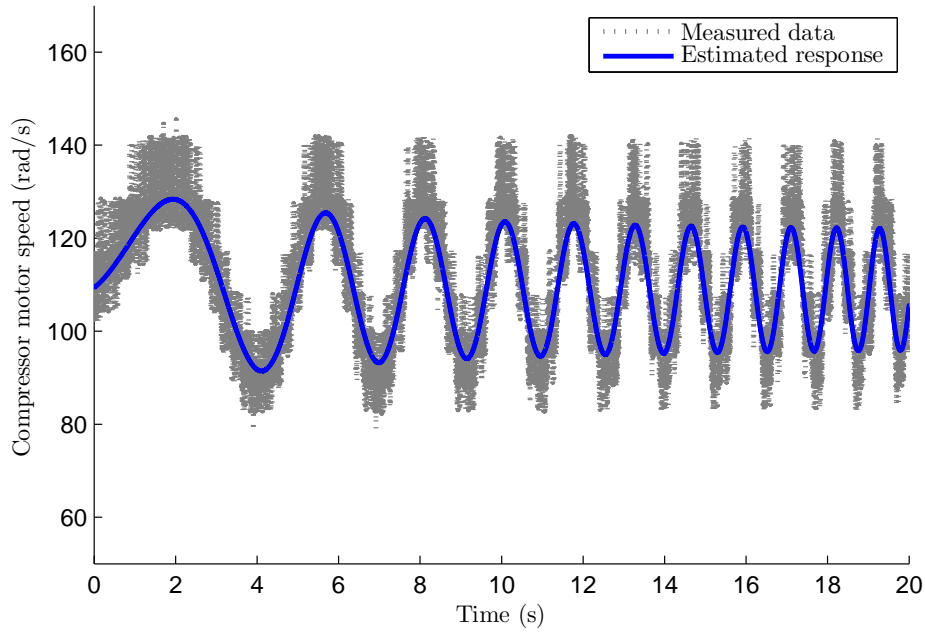


Figure 4.38: Compressor-motor speed dynamic identification with a chirp input.

with:

$$\begin{aligned}
 A &= \begin{bmatrix} -0.029 & -7.451 \\ 7.451 & -21.51 \end{bmatrix} & B &= \begin{bmatrix} 2231 & -5.013 \times 10^{-6} \\ -5.512 \times 10^4 & 1.156 \times 10^{-5} \end{bmatrix} \\
 C &= [-2231 \quad -5.512 \times 10^4] & D &= [3.964 \times 10^7 \quad -0.01884]
 \end{aligned}$$

where input vector is given by $u = [h_3(x_3, x_4) \quad \chi]^T$ and the system output is $y = x_4$.

Inputs for identification are shown in Figure 4.39. Identification result on x_4 , the supply manifold pressure, is given in Figure 4.40. These results were obtained for a PRBS input on the FC cathode pressure χ . This model was found using an *ARX* model structure and the iterative prediction-error minimization method with the *SI Toolbox*.

4.4.3.3 Compressor models identification

The identification problems described before have been limited to the identification of generic dynamic and static models for the compressor-motor system from real system measured data. The identification results for the static system $h_3(x_3, x_4) = W_{cp}$ is presented in Figure 4.41. The static model used to fit this compressor-map characteristic is a non-linear full cubic model. This non-linear regression could be used when precise values of the compressor flow are needed, as in the case of the system references computations. A map of the compressor power contours is presented in Figure 4.42.

A simplified linear system is obtained for the dynamic model of the compressor-motor system for simulations and to produce a control-oriented model. This linear system was computed using the *MATLAB Identification Toolbox* and a second-order state-space model structure. The iterative prediction-error minimization method was used to obtain the unknown parameters of the state-space model. The obtained model is given in the from:

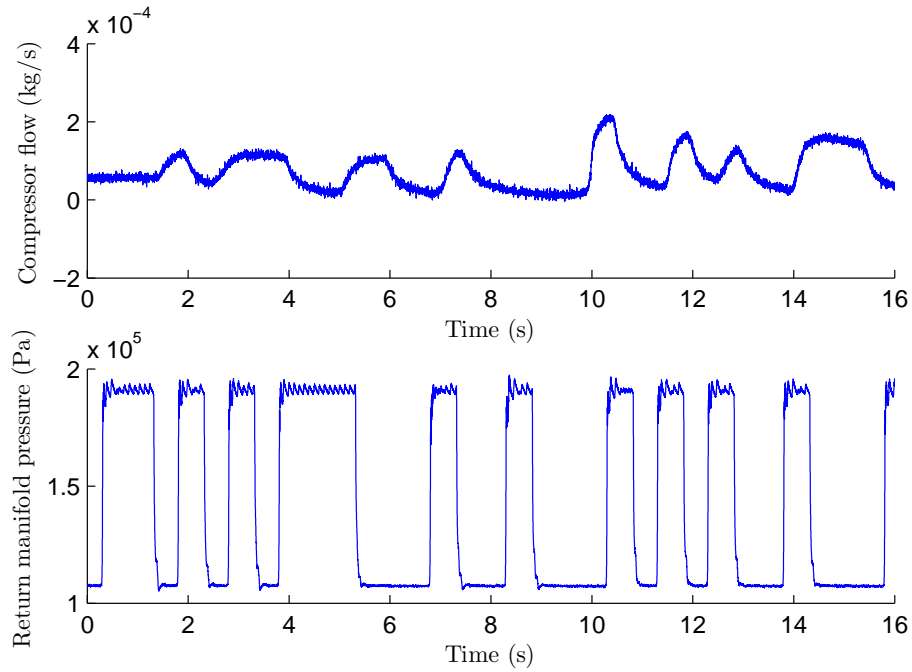


Figure 4.39: Input signals, compressor flow W_{cp} and return manifold pressure p_{rm} , for the supply manifold pressure dynamic identification.

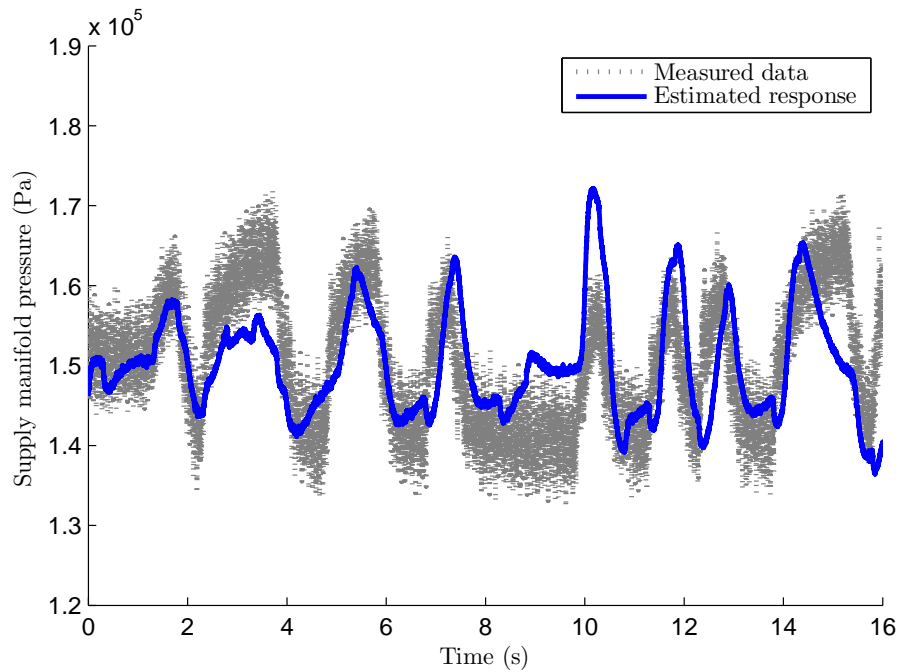


Figure 4.40: Supply manifold pressure p_{sm} dynamic identification with a PRBS input.

$$\begin{aligned} \dot{x} &= Ax + Bu \\ y &= Cx + Du \end{aligned}$$

with:

$$A = \begin{bmatrix} -1.81 & 3.792 \\ -0.6158 & -7.553 \end{bmatrix} \quad B = \begin{bmatrix} 0.01461 & -4.598 \times 10^{-5} \\ 0.1274 & -0.0001696 \end{bmatrix}$$

$$C = [0.0004138 \quad -9.53 \times 10^{-5}] \quad D = [0 \quad 0]$$

where input vector is given by $u = [\omega_{cp} \quad p_{sm}]^T$ and the system output is $y = W_{cp}$.

The model validation using as inputs the compressor-motor speed and the supply manifold pressure, shown in figures 4.37 and 4.40 respectively, is presented in Figure 4.43.

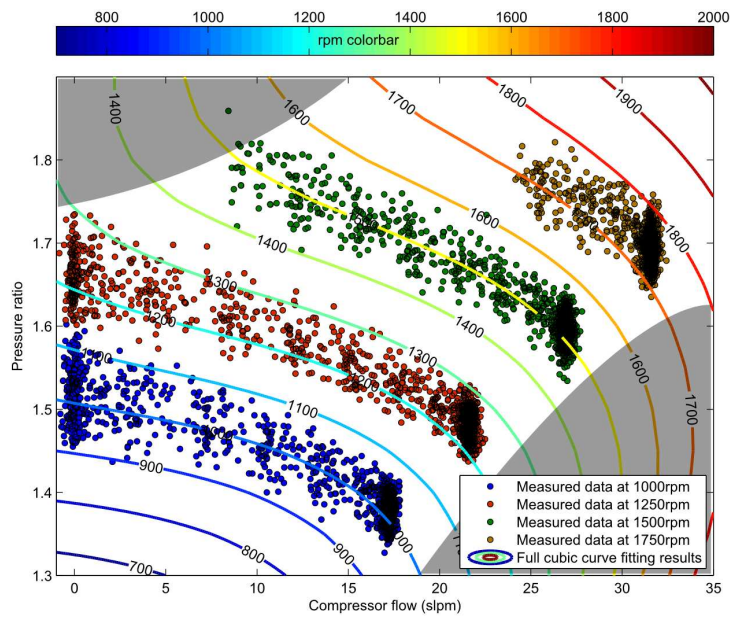


Figure 4.41: Compressor flow map (measured) and the non-linear regression model.

4.4.4 Experimental identification and validation of FCS linear model

A key parameter in the model proposed by [Gasser, 2006] is the FC stack pressure drop, which is computed on data obtained from real measurements. The pressure drop remains fairly linear when increasing the air flow, this is shown in Figure 4.44. With this measure the flow hydraulic resistance parameter k_h can be computed.

For the dynamic model a first set of parameters is identified using the model of the compressor motor without the pressure dynamics. These dynamic parameters identified are J_{cp} , k_f , L_{cm} and R_{cm} . The results obtained were used as a starting point guess on a second optimization problem involving the complete model (including the pressure dynamics). Identification was carried out again using the MATLAB *Identification Toolbox* with the least-square regression algorithm option.

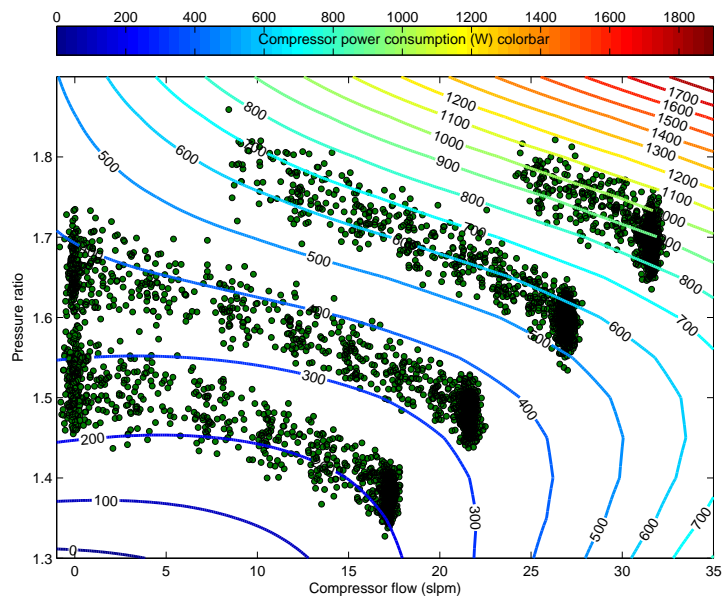


Figure 4.42: Compressor power contour map.

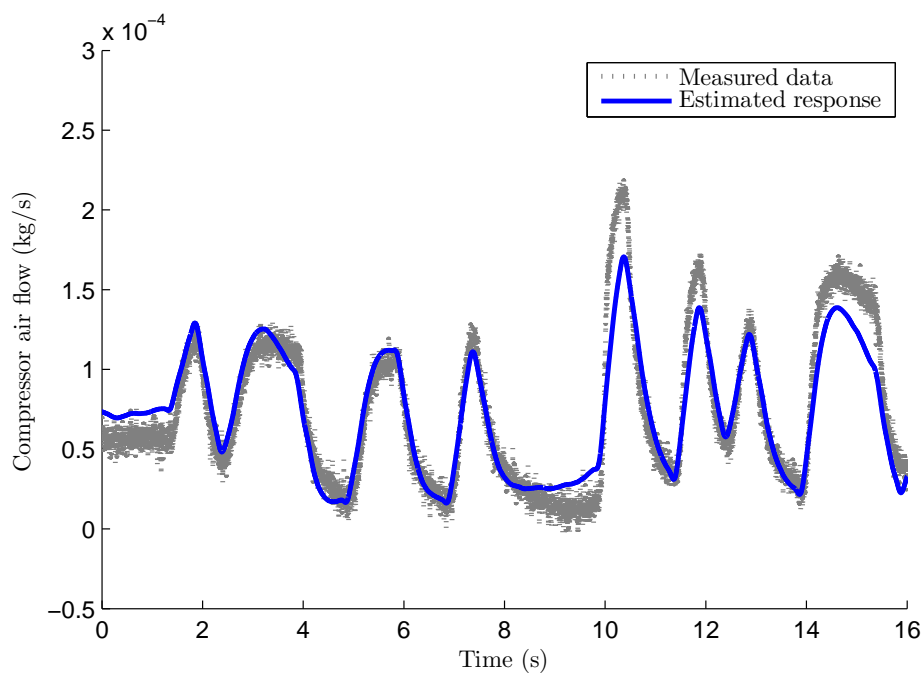
Figure 4.43: Validation of a linear dynamic model for $h_3(x_3, x_4) = W_{cp}$.

Figure 4.45 show the inputs used to identify this model. Measured and simulated results are compared in figure 4.46. Figure 4.47 show this comparison for the compressor output flow and pressure. Additionally the parameters of the PI (assumed) from the integrated speed control of the compressor are considered and identified. The parameters of the pressure dynamics model were also identified. Results are summarized at the end of this section in Table 4.5.

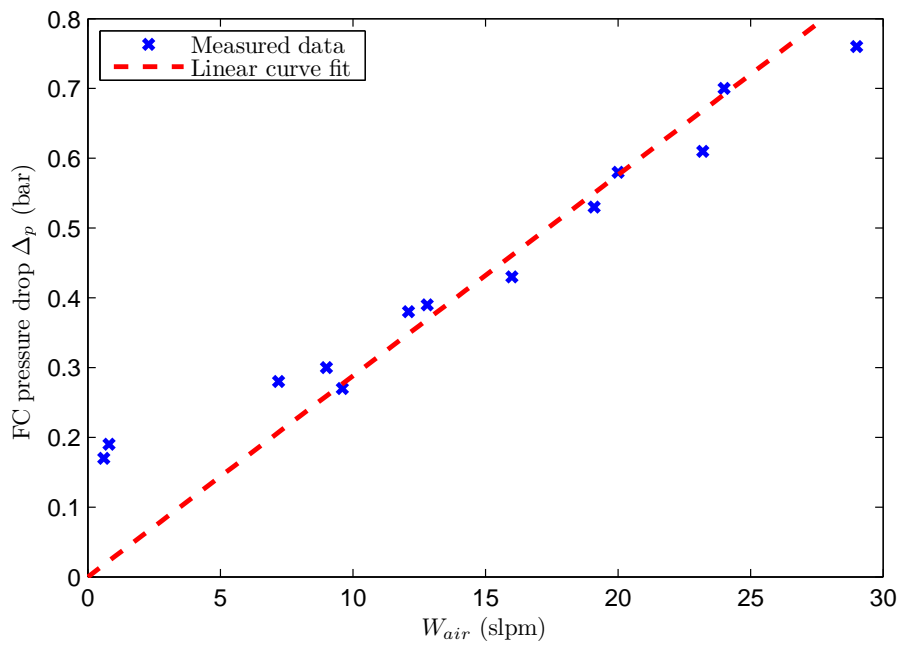


Figure 4.44: Fuel cell pressure drop constant computation.

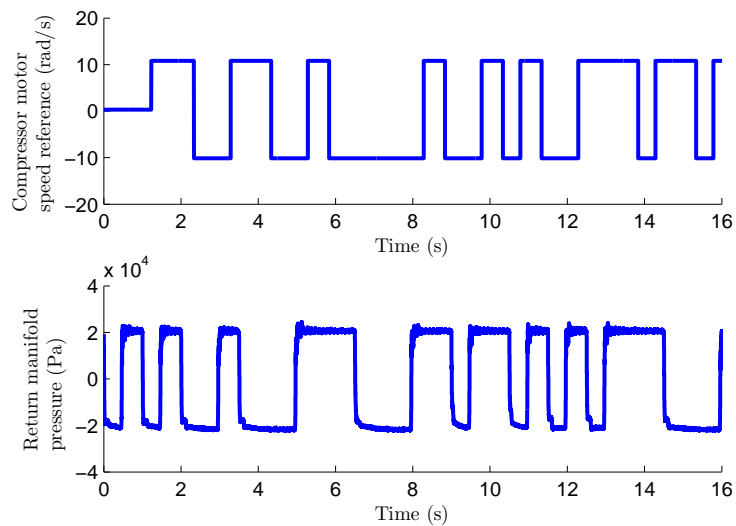


Figure 4.45: Inputs used to identify the model proposed by [Gasser, 2006].

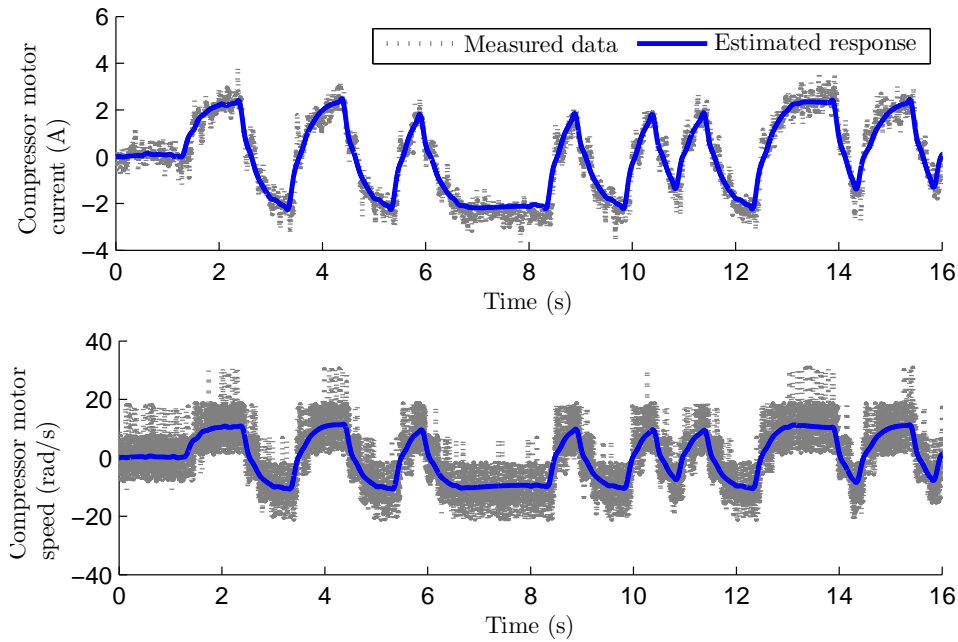


Figure 4.46: Measured and simulated results for current and speed using the model proposed by [Gasser, 2006].

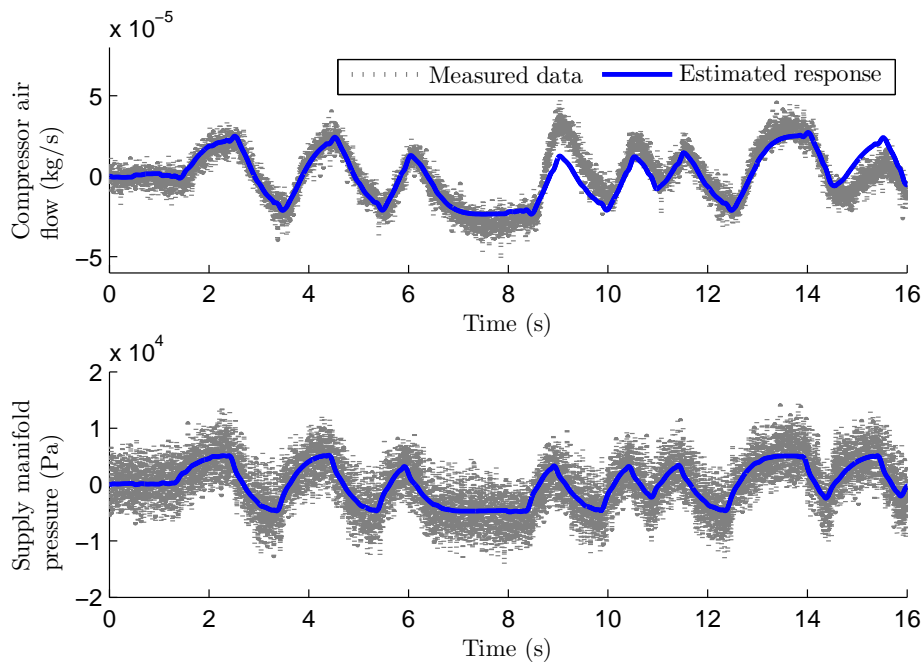


Figure 4.47: Measured and simulated results for mass flow and pressure using the model proposed by [Gasser, 2006].

Table 4.5: Identification results for the model proposed by [Gasser, 2006]

Parameter	Identified Values	Units
$k_{m,cp}$	1.7002×10^{-6}	$\frac{kg}{rad}$
k_h	6088.1×10^4	$Pa.s/kg$
k_p	3.7477×10^{-6}	m^3
k_e	0.2634	$V \frac{s}{rad}$
k_t	0.1936	$N.m/A$
k_d	0.0588	$N.m \frac{s}{rad}$
J_{cp}	2.4637×10^{-5}	$kg.m^2$
R_{cm}	2.1805	Ω
L_{cm}	0.0040	H
V_{sm}	0.0010	m^3
k_p (PI)	0.4912	–
k_i (PI)	5.9854	–

4.5 Conclusion

In this chapter the different models studied in this thesis dissertation were presented. The dedicated test-bench set-ups were described in details. A real FC stack was available within the GESI set-up, the stack is a PEM with a 1kW of maximal power capacity.

The system models and parameters were presented. An average model, non-linear and linear, is used to model power converters, including the parallel boost converter arrangement and a voltage inverter. These models were validated through simulations on the topological (exact) models.

Several FC models are also described. Two important models will be retained for the application of control strategies to the air supply system to the FC. The first, is a reduced third order model derived from known literature on FC, and specially from the complete FC model proposed by Pukrushpan et al. [2004a]. A second model presented is the linear model of the air supply system and FC proposed by Gasser [2006].

These models were identified using the identification methods described in chapter 3. A hard problem to solve was the existence of a feedback loop in the system measures used for identification.

Chapter 5

Control Applications

5.1 Introduction

In this chapter the control design proposed and the analysis of the results obtained in this dissertation are presented. The closed-loop analysis is completed on the open-loop systems described in chapter 4. In the first section, the control design methodology is detailed. Application of the control methodology is achieved using the control tools presented in chapter 3. The rest of this chapter is divided in two large sections: control of the electrical sub-system and control of the air supply sub-system.

The results obtained with simulation for the electrical sub-system are complemented with a validation of the control structure on a real-time test-bench. Robustness analysis results using μ -analysis are also presented. For the air supply sub-system an LPV methodology approach using gain-scheduling is proposed. The LPV control is also considered to deal with some given system uncertainties.

In a final section, a control strategy of the complete system including both, the electrical and air supply dynamics, is proposed.

A summary of the control application strategies is given in the following list:

- Electrical sub-system (FC+storage+DC/DC converters)
 - Hybrid boost converters
 - Hybrid boost converters with reversible converter for storage system
 - Hybrid boost converters with voltage inverter for AC load
- Air supply sub-system
 - Compressor system control
 - An introduction to LPV control
 - * LPV speed control
 - * An LPV controller to deal with system uncertainties
- Complete system control

5.2 Proposed control methodology

A generalized control methodology is used in this dissertation for controller design and computation.

As presented in the previous chapter, the dynamical equations and the equivalent average model (in the case of switching systems) are used to describe the behavior of a given real system. Linearizing these equations, for a given equilibrium state, a linear state-space model can be obtained. The open-loop system validation can be achieved using the topological model or real system tests.

Using a mixed sensitivity approach, performance and robustness specifications are introduced using weighting functions over particular closed-loop transfer functions [Sko-gestad and Postlethwaite, 1996]. An extended model including these weighting functions is then obtained, where uncertainties models could be introduced to consider parametric uncertainties or unmodeled dynamics.

The controller can now be computed using the control tools detailed in chapter 3. A final multivariable controller is obtained until all desired specifications are satisfied. For control validation, tests using the average or topological models are convenient. Implementation on the real system is the final step. The proposed methodology is resumed in Figure 5.1.

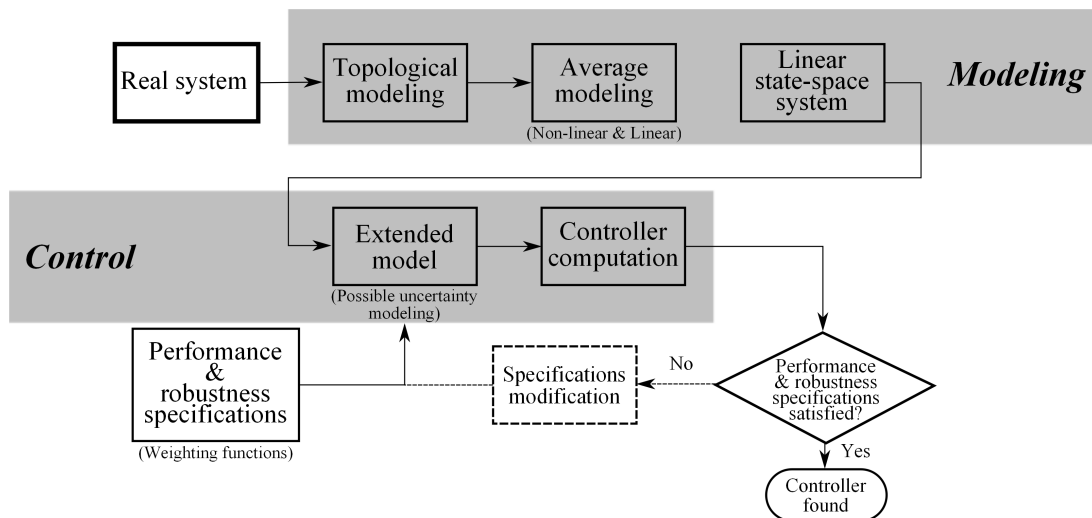


Figure 5.1: Proposed methodology.

As a general approach we also used closed-loop time domain simulations to test for desired controller performance validation. These simulations were implemented using MATLAB/SIMULINK and the average modeling methodology presented in the previous chapter 4. A schematic of the general approach used to obtain simulation results is presented in Figure 5.2.

5.2.1 Problem objectives

In a general basis, the control objective adopted in this thesis is the disturbance rejection. It is proposed that this approach will have an influence on the cells life-span, avoiding non-desired and harmful high energy transients. The optimization of control reference signals

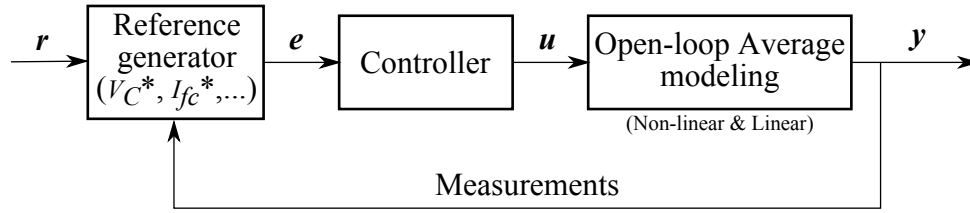
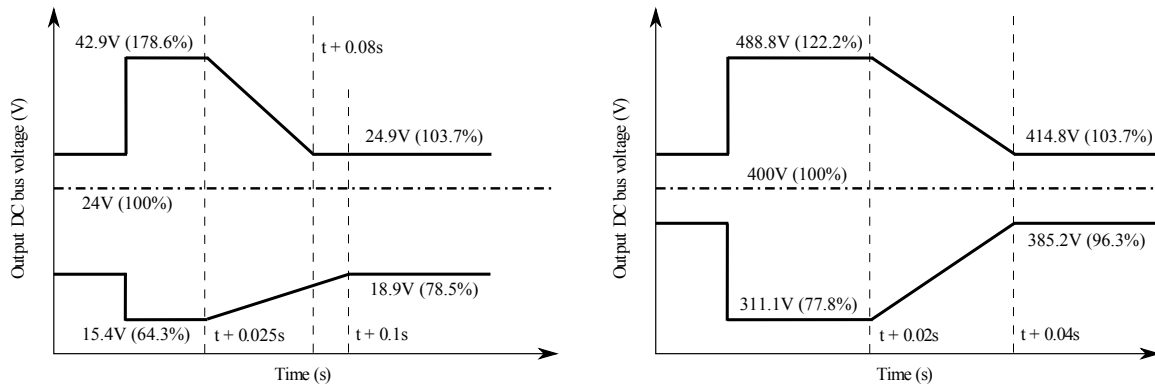


Figure 5.2: Approach for time-domain simulations.

variables (denoted hereby with the asterisk symbol $*$) was not considered in this thesis. However, as it was presented in the introductory chapter, the literature is rich and several optimization methodologies can be found, including the use of MPPT algorithms or the maximization of the overall system efficiency. The tracking problem is not of interest for the control of the electrical power management sub-system, since an application will always keep the same desired output voltage value, where in counterpart the regulation following a disturbance is a special concern. Despite this, in some cases the tracking performance of controllers is shown for illustrative purposes. A compressor-motor speed controller is proposed later in this chapter, in this case the tracking problem is analyzed.

We are interested on high delivered energy quality. A constant DC bus voltage is considered for evaluating the energy quality. However, other parameters may be considered as quality performance indicators, as the frequency for AC applications, the harmonics contents and the total harmonic distortion (THD), among others. Energy quality are commonly defined by norms. For AC application norms are very well defined, some restrictions can be found in *IEEE Standard C37.106-2003*¹ or in draft *IEEE Standard P1547/D07*², and their French and European equivalents, see a résumé in Valero [2004]. For DC applications we will introduce an example taken from aeronautics norms used resumed in the work of Sautreuil [2009], and adapted from the military aircraft norm *MIL-STD-704E*³. An adapted version of these norms for DC voltage aircraft application, to the voltage levels considered in this thesis, is presented in Figure 5.3.

Figure 5.3: Adaptation from the military aircraft norm *MIL-STD-704E* for: DC applications at 20-30V (left) and DC application for $>200V$ systems (right).

¹IEEE Std C37.106-2003: Guide for Abnormal Frequency Protection for Power generating Plants

²IEEE P1547/D07: Draft Standard for Interconnecting Distributed Resources with Electric Power Systems

³MIL-STD-704E: Department of Defense Interface Standard, Aircraft Electric Power Characteristics

5.3 Electrical sub-system

In this section the control applications to the electrical sub-system of the fuel cell system are presented. In a first part the control of the hybrid boost converters of the “GESI” system is described. In a second part, the control of the “Emulator” test-bench is presented. This system considers a reversible boost converter and, in a second section, a voltage inverter for AC loads applications. Note that, as presented before, the system parameters of the “GESI” and “Emulator” test-bench systems are totally different. Let us now present the control application for the “GESI” test-bench system.

5.3.1 Hybrid boost converters

In this section the control of the “GESI” test-bench system is presented. In a first approach some classical and the robust control methodologies are presented and compared using time-domain simulations and robustness analysis.

5.3.1.1 A classic control approach

(a) Control Strategy proposed by Valero [2004]

The classic control approach considered in Valero [2004] is based on multi-loop control. Multiple feedback control strategies are used to solve the stability problems associated with boost converter control [Middlebrook, 1987]. A single current loop is used for the FC boost converter. The SC boost converter is chosen to control the DC bus voltage with a square output voltage loop and a second stabilizing current loop. This structure is shown in Figure 5.4. For time-domain simulations this structure can be adapted to Figure 4.12 using the simulation approach presented in figure 5.2.

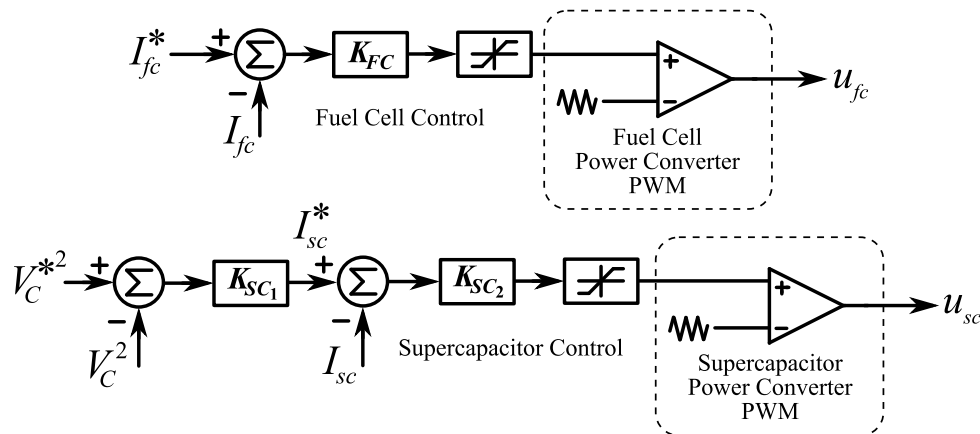


Figure 5.4: Hybrid system control strategy proposed in Valero [2004].

Simple PI controllers of the form $k_p(1 + k_i/s)$ are used for K_{FC} , K_{SC1} and K_{SC2} . The controller parameters are computed using pole compensation, approaching the system to a second order closed-loop transfer function. Usually the second order dynamics are defined by the damping ratio ζ and the undamped natural frequency ω_n . These parameters are obtained by mean of classic time domain performance parameters such as the maximum

overshoot, settling time, etc. The system equations are simplified to a first order transfer functions for each source.

The transfer functions for the FC and the SC are given respectively by:

$$\frac{I_{fc}}{\alpha_{fc}} = \frac{V_{C_e}}{L_{s_{fc}}s + R_{s_{fc}}} \quad (5.1)$$

$$\frac{I_{sc}}{\alpha_{sc}} = \frac{V_{C_e}}{L_{s_{sc}}s + R_{s_{sc}}} \quad (5.2)$$

with $R_{s_{fc}} = 0.0036\Omega$, $L_{s_{fc}} = 45\mu\text{H}$, $R_{s_{sc}} = 0.019$ and $L_{s_{sc}} = 50\mu\text{H}$. From further analysis in Valero [2004] and based on the structure in Figure 5.4, the controllers parameters for a desired settling time t_s were chosen as:

- FC current loop $K_{FC}(s)$:

$$k_p^{FC} = \frac{1}{V_{C_e}} \left(\frac{6L_{s_{fc}}}{t_s} - R_{s_{fc}} \right), k_i^{FC} = \frac{R_{s_{fc}}}{L_{s_{fc}}}$$

- SC voltage loop $K_{SC_1}(s)$:

$$k_p^{SC_1} = \frac{1}{V_{sc_e}} \left(C\zeta_v\omega_{nv} - \frac{1}{R_L} \right), k_i^{SC_1} = \frac{\omega_{nv}^2 C}{2k_p V_{sc_e}}$$

- SC current loop $K_{SC_2}(s)$:

$$k_p^{SC_2} = \frac{\omega_{ni}L_{s_{sc}} - R_{s_{sc}}}{V_{C_e}}$$

Using the system parameters and choosing $t_s = 5\text{msec}$, $\omega_{ni} = 1000\text{rad/s}$, $\omega_{nv} = 100\text{rad/s}$ and $\zeta_v = 1$, the simulation results, obtained with the non-linear average model for a 5% voltage reference step at $t = 1\text{sec}$ and a 50% disturbance step at $t = 2\text{sec}$, are shown in Figures 5.5 and 5.6.

For this test case, the current references I_{fc}^* and I_{sc}^* in Figure 5.4 are computed using an adapted filtered signal of the load current demand. The cut-off frequency of the filter is fixed at 1Hz. With this strategy the SC supplies the instantaneous transient current while the FC current has a smooth response to the disturbance, keeping a healthy FC operation as shown in Figure 5.6. Other constraints could be added to the FC dynamic, as the classic slope constraint with respect to the current density to avoid the so-called starvation⁴ problem Thounthong et al. [2009].

(b) Control Strategy proposed by Sailer [2008]

A slightly modified version of the control strategy proposed in Sailer [2008] is presented in Figure 5.7.

In this case, the FC control ensures the DC bus voltage control. Following the same procedure described before, the controller parameters are chosen as:

⁴Fall of the partial oxygen pressure below a critical level resulting in a fast decrease of the cell voltage.

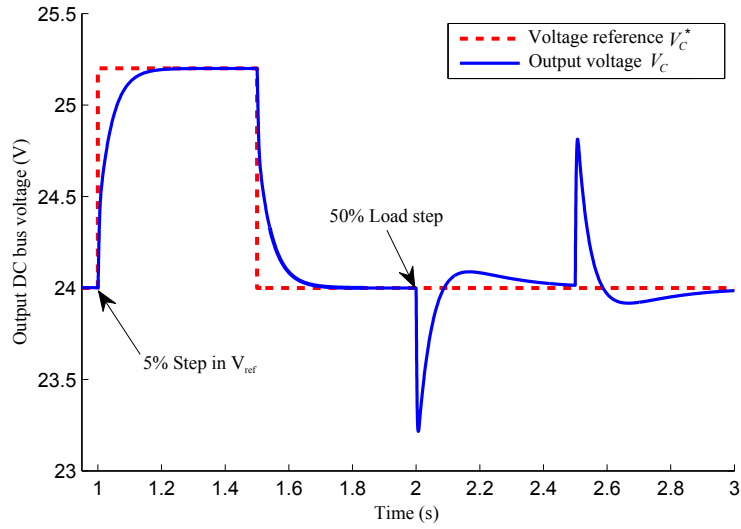


Figure 5.5: Output voltage time response, method Valero [2004].

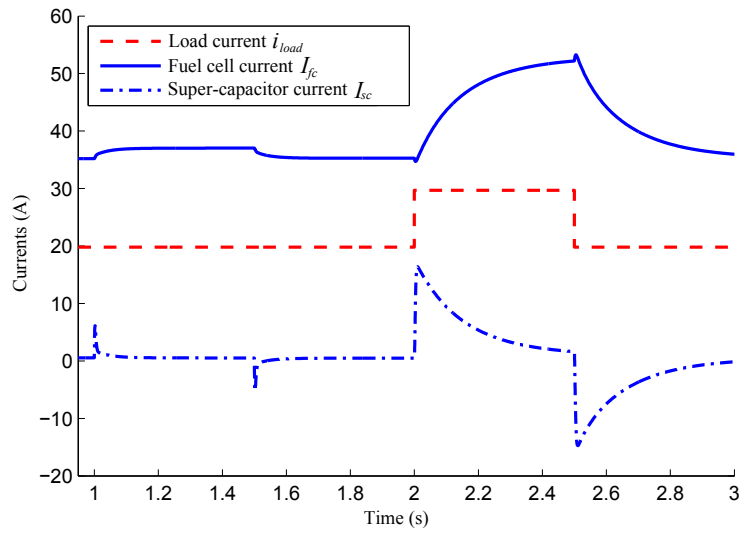


Figure 5.6: System currents time response, method Valero [2004].

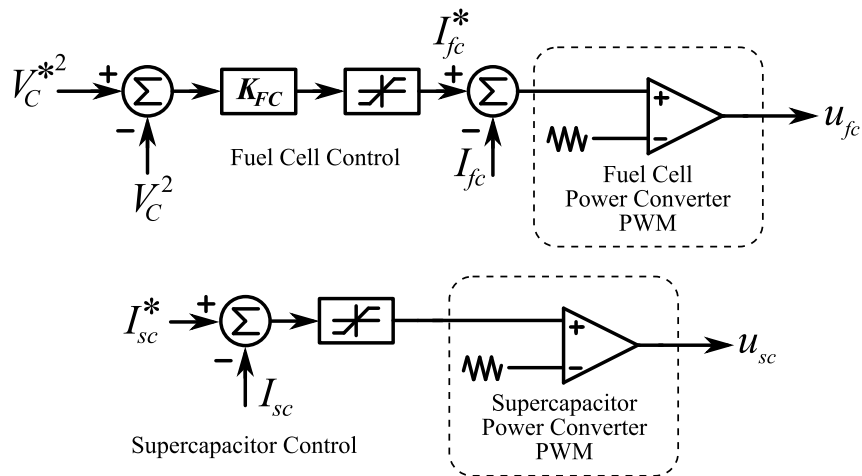


Figure 5.7: Hybrid system control strategy proposed in Sailer [2008].

- FC voltage loop:

$$k_p^{FC} = \frac{1}{V_{fce}} \left(C\zeta_v\omega_{nv} - \frac{1}{R_L} \right), \quad k_i^{FC} = \frac{\omega_{nv}^2 C}{2k_p V_{fce}}$$

For $\omega_{nv} = 480\text{rad/s}$ and $\zeta_v = 0.707$ the result shown in Figure 5.8 is obtained with the non-linear average model for a 5% voltage reference step at $t = 1\text{sec}$ and a 50% disturbance step at $t = 2\text{sec}$.

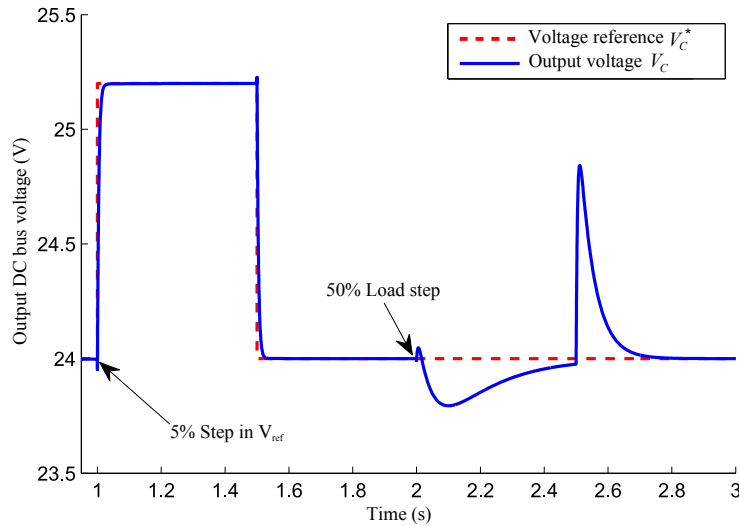


Figure 5.8: Output voltage time response, method Sailer [2008].

It should be noted that these “classic” control strategies presented are given as a reference from some previous works. However, other various control strategies are possible for this type of system. For illustration purposes see for example the interesting works of Thounthong et al. [2009] or Choe et al. [2007] for the implementation of other effective classic control methodologies.

5.3.1.2 Robust control approach

As FC are very sensitive to fast current transients that could shorten its lifespan, and to avoid harmful operating conditions, a disturbance rejection design is suggested. As opposed to those “classic” control designs shown in the previous section, we are also interested in guaranteeing robustness, especially for a system subject to parametric uncertainties.

Our control objective is to keep a desired output voltage level and to control the source currents in order to provide the fast transient currents in the case of a load disturbance. The voltage in the DC bus should comply a standard voltage maximum voltage deviation for a specific time, for example in the case of an on-board aircraft application this deviation stands approximately at $\pm 5\%$ over the first 40msec following a disturbance [Sautreuil, 2009].

The MIMO robust control synthesis proposed here is based on the general control configuration adapted to the hybrid FC/SC power boost converter system. In a first approach the DC bus output voltage ($V_C * -V_C$) and the FC current tracking errors ($I_{fc} * -I_{fc}$), as well as the control inputs (u_{fc} , u_{sc}), are chosen as performance outputs.

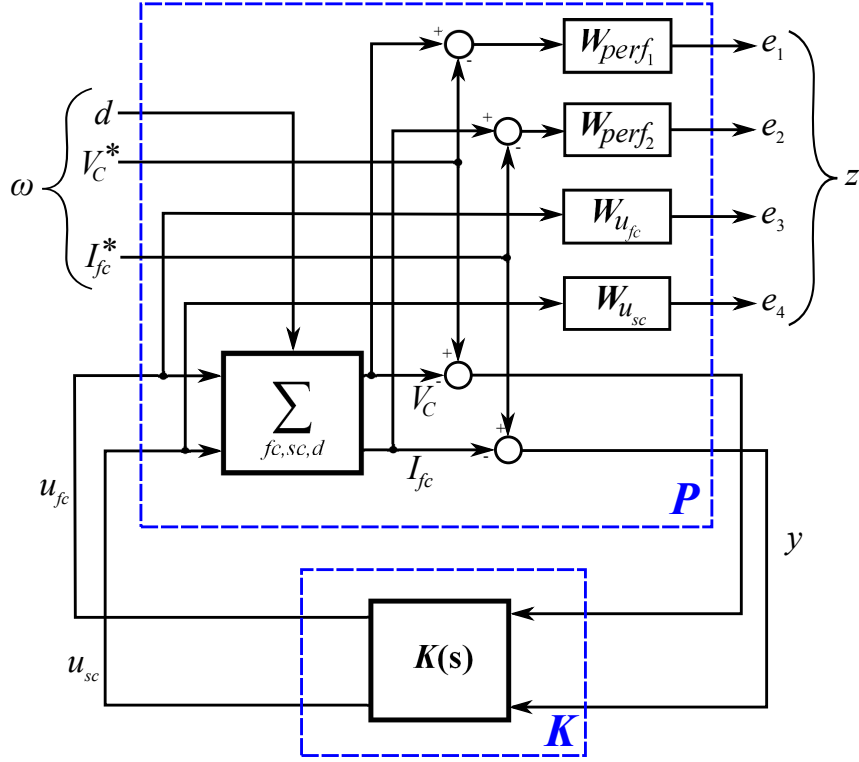


Figure 5.9: The first proposed control configuration.

The measured outputs are the DC bus output voltage and the FC current. This structure is detailed in Figure 5.9.

Weighting functions are chosen to keep a good trade-off between a relative fast time-domain response and the system robustness. The performance weights are designed for an imposed stabilization time of approximately $t_s = 0.3\text{sec}$ with a frequency pulsation of $\omega_B = 1\text{rad/s}$. The module margins of the sensitivity functions are limited to 2 to gain in robustness. For the control weighting functions, an input duty cycle limit of 0.95 is considered. Finally, these weighting functions are given by:

$$W_{perf} = \frac{0.8s + 0.1}{s + 0.001} \times I_2 \quad (5.3)$$

$$W_{u_1} = \frac{s + 15.79}{0.01s + 15.71} \quad (5.4)$$

$$W_{u_2} = \frac{s^2 + 3.947 \times 10^5 s + 6.2 \times 10^6}{0.01s^2 + 3.927 \times 10^5 s + 6.169 \times 10^4} \quad (5.5)$$

Using the control methodology presented in chapter 3, we compute first a full-order \mathcal{H}_∞ controller and then a MIMO PI controller using the iLMI algorithm. The iLMI algorithm yields a solution for the multivariable PI controller after five iterations, with a conditioning value of $\gamma = 1.45$. The full-order \mathcal{H}_∞ controller found has 11 states with a conditioning value of $\gamma = 1.25$.

The multivariable PI controller found is given by:

$$PI_{iLMI} = \begin{bmatrix} 0.0610/s & 0.0055 + 0.3217/s \\ 0.0034 + 0.0720/s & 0.0019 + 0.1292/s \end{bmatrix}$$

For the studied system, the sensitivity functions are defined by:

$$S_1 = \frac{V_C}{d}, S_2 = \frac{I_{fc}}{d}, S_1K_1 = \frac{u_{fc}}{d}, S_2K_2 = \frac{u_{sc}}{d}$$

The singular value plots of the MIMO sensitivity functions $S(s)$ and $SK(s)$, are shown in Figures 5.10 and Fig. 5.11 respectively. Results show how the shaping of \mathcal{H}_∞ performance is straightforward for the PI iLMI and the full order \mathcal{H}_∞ controllers using the templates weighting functions. The \mathcal{H}_∞ controller shows an overall better robustness when compared with the iLMI PI control; however, in both cases control performance specifications are respected. From analysis of Figure 5.11 it is clear that the control input energy is not minimized at low frequencies using the iLMI PI control, this is due to the control structure simplicity.

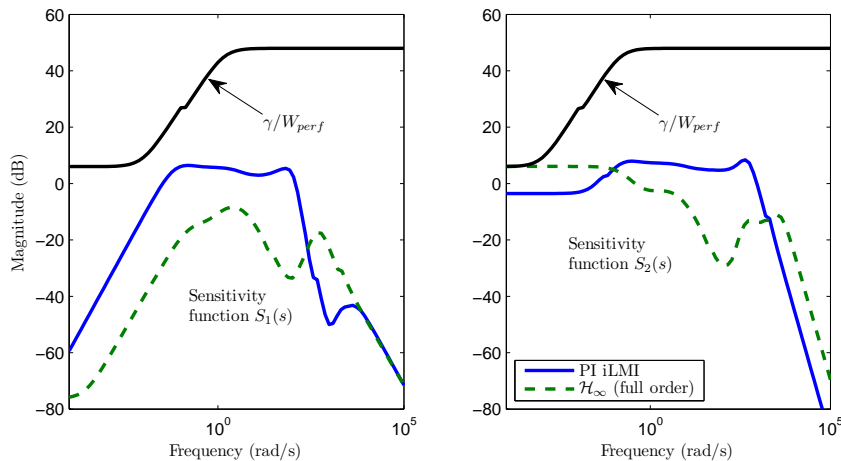


Figure 5.10: Sensitivity function.

These controllers were implemented using MATLAB/SIMULINK for time-domain simulations. For these simulations the non-linear average model is used. The current reference of the FC (I_{fc}^*), is computed filtering the load current by means of a second order low-pass filter with a cutoff frequency of 1Hz and a damping factor of 0.707. An important number of primary level control strategies are based on imposed reference signals related to the FC dynamic, as the Maximum Power Point Tracker (MPPT), a tracking on the FC efficiency curve, etc. Despite this, in this work the reference generation for the FC control is not optimized, we use instead a simple reference generation strategy by imposing the steady-state value of the primary energy source (the FC in this case). A rich literature can be found on this subject, see for example Han et al. [2007], Thounthong et al. [2009], Thounthong and Rael [2009], Suh and Stefanopoulou [2005] or even Valero et al. [2006] for several examples on primary level control methodologies.

Let us first compare the PI controllers computed with the classic method and the robust MIMO PI controller computed with the iLMI algorithm. The simulation is obtained

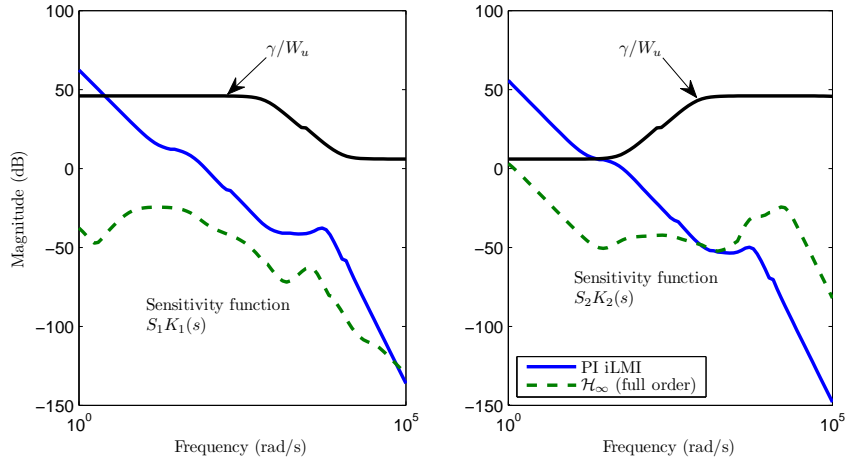


Figure 5.11: Complementary sensitivity function.

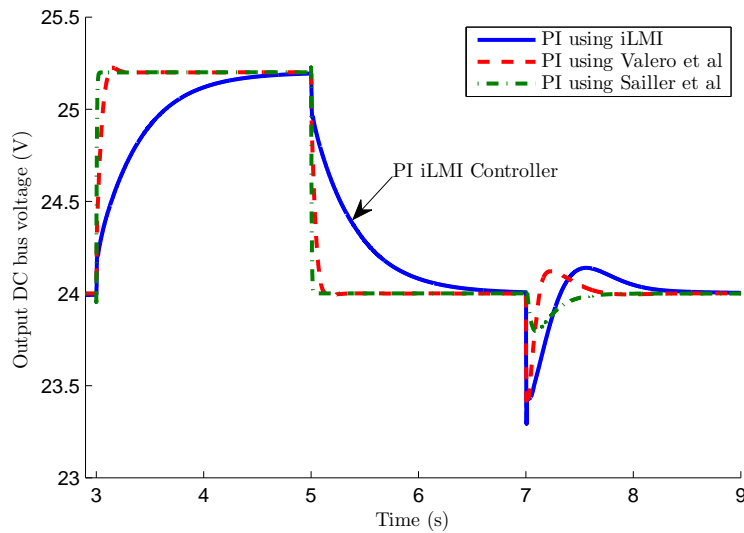


Figure 5.12: Simulation results using PI control (classic and robust).

for a 5% step in the voltage reference V_C^* at $t = 3$ s and for a 50% load disturbance $d = I_{load}$ at $t = 7$ s. The result is shown in Figure 5.12.

From these results it is clear that the disturbance rejection performance is not better with the robust MIMO PI controller. However, as it will be presented later, other control structures are possible in order to improve the disturbance rejection while keeping a good robustness trade-off, but at the cost of a higher number of measured variables.

Remark 1 A second option was proposed in Hernandez-Torres et al. [2010a] considering the SC current as a measure instead of the FC current. Good results were obtained for both dynamic disturbance rejection and robustness. However, the first solution is retained given the use of a direct control methodology on the FC current. This will allow us now to introduce a FC current rate limitation to 10A/s to reduce harmful effects of big load steps disturbances. This value could be different depending on the size and characteristics of the FC stack, some authors report typical values for this limitation between 4–18A/s [Thounthong et al., 2009],[Tritschler, 2010].

The Figure 5.13 show a comparison of the simulation response obtained for the FC current control using the iLMI PI control with and without the current rate limitation. The figure may also represent a simulation of a FC current start-up sequence, where the current limitation could play an important role given the big current step involved. A 10% load current step is applied at $t = 6$ s.

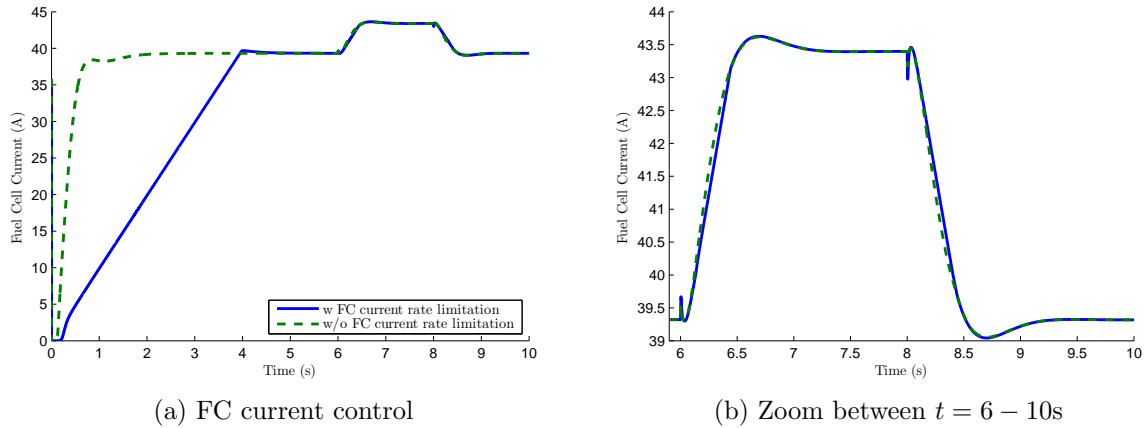


Figure 5.13: Simulation results.

Let us now present the simulation results obtained using the \mathcal{H}_∞ controller. The results with both the full order and the reduced order controllers are presented. The reduced order controller was obtained using the functions `balreal` and `modred` in MATLAB. In Figures 5.14 and 5.15 voltage and current responses are respectively compared after a 50% load disturbance at $t = 1$ s.

The results show that the order reduction of the controller, from a 11th to a 5th order, is effective. The \mathcal{H}_∞ controllers show a better disturbance rejection when compared to the classic and robust PI controllers. The effect of FC current limitation can be seen on the response obtained with the MIMO PI iLMI controller presented below.

Remark 2 We showed in Hernandez-Torres et al. [2010b] that the computation of fixed order controllers was also possible for this system. Good results were obtained using the function `hifoo` from Gumussoy et al. [2009].

Other proposed robust control structures

Other different **robust** control structures are also possible. We will now consider that three measures are available, with a measured output vector composed by:

$$y = [V_C \quad I_{fc} \quad I_{sc}]^T \quad (5.6)$$

This configuration is perfectly achievable since we have access to both voltage and current measurements. Using this structure, three other PI controllers using the iLMI algorithm are computed. These **proposed** controllers are subsequently named **prop1**, **prop2** and **prop3**. All structures considered are resumed in Table 5.1. Limitations on

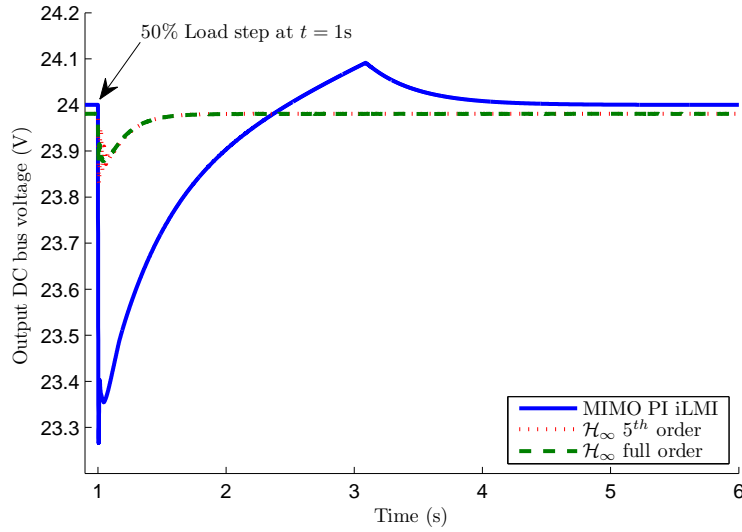


Figure 5.14: Simulation results, comparing several robust controllers.

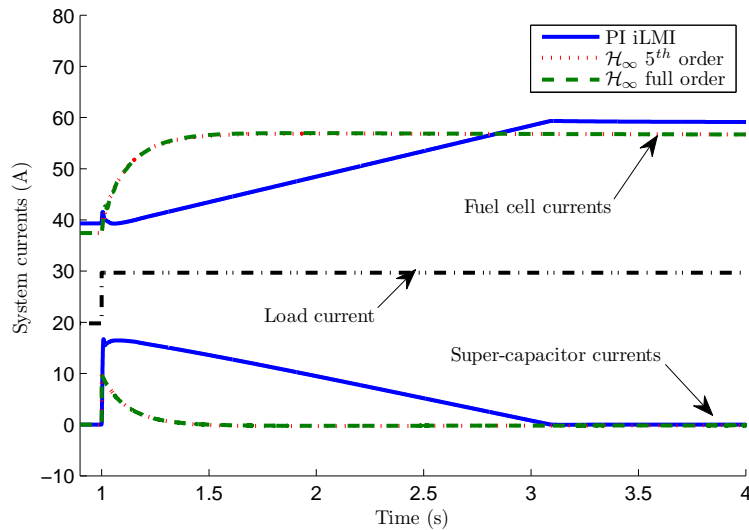


Figure 5.15: Simulation results, comparing several robust controllers.

Table 5.1: Control structures considered using the PI iLMI algorithm

Structure name	Performance output z	Measured output y
PI iLMI Original	$[W_{perf1}V_C \quad W_{perf2}I_{fc}]^T$	$[V_C \quad I_{fc}]^T$
prop1	$[W_{perf1}V_C]^T$	$[V_C \quad I_{fc} \quad I_{sc}]^T$
prop2	$[W_{perf2}I_{sc}]^T$	$[V_C \quad I_{fc} \quad I_{sc}]^T$
prop3	$[W_{perf1}V_C \quad W_{perf2}I_{sc}]^T$	$[V_C \quad I_{fc} \quad I_{sc}]^T$

the control inputs were also included using the same weighting function W_u presented in expressions (5.4) and (5.5).

The singular values plot of the sensitivity functions for each controller is presented

in Figure 5.16. These controllers were implemented using again the non-linear average model. A +10% load step at $t = 10$ s and a -10% load step at $t = 14$ s are applied. The disturbance rejection responses are presented in Figure 5.17 and Figure 5.18 show a zoom at the first load step at $t = 10$ s. The system currents are given in figure 5.19. For these time simulations, the FC current rate limitation was temporarily removed to show the natural dynamic response of each controller.

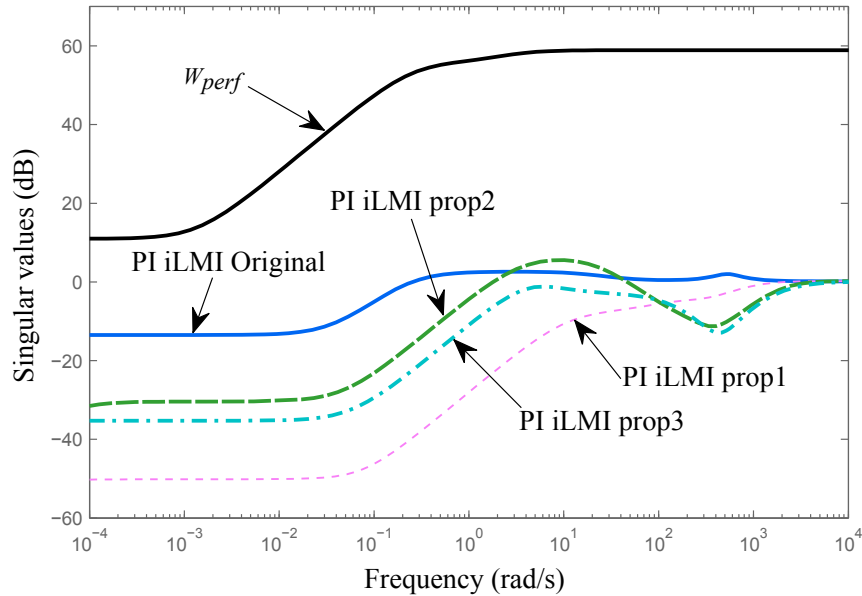


Figure 5.16: Sensitivity functions singular value plot for proposed robust PI controllers.

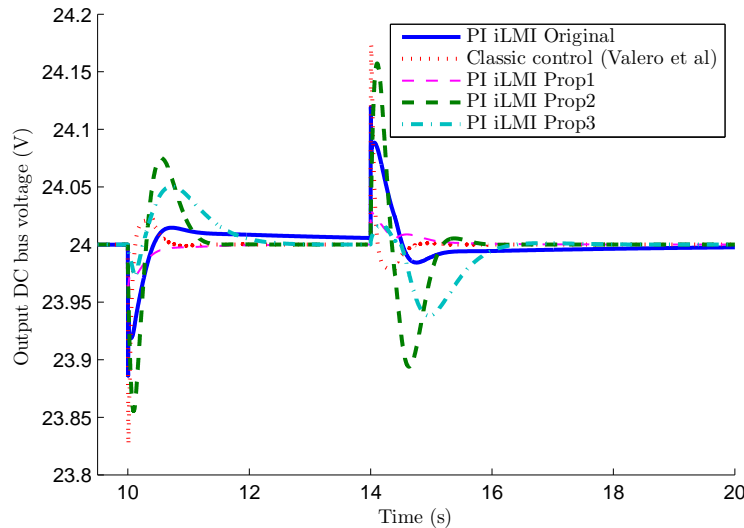


Figure 5.17: Simulation results of several proposed control structures.

These results show an overall good disturbance rejection for all controllers. A direct control of the auxiliary source current, as in the new proposed structures **prop2** and **prop3**, could be interesting if an optimal reference signal generation strategy is to be applied. In the literature this has been shown to be a more common case when using

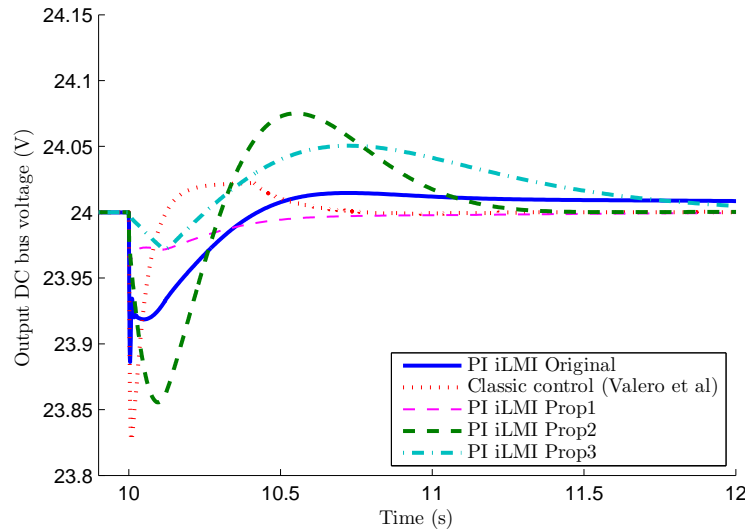


Figure 5.18: Simulation results of several proposed control structures.

a battery, actually the auxiliary source may be managed to operate at its maximum efficiency manipulating its operating point. It is clear from Figure 5.19 that the use of a given control structure has a performance improvement on the DC bus voltage disturbance rejection and not on the system currents. Again, this may be different using an optimal reference generation strategy.

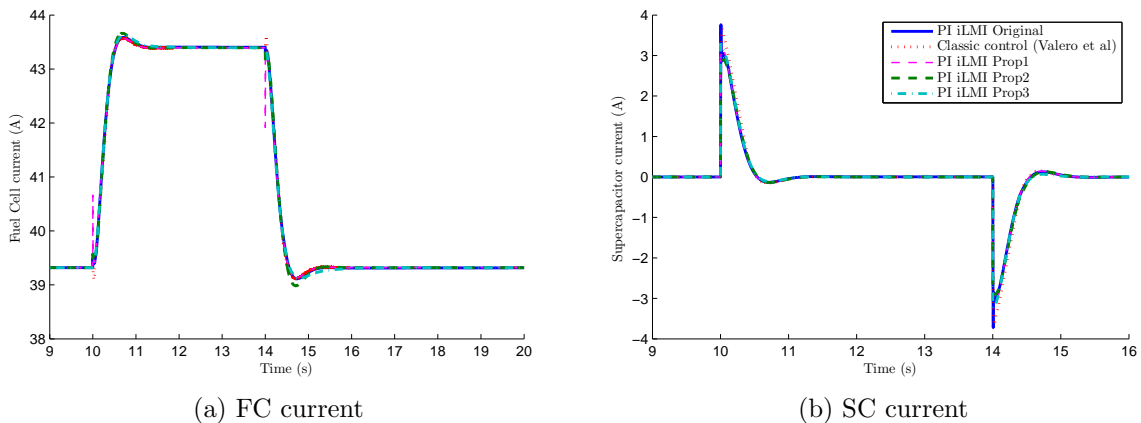


Figure 5.19: Simulation results.

Finally, in Figure 5.20, the control input simulation results are shown for a +50% load step at $t = 7$ s. These results are obtained using the non-linear average model of the hybrid generation system.

Experimental implementation on real-time test-bench

The GESI test-bench was used to implement the PI iLMI controller (Original) under a real-time environment. The fuel cell, a 1kW PEMFC was emulated by a 100A-60V DC programmable source and a SIMULINK/SPACE real-time environment. The source

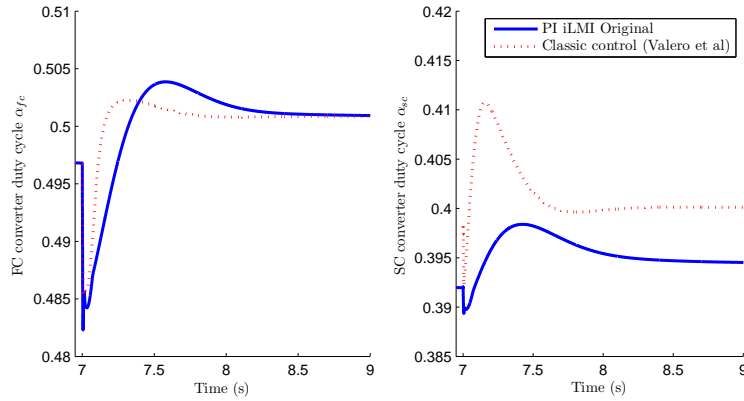


Figure 5.20: Simulation results for the control inputs α_{fc} and α_{sc} .

was prepared under the remote voltage control mode and was controlled through a 0–10V signal. The real measured polarization curve of the FC and the electrical equivalent models are used for static and dynamic modeling respectively. The SIMULINK model used to emulate the FC is presented in Figure 5.21.

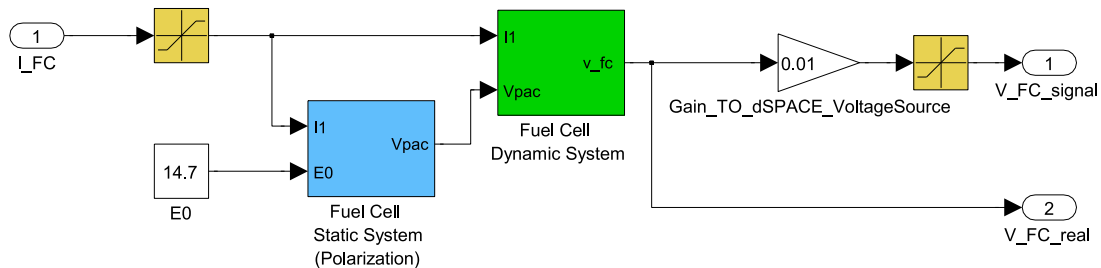


Figure 5.21: FC emulator model in MATLAB/SIMULINK.

The emulator is validated using load steps from a pure resistance load obtained under the “Resistance Mode” of a TDI RBL488 electronic load. The validation results obtained for load steps of 25% (0 – 10A) and 100% (0 – 35A) are presented in Figures 5.22 and 5.23 respectively. In the oscilloscope screen-shoots the channel 1 is the FC voltage and the channel 2 is the load current. These results are validated by comparison to the results obtained with computer simulation of the open loop system (no control).

The 1kW PEMFC chosen has fast dynamics, since the voltage response to a load step is around 10ms. Due to the DC programmable source limitations and the inherent electronic load dynamics, a voltage overshoot is observed in Figure 5.23. However, this should not be a problem since for closed-loop control validation dynamics are around 0.5sec. Moreover, load steps for control validation will be limited to a 50% maximum.

The oscilloscope screen-shoot of the closed-loop system implementation for the PI iLMI **original** controller is given in Figure 5.24. For this test a 20% load step was applied using the electronic load.

Implementation results and the comparison with the simulation results are presented in Figures 5.25 and 5.26 for the **original** proposed strategy using iLMI from Table 5.1. The results are shown for 5%, 10% and 20% load steps.

The results obtained with the real-time tests are interesting. The output DC bus voltage is properly regulated within the desired limits presented in Figure 5.3 for an

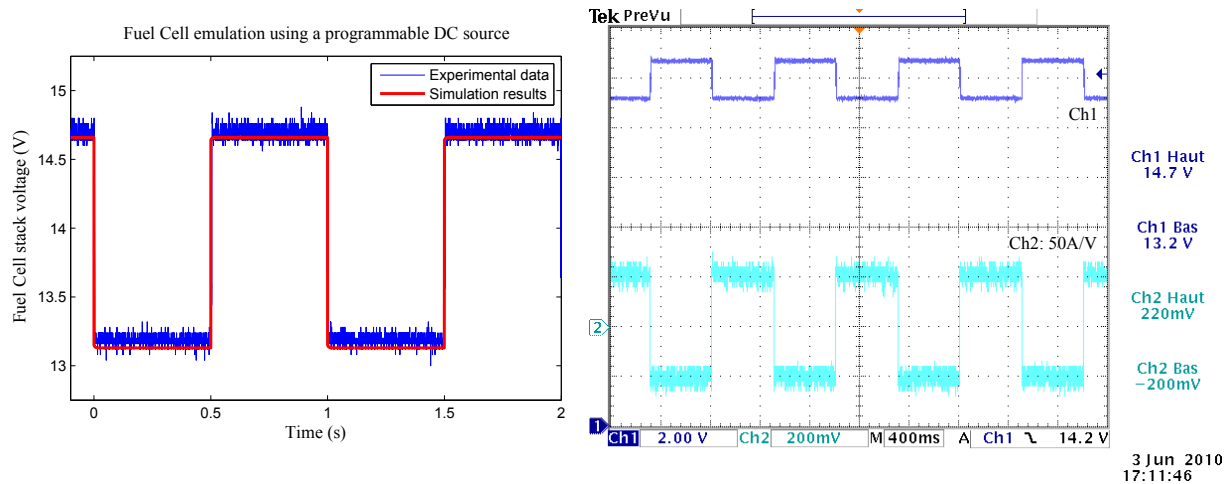


Figure 5.22: FC emulator validation (0 – 10A step), open-loop.

output voltage level at 24V. The instantaneous voltage drop in the real-time case is still high ($\sim 0.5V$) as seen in figure 5.25(b) and slightly different from that obtained using the average model simulation, this is probably due to high system losses in the power wiring. Despite this, this instantaneous voltage drop is still far from even the steady-state allowed lower limit which stands at 18.9V ($\approx 78.5\%$ of the nominal DC bus voltage), according to the standard described in Figure 5.3. We compare now the experimental results obtained when comparing the proposed PI iLMI **original** and the classic control structure from Valero [2004]. These results are compared in Figures 5.27 and 5.28 for the system currents and the output DC bus voltage respectively. The results obtained are similar to those obtained with the simulations. The classic PI has a faster regulating response time, however it presents a high current ripple with some small scale oscillations. These oscillations are not visible when using the PI iLMI control.

5.3.1.3 Robustness analysis

The robustness analysis in this dissertation is based on the computation of the structured singular value, i.e. the μ -analysis. However, at the cost of some conservatism, but for simplicity, the unstructured multiplicative input model is used to represent uncertainties for simplicity. Robust stability and robust performance are considered. The structured singular value is computed for the different studied (designed) controllers under the general control configuration forms. In the case of the studied hybrid system, uncertainties are given first by the electrical system parameters (inductances, capacitors and resistances), but are also representative of variations in the FC stack polarization curves as a consequence of degradation of cells. They could also represent slight changes in the FC humidification or temperature.

We consider parametric uncertainties on the hybrid system physical parameters. Resistance variations are a consequence of possible variations in the temperature, in addition to the component tolerance. See for example in Figure 5.29. the temperature evolution from an ambient temperature of 25°C after a continuous 1h operation (at nominal loading conditions) of the converters arrangement of the GESI test-bench.

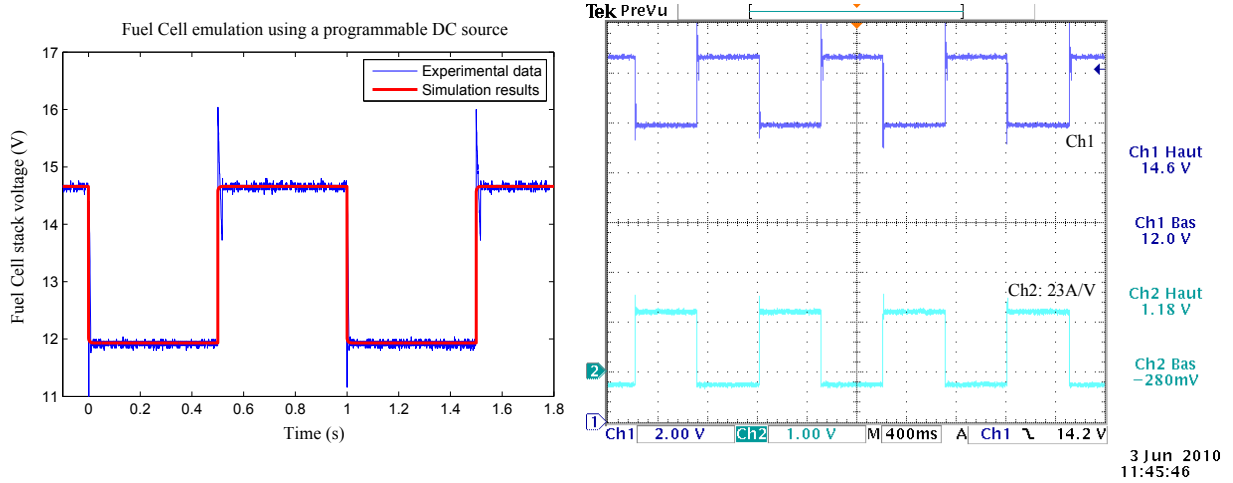


Figure 5.23: FC emulator validation (0 – 35A step), open-loop.

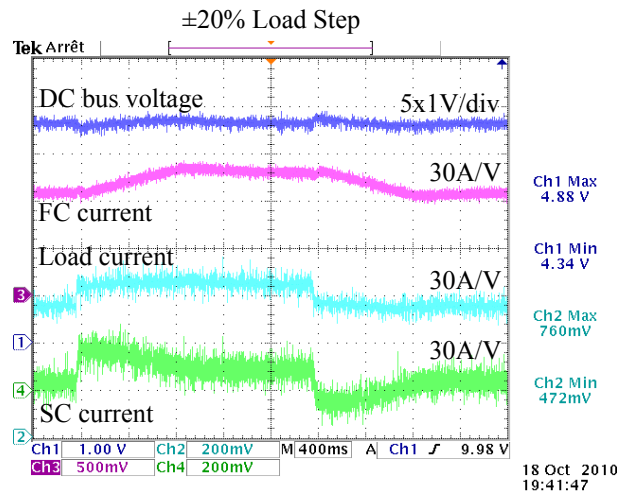


Figure 5.24: Experimental results for 20% load step.

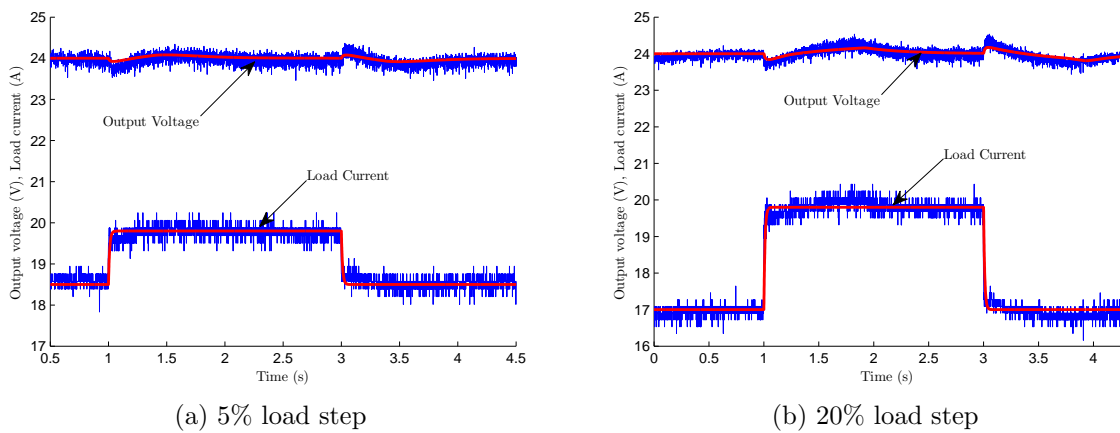


Figure 5.25: Experimental results for 5 and 20% load steps.

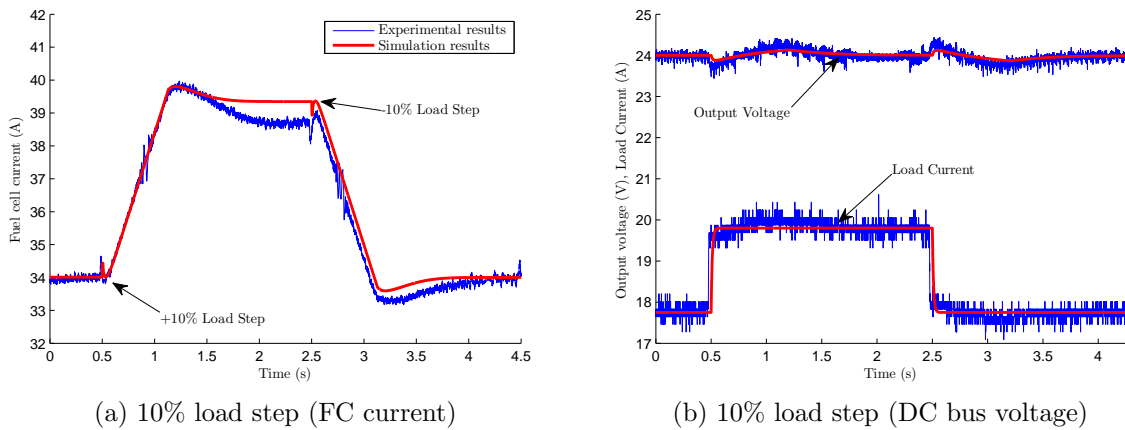


Figure 5.26: Experimental results for 10% load step (current and voltage).

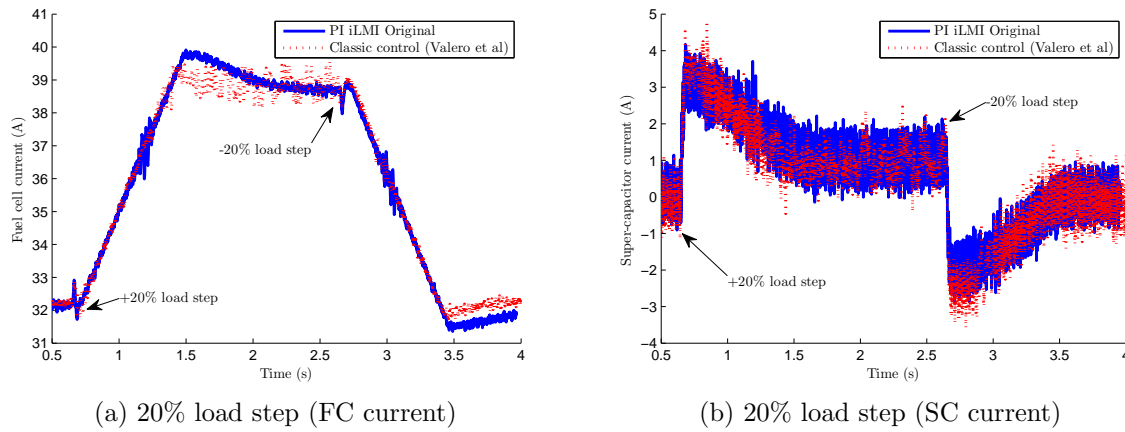


Figure 5.27: Experimental results for $\pm 20\%$ load step, comparison between robust and classic PI controllers.

The resistance variation with the temperature follows the well-known linear approximation given by:

$$R = R_0 [1 + \alpha(T - T_0)] \quad (5.7)$$

with α the temperature coefficient based on the conductor material (for cooper $\alpha = 3.9 \times 10^{-3}/^\circ\text{C}$).

If we take for example the resistance associated with the boost converter inductance $R_L = 0.0024\Omega$, a variation of 10°C could have an effect of a $\sim 5\%$ variation in R_L . Using this linear approximation of the resistance variation with temperature, an estimated $\pm 25\%$ variation in the value of resistances is considered, assuming higher temperature variations for longer operation times. In the case of capacitors, according to several manufacturers, a capacitor tolerance varies between $\pm 10\%$ and $\pm 20\%$ of the nominal value of the capacitor. In this work a scenario with a $\pm 10\%$ variation in the capacitor value is considered. Resistances, inductances and SC values may vary significantly during different loading and temperature conditions [Gualous et al., 2003]. Even when a maximum

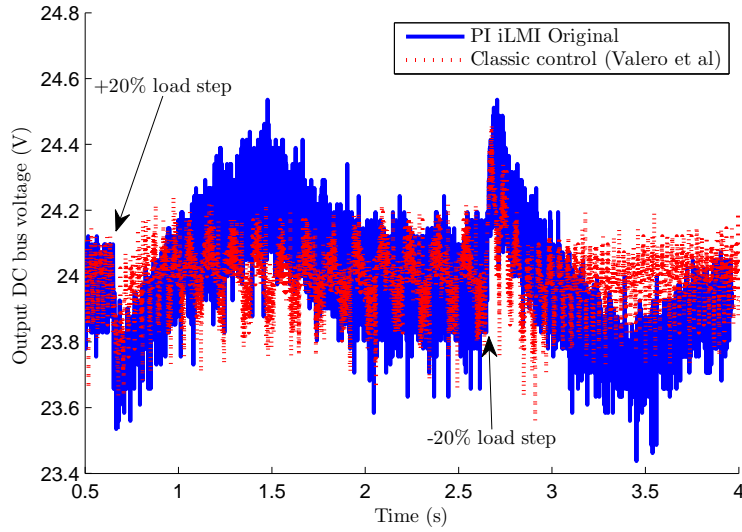


Figure 5.28: Experimental results comparison for 20% load step, output voltage.

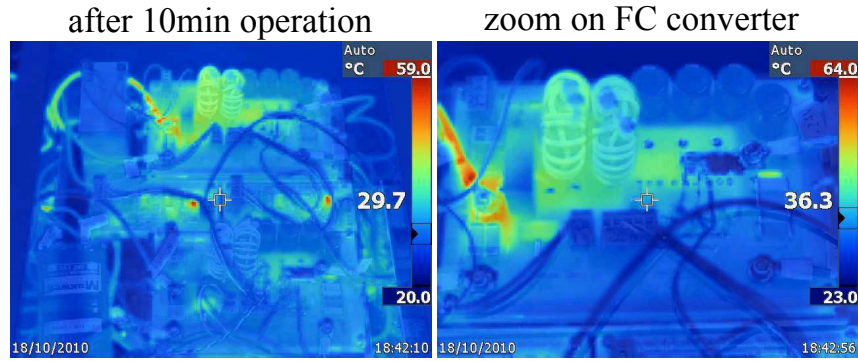


Figure 5.29: Temperature of the power converters after 1h operation at rating load.

variation of 20% in the loading conditions was considered, a pessimistic variation of 40% in the system inductances is studied. In the case of the SC different loading conditions are considered by taking different states of charge (SOC) of the SC. The SOC_{sc} is defined by:

$$SOC_{sc} = \left(\frac{v_{int_{sc}}}{v_{max_{sc}}} \right)^2 \quad (5.8)$$

with $v_{int_{sc}}$ the internal SC voltage and $v_{max_{sc}}$ the maximum possible SC voltage. This could lead to a capacitance variation of as much as -40% and $+10\%$ [Hernandez-Torres et al., 2011].

In Table 5.2 a summary of the considered uncertainties is presented.

With the open-loop system subject to these uncertainties the function `ucover` is used to compute the appropriate weighting functions that model the complex uncertainties. The bode plot of the different transfer functions and their respective obtained weighting function modeling uncertainties is presented in figure 5.30.

The obtained weighting functions are given by:

Table 5.2: Considered uncertainties levels

Parameter	Uncertainty
Resistances	$\pm 25\%$
Filter capacitors	$\pm 10\%$
Inductances	$+40\%$
Super-capacitor value	$-40\%, +10\%$

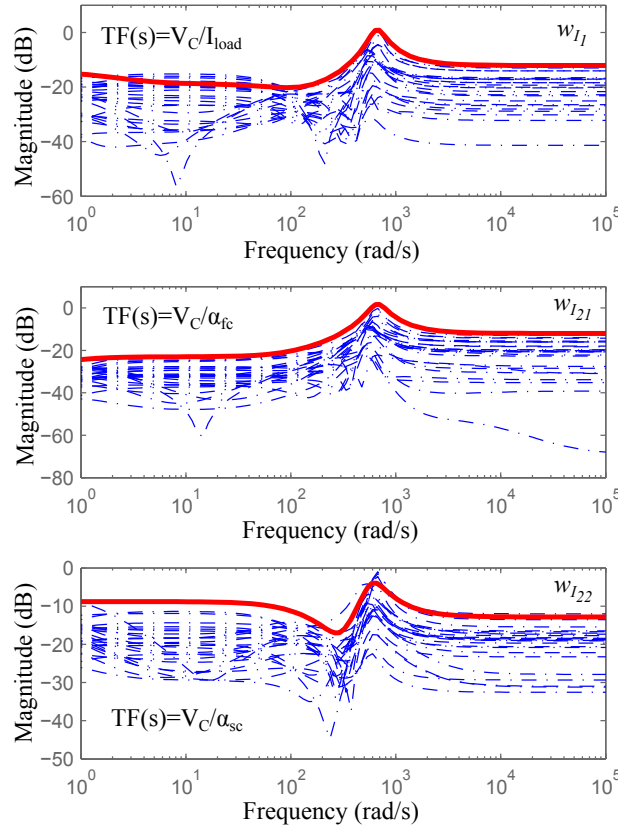


Figure 5.30: Weighting functions to model complex uncertainties .

$$w_{I_1} = \frac{0.109s^4 + 83.01s^3 + 1.085 \times 10^4 s^2 + 4.67 \times 10^5 s + 2.265 \times 10^5}{s^4 + 724.3s^3 + 4.978 \times 10^5 s^2 + 1.941 \times 10^8 s + 5.775 \times 10^9}$$

$$w_{I_{21}} = \frac{0.1133s^4 + 53.49s^3 + 3.792 \times 10^4 s^2 + 4.606 \times 10^6 s + 8.307 \times 10^6}{s^4 + 471.7s^3 + 7.007 \times 10^5 s^2 + 1.56 \times 10^8 s + 9.899 \times 10^{10}}$$

$$w_{I_{22}} = \frac{0.1017s^4 + 74.72s^3 + 5.004 \times 10^4 s^2 + 5.537 \times 10^6 s + 1.078 \times 10^7}{s^4 + 689.9s^3 + 8.198 \times 10^5 s^2 + 2.451 \times 10^8 s + 1.237 \times 10^{11}}$$

with:

$$w_{I_2} = \begin{bmatrix} w_{I_{21}} & 0 \\ 0 & w_{I_{22}} \end{bmatrix}$$

Robust stability (RS) and robust performance (RP) plots are obtained following the procedure described in chapter 3. To compute these plots we use the N-structure described in Figure 5.31.

The results obtained for robustness analysis (RS and RP) are given in Figure 5.32 for the uncertainties levels described before. From the results obtained it is clear that both controllers achieve robust stability and robust performance ($\mu < 1$). In the case of RS, for a maximum value of $\mu \approx 0.5$, this means that the closed-loop system can stand up to 200% the uncertainties levels before becoming unstable. RP performance is better for the full order \mathcal{H}_∞ controller. For a special uncertainty case before instability, given by $\pm 40\%$ uncertainty in all resistances and $\pm 20\%$ uncertainty in all capacitors and inductances, we compare the robust controllers presented in this section with the classic PI controller described earlier. The results are compared in Table 5.3.

In a final robustness test we considered uncertainty in the steady-state value of the SC voltage. This can be translated in the computation of a robust controller for different SOC_{sc} values. The uncertainty level was fixed to $0.5 < SOC_{sc} < 0.96$. Again, in this case the PI iLMI controller, guarantees RS and RP. Using the test-bench, an $SOC_{sc} = 0.5$ was found to be minimum possible capacitor charging for proper operation. Figure 5.34 show the real-test system response to $\pm 10\%$ load steps for $SOC_{sc} = 0.5$ and $SOC_{sc} = 0.75$. As predicted by the robustness analysis, the closed-loop control performances are preserved.

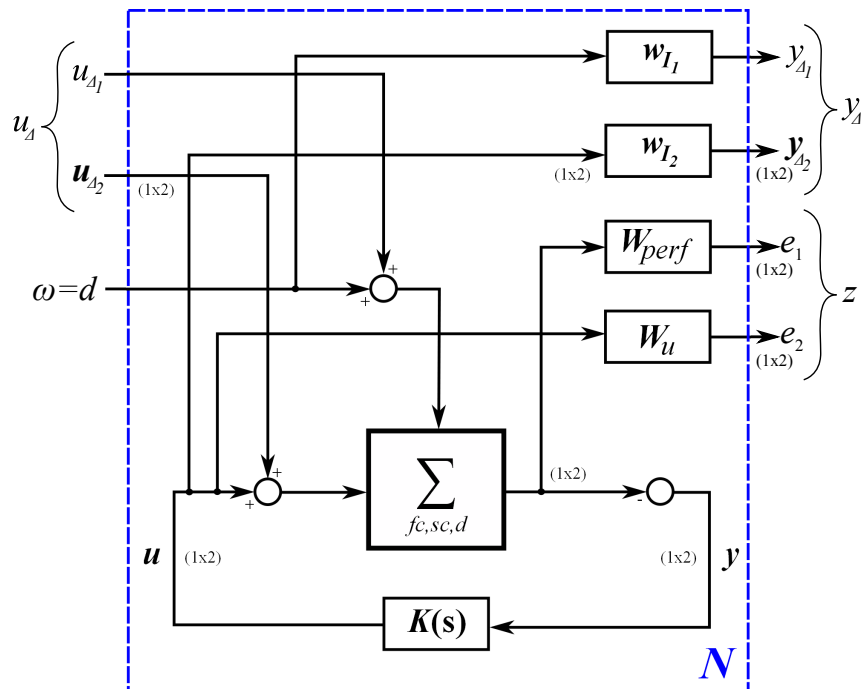


Figure 5.31: N-structure used to compute structured singular values plot.

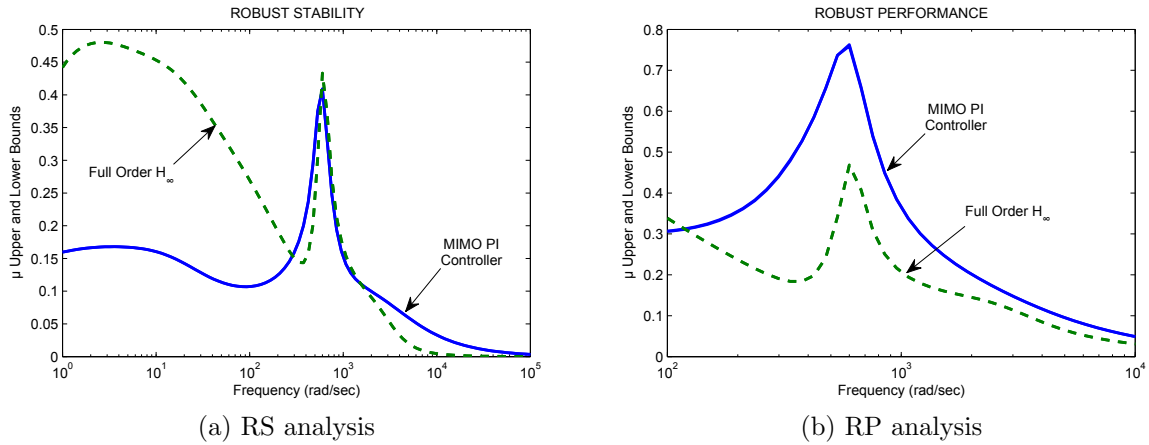


Figure 5.32: Robustness analysis using μ -analysis.

Table 5.3: Maximum μ values for RS

Method	$\mu_{max}(RS)$
Valero et al	1.4564
Sailler et al	1.4254
PI iLMI	1.0312
Full order \mathcal{H}_∞	0.9038

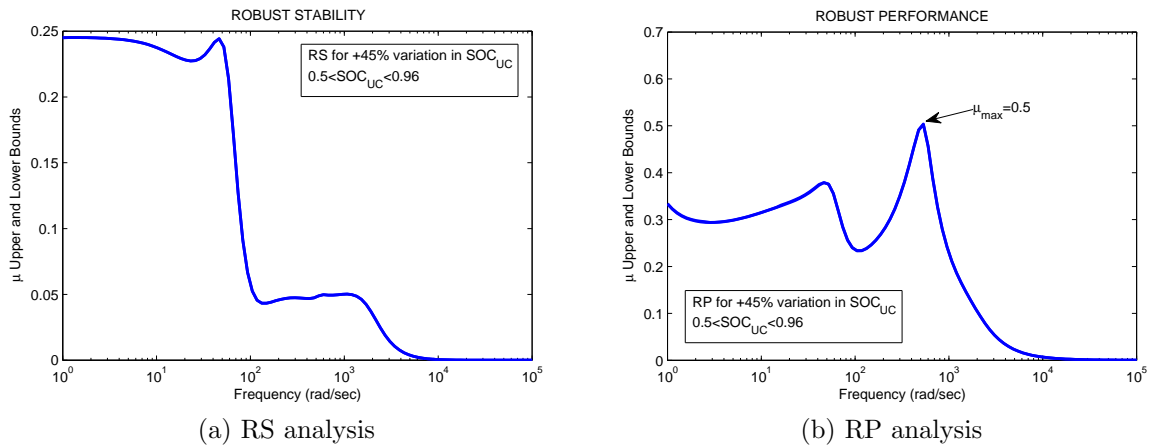


Figure 5.33: Robustness analysis with μ -analysis using the iLMI PI controller.

Component design after robustness

An analysis on the importance of robustness and its relationship with the entire design system procedure can be done. The robustness analysis of the whole control strategy can be exploited in different ways. In the design process of an equipment, in this case the hybrid power generator, it could be important to minimize certain physical parameters, as the mass or the volume in the case of an on-board or a transport application. In that case robustness can be linked to the system mass minimization through the adequate choice

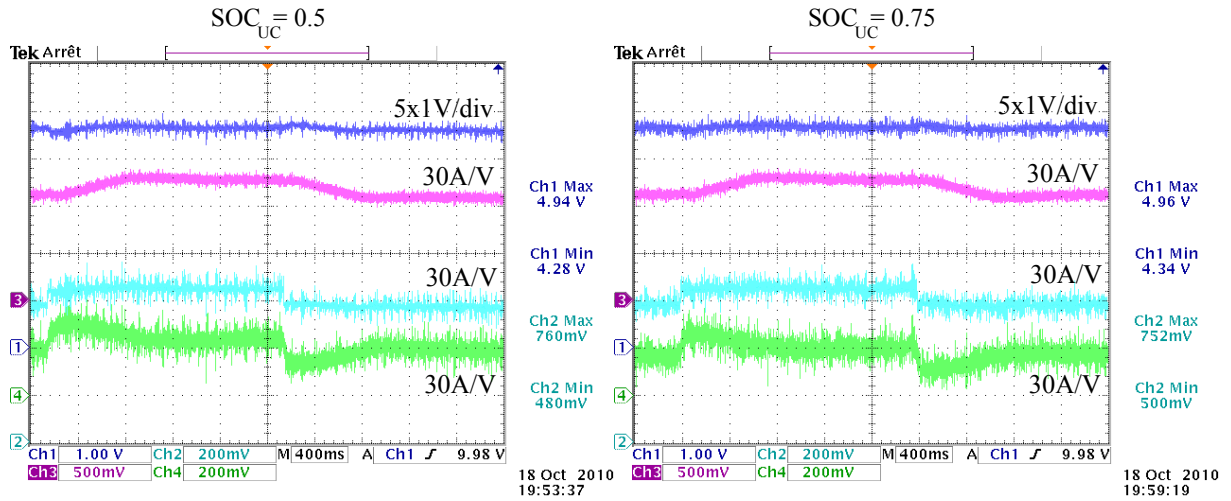


Figure 5.34: Experimental results for several SOC_{sc} values.

of system components.

As it was presented in Hernandez-Torres et al. [2011] and in the work of Sautreuil [2009], in the design process of a system, a dedicated tool that considers the final complete system performance from the beginning of the design process could be very interesting. The system components variations are then defined as the parametric uncertainties. In order to account for the performance specifications parameters influence on system robustness, several curves, that can be assimilated in some extent to Pareto curves, were plotted for some variations on the DC bus filter capacitance. With the single parameter variation defined as:

$$q_p = q_{nom}(1 + k_q p_q \Delta) \quad (5.9)$$

with q_{nom} the nominal value of the parameter and p_q the parameter variation, a new parameter, the “robustness factor”, defines the deviation from the fixed parameter variation level, i.e.:

$$\text{Robustness factor} = \max |q - q_{nom}| \text{ s.t. } \mu < 1 \quad (5.10)$$

In Figure 5.35 the curves for the maximum peak magnitude (top-left) and the closed-loop bandwidth (top-right) are presented. These curves corresponds to variations in the DC bus capacitor value and the robustness factor is the maximum level of allowable parameter variation to guarantee robust performance ($\mu = 1$). The robustness factor gives the level of variation for the capacitance C and the difference between this capacitance and the nominal value is defined as the improvement, since the relation between the volume and the value of the capacitance is linear, this could be translated into a gain in volume. For the specific case of the considered hybrid system, this gain is around 1800cm^3 , proving the contribution of the robust control strategy to component design. Of course, the limitation of the desired filter frequency value and the capacitor satisfying this frequency should be respected. However as a drawback this procedure cannot be applied to the sizing of the SC for example, since the natural frequency of SC's are lower than 1Hz, far from the natural frequency of the DC bus filter.

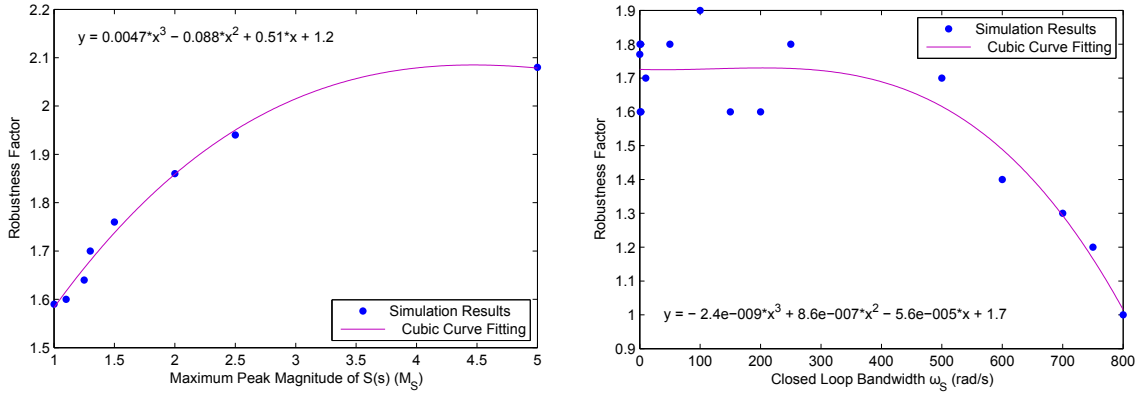


Figure 5.35: Pareto curves for a proposed component design.

5.3.2 Hybrid boost system with reversible converter

In this section the control design of the hybrid system composed by two parallel-connected boost converters with reversibility for the converter dedicated to the auxiliary source. The use of a second reversible converter is a more common solution for charging the auxiliary source. Let us recall that, in the previous case the use of a flyback converter was bounded to the availability of the GESI set-up for experimental tests. In the latter case, the system parameters were taken from the “Emulator” test-bench. Even when a new parallel boost arrangement, with a second reversible converter, was recently installed in the “Emulator” test-bench at G2ELab during the thesis experimental works for Tritschler [2010], some problems related to the original IGBT power switches design have made it impossible to experimentally validate the results that will be described in this section. For these reason only simulation results using MATLAB/SIMULINK are presented.

As presented in the chapter 4, in section 4.3.3, the average modeling is very similar to the case of non-reversible converter and so is the control strategy developed for this system. The proposed control configuration extended with the performance weighting functions is presented in Figure 5.36. In order to guarantee a fast transient response, and given the high values obtained for the conditioning number γ , the cut-off frequency for W_{perf_1} was fixed at $\omega_B = 50\text{rad/s}$. For a faster current response, ω_B for weight W_{perf_2} was fixed three times higher at 150rad/s . The module margin for the sensitivity function was fixed for both cases at $M_S = 2.67$.

The performance weighting functions are given by:

$$W_{perf_1} = \frac{0.375s + 50}{s + 0.005} \quad (5.11)$$

$$W_{perf_2} = \frac{0.375s + 150}{s + 0.015} \quad (5.12)$$

Weighting functions W_u are identical to those considered in the previous case with expressions (5.4) and (5.5). The iLMI algorithm yields a solution for a MIMO PI controller, after nine iterations. The conditioning values are respectively $\gamma = 124.16$ for the full order \mathcal{H}_∞ controller (11^{th} order) and $\gamma = 1.0655 \times 10^5$ for the PI controller. The MIMO PI controller is given by:

$$PI_{iLMI} = \begin{bmatrix} 0.0002 + 0.0807/s & 0.0001 + 0.0299/s \\ 0.0001 + 0.0916/s & 0.0075/s \end{bmatrix}$$

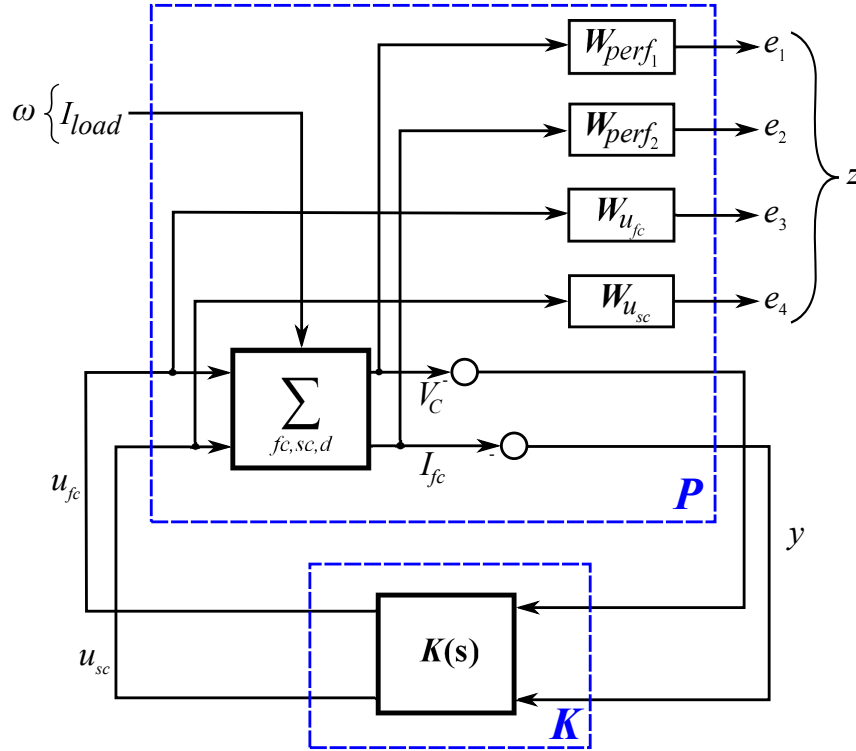


Figure 5.36: The proposed control configuration.

The singular values plots of the sensitivity functions are given in Figure 5.37. The \mathcal{H}_∞ controller order reduction was found feasible to a 4th order system. In Figure 5.38 the full and reduced order sensitivity functions are compared. Despite the high value obtained for the conditioning number γ , the robust controllers gain performances are within the desired and acceptable bounds. A better disturbance rejection is obtained for both \mathcal{H}_∞ controllers compared to the PI iLMI, for which a non-zero steady-state error may occur. Gain performances (closed-loop system \mathcal{H}_∞ gain) for the obtained controllers are summarized in Table 5.4.

Table 5.4: Closed-loop system \mathcal{H}_∞ gain

Controller	Performance
PI iLMI	$\mathcal{H}_\infty < 2.9992$
Full order \mathcal{H}_∞	$\mathcal{H}_\infty < 2.5722$
Reduced order \mathcal{H}_∞	$\mathcal{H}_\infty < 3.4782$

Finally time-domain simulation results are presented. Computing the linear closed-loop model, the controllers responses to a unitary step on the load current are given in Figure 5.39. The reduced order controller yields to a few oscillatory response, but small

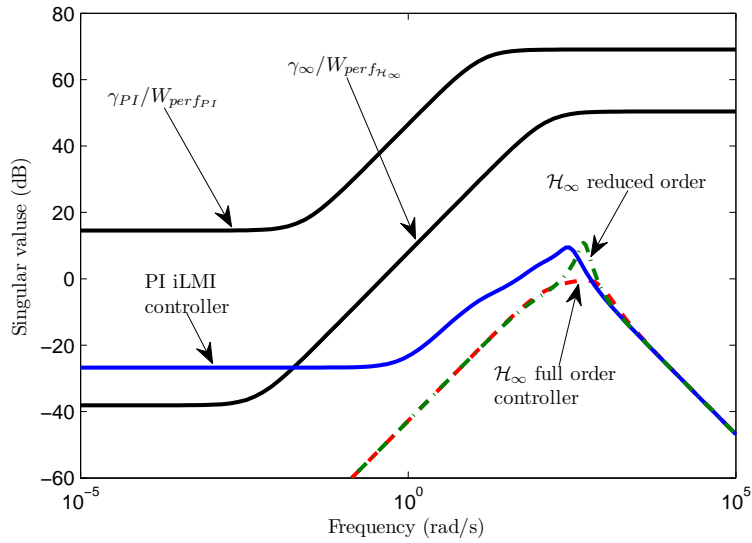


Figure 5.37: Singular values plots of the sensitivity functions $S(s)$.

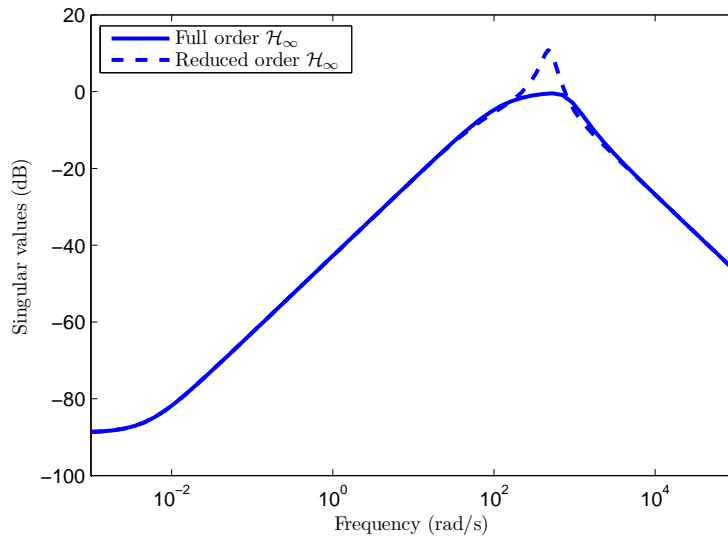


Figure 5.38: Singular values plots of the sensitivity functions for the full and reduced order controllers.

in amplitude and still with a fast and good disturbance rejection. Using the MIMO PI controller, the system stabilizes within the desired bounds after 20msec approximately.

Figure 5.40 show the simulation response of the MIMO PI controller using the non-linear average model of the hybrid boost system with reversible converter. The simulation corresponds to the response to a 50% load step. The dynamical norm envelope limiting the DC bus voltage is included for illustration purposes in the figure. The results are similar to those obtained with the linear simulations. Finally, a series of load steps is applied to the non-linear average closed-loop model. The results obtained for these series steps are given in Figure 5.41 for the output DC bus voltage and in Figure 5.42 for the system currents respectively. Note the important contribution of the SC to the transient load current requirement, avoiding large and fast current transients on the FC current

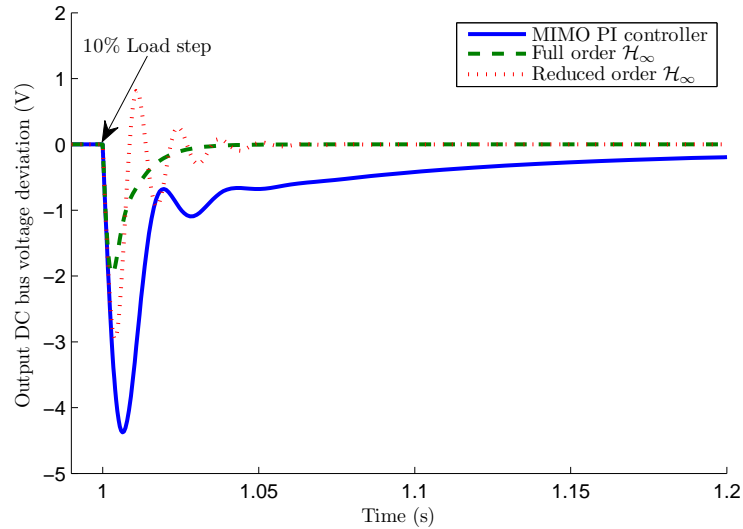


Figure 5.39: Simulation results using linear system (DC bus voltage).

dynamic. As with the initial hybrid boost system, a current rate limitation can be included for FC protection in the case of a real-time application.

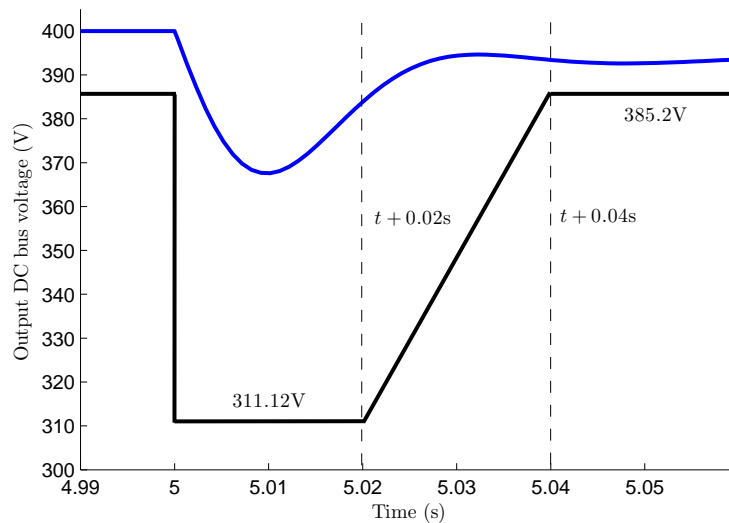


Figure 5.40: Simulation results using non-linear system (DC bus voltage) with PI iLMI controller.

5.3.3 Hybrid boost converters with voltage inverter

As an extension to the previous system, now a voltage inverter is considered. The use of a voltage inverter is of interest for connection to the network or for an isolated (islanded) operation with an AC application. In this dissertation only the hybrid system with a voltage inverter operating as a voltage source is considered. However, the control strategies presented can be also adapted to the current source operating mode, considering connec-

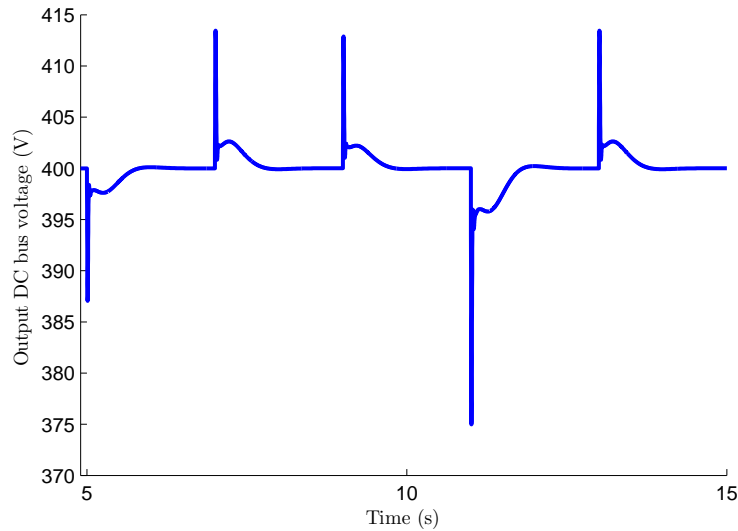


Figure 5.41: Simulation results for series of load current steps (DC bus voltage) with PI iLMI controller.

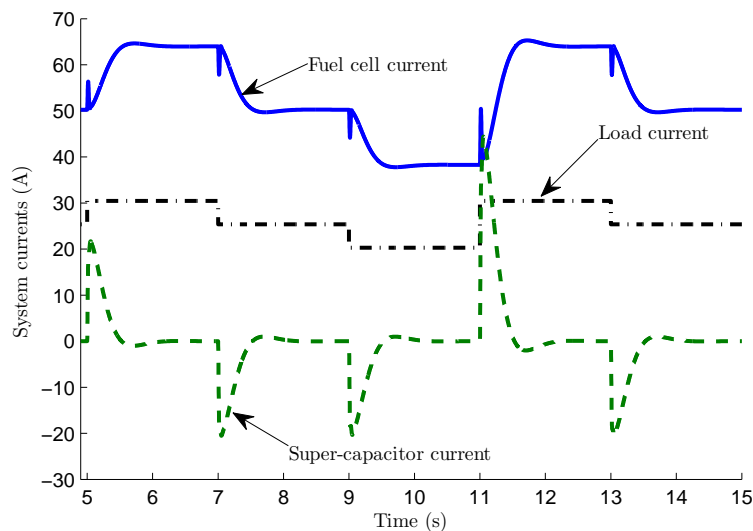


Figure 5.42: Simulation results for series of load current steps (DSystem currents) with PI iLMI controller.

tion to the power network. The voltage inverter model was presented in chapter 4, in section 4.3.4. The topology of the hybrid system with voltage inverter was presented in Figure 4.24. A block diagram recalling both input and output variables of the inverter system is presented in Figure 5.43. The interconnection of this system to the hybrid boost converter system is then considered. Note that considering separate decoupled system is possible since, using Equations (4.16), both models are connected through variables $I_{inv,d,q}$, $\beta_{d,q}$ and output DC bus voltage V_C (which is not a state-variable in the inverter system).

In this section a focus is given to reduced and fixed order \mathcal{H}_∞ controllers. Indeed, as a limitation to the iLMI algorithm, the computation of MIMO PI controller for the complete system was found to be an almost unfeasible problem. Convergence was **not** obtained

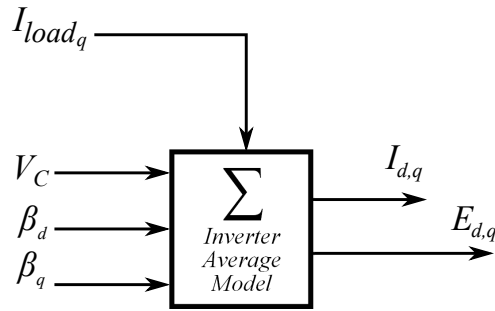


Figure 5.43: Block diagram of the voltage inverter system.

using the iLMI algorithm, or, when obtaining convergence, the conditioning number γ was too high to guarantee desired performances. For this reason we focused on robust reduced and fixed order \mathcal{H}_∞ controllers. Fixed order controllers were computed using the function `hifoo` from Gumussoy et al. [2009].

In a first approach, the decentralized system of the voltage inverter is considered for control, in that case, the hybrid boost system control is assumed perfect. Then, a complete system including the hybrid boost converters is analyzed. Let us now describe the “classic” control strategy associated with the voltage inverter.

5.3.3.1 “Classic” control approach

The classic approach for inverter control as a voltage source is given in figure 5.44. Again, as for the control of the hybrid boost converters, the use of a multi-loop structure is a common practice. In this structure the external loop controls the voltage $E_{d/q}$ at the capacitor C_{AC} terminals. The inner loop controls the inverter output current $I_{inv d/q}$ or the current through inductance L_{AC} . For this review of a classic control strategy, we will focus on simple PI control, based on the principle of a controller under a rotating frame. This is why the inverter model is given under Park’s referential. As before, several other options are possible. In the interesting work of Valero [2004] different “classic” control methodologies were tested, including validation on the “Emulator” test-bench. These methodologies include: simple PI under Park’s referential, the “generalized integrator” for voltage regulation at different resonant frequencies, and even the RST controller. Note also that in the classic approach the inverter system is decoupled. The system is decoupled by simplifying the terms $I_{inv d/q} \omega_{net}$ and $E_{d/q} \omega_{net}$ in the average inverter model (see inverter model in chapter 4).

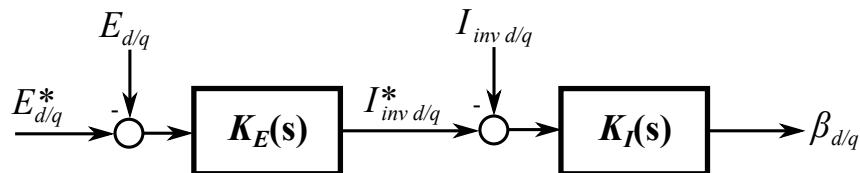


Figure 5.44: Classic voltage inverter control strategy.

For the classic PI controller we consider a similar control strategy as in section 5.3.1. The controller design is based on the frequency dynamic of the closed-loop and the PI constants are computed using the dominant poles approximation and the classic second order desired transfer function.

For the given values of R_{AC} , C_{AC} and L_{AC} , it can be easily shown that for the voltage and current loops we have:

- Inverter voltage loop $K_E(s)$:

$$k_p^E = 2\zeta_e\omega_{n_e}C_{AC}, k_i^E = \frac{C_{AC}\omega_{n_e}^2}{k_p^E}$$

- Inverter current loop $K_I(s)$:

$$k_p^I = \frac{\omega_{n_i}L_{AC} - R_{AC}}{(V_{C_e}/2)} \quad (5.13)$$

For a faster dynamic of the inverter currents and to avoid disturbance from the switching frequency, the current loop bandwidth frequency is fixed at $\omega_{n_i} = 5000\text{rad/s}$. For the voltage loop the bandwidth frequency is fixed for a slower response in voltage at $\omega_{n_e} = 500\text{rad/s}$ with a damping factor $\zeta_e = 1$.

With these settings, simulation results are obtained for the complete hybrid boost converters plus inverter system using the linear average model. Results are given in Figure 5.45 for the DC bus voltage V_C , and the inverter currents $I_{d/q}$ and voltages $E_{d/q}$. The three-phase currents delivered by the voltage inverter are presented in Figure 5.46. These results were obtained for a 20% load step in the three-phase load currents, given by a 20% load step in current I_{load_q} . This classic control methodology has an effective and fast disturbance rejection (5msec). Moreover, this approach has the advantage of simplicity in both design and implementation.

5.3.3.2 Robust control approach

In a first proposition we will consider the robust control of the inverter system only. This considers a control decoupled from the hybrid boost converters system. We will compare later the results obtained with the centralized controller of the complete electrical system.

The robust control configuration approach for the voltage inverter system control is given in Figure 5.47.

Weighting functions are designed in a similar manner as in the classic control methodology in terms of the desired frequency dynamic. The performance weight for the current loop is fixed with a cut-off frequency $\omega_B = 5000\text{rad/s}$. The module margin for the sensitivity function was fixed at $M_S = 1.5$. The \mathcal{H}_∞ controller is obtained with a conditioning number $\gamma = 1.9983 \times 10^4$. Despite this, the desired gain performances are met. A fixed order controller is also computed using `hifoo`, the order is fixed at 4th. The full order \mathcal{H}_∞ controller can be reduced to a 6th order system.

The singular values plots of the sensitivity functions is presented in Figure 5.48. As it will be presented in the following section, the improvement in robustness is important when compared to the classic methodology. Moreover, the time response is again representative of a good disturbance rejection system. Time-domain simulation results are given in Figure 5.49 for a 10% load step. A better disturbance rejection is obtained with the fixed order controller. The different controllers gain performances (closed-loop \mathcal{H}_∞ gain) are summarized in Table 5.5.

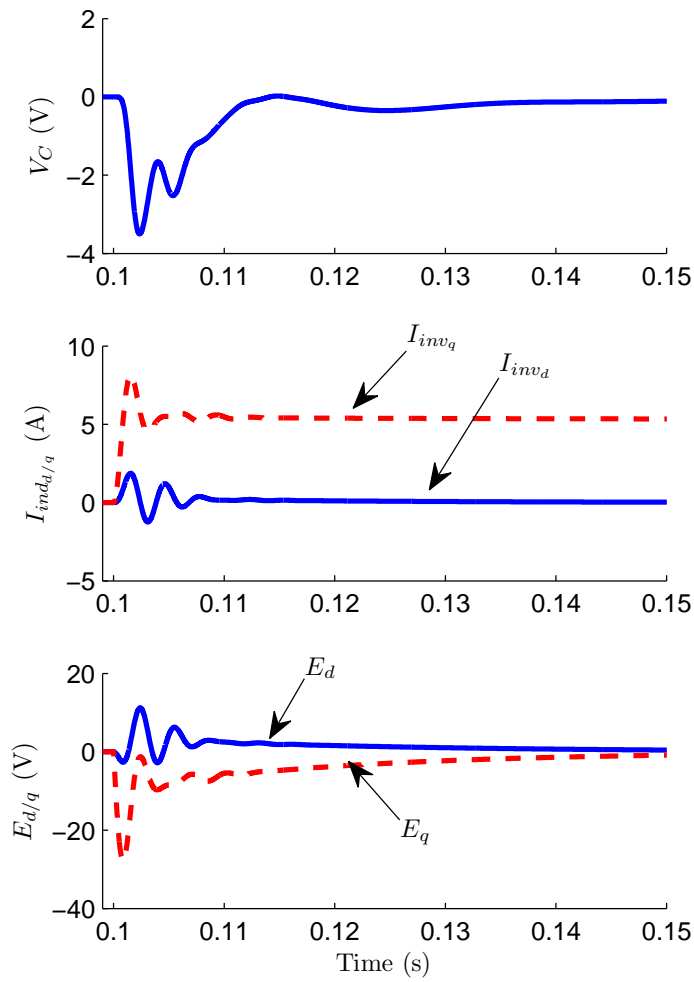


Figure 5.45: Simulation results using classic control.

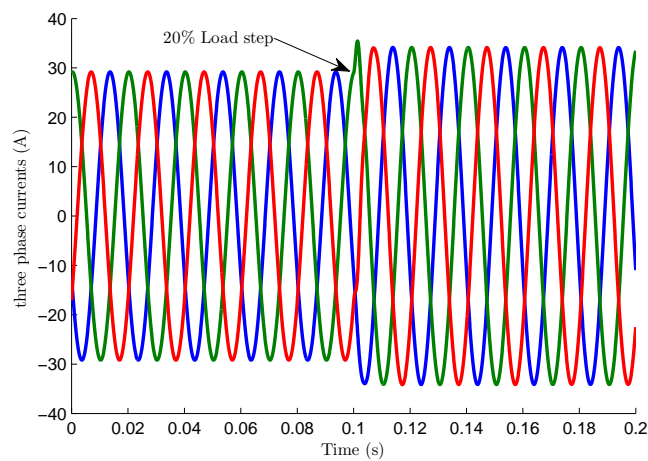


Figure 5.46: Three-phase simulation results using classic control.

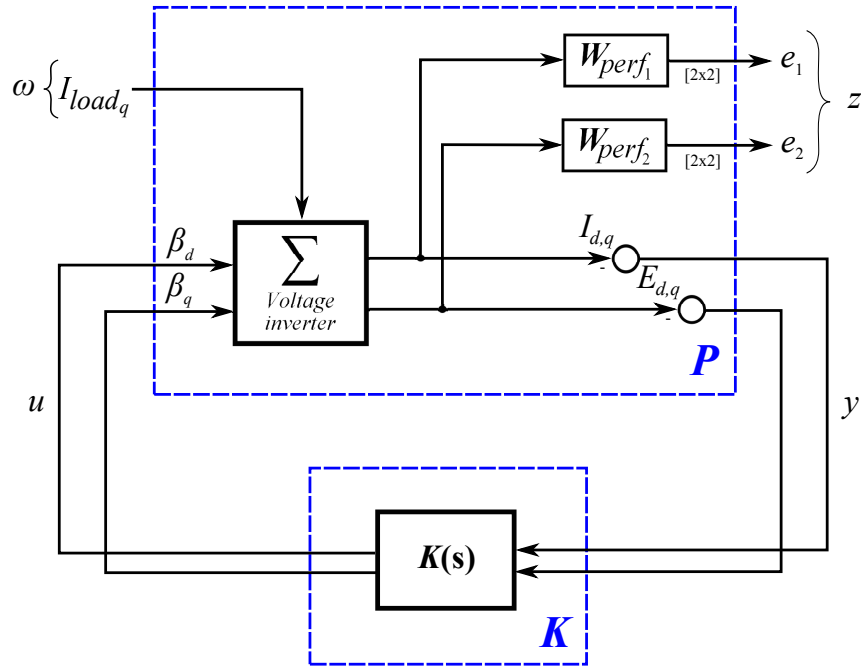


Figure 5.47: Control configuration in the P-K form for the inverter system.

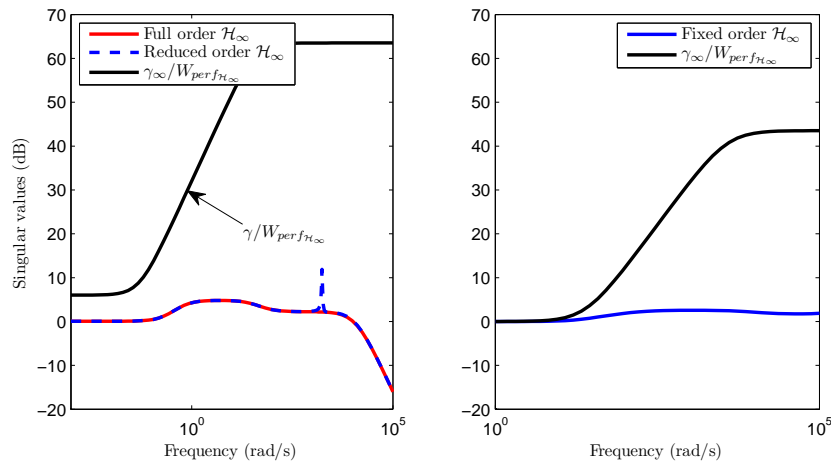


Figure 5.48: Singular values plots of the sensitivity functions $S(s)$.

Table 5.5: Closed-loop \mathcal{H}_∞ gain

Controller	Performance
Full order \mathcal{H}_∞	$\mathcal{H}_\infty < 1.7394$
Reduced order \mathcal{H}_∞	$\mathcal{H}_\infty < 3.9313$
Fixed order \mathcal{H}_∞	$\mathcal{H}_\infty < 4.3548$

Complete electrical sub-system control

Now the control of the complete electrical system is presented. The complete electrical sub-system model is given by the interconnection of non-linear systems , and . The

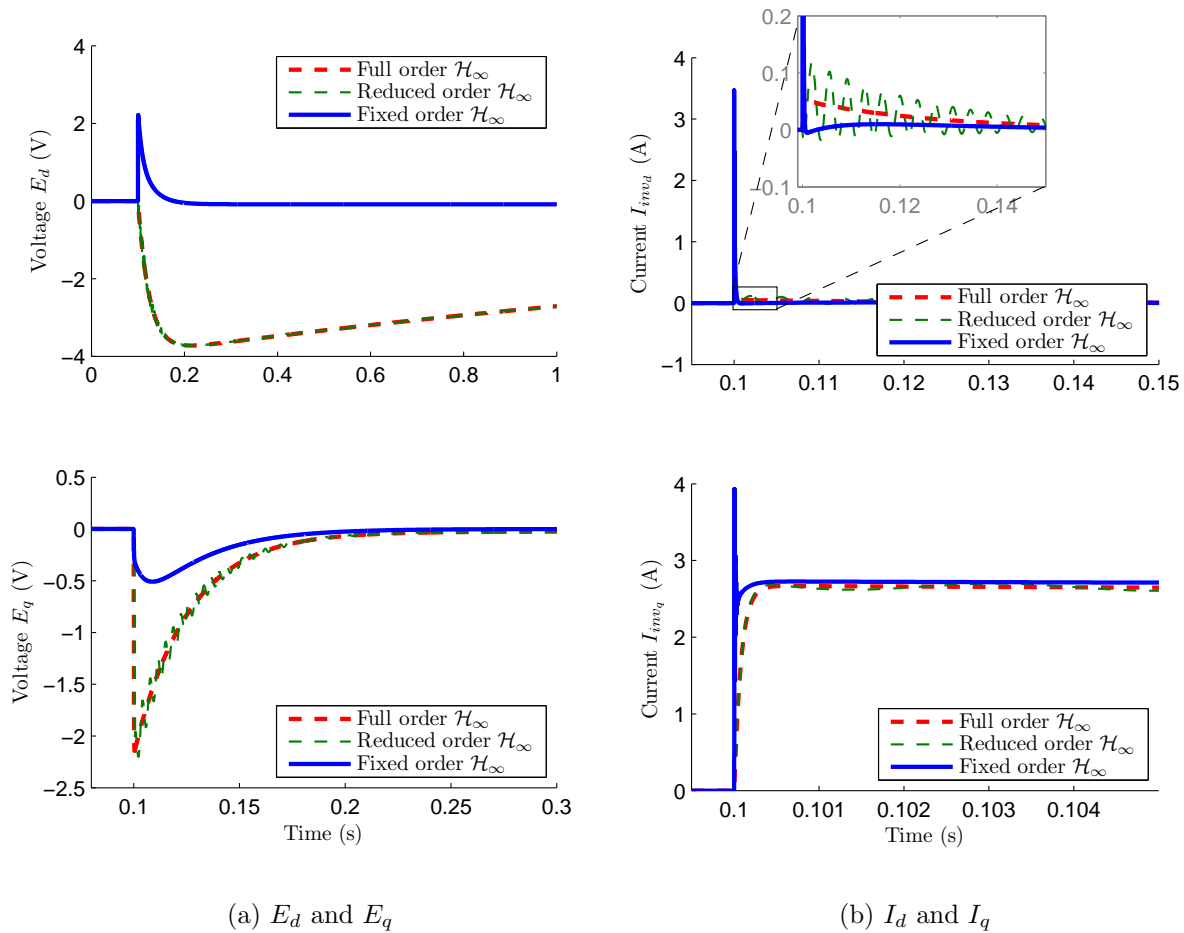


Figure 5.49: Simulation results for several control structures.

complete non-linear system is then linearized for an operating condition corresponding to a 5.27kW load power or a 15.37A load current at $fp = 0.9$. The proposed robust control configuration approach is given in Figure 5.50. Weights for the hybrid boost converters (W_{perf_1} and W_{perf_2}) are the same as described in section 5.3.2. The inverter control weights were presented in the previous section.

A full order \mathcal{H}_∞ controller and a fixed order \mathcal{H}_∞ controller using `hifoo` are computed. Both, the reduced order and the fixed order controllers, are given by an 8th order system. The full order controller was obtained with a conditioning number $\gamma = 2.1391 \times 10^4$. The closed-loop \mathcal{H}_∞ gains obtained are $\mathcal{H}_\infty < 2.0886$ and $\mathcal{H}_\infty < 2.8653$ for the full order and the fixed order controllers respectively. The low frequency gain A_ϵ for the performance weights with the fixed order controller were fixed at 1×10^{-1} for better convergence in the `hifoo` function.

The singular values plot of the sensitivity function $S(s)$ is given in figure 5.51. In figure 5.52 we compare the sensitivity of the robust fixed order controller and the classic PI control, illustrating the gain in robustness.

As in the previous case, we use now the linear average model to obtain the time-domain response of the system to a load disturbance. Figure 5.53 compares the full and fixed order \mathcal{H}_∞ controllers with the classic PI control after a 10% load step. Disturbance rejection is achieved by all controllers within the desired bounds presented in Figure 5.3 for systems

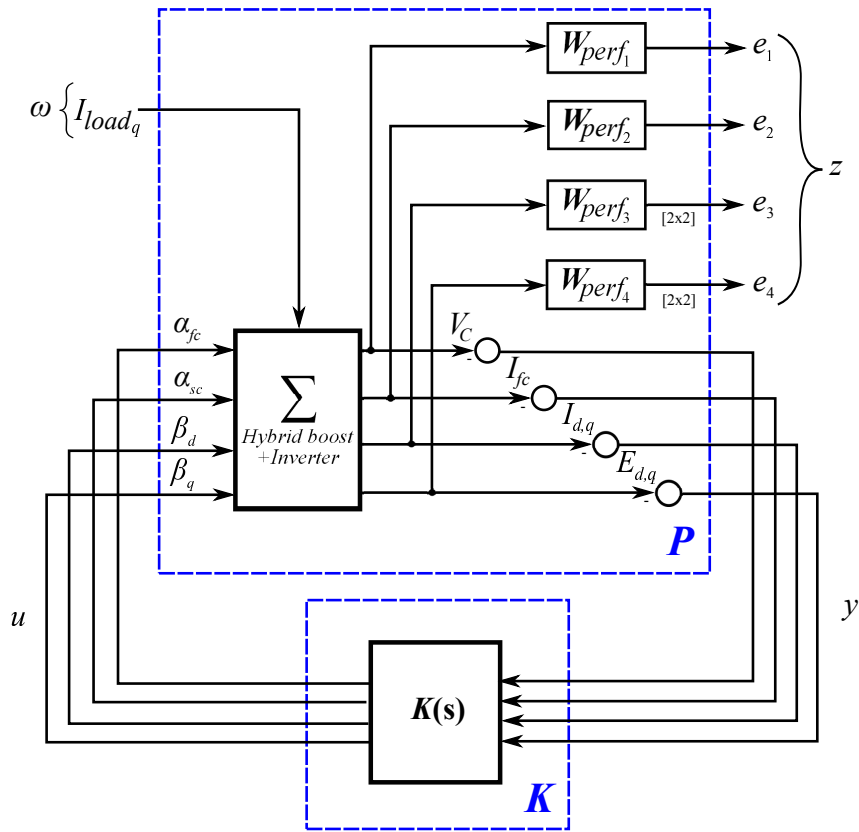


Figure 5.50: Control configuration in the P-K form for the complete electrical system.

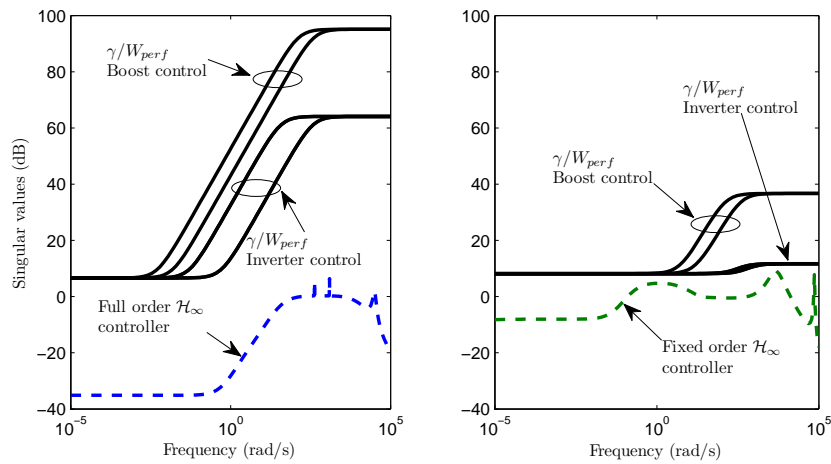


Figure 5.51: Singular values plot of the sensitivity function $S(s)$.

with DC voltages $> 200V$. The dynamic behaviour of voltages $E_{d/q}$ and currents $I_{invd/q}$ are very similar to those obtained in the previous section with the decentralized controller methodology. Finally, Figure 5.54 presents the three-phase current rejection of the load disturbance. Note the similarity on this result with the obtained for the classic PI control shown in Figure 5.46.

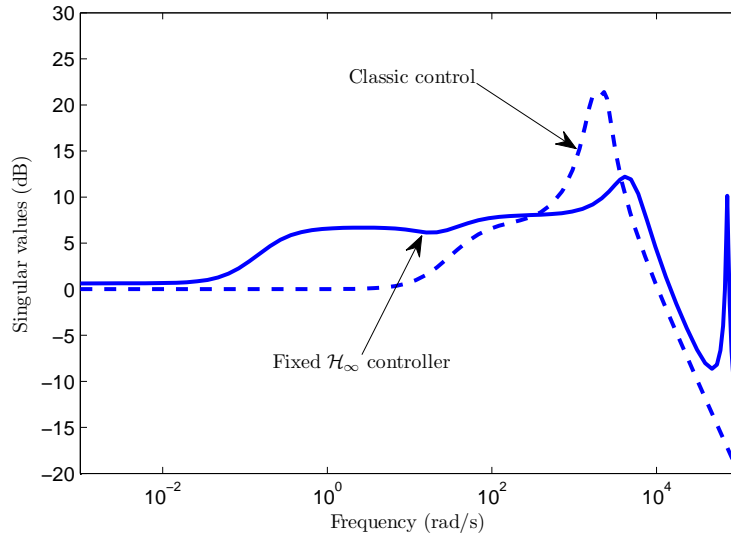


Figure 5.52: Closed-loop singular values plot, comparison fixed order \mathcal{H}_∞ and classic control.

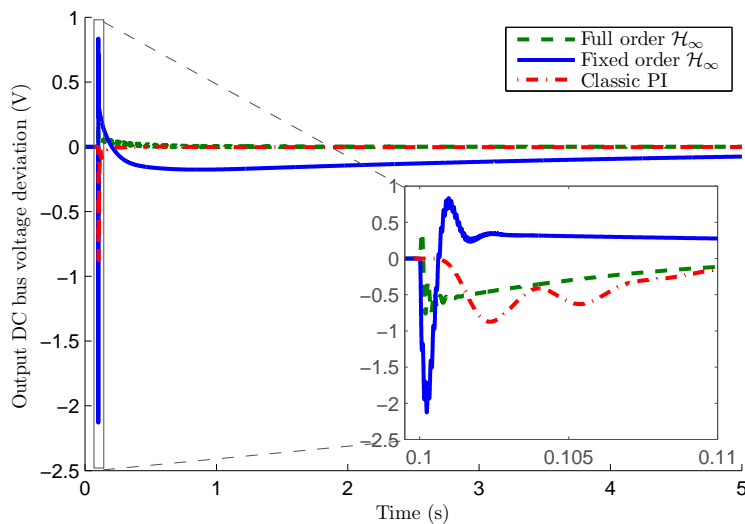


Figure 5.53: Simulation results, comparison of full and fixed order \mathcal{H}_∞ controllers with classic PI control.

A brief robustness test

A robustness test on the control of the complete electrical system is presented. Robustness of the control methodology is tested for parametric variations in the AC side filter dynamical parameters (L_{AC} and C_{AC}).

For this test we consider parameter variations of $\pm 10\%$. The robust fixed order controller is compared with the classic PI control methodology. The singular values plots of the sensitivity function under parametric variations are presented in Figure 5.55. The figure shows the evolution of the sensitivity function when varying uncertain parameters from -10% to $+10\%$.

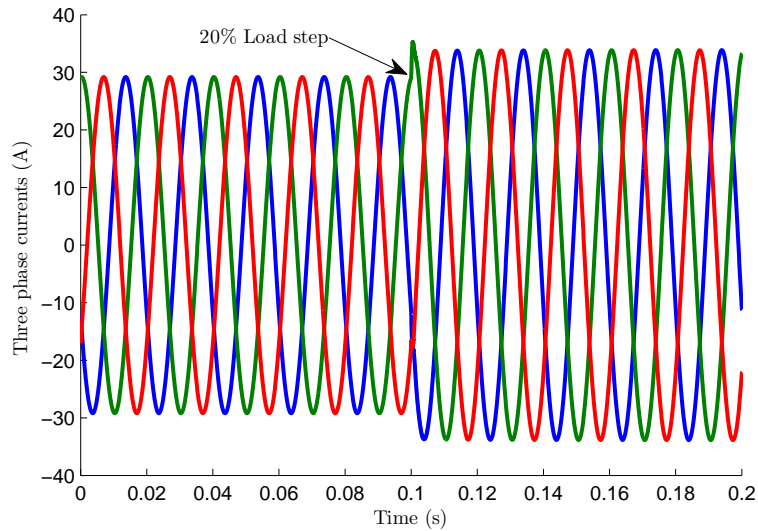


Figure 5.54: Three-phase simulation results using fixed order \mathcal{H}_∞ .

The gain in robustness using the fixed order \mathcal{H}_∞ controller is considerable. Returning to the analysis of the design of the system components, the robustness analysis results can be directly used to help the system designer in optimizing his choice in the conception stage.

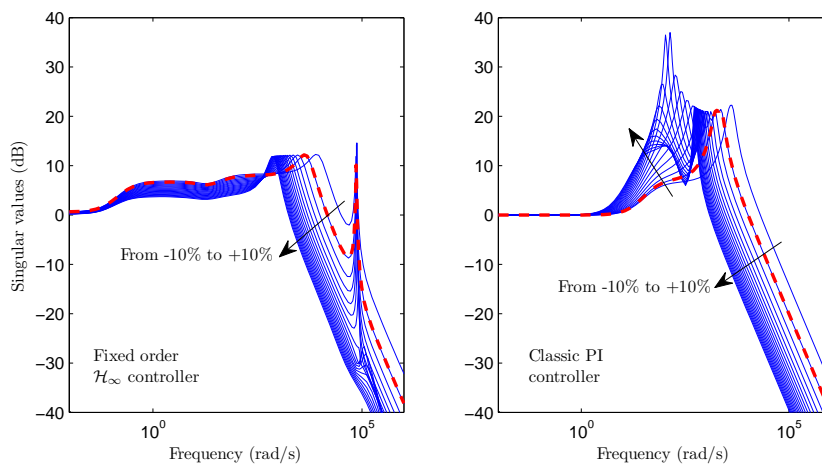


Figure 5.55: Robustness analysis of the closed-loop systems.

5.4 Air supply sub-system

In this section, some control methodologies for the compressor system are proposed. Two main problems are tackled. In the first problem, a control strategy for the compressor system using the linear model and the robust control methods is proposed. A second problem is dealing with the high non-linearities in the compressor model. A complement of this problem is considering uncertainties in design of a speed controller for the compressor system. In order to solve these problems, the use of LPV control using gain-schedule methods is proposed.

The air input dynamic behavior plays a very important role on the FC dynamic. The control objectives for the compressor system are chosen to comply with the desired performance of the FC. Two main objectives are considered: keep a desired oxygen excess ratio λ_{O_2} and maximizing the net power delivered to the load. Note that we consider an autonomous system, i.e., the compressor energy is taken from the DC bus. This is not an easy requirement to meet, a trade-off has to be made because rising the supply manifold pressure increases the FC performance, but rising the pressure increases the current consumed by the compressor directly from the FC stack itself. In a simplistic solution, this is partially achieved minimizing the overshoots and properly rejecting disturbance transients on the supply manifold pressure and on the compressor speed. Note that at higher speeds more current is consumed by the compressor-motor.

Under these assumptions, let us now present the proposed compressor system control.

5.4.1 Compressor system control

The compressor system dynamic is composed by the compressor-motor and the FC supply manifold dynamic. The control strategies described in this section are motivated by the GESI test-bench and the air compressor acquired within the thesis framework for operation of the FC under dry air conditions.

The compressor-motor delivered by Vairex© includes the speed controller along with the several protection devices (over-heat, over-speed,...) into a dedicated under closed package. To avoid warranty limitations issues and guarantee safe operation of the compressor, we decided to keep the manufacturer speed controller in operation. Test-bench tests were performed on this system including a feedback loop in the compressor speed. The identification problem was solved with an iteration process from a starting guess of controller gains (supposing a simple PI control structure). As explained in chapter 4, section 4.4.2.4, the linear model proposed by Gasser [2006] was found to be well adapted to the design of the compressor system control for mainly two reasons: identification results were actually good and this model includes the dynamic of the compressor motor current, which will be used later to consider a true autonomous system.

Note that considering an autonomous system the following system currents relationship can be established:

$$I_{DC} = I_{load} + I_{cm} \quad (5.14)$$

where I_{DC} is the current delivered by the hybrid boost converters at the DC bus.

Recalling the modeling of the compressor in the FC system presented in section 4, a block diagram of the model, showing input and output variables, is given in Figure 5.56.

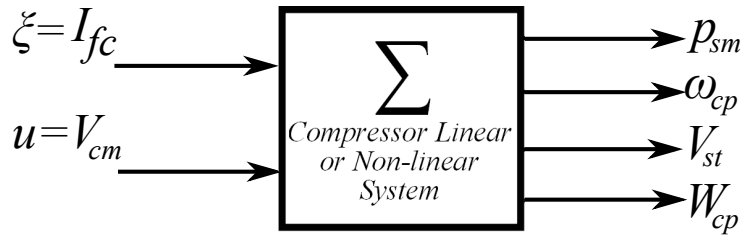


Figure 5.56: Block diagram of the FC system with compressor-motor model.

We will present now the classic strategy used to obtain a simple PI controller for this system.

5.4.1.1 Classic control approach

A very simple control design for a PI is presented. We used the function `sisotool` in MATLAB to find a PI controller that satisfies a gain margin larger than 6dB and a phase margin larger than 45° . A design that presents a good trade-off between the overshoot and a stabilization time t_s around 2s was chosen. The controller found satisfies $GM = 12.2\text{dB}$ and a $PM = 60^\circ$. The gains are given by $k_p = 8.33 \times 10^4$ and $k_i = 5.21 \times 10^5$. This PI controller for $K_{\lambda_{O_2}}$ has the classic structure $K_{\lambda_{O_2}} = k_p + k_i/s$.

A proposed strategy for oxygen excess ratio control is presented in Figure 5.57. In this case the speed controller $K_\omega(s)$ is given by the identified PI controller with gains $k_p = 0.4912$ and $k_i = 5.9854$, as it was shown in chapter 4.

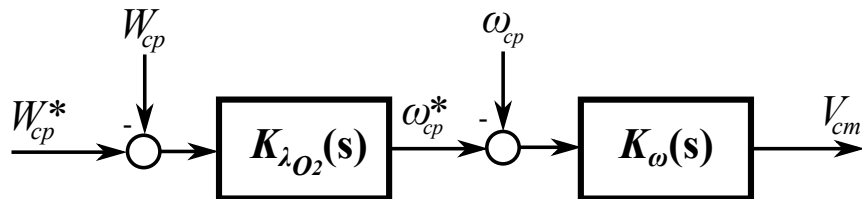


Figure 5.57: Compressor proposed control strategy.

Time-domain simulations results are computed for the closed-loop system and step inputs are applied to the FC current I_{fc} simulating changes in the load current. The simulation result is presented in Figure 5.58 for $\pm 20\%$ load steps. Figure 5.59 show the compressor flow error ($W_{cp}^* - W_{cp}$) to obtain the desired oxygen excess ratio. Results are compared to the open-loop system (no control). The system regulation to the desired $\lambda_{O_2} = 1.6$ is effectively achieved. In Pukrushpan et al. [2004a] this value was fixed at 2 and was chosen for the maximum net power delivered to the load. In our case, after several tests on the real FC stack, this value was fixed to 1.6, for which the best performance was obtained for the FC operating under dry air conditions (without humidification) in terms of the FC stack voltage stabilization.

5.4.1.2 Robust control approach

In the robust control approach we compute both full and reduced order \mathcal{H}_∞ controllers.

The compressor system block diagram is presented in Figure 5.61 for the system proposed by Gasser [2006] and detailed in chapter 4, section 4.4.2.4. The complete open-loop

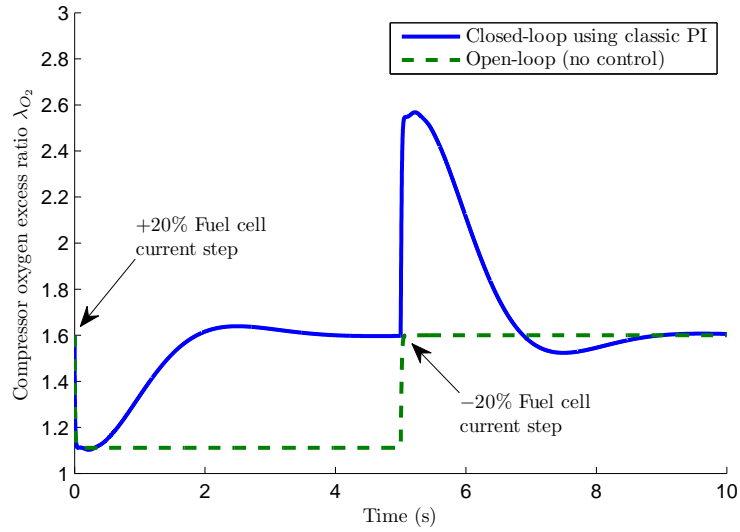


Figure 5.58: Oxygen excess ratio using linear model.

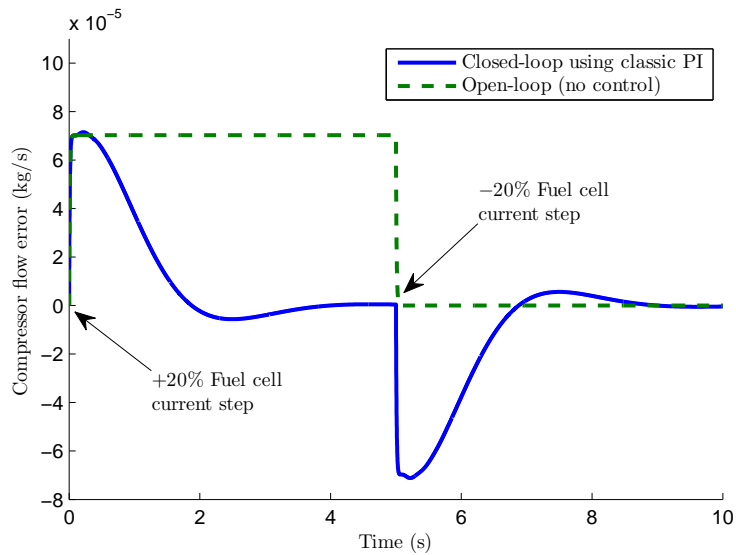


Figure 5.59: Oxygen excess ratio using linear model.

state-space matrices for this system are presented in appendix B. The proposed control configuration with a single performance weighting function is presented in Figure 5.60.

The weighting function is fixed for a stabilization time $t_s = 1$ s. Using the classic 5% criterion and the approximation to dominant poles, the expression $t_s = \frac{3}{\zeta\omega_n}$ can be used to obtain the natural frequency of the desired closed-loop. With $\zeta = 0.6$, we obtain $\omega_n = 5$ rad/s. The performance weight is then given by:

$$W_{perf} = \frac{0.5s + 5}{s + 5 \times 10^{-8}} \quad (5.15)$$

The full order \mathcal{H}_∞ controller (order 5) obtained can be reduced to 1st order system, given by:

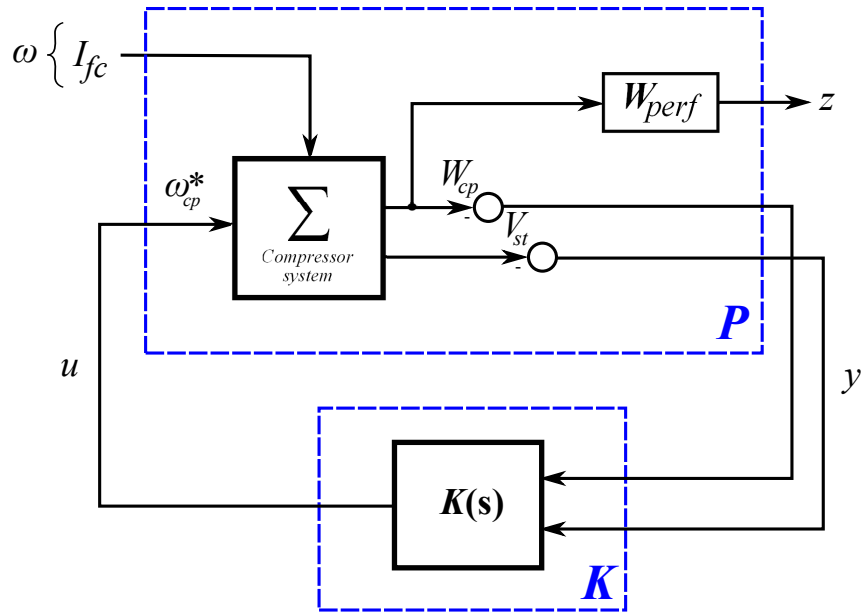


Figure 5.60: Control configuration in the P-K form for the compressor system.

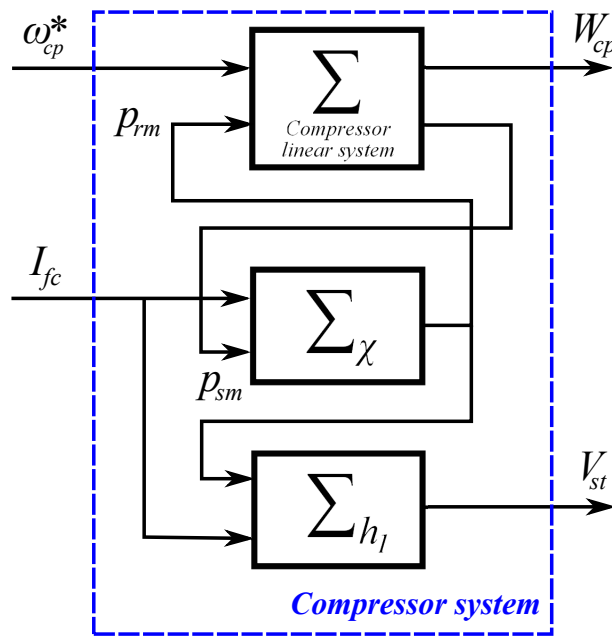


Figure 5.61: Compressor system block diagram.

$$K_{\mathcal{H}_\infty}(s) = \begin{bmatrix} \frac{2.587 \times 10^5 s + 7.036 \times 10^5}{s - 0.0001521} \\ \frac{9.747 \times 10^{-5} s + 2.543 \times 10^{-8}}{s - 0.0001521} \end{bmatrix}$$

A robust controller was also computed using the function `hinfstruct` and fixing the controller structure to a MIMO PI. The closed-loop \mathcal{H}_∞ gain for each robust controller found are summarized in Table 5.6. The singular values plots of the sensitivity functions are compared in Figure 5.62. A slightly more robust controller is obtained with the full and reduced order \mathcal{H}_∞ controllers.

Table 5.6: Closed-loop \mathcal{H}_∞ gain

Controller	Performance
Full order \mathcal{H}_∞	$\mathcal{H}_\infty < 0.0788$
Reduced order \mathcal{H}_∞	$\mathcal{H}_\infty < 0.1848$
Using <code>hinfstruct</code>	$\mathcal{H}_\infty < 0.1865$
Classic PI	$\mathcal{H}_\infty < 0.1933$

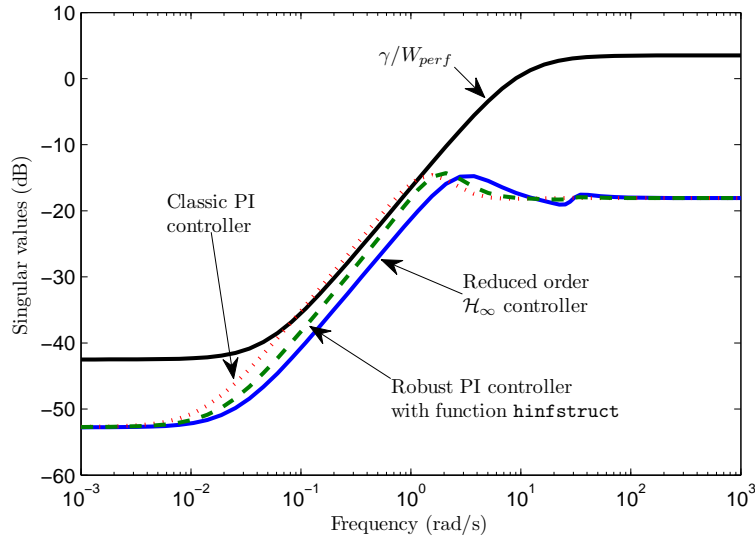


Figure 5.62: Closed-loop singular values plot.

In Figures 5.63a and 5.63b the controllers regulation of the oxygen excess ratio are compared using the linear and non-linear models (cf to models equations (4.58) and (4.66) in chapter 4). The reduced order \mathcal{H}_∞ controller is not shown in the non-linear simulations because the results obtained are very similar to those obtained with the full order \mathcal{H}_∞ control. In the linear simulation 20% load step are applied. In the non-linear case a 75% load step is applied. The non-linear simulation results show a clearly better disturbance rejection using the proposed robust control. The Figure 5.64 show the evolution of the net power delivered by the FC after a series of load steps. Note the several overshoots in the transient response using the classic control. Using the same series of load step a different set of system variables is presented in Figure 5.65.

Using the non-linear model of the compressor system, validation of robust controller is obtained. Dynamic variations on the operating point of the FC polarization curve and the compressor flow map are presented in Figures 5.66 and 5.67 respectively after $\pm 75\%$ load steps. According with these results, and associating these results with the overshoot peaks shown in Figures 5.63b and 5.64, an improvement of the net power delivered by the FC is obtained with the MIMO \mathcal{H}_∞ control methodology. The evolution of the operating point in the polarization curves given an idea of the degradation of cell performance after a big load current step, and the influence of the supply manifold pressure p_{sm} variation.

Finally, several other dynamic results are obtained using the non-linear model, and applying a second series of load steps. A final result sequence is given in Figure 5.68. Note

the slight oscillatory behavior of the compressor motor speed using the classic methodology. A smooth disturbance rejection is achieved on the supply manifold pressure. When comparing with results presented in Figure 5.65, these results obtained with the linear and non-linear models are very similar. Figure 5.68 shows the good regulation of the compressor speed and the drop on the FC stack voltage after the disturbances.

In the following section a new speed controller using LPV control is proposed to deal with non-linearities in the system and parametric uncertainties.

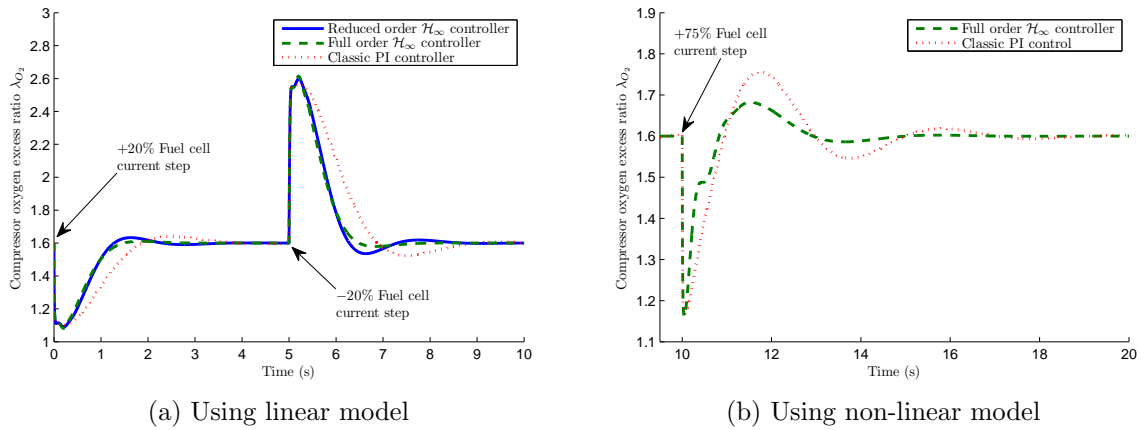


Figure 5.63: Oxygen excess ratio simulation results.

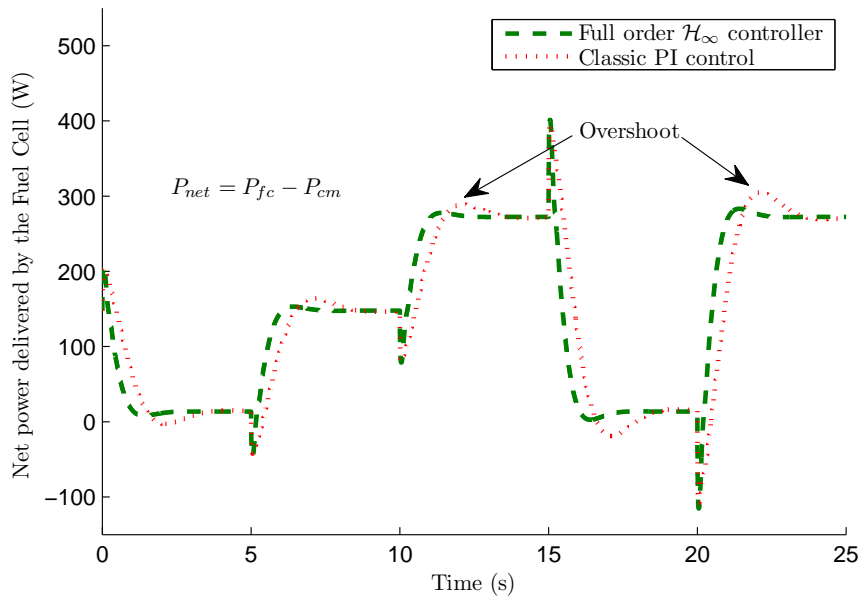


Figure 5.64: Net power delivered by the FC.

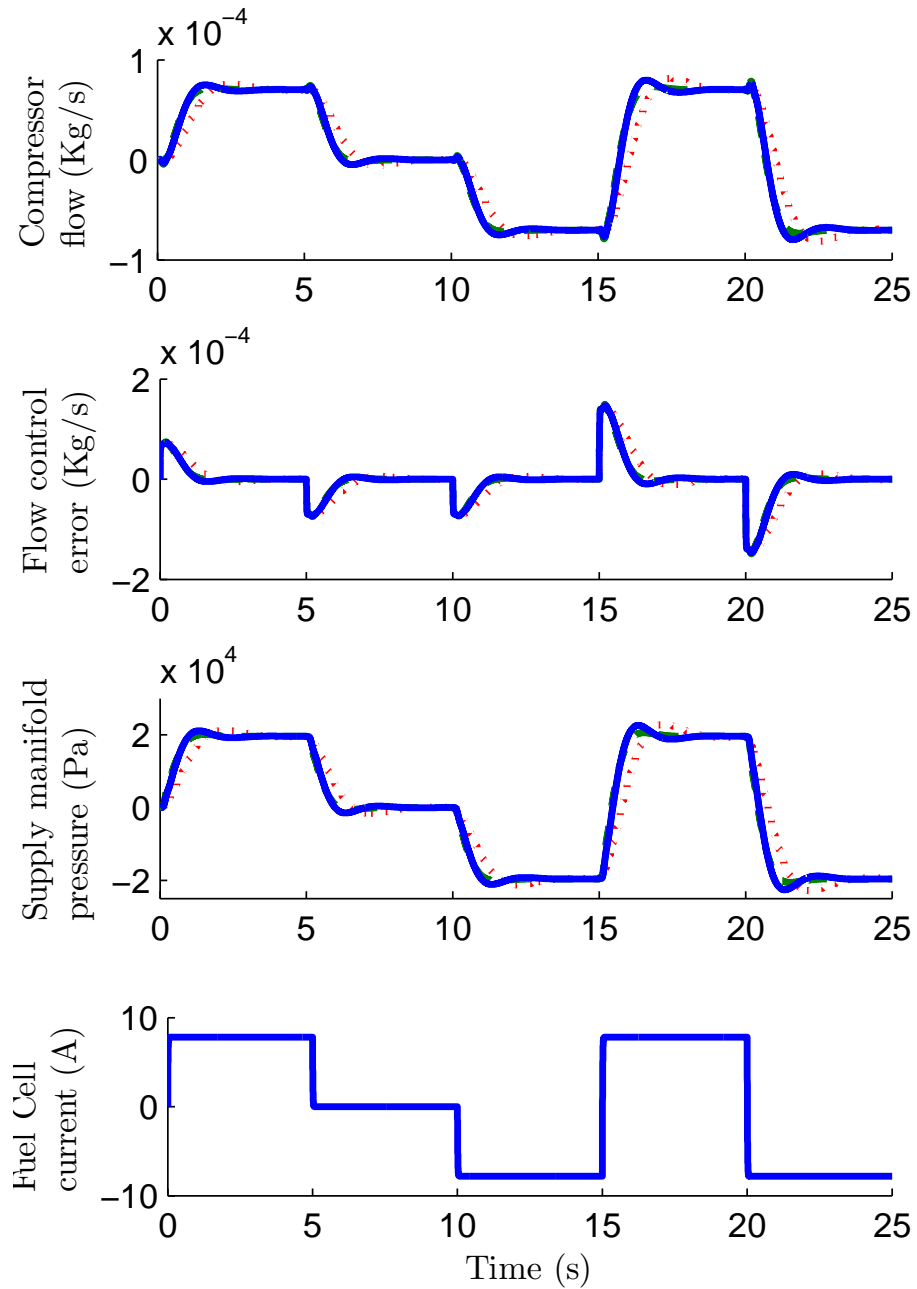


Figure 5.65: Simulation results using linear model (reduced order controller in continuous line, full order controller in dashed line and classic PI controller in dotted line).

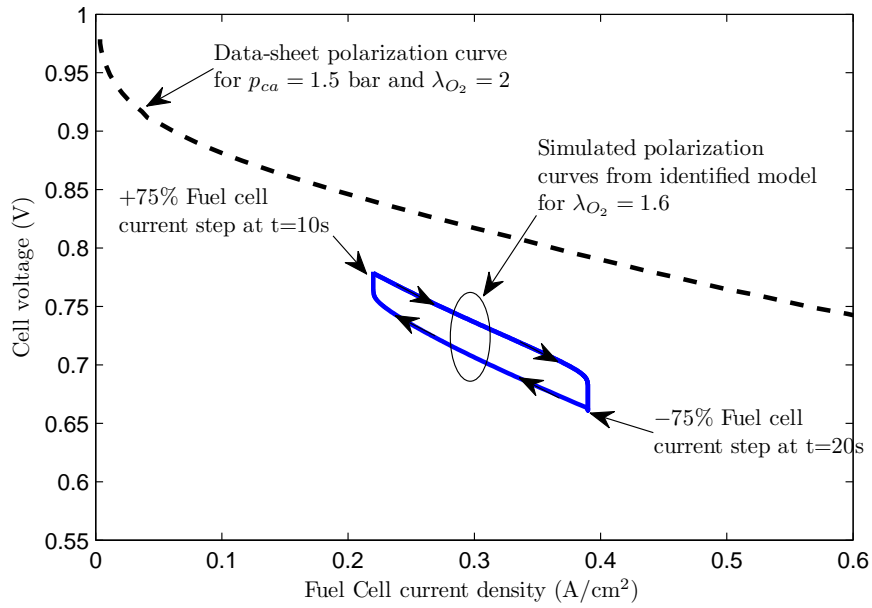


Figure 5.66: Polarization curve.

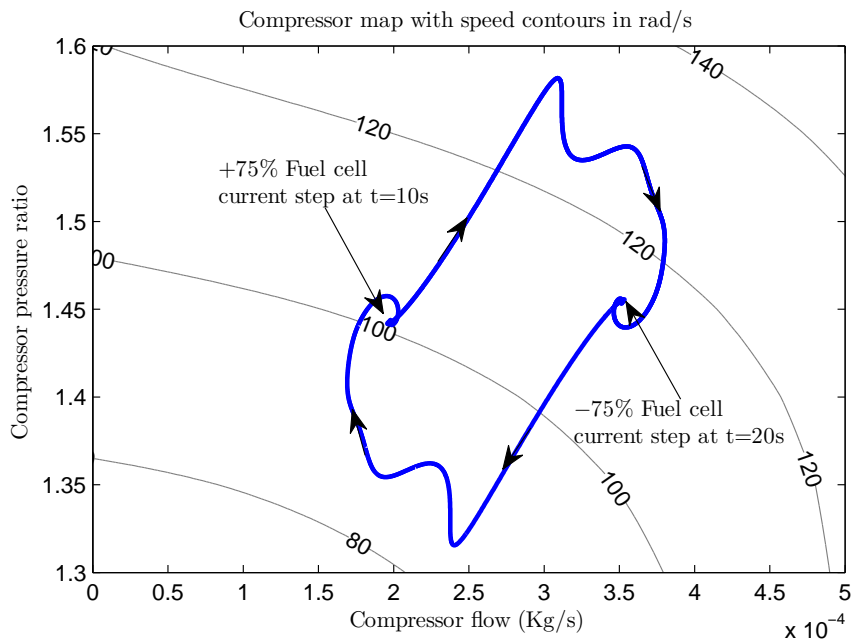


Figure 5.67: Compressor map.

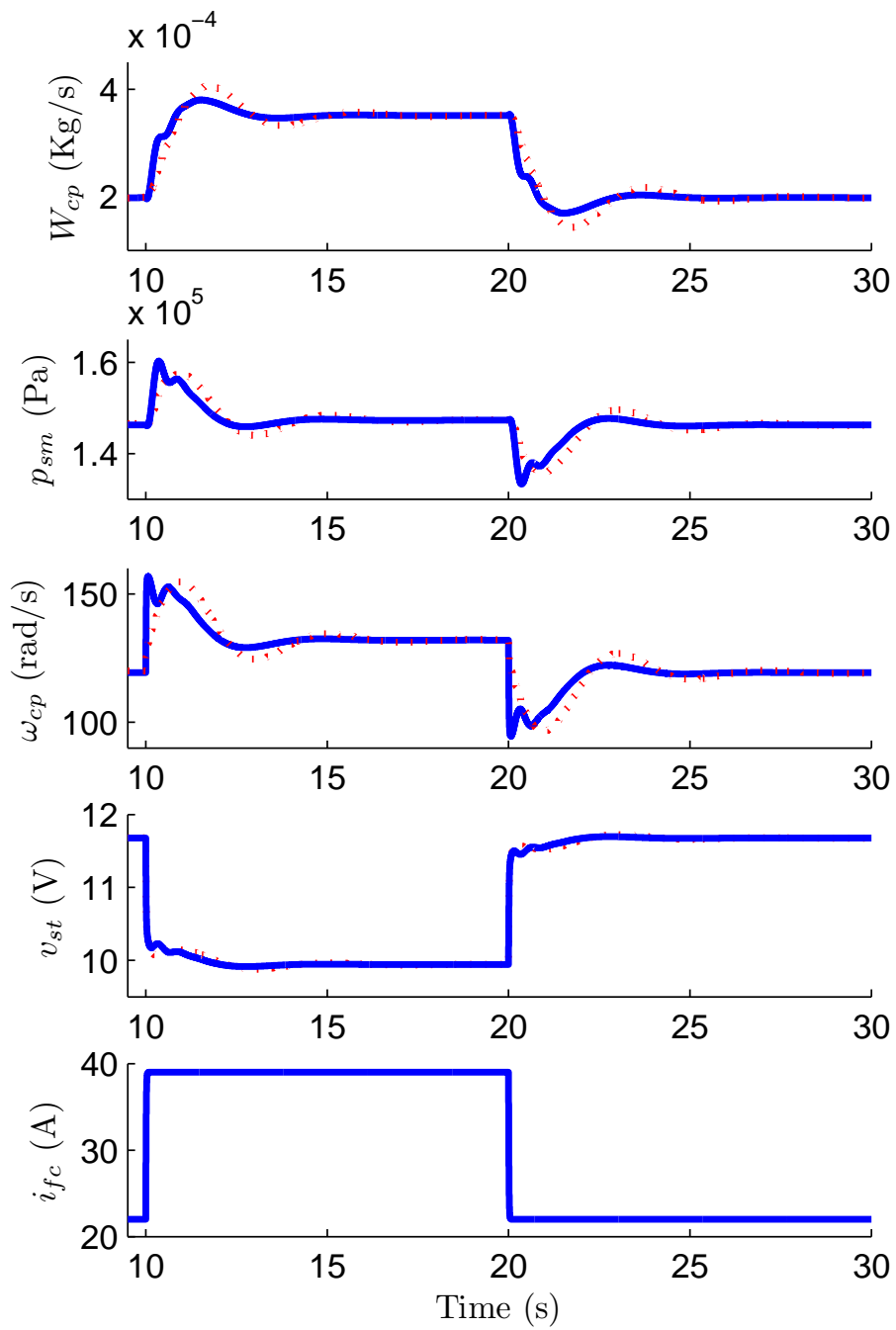


Figure 5.68: Simulation results using non-linear model (reduced order controller in continuous line and classic PI control in dotted line).

5.4.2 LPV speed control

In the previous section a multivariable controller of the oxygen excess ratio was presented. Now we will assume that the speed controller of the compressor motor is removed. A new speed control is then proposed.

In this section two problems are solved: the control problem of the non-linear 3rd order system (presented hereafter in system of equations (5.16)) and the computation of a robust speed controller for the system subject to some parametric uncertainty.

5.4.2.1 Solution to the control of the non-linear compressor model

To solve this problem, an affine representation of the Fuel Cell compressor system is presented first. The non-linear model is obtained from the reduced order model developed by Suh [2006] and detailed in chapter 4.

This model presented in Suh [2006] represents the reduced form of the complete order model presented by Pukrushpan et al [2004a]. Here, for simplicity, we use the notation retained in Talj et al. [2009]. Recalling from chapter 4, the final reduced order non-linear system was given by:

$$\begin{aligned}\dot{\chi} &= -\mu_1\chi + \mu_2x_4 + \mu_3 - \mu_4\xi \\ \dot{x}_3 &= -c_9x_3 - \frac{c_{10}}{x_3} \left[\left(\frac{x_4}{c_{11}} \right)^{c_{12}} - 1 \right] h_3(x_3, x_4) + c_{13}u \\ \dot{x}_4 &= c_{14} \left[1 + c_{15} \left[\left(\frac{x_4}{c_{11}} \right)^{c_{12}} - 1 \right] \right] [h_3(x_3, x_4) - c_{16}(-\chi + x_4)]\end{aligned}\tag{5.16}$$

Let us recall that the states of the system are χ , the air pressure given in Pa at the fuel cell cathode (remember that this can be measured at the fuel cell output and that it is considered that the air has reached the saturated state within the fuel cell channels), x_3 is the compressor speed in rad/s and x_4 given in Pa is the compressor output pressure or the pressure in the supply manifold chamber. The input ξ is the fuel cell current in A and is considered as the system disturbance. The control input u is the compressor-motor control voltage in V. $h_3(x_3, x_4)$ is the compressor flow in slpm. Constants μ_i and c_j with $i \in [1, 4]$, and $j \in [9, 16]$ are parameters dependent on physical characteristics of the fuel cell and compressor systems and on physical properties of the air.

The goal now is to find an affine LPV model of this system. Given the non-linearities and avoiding the possibility of a high number of varying parameters, four propositions are presented. In these propositions the systems may be separated in the cascade form (cf to the system model diagram presented in Figure 4.31). In the first proposition, an LPV affine system representation considering all model state-space variables (χ, x_3, x_4) is presented. The second, third and fourth propositions are a reduction of the first method, then considering subsequently affine LPV models of sub-systems (χ, x_4) , (χ, x_3) and (x_3, x_4) respectively.

First method: Full reduced-order LPV system

From the original system we define a first varying parameter given by:

$$\rho_1 = -\frac{c_{10}}{x_3 x_4} \left[\left(\frac{x_4}{c_{11}} \right)^{c_{12}} - 1 \right] h_3(x_3, x_4) \quad (5.17)$$

With this, the equation in x_3 becomes:

$$\dot{x}_3 = -c_9 x_3 + \rho_1 x_4 + c_{13} u \quad (5.18)$$

To parametrize the equation in x_4 we define:

$$\rho_2 = \frac{c_{14}}{x_3} \left[1 + c_{15} \left[\left(\frac{x_4}{c_{11}} \right)^{c_{12}} - 1 \right] \right] h_3(x_3, x_4) \quad (5.19)$$

$$\rho_3 = c_{14} c_{16} \left[1 + c_{15} \left[\left(\frac{x_4}{c_{11}} \right)^{c_{12}} - 1 \right] \right] \quad (5.20)$$

Some conservatism may then appear noting moreover that ρ_2 and ρ_3 are linked by:

$$\rho_2 = \rho_3 \frac{h_3(x_3, x_4)}{c_{16} x_3} \quad (5.21)$$

A fourth parameter may be defined as:

$$\rho_4 = \mu_2 + \frac{\mu_3}{x_4} \quad (5.22)$$

With this the complete system becomes:

$$\begin{cases} \dot{\chi} &= -\mu_1 \chi + \rho_4 x_4 - \mu_4 \xi \\ \dot{x}_3 &= -c_9 x_3 + \rho_1 x_4 + c_{13} u \\ \dot{x}_4 &= \rho_2 x_3 - \rho_3 x_4 + \rho_3 \chi \end{cases} \quad (5.23)$$

Second method: An LPV (χ, x_4) model

Following the same procedure we define now for this sub-system:

$$\rho_1 = c_{14} c_{16} \left[1 + c_{15} \left[\left(\frac{x_4}{c_{11}} \right)^{c_{12}} - 1 \right] \right] \quad (5.24)$$

$$\rho_2 = \mu_2 + \frac{\mu_3}{x_4} \quad (5.25)$$

With this the following LPV sub-system is obtained:

$$\begin{cases} \dot{\chi} &= -\mu_1 \chi + \rho_2 x_4 - \mu_4 \xi \\ \dot{x}_4 &= \rho_1 \chi - \rho_1 x_4 + \rho_1 \frac{h_3(x_3, x_4)}{c_{16}} \end{cases} \quad (5.26)$$

In this case now the compressor flow $h_3(x_3, x_4)$ can be considered as the control input and then only two varying parameters are used but, in contrast, the equation in x_3 is still non-linear and is possibly challenge to control.

Third method: An LPV (χ, x_3) model

For this approach, a reduction of the full reduced-order LPV system, the following varying parameters are considered:

$$\rho_1 = \mu_2 + \frac{\mu_3}{x_4} \quad (5.27)$$

$$\rho_2 = -\frac{c_{10}}{x_3 x_4} \left[\left(\frac{x_4}{c_{11}} \right)^{c_{12}} - 1 \right] h_3(x_3, x_4) \quad (5.28)$$

The obtained LPV sub-system is given by:

$$\begin{cases} \dot{\chi} &= -\mu_1 \chi + \rho_1 x_4 - \mu_4 \xi \\ \dot{x}_3 &= -c_9 x_3 + \rho_2 x_4 + c_{13} u \end{cases} \quad (5.29)$$

Fourth method: Towards an LPV (x_3, x_4) model In this fourth method, we keep the notation presented for the full reduced order LPV system (first method), but we decouple the equation of χ from the system. The reduced LPV sub-system obtained is then given by:

$$\begin{cases} \dot{x}_3 &= -c_9 x_3 + \rho_1 x_4 + c_{13} u \\ \dot{x}_4 &= \rho_2 x_3 - \rho_3 x_4 + \rho_3 \chi \end{cases} \quad (5.30)$$

As an advantage using this approach the remaining sub-system in χ is linear and easy to control.

For convenience, we will keep this proposed model for sub-system (x_3, x_4) . From time-domain simulations with the non-linear model, it has been observed that the variation range of ρ_3 can be neglected. The LPV is finally reduced to two varying parameters. From non-linear simulations the varying parameters range is given by:

$$\begin{aligned} \rho_1 &\in [2.577 \times 10^{-5}, 2.388 \times 10^{-4}] \\ \rho_2 &\in [4200, 38068] \end{aligned}$$

The compressor LPV system block diagram is given in Figure 5.69. The proposed control configuration using gain scheduling and including the performance weighting functions, is presented in Figure 5.70.

The cut-off frequency ω_B is fixed for a sufficient fast speed response. The weighting function is given by:

$$W_{perf} = \frac{500s + 2000}{s + 0.002}$$

A full order \mathcal{H}_∞ polytopic controller is computed with a conditioning number $\gamma = 1.3478$. The singular values plot of the sensitivity function at each corner of the polytope is given in Figure 5.71.

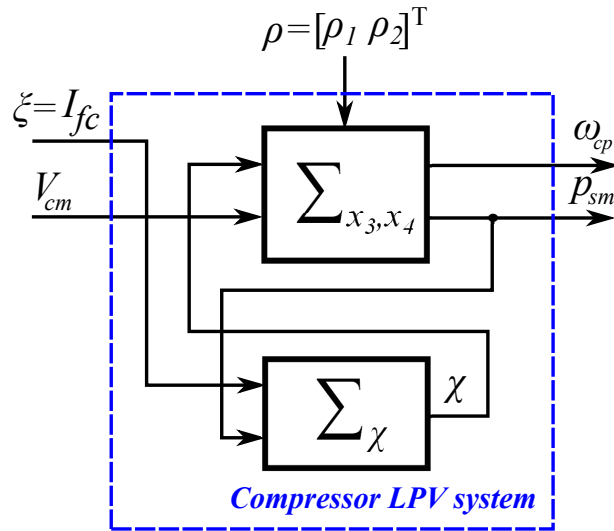


Figure 5.69: Compressor LPV system block diagram.

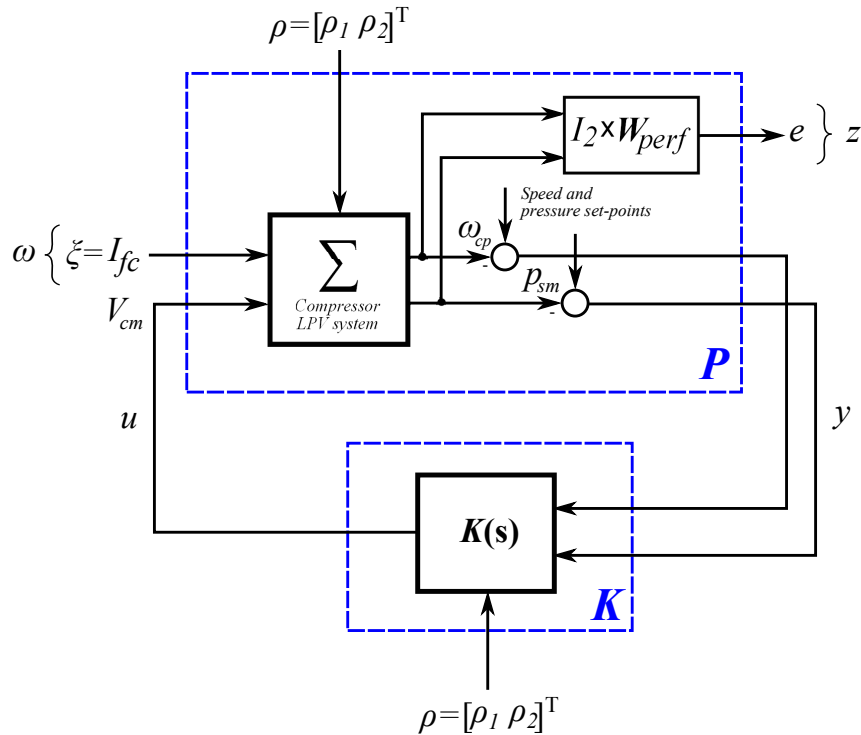


Figure 5.70: Control configuration in the P-K form for the LPV system.

Evaluating at each corner of the closed-loop polytope a time-domain simulation response to a unitary impulse disturbance is presented in Figure 5.72.

The system achieves good disturbance rejection at each polytopic vertex, however the validation inside the polytopic set is necessary to verify the control performances. For this we use the gain scheduling approach. The gain scheduled controller simulation was obtained using SIMULINK and the given functions for polytopic set definition: `pvec` and `polydec`. The system response to a FC load step and the system response to the tracking problem of the speed reference signal are presented in Figures 5.73 and 5.74 respectively. These results demonstrate the effectiveness of the speed control strategy proposed, robust

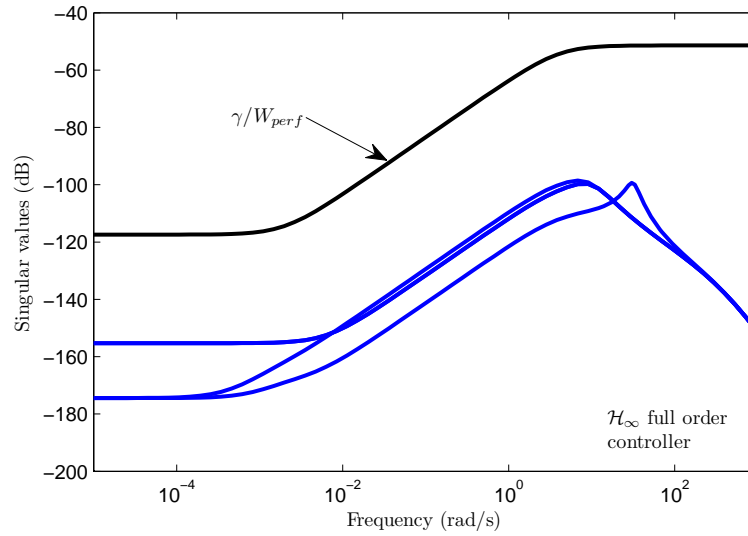


Figure 5.71: Singular values plot of the sensitivity function for \mathcal{H}_∞ polytopic controller.

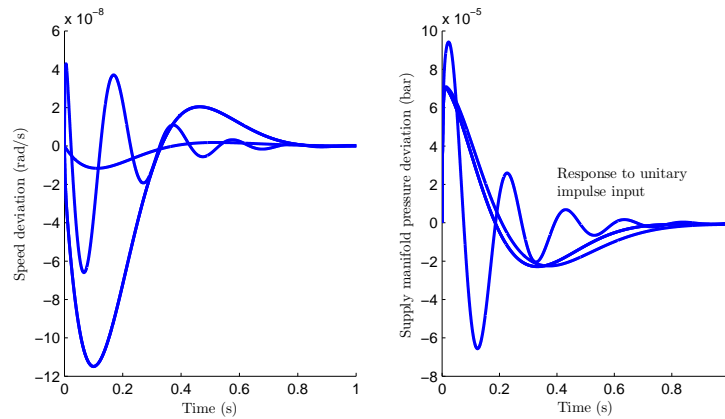


Figure 5.72: Impulse response for \mathcal{H}_∞ polytopic controller at each vertex.

to non-linearities in the model. In the following section a similar problem is treated for the solution of the control problem of a system subject to model uncertainties. The defined parameter variation trajectory used for time-domain simulations is presented in Figure 5.75.

5.4.2.2 Model uncertainties problem solution

Following a similar approach, the problem of a model subject to uncertainties is now solved using LPV control.

The proposed control configuration using gain scheduling and including the performance weighting functions, is identical to the previous case, in contrast the compressor LPV model is given by the sub-system (χ, x_3) (cf to the third proposed method). From this system, parameters c_9 and c_{13} of the 3rd order non-linear system are assumed to be uncertain. These parameters are directly dependent on the compressor-motor inertia constant J_{cp} , which may assumed to be variable or with uncertainty on its identified value.

The LPV system block diagram is given in Figure 5.76.

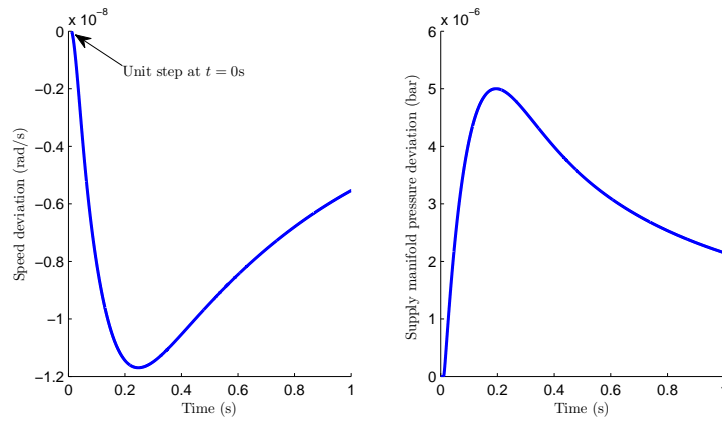


Figure 5.73: System response to a load step using gain scheduling approach.

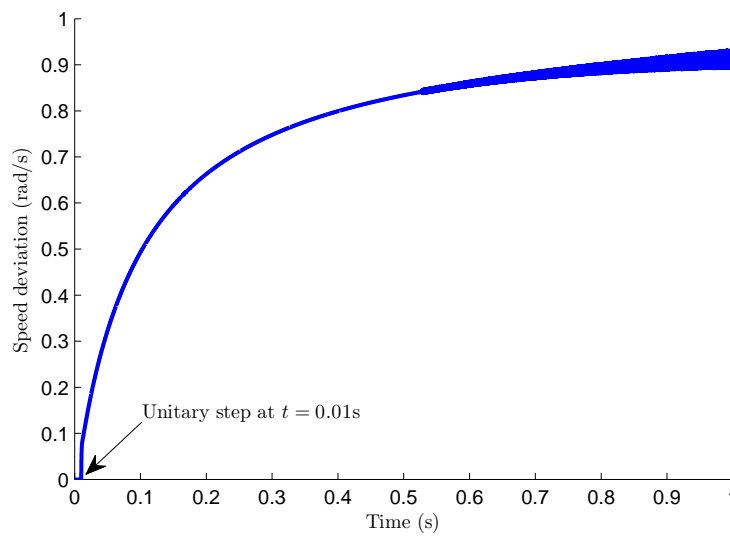


Figure 5.74: System response to a speed reference step using gain scheduling approach.

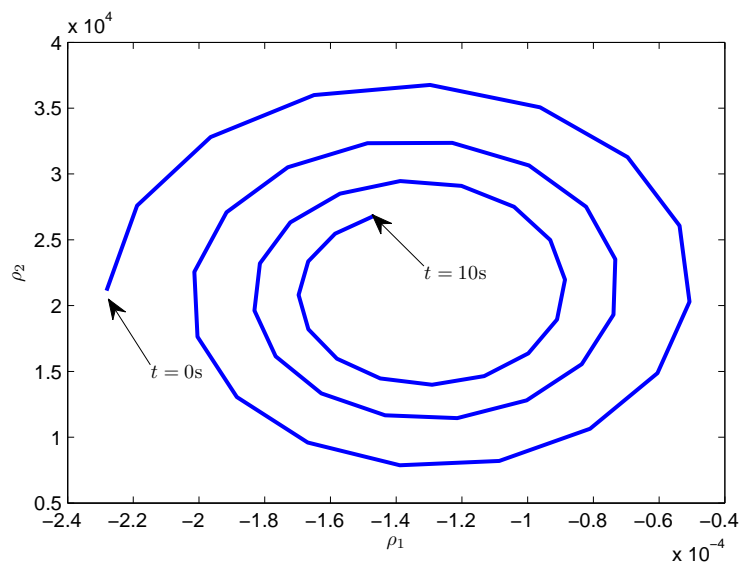


Figure 5.75: Varying parameter trajectory.

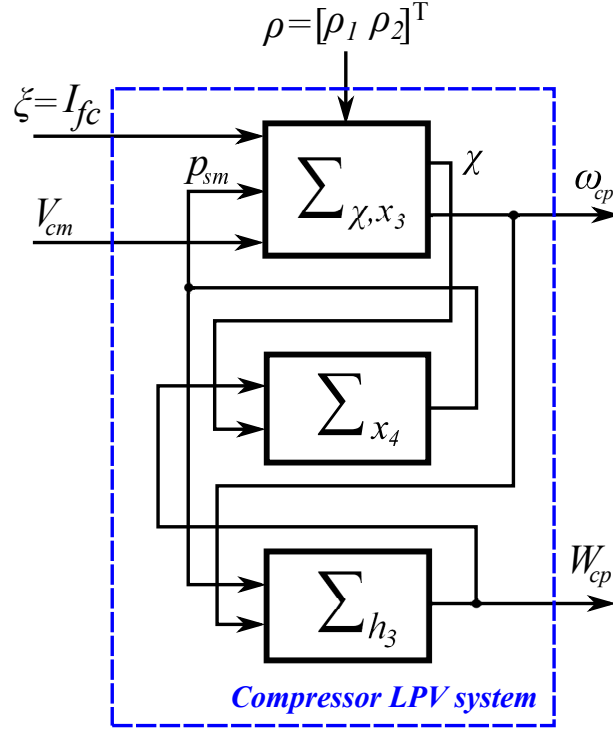


Figure 5.76: Compressor LPV system block diagram.

The varying parameters were computed from non-linear simulation values, they are defined as:

$$\begin{aligned}\rho_1 &= c_9 \in [930.26, 2300] \\ \rho_2 &= c_{13} \in [1069.5, 3531.7]\end{aligned}$$

From these values, the model is linearized for given steady-state values of $x_{3_e} = 110\text{rad/s}$ and $x_{4_e} = 1.512\text{bar}$, to obtain a state-space representation in the form $\dot{x} = Ax + Bu$, with state matrices:

$$A = \begin{bmatrix} -\mu_1 & 0 \\ 0 & -\rho_1 \end{bmatrix} \text{ and } B = \begin{bmatrix} k_2 & -\mu_4 & 0 \\ k_1 & 0 & \rho_2 \end{bmatrix} \quad (5.31)$$

with:

$$k_1 = -\frac{c_{10}}{x_{3_e} x_{4_e}} \left[\left(\frac{x_{4_e}}{c_{11}} \right)^{c_{12}} - 1 \right] h_3(x_{3_e}, x_{4_e}) \quad (5.32)$$

$$k_2 = \mu_2 + \frac{\mu_3}{x_{4_e}} \quad (5.33)$$

where:

$$x = [\chi \quad x_3]^T \quad (5.34)$$

$$u = [x_4 \quad \xi \quad V_{cm}]^T \quad (5.35)$$

Both a full order \mathcal{H}_∞ polytopic controller and a PI LPV controller are computed following the methodology described in chapter 3, section 3.3.4.2. The weighting functions for the \mathcal{H}_∞ and PI controllers are respectively given by:

$$W_{perf_{\mathcal{H}_\infty}} = \frac{500s + 20000}{s + 0.02}$$

$$W_{perf_{PI}} = \frac{50s + 20000}{s + 20}$$

Conditioning numbers for each controller are $\gamma_{\mathcal{H}_\infty} = 210.96$ and $\gamma_{PI} = 5.72$. The closed-loop systems are stable for each corner of the polytopic representation, however the PI LPV controller is not gain scheduled, i.e. the obtained controller is not parameter-dependent. As before, the singular values plot of the sensitivity function for \mathcal{H}_∞ polytopic and the PI LPV controllers are shown in Figure 5.77. More robustness is obtained with the \mathcal{H}_∞ polytopic control.

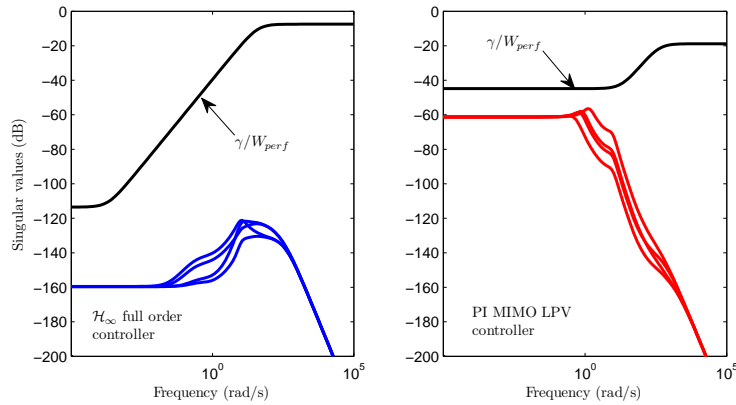


Figure 5.77: Singular values plot of the sensitivity function for \mathcal{H}_∞ polytopic and PI LPV controllers.

The control procedure is validated from time-domain simulation results using gain scheduled systems. The system response to a FC load step and the system response to the tracking problem of the speed reference signal are presented in Figures 5.78 and 5.79 respectively. The defined parameter variation trajectory used for gain scheduled simulation is presented in Figure 5.80. The closed-loop simulation results show a good disturbance rejection for the \mathcal{H}_∞ polytopic controller, however an undesired overshoot appears in the speed reference tracking response. Despite this, the system remains stable for the uncertainties level defined. Disturbance rejection and reference tracking performances are not entirely met by the PI LPV controller. These results emphasize the interest of the LPV methodology which needs to be further studied.

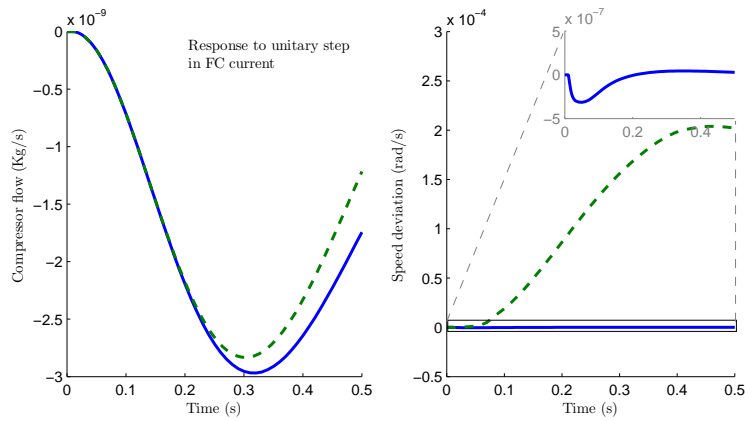


Figure 5.78: System response to a load step using gain scheduling approach (\mathcal{H}_∞ polytopic controller in continuous line and PI LPV controller in dashed line).

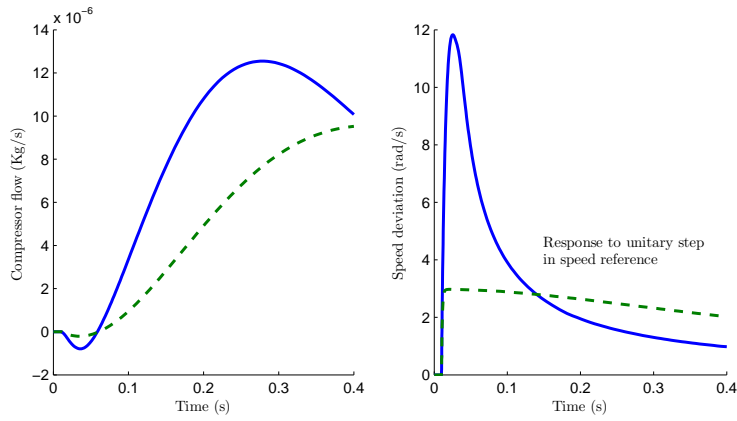


Figure 5.79: System response to a speed reference step using gain scheduling approach (\mathcal{H}_∞ polytopic controller in continuous line and PI LPV controller in dashed line).

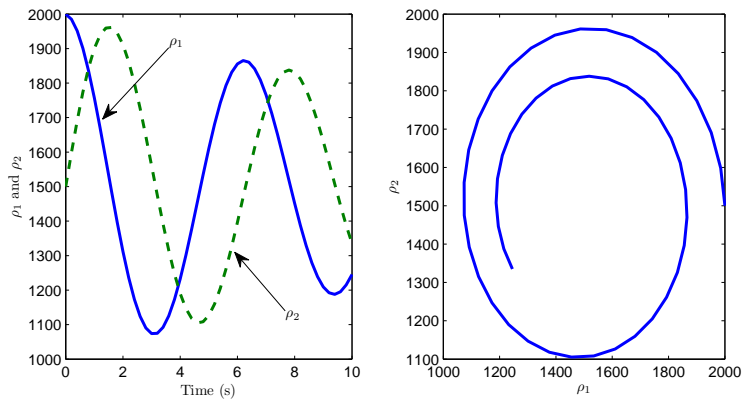


Figure 5.80: Varying parameter trajectory.

5.5 Complete system control

In the previous systems, the effect of a true autonomous system was not considered. Taking a complete system composed by the hybrid boost converters and the compressor-motor systems, the effect of the coupled currents I_{DC} , I_{cm} and I_{load} is taken into account. The two systems are also coupled by the FC stack voltage.

The linear model of the compressor-motor system is used here (cf to model (4.58) presented in chapter 4 section 4.4.2.4). The classic control methodology is a combination of the classic controller presented in the previous sections. With respect to robust controllers, full and reduced order \mathcal{H}_∞ controllers are computed, along with the MIMO PI using the iLMI algorithm.

The complete system block diagram is presented in Figure 5.81 and the proposed control configuration is presented in Figure 5.82. The open-loop state-space matrices for this system are presented in appendix B.

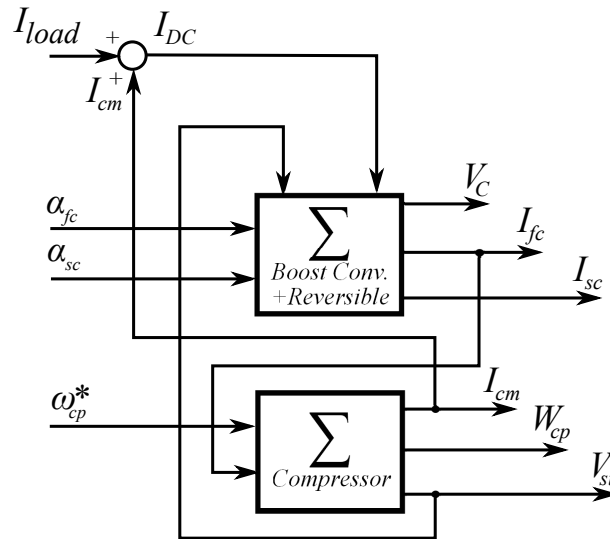


Figure 5.81: Complete system block diagram.

Two variables are chosen to be controlled:

- The DC bus voltage V_C , to guarantee desired regulation.
- The compressor output air flow W_{cp} , to obtain the desired tracking of the oxygen excess ratio λ_{O_2} .

The system measurements are the DC bus voltage V_C , the fuel cell current I_{fc} , the super-capacitor current I_{sc} , the compressor air flow W_{cp} and the fuel cell stack voltage V_{st} .

The performance weighting functions are defined as:

$$W_{perf_1} = W_{perf_2} = \frac{0.05s + 5}{s + 5 \times 10^{-5}} \quad (5.36)$$

The module margin for the PI iLMI controller is fixed at $M_S = 2$. The iLMI algorithm yields in this case a solution after 8 iterations. The full order \mathcal{H}_∞ controller (order 6)

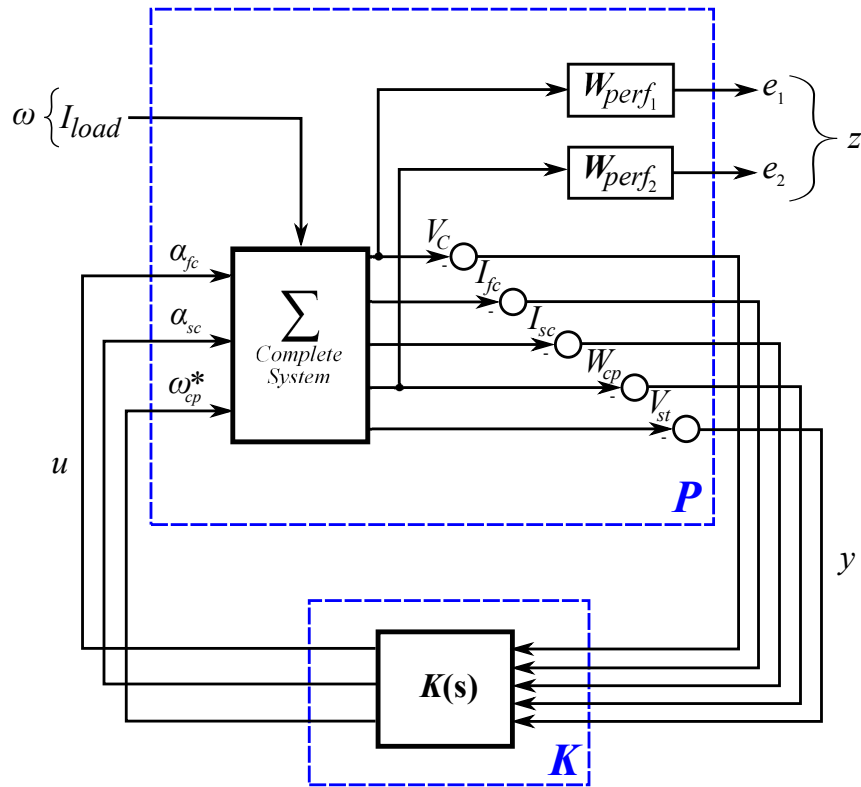


Figure 5.82: Control configuration in the P-K form for the complete system.

can be reduced to a 2^{nd} order system. The better robustness for the proposed controllers is clear from Figure 5.83, the singular values plot of the sensitivity function. Robust controllers are compared in more detail in Figure 5.84.

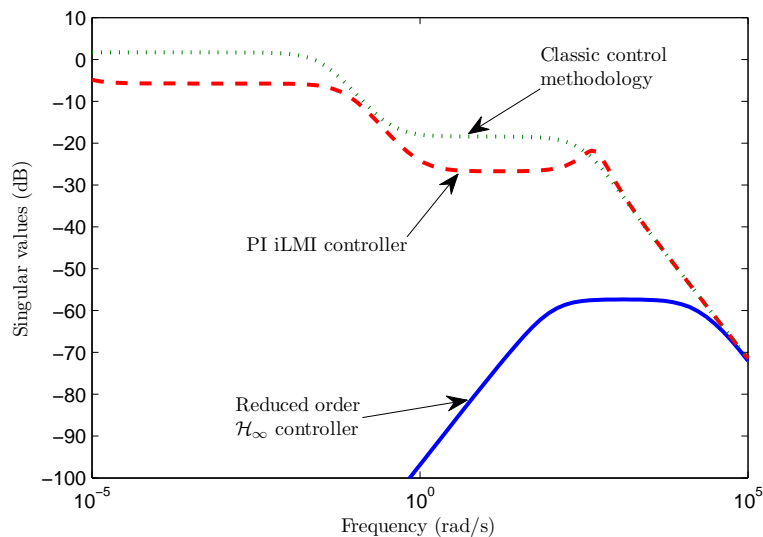


Figure 5.83: Closed-loop singular values plot.

Using the linear model, time-domain simulation results are obtained. The closed-loop response in the DC bus voltage for a 10% load step is presented in Figure 5.85. The reduced order \mathcal{H}_∞ controller show the best performance for all the controllers considered

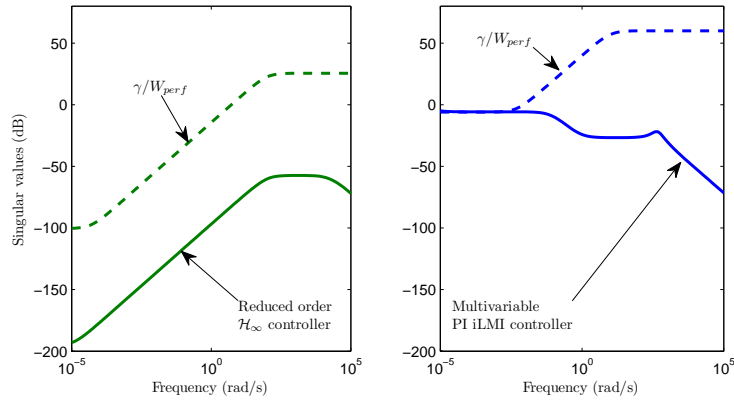


Figure 5.84: Closed-loop singular values plot.

in this complete case study. Disturbance rejection for the DC bus voltage is effective.

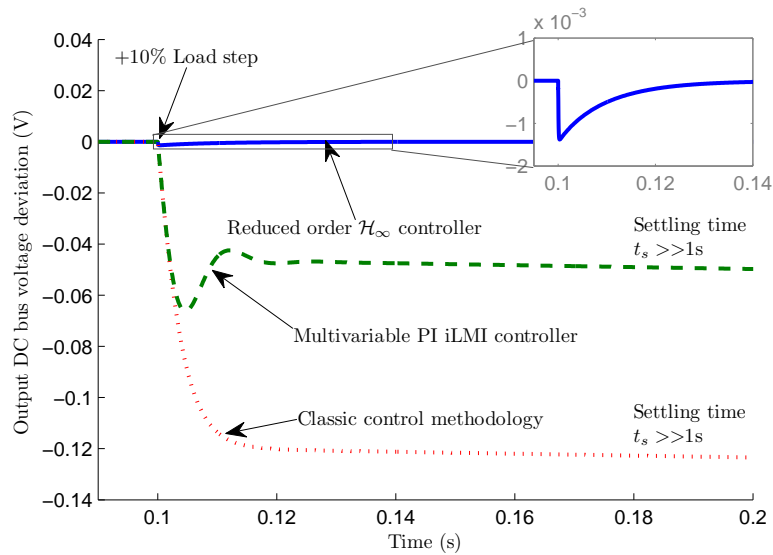


Figure 5.85: Simulation results, DC bus voltage.

Simulation results on the oxygen excess ratio regulation and the net power delivered by the FC and the output DC bus voltage are given in Figures 5.86 and 5.87 respectively. These results were obtained for a series of load current steps (presented afterward in Figure 5.88). Note the advantage of the proposed multivariable approach, the result obtained show a better regulation for the oxygen excess ratio λ_{O_2} , with overshoot peaks that are higher for the case of a decoupled system. This can be demonstrated by inspection of the closed-loop system response at $t = 5s$ (corresponding to a -20% load step), compare, at this point, the results of Figure 5.86 and Figure 5.63a in section 5.4.1.2. A final simulation result series of other several system variables was obtained for illustration purposes, using the reduced order \mathcal{H}_∞ controller. Results are presented in Figure 5.88.

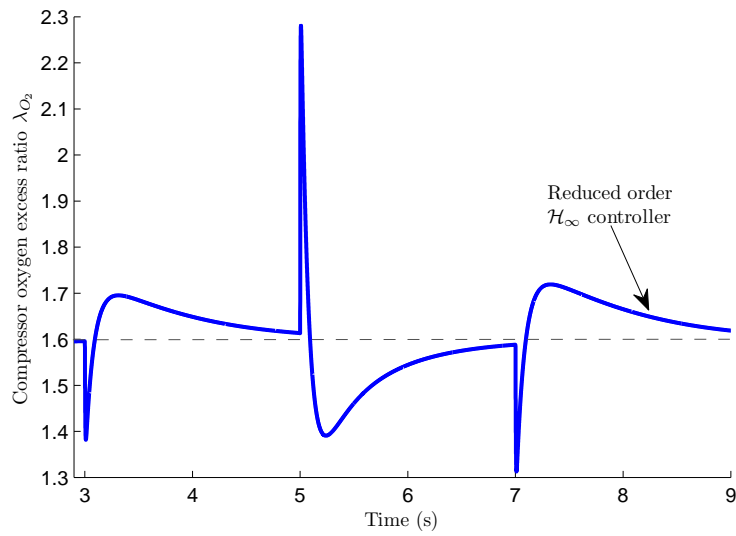


Figure 5.86: Simulation results, oxygen excess ratio.

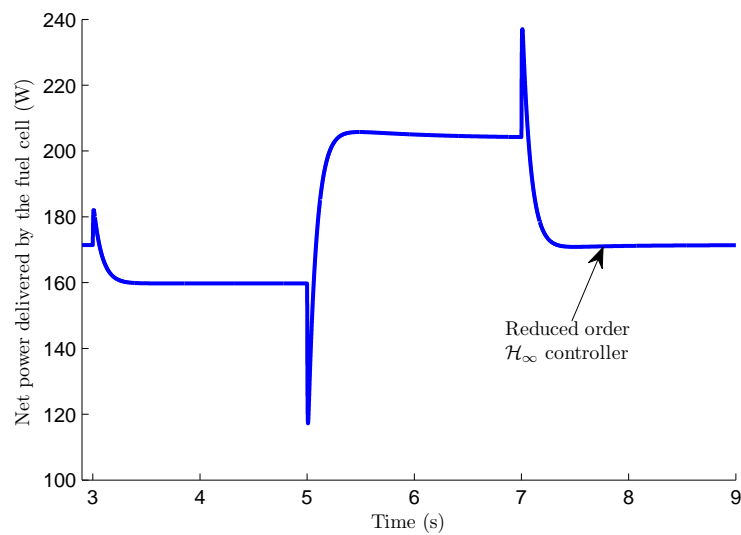


Figure 5.87: Simulation results, net power delivered to the load.

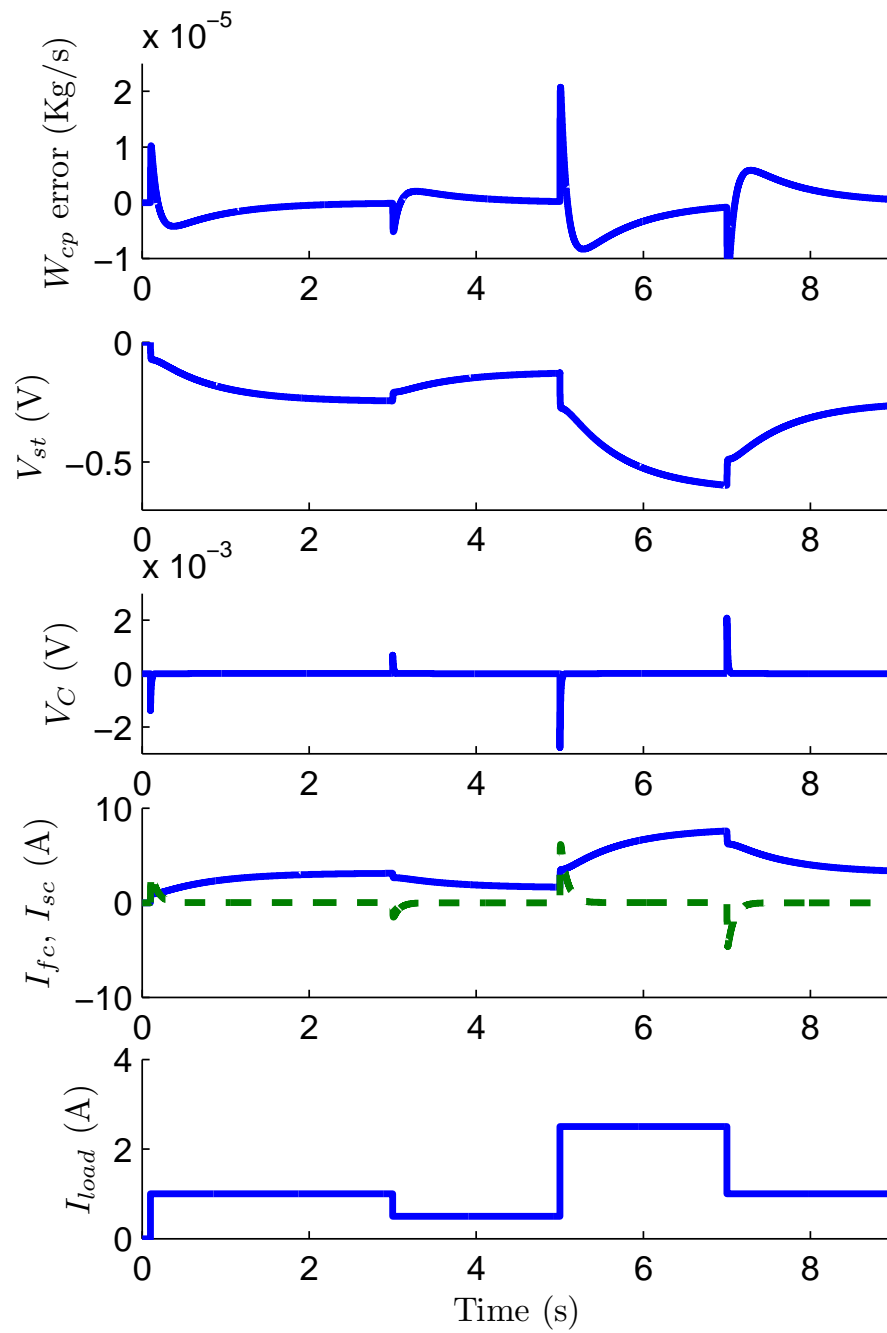


Figure 5.88: Simulation using linear system results and the reduced order \mathcal{H}_∞ controller for several complementary variables for a series steps in the load current.

5.6 Conclusion

In this chapter the results obtained for robust controller synthesis were presented. A main conclusion for all robust controller described is the significant improvement in robustness, in the sense of minimization of the closed-loop \mathcal{H}_∞ norm, when compared to the classic methodologies. It should also be noted however that the classic methodologies presented are not unique and maybe a better robust disturbance rejection performance can be obtained if these controllers are meticulously designed. They were presented here for illustrating the clear advantage of the robust methods. A great advantage of the classic methodology is its simplicity, the drawback is the possible lack of robustness and the time spent to design them for systems with closer or complex interactions. For the robust methods we have shown in this chapter that a robust implementation of a simplified controller was possible, while always keeping the robust property. This was realized with reduced order \mathcal{H}_∞ , fixed order \mathcal{H}_∞ and robust PI controllers. In general good results were obtained achieving our goal of a disturbance rejection control. In some specific cases, as in the FC current and the oxygen excess ratio, the disturbance effective rejection mitigates the harmful effects of large load transients on the FC, preserving its life span.

Another very important characteristic is the multivariable feature of the proposed methodologies. This means that, along with methodology described in Figure 5.1, a generalized approach to multivariable robust control system can be developed. It should be noted that almost every robust controller presented was computed using the same methodology. The final robust controllers were obtained using very similar procedures, this may offer a better flexibility to the control designer. The proposed methodology focus on robust control, for this, a complete robustness analysis was proven to be a critical part of the strategy.

Some problems were however reported using some robust methods described in this chapter. For example, the convergence problem of the iLMI algorithm for the control of the complete electrical sub-system. Other problem was the impossibility of control validation using the dedicated test-bench set-ups. This will presented as a part of the future work in this area.

Conclusions and Perspectives

Summary

A methodology has been proposed in this thesis for a hybrid fuel cell system control. Two main important features are the *multivariable* structure and *robustness* in the control strategies. A may concern is to protect the FC stack to load current transients, this is why a disturbance rejection approach was introduced.

Comparison with classic control strategies was used to show that, even when classic control may be straightforward, important gains may be obtained from advanced control tools.

To cope with the simplicity of classic control approaches, reduced order robust controllers were of interest during this thesis. A special interest was given to simple PI control designed in the \mathcal{H}_∞ /LMI frame-work. Good results on time transient simulations and robustness performance were obtained. However, the limitations of the algorithms involved to compute multivariable PI controllers were also shown. A special limitation is the size of the multivariable problem. Attention was also given to fixed order controllers with \mathcal{H}_∞ performance. Fixed order strategies are very powerful, the results obtained with these controllers are encouraging. Fixed order controllers were computed to solve the problem of simple control strategies for the special cases where the multivariable complexity was too important and the proposed iLMI algorithm was not a sufficient solution. For the MIMO iLMI PI control methodology, it was obtained that for large multivariable problems, the system order will affect the optimization algorithm efficiency and convergence problems may arise. In the specific case of the complete electrical sub-system control, including the voltage inverter, no solution was found using the proposed algorithm. While in the simplified case of a decoupled electrical sub-system (without voltage inverter), the algorithm retrieved good results including robust performance.

The multivariable approach considered in the methodology proposed, aims to the implementation of a *generalized* control strategy that helps the control engineer to consider the advantages obtained with the robust property. In some special cases, as in on-board applications, it could be very interesting to introduce critical physical parameters as the complete system weight and volume. A first approach was presented for the design and sizing of the DC bus filter parameters.

Perspectives

As a consequence of the results obtained during this thesis, some interesting research perspectives in this topic may be proposed:

Mid-term perspectives

- The methodologies proposed during this thesis may be completed using classical power management approaches. Many interesting methods can be found in the literature including the use of efficiency curves and MPPT algorithms. These strategies are a very important complement for safe and *optimal* operation of the FC stack.
- Analysis and consideration of other control methodologies and a deeper comparison with classic and effective control methods. Compare the results obtained with other more complex classic methodologies as the RST for parallel boost converter control or the “generalized integrator” for current-mode control of voltage inverters and the solution of the harmonics control problem.
- A further analysis and comparison of results obtained for the compressor-motor system and the complete system with other *classic* control schemes proposed in the literature.
- It may be also interesting to test the proposed methodologies on real-world FC applications, stationary or mobile, including its use hybrid electrical vehicle applications with real load demand profiles.

Long-term perspectives

- Analysis of several *application topologies*. For example, considering multiple fuel cells for high-voltage/high-power applications may be a challenging problem that includes several FC modules connected in series. An interesting approach may also lead to the use of the multivariable control strategy presented in this thesis to solve the multilevel DC-DC converter topology, distinctive in DC bus distribution architectures. See Yu et al. [2007] for a summary on different power conditioning topologies.
- Further develop the advantage of robust methods and a *generalized* strategy. A general component optimization may be proposed to reduce the overall components weight/volume values. This may be continuation of the work of Huu [2008] on component device size/volume optimization, interesting for *on-board* applications. An interesting option may consider the design optimization of the energy sources, in this case, a leading perspective, may be to analyze the use of the double layer capacitance of the fuel cell as a parameter for component optimization.
- Experimental implementation for control methodology validation of compressor and voltage inverter systems using the GESI and the Universal test-bench set-ups respectively.
- Design an LPV control approach for a more wide operating range, and then include the influence of temperature and cell humidification in the FC operating point.

Appendix A

Matlab functions used for control

In this appendix, some MATLAB functions developed and used for control are presented. The functions presented in this section, are used for the computation of PI controllers. Two main functions are presented: the iLMI algorithm for computation of a PI controller in an LTI system and the function used for computation of a gain-scheduled PI controller for an LPV system. The functions used to compute the \mathcal{H}_∞ controller for both LTI and LPV systems are not presented, they were developed in the work of Poussot-Vassal [2008].

A.1 PI controller for an LTI system

The function *Paper_ILMI_SOFHinf_yalmip* calls two other functions: *SOF_model* and *GEVP_Hinf_Yalmip* presented hereafter.

A.1.1 The iLMI algorithm

```
function [Fend, alphaFinal, Poles, NormHinf,...
    i, k] = Paper_ILMI_SOFHinf_yalmip(Plant, nmeas, ncon, gamma)

% This function computes a controller using a PID H-infinity
% formulated as an LMI iterative problem.
% This function is divided in two parts. In the first part the
% algorithm 3 (see Yong et al) is coded.
% This algorithm finds an initial decision variable P for
% algorithm 4. The second part computes algorithm 4. In this
% part three optimization problem are solved if necessary, OP1,
% OP2, and % OP3. The function "GEVP_Hinf_Yalmip" is called if
% necessary, this function solves the generalized eigenvalue
% problem and is the same as the "gevp" function in the Matlab's
% LMILab but using Yalmip instead.
% Input and output variables are the same as in the
% "Paper_ILMI_SOFHinf_yalmip" function.
% Input variables:
% - System variables: A, B1, B2, C1, C2, D11, D12, D21.
% - H-infinity optimization parameter: gamma (>0).
% - Angle "theta" for pole placement.
```

```

% Output variables:
% - Controller: F = [F1 F2 F3]'
% - LMI optimization parameter: alpha (<=0).
% - System closed loop eigenvalues: Poles.
% - Closed loop H-infinity norm: NormHinf.
% - Iteration variables: i for iteration number of
%   algorithm 1 and k for iteration number of algorithm 2
%   (see Yong et al).
% This algorithm is proposed in:
% An Improved ILMI Method for Static Output Feedback
% Control With Application to Multivariable PID Control
% Yong He and Qing-Guo Wang
%
% NOTE: SOF Hinf example and Yalmip code is used.
%
% David HERNANDEZ - January 2010
% Grenoble Electrical Engineering Laboratory (G2ELab)

%*****
%*****
% Begins Algo 3:
disp('CONTROLLER CALCULATION IN PROGRESS...')

% The SOF model:
[A, B1, B2, C1, C2, D11, D12, D21] = SOF_model(Plant,nmeas,ncon);

i = 1;
[Nx,Nu]=size(B2); [Nys,Nx]=size(C2); [Nz,Nomega]=size(D11);
P0=eye(size(A,1)); L0=eye(size(A,1)); epsilon = 0.3;

% Method #1: Algorithm using Yalmip:
P = sdpvar(Nx);
L = sdpvar(Nx);
V1 = sdpvar(Nx,Nys);
V2 = sdpvar(Nu,Nx);
F = sdpvar(Nu,Nys);

while i < 200
    % OP1:
    G = set([P*A+A'*P+V1*C2+C2'*V1' P*B1+V1*D21 C1'+C2'*F'*D12';...
            B1'*P+D21'*V1' -gamma*eye(Nomega) D11'+D21'*F'*D12';...
            C1+D12*F*C2 D11+D12*F*D21 -gamma*eye(Nz)] < 0);
    G = G + set([A*L+L*A'+B2*V2+V2'*B2' B1+B2*F*D21 L*C1'+V2'*D12';...
                B1'+D21'*F'*B2' -gamma*eye(Nomega) D11'+D21'*F'*D12';...
                C1*L+D12*V2 D11+D12*F*D21 -gamma*eye(Nz)] < 0);
    G = G + set([P eye(size(A,1));eye(size(A,1)) L] >= 0);
    G = G + set(F > 0);

```

```

options = sdpsettings('solver','sedumi','usex0',1,'verbose',0);
solvesdp(G,trace(P*L0+L*P0),options);
fprintf('Iteration: %d - Condition: %4.4f for %2.0f\n',i,...
        trace(double(P)*double(L)),Nx)
if abs(trace(double(P)*double(L))-Nx) <= epsilon
    Pnum = double(P);theflag = 1
    break
end
if abs(trace(double(P)*double(L))-trace(P0*L0)) <= epsilon*0.001
    theflag = 2
    break
end
i = i + 1;
P0 = double(P); L0 = double(L);
end
Pnum = double(P);
% Algo 3 ends
%*****
%*****
% Begins Algo 4:
k = 1
while k <= 100
% >>> OP1:
% Method #1: Algorithm using Yalmip:
alpha = sdpvar(1,1); F0 = ones(Nu,Nys);
if k == 1; assign(F,F0); end
H = set([Pnum*A+A'*Pnum+Pnum*B2*F*C2+C2'*F'*B2'*Pnum'...
        -alpha*Pnum Pnum*B1+Pnum*B2*F*D21 C1'+C2'*F'*D12';...
        B1'*Pnum+D21'*F'*B2'*Pnum -gamma*eye(Nomega)...
        D11'+D21'*F'*D12';...
        C1+D12*F*C2 D11+D12*F*D21 -gamma*eye(Nz)] < 0);
H = H + set(F > 0);
options = sdpsettings('solver','sedumi','verbose',0);
solvesdp(H,alpha,options);
Fend = double(F);
alpha = double(alpha);
% Imposing positive Fend coefficients:
check = Fend > 0; check2 = prod(double(check));

if alpha <= 0 %&& check2 == 1
    disp('SOF GOOD! Stop1!'),break;
end
% >>> OP2:
k = k + 1
[Pnum, alpha] = GEVP_Hinf_Yalmip(A,B1,B2,C1,C2,D11,...

```

```

        D12,D21,Nx,Fend,gamma);

if alpha <= 0 %&& check2 == 1
    disp('SOF GOOD! Stop2!'),break;
end
% >>> OP3:
% Method #1: Algorithm using Yalmip:
assign(P,Pnum);
I = set([P*A+A'*P+P*B2*Fend*C2+C2'*Fend'*B2'*P-alpha*P...
        P*B1+P*B2*Fend*D21 C1'+C2'*Fend'*D12';...
        B1'*P+D21'*Fend'*B2'*P -gamma*eye(size(D11,2))...
        D11'+D21'*Fend'*D12';...
        C1+D12*Fend*C2 D11+D12*Fend*D21...
        -gamma*eye(size(D11,1))] < 0);
options = sdpsettings('solver','sedumi','verbose',0);
solvesdp(I,trace(P),options);
Pnum = double(P);
%     if (norm(Pii_num2 - Pnum) / norm(Pii_num2)) < 0.001
%         break;
%     else
%         Pnum = Pii_num2;
%     end
    k = k + 1
    %[P]=P_min(A,B2,C2,alpha,Fend,Pnum);
end
% Algo 4 ends
%*****

% Calculation of closed loop system:
Acl = A + B2*Fend*C2;
Bcl = B1 + B2*Fend*D21;
Ccl = C1 + D12*Fend*C2;
Dcl = D11 + D12*Fend*D21;
SystBF = ss(Acl, Bcl, Ccl, Dcl);
% bode(SystBF)
Poles = eig(Acl);
NormHinf = norm(SystBF,inf);
alphaFinal = alpha;

```

A.1.2 Function for Static Output Feedback

```

function [Ab, B1b, B2b, C1b, C2b, D11b, D12b,...
        D21b] = SOF_model(P,nmeas,ncon)

```

```

Nz = size(P,1)-nmeas;
Nomega = size(P,2)-ncon;

```



```

t_lower = 1e-10;
t_upper = 1e10;

ops = sdpsettings('verbose',0,'warning',0,'solver','sedumi');

% Bisection Algorithm:
tol = 1e-5;
t_works = t_lower;
while (t_upper-t_lower)>tol
    t_test = (t_upper+t_lower)/2;
    %disp([t_lower t_upper t_test])
    H2 = [Pi>eye(N) , [Pi*A+A'*Pi+Pi*B2*Fend*C2+C2'*Fend'*B2'*...
        Pi+2*t_test*Pi Pi*B1+Pi*B2*Fend*D21 C1'+C2'*Fend'*D12';...
        B1'*Pi+D21'*Fend'*B2'*Pi -gamma*eye(Nomega) D11'+...
        D21'*Fend'*D12';...
        C1+D12*Fend*C2 D11+D12*Fend*D21 -gamma*eye(Nz)] < 0];
    sol = solvesdp(H2, [], ops);
    if sol.problem==1
        t_upper = t_test;
    else
        t_lower = t_test;
        t_works = t_test;
    end
end
end
Pii_num = double(Pi);
alphaii_num = -2*t_upper;
end

```

A.2 PI controller for an LPV system

```

function [K1,K2,GAMMA] = pi_mimo_lpv_function(listP,...
    Nys, Nu, percentage, solver, G_I, beta)

% Author: David HERNANDEZ-TORRES
% Date: March 2011

% Function solver for the MIMO PI LPV controller.
% This function is based on the template Hinf controller
% function developed by Charles Poussot-Vassal.

% Description
% In this file the problem of finding a multivariable
% PI controller guaranteeing QS of the closed loop system and
% an  $H_{\infty}$  norm bound less than a specified  $\gamma > 0$ .

```

```

% This file solves the numeric example and uses the problem
% solution using collorary 7 to solve problem 2 of the paper:
% M. Mattei/Automatica 37 (2001) 1997-2003.
% To use this function one have to create the generalized
% plant P:
% Xdot   A  B1 B2   X
% Z   =  C1 D11 D12  W
% Y      C2 D21 D22  U
% and to input them as a list of systems
%
% Input
% listP  : list of plants
% Nys    : number of measures
% Nu     : number of control signals
% percentage : percentage added to the gamma optimal to
%             conditionate the controller
% solver  : name of the solver used ('dsdp','sedumi'...)
% G_I    : contant matrix indicating output measures
%         with integral action
% beta   : desired decay rate
%
% Output
% K1, K2 : controller matrices used to reconstruct
%         gain-scheduled control
% GAMMA  : optimal gamma

%%% Size of the generalized plant
Nx = size(listP{1}.a,1);
Nz = size(listP{1},1)-Nys; % number of controlled output -
%                          number of measure
Nomega = size(listP{1},2)-Nu; % number of input -
%                          number of control
Nc = size(G_I,1);

%%% To tackle with some strict inequalities problems
% not well implemented in Yalmip

%%% Cut the system
for i = 1:size(listP,2)
    A{i} = listP{i}.a(1:Nx,1:Nx);
    B1{i} = listP{i}.b(1:Nx,1:Nomega);
    B2{i} = listP{i}.b(1:Nx,Nomega+1:Nomega+Nu);
    C1{i} = listP{i}.c(1:Nz,1:Nx);
    D11{i} = listP{i}.d(1:Nz,1:Nomega);
    D12{i} = listP{i}.d(1:Nz,Nomega+1:Nomega+Nu);
    C2{i} = listP{i}.c(Nz+1:Nz+Nys,1:Nx);
    D21{i} = listP{i}.d(Nz+1:Nz+Nys,1:Nomega);

```



```

        Cz_final{i}*Q Dzw_final{i} -eye(Nz)*gamma];
    %% Add sets
    G = G + set(H{i}<-eps);
end

options = sdpsettings('solver',solver,'usex0',1,'verbose',1,...
    'showprogress',1);
solvesdp(G,gamma,options);

GAMMA = double(gamma)*(1+percentage/100);

%% Numerical aspects
alpha = sdpvar(1,1,'full');

G0 = [Q -alpha*eye(Nx+Nc); -alpha*eye(Nx+Nc) ...
    [Wy';zeros(Nx-Nys,Nu)],zeros(Nx+Nc,Nx+Nc-Nu)];
Gn = set(G0>eps,'X and Y alpha constraint');

for i = 1:size(listP,2)
    F{i} = [A_final{i}*Q+Q*A_final{i}+[Wy';...
        zeros(Nx-Nys,Nu)]*B_final{i}'+B_final{i}*...
        [Wy';zeros(Nx-Nys,Nu)]' Bw_final{i} ...
        (1/GAMMA)*Q*Cz_final{i}';...
        Bw_final{i}' -eye(Nomega) ...
        (1/GAMMA)*Dzw_final{i}';...
        (1/GAMMA)*Cz_final{i}*Q ...
        (1/GAMMA)*Dzw_final{i} -eye(Nz)];
    %% Add sets
    Gn = Gn + set(F{i}<-eps);
end

options = sdpsettings('solver',solver,'usex0',1,...
    'verbose',1,'showprogress',1);
solvesdp(Gn,alpha,options);

Ky = double(Wy)/(double(Q1));

K1 = Ky(1:Nu,1:Nys);
K2 = Ky(1:Nu,Nys+1:Nys+Nc);

```


Appendix B

Open-loop state-space matrices

In this section, the state-space matrices representations of the open-loop systems used for computation of robust controllers are presented. The matrices presented here are the numerical representation of the state-space systems given in the dissertation, references to those systems are given when necessary.

B.1 Hybrid boost converter system

The state-space system is in the form given by equations (4.3), where the system matrices are given by:

$$A = \begin{pmatrix} 0 & 14.6848 & 0 & 0 & 16.2736 & 0 \\ -11054 & -1525.6 & -20000 & -20000 & 0 & 0 \\ 0 & 0.4717 & -231.2246 & 0 & 0 & 0 \\ 0 & 0.4717 & 0 & -999.3604 & 0 & 0 \\ -12250 & 0 & 0 & 0 & -380 & 20000 \\ 0 & 0 & 0 & 0 & -0.017241 & 0 \end{pmatrix} \quad (\text{B.1})$$

$$B_1 = \begin{pmatrix} -26.5692 \\ 0 \\ 0 \\ 0 \\ 0 \\ 0 \end{pmatrix} \quad (\text{B.2})$$

$$B_2 = \begin{pmatrix} -951.4608 & 0 \\ 480000 & 0 \\ 0 & 0 \\ 0 & 0 \\ 0 & 480000 \\ 0 & 0 \end{pmatrix} \quad (\text{B.3})$$

B.1.1 Hybrid boost system with reversible converter

This system is very similar with the previously system presented but with the modifications coming from equations (5.3.3.2).

For this system we considered a simplified electric equivalent model for the fuel cell. The dynamic equation for the fuel cell current I_{fc} becomes:

$$\frac{dI_{fc}}{dt} = \frac{1}{L_{fc}} [E_0 - R_{ohm}I_{fc} - (1 - \alpha_{fc})V_C] \quad (\text{B.4})$$

The state vector is $x = [I_{fc} \ I_{sc} \ V_{sc} \ V_C]^T$, the disturbance is $\omega = I_{load}$ and the control input $u = [\alpha_{fc} \ \alpha_{sc}]^T$.

The system matrices are then given by:

$$A = \begin{pmatrix} -141.5 & 0 & -84.1425 & 0 \\ 0 & -231.7073 & -457.3171 & 1219.5122 \\ 229.4795 & 170.4545 & 0 & 0 \\ 0 & -0.17241 & 0 & 0 \end{pmatrix} \quad (\text{B.5})$$

$$B_1 = \begin{pmatrix} 0 \\ -487804.878 \\ 0 \\ 0 \end{pmatrix} \quad (\text{B.6})$$

$$B_2 = \begin{pmatrix} 0 & 66666.6667 \\ 0 & 0 \\ -454.5455 & -22838.6502 \\ 0 & 0 \end{pmatrix} \quad (\text{B.7})$$

B.2 Voltage inverter system

The state-space system is in the form given by equations (4.23), where the system matrices are given by:

$$A = \begin{pmatrix} -0.33333 & 314.1593 & -333.3333 & 0 \\ -0.33333 & -314.1593 & 0 & -333.3333 \\ 10000 & 0 & 0 & 314.1593 \\ 0 & 10000 & -314.1593 & 0 \end{pmatrix} \quad (\text{B.8})$$

$$B_1 = \begin{pmatrix} 0 \\ 0 \\ -10000 \\ 0 \end{pmatrix} \quad (\text{B.9})$$

$$B_2 = \begin{pmatrix} 66666.6667 & 0 & -20.9217 \\ 0 & 66666.6667 & 308.1628 \\ 0 & 0 & 0 \\ 0 & 0 & 0 \end{pmatrix} \quad (\text{B.10})$$

B.3 Air supply system model

The linear model for the air supply system presented here, corresponds to the system proposed by Gasser [2006] extended with some of the linear models identified and pre-

sented in section 4.4.4. The block diagram of the state-space model presented here is given in Figure 5.61. The system inputs are $u = [\omega_{cp}^* \ I_{fc}]^T$ and the system output is $y = [W_{cp} \ V_{st}]^T$.

The numerical representation of this system is given by state-space matrices:

$$A = \begin{pmatrix} -110.18 & 26.43 & -0.02 & 3.96 \times 10^6 & 0 & 0 & -6.86 \times 10^{-5} \\ -309.67 & 88.87 & -0.11 & 1.49 \times 10^7 & 0 & 0 & -0.00048 \\ 202625.81 & -30620.96 & -13.07 & -3.67 \times 10^9 & 0 & 0 & -0.16 \\ -0.00093 & 0.00015 & 5.379 \times 10^{-8} & 12.59 & 0 & 0 & 9.38 \times 10^{-10} \\ 0 & 0 & 0 & 0 & -231.22 & 0 & 0 \\ 0 & 0 & 0 & 0 & 0 & -999.36 & 0 \\ 0 & 0 & -7718.84 & 0 & 0 & 0 & -399.34 \end{pmatrix} \quad (\text{B.11})$$

$$B = \begin{pmatrix} 0 & -0.23901 \\ 0 & 0.013232 \\ 0 & 851.3572 \\ 0 & -3.3136 \times 10^{-6} \\ 0.4717 & 0 \\ 0.4717 & 0 \\ 391.1566 & 0 \end{pmatrix} \quad (\text{B.12})$$

$$C = \begin{pmatrix} 0 & 0 & 0 & 1 & 0 & 0 & 0 \\ 0 & 0 & 0 & 0 & -1 & -1 & 0 \\ 0 & 0 & 0 & 1 & 0 & 0 & 0 \\ 0 & 0 & 0 & 0 & -1 & -1 & 0 \end{pmatrix} \quad (\text{B.13})$$

$$D = \begin{pmatrix} 0 & 0 \\ -0.07628 & 0 \\ 0 & 0 \\ -0.07628 & 0 \end{pmatrix} \quad (\text{B.14})$$

B.4 Complete system model

The model presented here was used to compute the robust controllers in section 5.5. The block diagram of the model is given in Figure 5.81. The system inputs are $u = [I_{load} \ \alpha_{fc} \ \alpha_{sc} \ \omega_{cp}^*]^T$ and the system outputs are $y = [V_C \ I_{fc} \ I_{sc} \ W_{cp} \ V_{st} \ I_{cm}]^T$.

The numerical representation of this system is given by state-space matrices:

$$A = \begin{pmatrix} 0 & 14.6848 & 16.2736 & 0 & 0 & 0 & 17.505 & -24.0811 & -11.216 & -4.8386 \\ -11054 & -3101.44 & 0 & -20000 & -20000 & 0 & -0.00046138 & -0.016693 & 0.012326 & 0.0024596 \\ -12250 & 0 & -380 & 0 & 0 & 20000 & 0 & 0 & 0 & 0 \\ 0 & 0.4717 & 0 & -231.2246 & 0 & 0 & 0 & 0 & 0 & 0 \\ 0 & 0.4717 & 0 & 0 & -999.3604 & 0 & 0 & 0 & 0 & 0 \\ 0 & 0 & -0.017241 & 0 & 0 & 0 & 0 & 0 & 0 & 0 \\ 0 & -2.1268 \times 10^{-6} & 0 & 0 & 0 & 0 & -1.6177 & 6.1289 & 1.7741 & 0.95281 \\ 0 & -5.4066 \times 10^{-5} & 0 & 0 & 0 & 0 & -6.1289 & -11.1813 & -27.0734 & -3.6704 \\ 0 & -6.9618 \times 10^{-5} & 0 & 0 & 0 & 0 & 1.7741 & 27.0734 & -3.9422 & -5.3516 \\ 0 & 3.3212 \times 10^{-5} & 0 & 0 & 0 & 0 & -0.95281 & -3.6704 & 5.3516 & -2.0133 \end{pmatrix} \quad (\text{B.15})$$

$$C = \begin{pmatrix} 1 & 0 & 0 & 0 & 0 & 0 & 0 & 0 & 0 & 0 \\ 0 & 1 & 0 & 0 & 0 & 0 & 0 & 0 & 0 & 0 \\ 0 & 0 & 1 & 0 & 0 & 0 & 0 & 0 & 0 & 0 \\ 0 & -2.6011 \times 10^{-12} & 0 & 0 & 0 & 0 & -2.3054 \times 10^{-6} & -2.4962 \times 10^{-7} & -1.9313 \times 10^{-6} & 2.3059 \times 10^{-5} \\ 0 & -0.078792 & 0 & 0 & 0 & 0 & -2.3069 \times 10^{-8} & -8.3466 \times 10^{-7} & 6.163 \times 10^{-7} & 1.2298 \times 10^{-7} \\ 0 & 1.6125 \times 10^{-7} & 0 & 0 & 0 & 0 & -0.65885 & 0.90635 & 0.42214 & 0.18211 \end{pmatrix} \quad (\text{B.16})$$

$$B = \begin{pmatrix} -26.5692 & -951.4608 & 0 & -0.00018661 \\ 0 & 480000 & 0 & -0.00019358 \\ 0 & 0 & 480000 & 0 \\ 0 & 0 & 0 & 0 \\ 0 & 0 & 0 & 0 \\ 0 & 0 & 0 & 0 \\ 0 & 0 & 0 & -0.65885 \\ 0 & 0 & 0 & -0.90635 \\ 0 & 0 & 0 & 0.42214 \\ 0 & 0 & 0 & -0.18211 \end{pmatrix}, \quad D = \begin{pmatrix} 0 & 0 & 0 & 0 \\ 0 & 0 & 0 & 0 \\ 0 & 0 & 0 & 0 \\ 0 & 0 & 0 & -1.0776 \times 10^{-10} \\ 0 & 0 & 0 & -9.6789 \times 10^{-9} \\ 0 & 0 & 0 & 7.0235 \times 10^{-6} \end{pmatrix} \quad (\text{B.17})$$

Appendix C

Some thermo-dynamical principles

This section intends to present a brief review on some important thermodynamical principles used in the FC system modelling. An extensive (and somehow classical) theory review in thermodynamics can be found in Sonntag et al. [2003]. According to the dynamic phenomena in relation with the FC operation, we will focus this review in two subjects: the mass conservation principle and the mixture involving gases and water vapor.

The physical laws concerning mass says that we cannot create or destroy mass, thus the mass conservation principle states that the rate of change of mass inside a *control volume* can be different from zero if we add or take a flow of mass out as Sonntag et al. [2003]:

$$\text{Rate of change} = +\text{Input Flow} - \text{Output Flow}$$

If several possible flows are considered, then we have:

$$\frac{dm_{CV}}{dt} = \sum W_{in} - \sum W_{out} \quad (\text{C.1})$$

where $\frac{dm_{CV}}{dt}$ is the mass rate of change in a control volume and W is the input or output mass flow in kg/sec.

This mass conservation principle will be used to model the mass evolution in the different flows involved in the process: air, water, oxygen, nitrogen, hydrogen, etc.

Some thermodynamical principles based on the mixture of gases will also be used. So let us consider a mixture of two gases A and B. The ideal gas law states that Pukrushpan et al. [2004a]:

$$pV = n\bar{R}T = mRT \quad (\text{C.2})$$

where p is the gas pressure, V is the gas volume, n is the number of moles of the gas, m is the mass of the gas, \bar{R} is the universal gas constant, R is the gas constant and T the gas temperature.

The number of moles of the mixture is the sum $n = n_A + n_B$ and considering each component as an ideal gas, then:

$$\begin{aligned} p_A V &= n_A \bar{R} T \\ p_B V &= n_B \bar{R} T \end{aligned} \quad (\text{C.3})$$

where p_A and p_B are the partial pressure of each component.

Using the total number of moles n we obtain that the pressure of the mixture is the sum of the partial pressures, i. e.:

$$p = p_A + p_B \quad (\text{C.4})$$

Considering this mixture as composed by air and water vapor. The humidity ratio ω (ratio between water vapor mass m_v and air mass m_a) is now defined as:

$$\omega = \frac{m_v}{m_a} \quad (\text{C.5})$$

However the relative humidity is widely used instead, because the maximum amount of water vapor that the air is able to contain in saturation is dependent on the temperature and pressure of the air Pukrushpan et al. [2004a]. The relative humidity ϕ is the ration between the mole fraction of water vapor and the mole fraction of vapor in a saturated mixture, assuming ideal gases:

$$\phi = \frac{p_v}{p_{sat}} \quad (\text{C.6})$$

where p_{sat} is the saturation pressure.

For a mixture of air and water vapor, p_{sat} is the water saturation pressure. This is a temperature dependent value as seen in the Table C.1¹. In literature, several equations for the water vapor saturation pressure could be found. From the data in Table C.1, the water saturation pressure equation is obtained using the *Curve Fitting Toolbox* in Matlab. The fitted equation is in the form:

$$p_{sat} = a \exp(b \times (T_{st} - 273.15)) \quad (\text{C.7})$$

with $a = 0.01738$ and $b = 0.04081$, the curve fitting results, and where T_{st} is the stack temperature in °K.

In Pukrushpan et al. [2004a] this data is used to obtain the following 4th order equation:

$$\log(p_{sat}) = -1.69 \times 10^{-10}T^4 + 3.85 \times 10^{-7}T^3 - 3.39 \times 10^{-4}T^2 + 0.143T - 20.92 \quad (\text{C.8})$$

where p_{sat} is in kPa and T in °K.

However, a typical procedure to compute this pressure is the use of the Antoine equation:

$$\log(p_{sat}) = A - \frac{B}{C + T} \quad (\text{C.9})$$

¹Data from: http://www.engineeringtoolbox.com/water-vapor-saturation-pressure-d_599.html

Table C.1: Water Saturation Pressure

Temperature (°C)	Absolute Water Pressure (kPa)
0	0.6105
5	0.8722
10	1.228
20	2.338
30	4.243
40	7.376
50	12.33
60	19.92
70	31.16
80	47.34
90	70.10
100	101.3

where p_{sat} is the saturation pressure, T is the temperature, A , B and C are component-specific constants. For water vapor pressure, and pressure given in Pa and temperature in °K: $A = 10.32907$, $B = 1642.89$ and $C = -42.85$.

A comparison graph of the different water saturation pressure procedures described here is presented in Figure C.1.

Finally, the humidity ratio and the relative humidity can be related using the ideal gas law:

$$\omega = \frac{m_v}{m_a} = \frac{p_v V / R_v T}{p_a V / R_a T} = \frac{R_a p_v}{R_v p_a} = \frac{M_v p_v}{M_a p_a} \quad (\text{C.10})$$

where M_v and M_a are the molar mass of water vapor and air respectively in kg/mol.

Now using equations (C.4) and (C.6) the relationship is given by:

$$\phi = \omega \frac{M_a p_a}{M_v p_{sat}} \quad (\text{C.11})$$

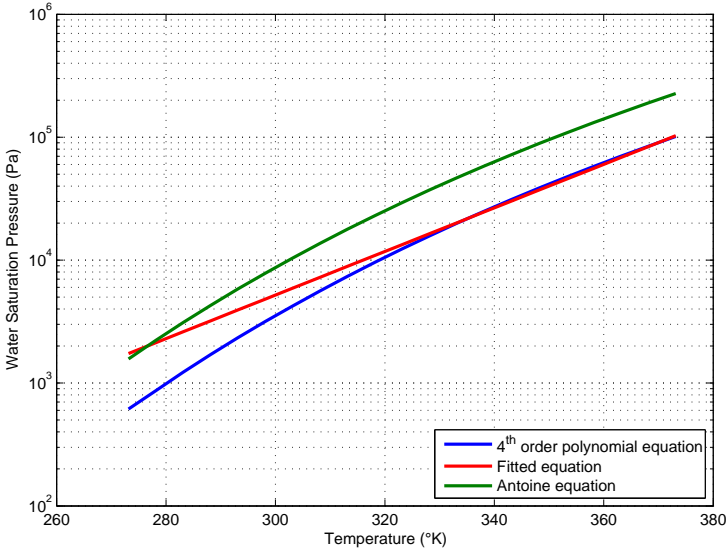


Figure C.1: Water saturation pressure calculation comparison.

Bibliography

- J. Alvarez-Ramirez, I. Cervantes, G. Espinosa-Perez, P. Maya, and A. Morales. A stable design of PI control for DC-DC converters with an rhs zero. *Circuits and Systems I: Fundamental Theory and Applications, IEEE Transactions on*, 48(1):103–106, Jan. 2001.
- P. Apkarian and D. Noll. Nonsmooth \mathcal{H}_∞ synthesis. *Automatic Control, IEEE Transactions on*, 51(1):71 – 86, jan. 2006. ISSN 0018-9286.
- S. Bacha, M. Brunello, and A. Hassan. A general large signal model for DC-DC symmetric switching converters. *Electric Machines and Power Systems*, 22:493–510, July 1994.
- S. L. Malo Barragán. *Design and Control of an Electric Energy Conditioning System for a PEM Type Fuel Cell*. PhD thesis, Universitat Politècnica de Catalunya, Institut d’Organització i Control de Sistemes Industrials, Barcelona, Spain, 2009.
- M. Becherif and D. Hissel. MPPT of a PEMFC based on air supply control of the motocompressor group. *International Journal of Hydrogen Energy*, (35):12521–12530, 2010.
- B. Blunier. *Modélisation de moto-compresseurs en vue de la gestion de l’air dans les systèmes piles à combustible, simulation et validation expérimentale (in French)*. PhD thesis, Université de Technologie de Belfort-Montbéliard,, Belfort, 2007.
- B. Boivin, L. Rambault, P. Coirault, and D. Mehdi. Multivariable PID Controllers via LMI Approach Applied to a Gyrometer. In *European Control Conference*, Cambridge, UK, 2003.
- S. Boyd, L. El Ghaoui, E. Feron, and V. Balakrishnan. *Linear Matrix Inequalities in System and Control Theory*. Society for Industrial and Applied Mathematics (SIAM), Philadelphia, 1994.
- J. Brely. *Commande Multivariable de Filière de Production de Fibres de Verre (in French)*. PhD thesis, Institut National Polytechnique de Grenoble, Laboratoire d’Automatique de Grenoble LAG (now Gipsa-Lab), 2003.
- C. Briat. *Commande et Observation Robustes des Systèmes LPV Retardés*. PhD thesis, Institut National Polytechnique de Grenoble, Gipsa-Lab, Grenoble, France, 2008.
- F. Bruzelius. *Linear Parameter-Varying Systems, an approach to gain scheduling*. PhD thesis, Department of Signals and Systems, Chalmers University of Technology, Göteborg, Sweden, 2004.

- S. Buller, E. Karden, D. Kok, and R.W. de Doncker. Modeling the dynamic behaviour of supercapacitors using impedance spectroscopy. *IEEE Trans. on Industry Applications*, 38(6):1622–1626, November/December 2002.
- D. Candusso. *Hybridation du groupe électrogène à pile à combustible pour l'alimentation d'un véhicule électrique (in French)*. PhD thesis, Institut National Polytechnique de Grenoble, Laboratoire d'Électrotechnique de Grenoble LEG (now G2ELab), Grenoble, France, 2002.
- Y. A. Chang and S. J. Moura. Air Flow Control in Fuel Cell Systems: An Extremum Seeking Approach. In *IEEE American Control Conference*, pages 1052–1059, St. Louis, MO, USA, June 2009.
- S. Choe, J. Lee, J. Ahn, and S. Baek. Integrated modeling and control of a PEM fuel cell power system with a PWM DC/DC converter. *Journal of Power Sources*, (164): 614–623, 2007.
- B. Cook. Introduction to Fuel Cells and Hydrogen Technology. *Engineering Science and Education Journal*, pages 205–216, 2002.
- B. V. Dang. *Conception d'une interface d'électronique de puissance pour Pile à Combustible (in French)*. PhD thesis, Institut National Polytechnique de Grenoble, Laboratoire d'Électrotechnique de Grenoble LEG (now G2ELab), Grenoble, France, 2006.
- S. Dasgupta and B. Anderson. A parametrization for the closed-loop identification of nonlinear time-varying systems. *Automatica*, 32(10):1349 – 1360, 1996. ISSN 0005-1098.
- D. Di Domenico, C. Speltino, and G. Fiengo. Power Split Strategy for Fuel Cell Hybrid Electric System. *Oil & Gas Science and Technology - Rev. IFP*, 65:145–154, 2010.
- M. W. Ellis, M. R. Von Spakovsky, and D. J. Nelson. Fuel Cells Systems: Efficient, Flexible Energy Conversion for the 21st Century. *Proceedings of the IEEE*, 89(12): 1808–1818, Dec. 2001.
- G. Fontes, C. Turpin, S. Astier, and T. A. Meynard. Interactions Between Fuel Cells and Power Converters: Influence of Current Harmonics on a Fuel Cell Stack. *IEEE Trans. on Power Electronics*, 22(2):670–678, March 2007.
- M. Frati. Rapport de stage: Dispositifs à convertisseurs statiques pour pile à combustible (PAC) (in French). Technical report, Internship report at Laboratoire d'Électrotechnique de Grenoble LEG (now G2ELab), 2006.
- I. Gadoura, T. Suntio, and K. Zenger. Robust control design for paralleled DC/DC converters with current sharing. In *Proceedings of the 15th IFAC World Congress on Automatic Control*, Barcelona, Spain, 2002.
- P. Gahinet, A. Nemirovski, A. J. Laub, and M. Chilali. *LMI Control Toolbox, for use with MATLAB*. The MathWorks, Inc., Natick, MA, 1995.
- F. Gasser. *An Analytical, Control-Oriented State Space Model for a PEM Fuel Cell System*. PhD thesis, École Polytechnique Fédérale de Laussane, 2006.

- H. Gaztañaga. *Etude de structures d'intégration des systèmes de génération décentralisée: Application aux micro-réseaux (in French)*. PhD thesis, Institut National Polytechnique de Grenoble, Laboratoire d'Électrotechnique de Grenoble LEG (now G2ELab), Grenoble, France, 2006.
- C. Gombert. *Simulations temps-réel des dispositifs d'électronique de puissance dédiés aux réseaux d'énergie électrique (in French)*. PhD thesis, Institut National Polytechnique de Grenoble, Laboratoire d'Électrotechnique de Grenoble LEG (now G2ELab), Grenoble, France, 2005.
- H. Gualous, D. Bouquain, A. Berthon, and J. M. Kauffmann. Experimental study of supercapacitor serial resistance and capacitance variations with temperature. *Journal of Power Sources*, (123):86–93, 2003.
- S. Gumussoy, D. Henrion, M. Millstone, and M.L. Overton. Multiobjective Robust Control with HIFOO 2.0. In *Proc. of the IFAC Symposium on Robust Control Design*, 2009.
- Y. Song Han, S.B. Li, X. Park, S.I. Jeong, H.G. Jung, and B.M. Jung. A power control scheme to improve the performance of a fuel cell hybrid power source for residential application. In *Power Electronics Specialists Conference, 2007. PESC 2007. IEEE*, pages 1261 – 1266, June 2007.
- F. Hansen, G. Franklin, and R. Kosut. Closed-Loop Identification via the Fractional Representation: Experiment Design. In *American Control Conference, 1989*, pages 1422 –1427, 1989.
- M. Hauck. Operation of Grid-Connected Cross-Flow Water Turbines in the Stall Region by Direct Power Control. *IEEE Trans. on Industrial Electronics*, 58(4):1132–1140, April 2011.
- Y. He and Q. Wang. An Improved ILMI Method for Static Output Feedback Control With Application to Multivariable PID Control. *IEEE Transactions on Automatic Control*, 51:1678–1683, 2006.
- D. Hernandez-Torres, D. Riu, O. Sename, and F. Druart. Robust optimal control strategies for a hybrid fuel cell power management system. In *36th Annual Conference on IEEE Industrial Electronics Society IECON*, pages 698–703, Nov. 7–10 2010a.
- D. Hernandez-Torres, D. Riu, O. Sename, and F. Druart. On the Robust Control of DC-DC Converters: Application to a Hybrid Power Generation System. In *4th IFAC Symposium on system, structure and control SSSC*, Sep. 15–17 2010b.
- D. Hernandez-Torres, D. Riu, O. Sename, and F. Druart. Robust control analysis using real-time implementation of a hybrid fuel cell power generation system. In *Fundamentals and Developments of Fuel Cells Conference FDFC*, Jan. 19–21 2011.
- D. Hissel and C. Turpin. A review on existing modeling methodologies for PEM fuel cell systems. In *Proceeding of the Fundamentals and Developments of Fuel Cells Conference (FDFC)*, Nancy, France, 2008.

- C. W. J. Hol, C. W. Scherer, E. G. van der Meché, and O. H. Bosgra. A Non-linear SDP Approach to Fixed-Order Controller Synthesis and Comparison with Two Other Methods Applied to an Active Suspension System. *European Journal of Control*, 9: 13–28, 2003.
- H. Nguyen Huu. *Méthodes et outils pour la conception de composants intégrés dans un réseau électrique embarqué*. PhD thesis, Université Joseph Fourier, G2ELab, Grenoble, France, 2008.
- Z. Jiang, L. Gao, and R. A. Dougal. Adaptive Control Strategy for Active Power Sharing in Hybrid Fuel Cell/Battery Power Sources. *IEEE Transactions on Energy Conversion*, 22(2):507–515, June 2007.
- I. H. Kazmi and A.I. Bhatti. Robust Controller Using LMI Framework for PEM Fuel Cell System. In *IEEE International Conference on Emerging Technologies (ICET)*, pages 136–141, Islamabad, Pakistan, 2009.
- P. Kundur. *Power System Stability and Control*. McGraw-Hill, Inc, New York, 1993.
- I. D. Landau. *Identification et Commande des Systèmes*. Hermes, 1993.
- I. D. Landau and A. Karimi. Recursive algorithms for identification in closed loop: A unified approach and evaluation. *Automatica*, 33(8):1499 – 1523, 1997. ISSN 0005–1098.
- E. Laroche. *Identification et Commande Robuste de Systèmes Électromécaniques (Habilitation à Diriger des Recherches)*. Université Louis Pasteur de Strasbourg, 2007.
- M. A. Laughton. Fuel Cells. *Engineering Science and Education Journal*, pages 7–16, 2002.
- H. B. Le. *Contribution aux méthodes de synthèse de correcteurs d'ordres réduits sous contraintes de robustesse et aux méthodes de réduction de modèles pour la synthèse robuste en boucle fermée (in French)*. PhD thesis, Université de Grenoble / Institut Polytechnique de Grenoble, LCIS, Grenoble, France, 2010.
- Q. Li, W. Chen, Y. Wang, S. Liu, and J. Jia-Yush. Robust control based on linear matrix inequality of fuel cell system with μ analysis. In *IEEE International Conference on Control and Automation*, pages 339–344, Xiamen, China, June 2010.
- L. Ljung. *System Identification: Theory for the User*. Prentice-Hall, Englewood Cliffs, New Jersey, 1987.
- L. Ljung. *System Identification Toolbox User's Guide*. The MathWorks, Inc., Natick, MA, 1988.
- L. Ljung. System Identification, To be included in the Control Handbook, edited by W. Levine. Technical Report LiTH-ISY-R-1763, Dept of EE. Linköping University, S-581 83 Linköping, Sweden, 1995.
- J. Löfberg. YALMIP : A Toolbox for Modeling and Optimization in MATLAB. In *Proceedings of the CACSD Conference*, Taipei, Taiwan, 2004.

- M. Mattei. Robust multivariable PID control for linear parameter varying systems. *Automatica*, 37(10):1997 – 2003, 2001. ISSN 0005-1098.
- B. A. McCain, A. G. Stefanopoulou, and I. V. Kolmanovsky. Stability Analysis for Liquid Water Accumulation in Low Temperature Fuel Cells. In *Proc. of the 47th IEEE Conf. on Decision and Control*, pages 859–864, Cancun, Mexico, 2008.
- R. D. Middlebrook. Topics in multiple-loop regulators and current-mode programming. *Power Electronics, IEEE Trans. on*, PE-2(2):109–124, April 1987.
- M.C. Pera, D. Candusso, D. Hissel, and J.M. Kauffmann. Power generation by fuel cells. *Industrial Electronics Magazine, IEEE*, 1(3):28–37, Fall 2007.
- B. Petrovic and Z. Rakic. Linear robust control of DC/DC converters: Part I - deterministic switching. *Electrical Engineering (Archiv fur Elektrotechnik)*, 87(2):57–68, Feb. 2005.
- D. Picault. *Reduction of mismatch losses in grid-connected photovoltaic systems using alternative topologies*. PhD thesis, Institut National Polytechnique de Grenoble, G2ELab, Grenoble, France, 2009.
- C. Poussot-Vassal. *Commande Robuste LPV Multivariable de Châssis Automobile*. PhD thesis, Institut National Polytechnique de Grenoble, Gipsa-Lab, Grenoble, France, 2008.
- J. T. Pukrushpan, A. G. Stefanopoulou, and H. Peng. *Control of Fuel Cell Power Systems. Principles, Modeling, Analysis and Feedback Design*. Springer, 2004a.
- J. T. Pukrushpan, A. G. Stefanopoulou, and H. Peng. Control of Fuel Cell Breathing. *IEEE Control Systems Magazine*, pages 30–46, April 2004b.
- S.M.R. Rafiei, R. Ghazi, R. Asgharian, M. Barakati, and H.A. Toliyat. Robust control of DC/DC PWM converters: a comparison of \mathcal{H}_∞ , μ , and fuzzy logic based approaches. In *Control Applications, 2003. CCA 2003. Proceedings of 2003 IEEE Conference on*, volume 1, pages 603–608, June 2003.
- Y. Riffonneau. *Gestion des flux énergétiques dans un système photovoltaïque avec stockage connecté au réseau (in French)*. PhD thesis, Université Joseph Fourier, G2ELab, Grenoble, France, 2009.
- S. Sailler. *Commande du convertisseur électrochimie ilôté GESI (in French)*. PhD thesis, Institut National Polytechnique de Grenoble, G2ELab/LEPMI, Grenoble, France, 2008.
- A. Sakhare, A. Davari, and A. Feliachi. Fuzzy logic control of fuel cell for stand-alone and grid connection. *Journal of Power Sources*, 135:165–176, July 2004.
- M. Sautreuil. *La Robustesse: Une nouvelle approche pour l'intégration des systèmes de génération aéronautique (in French)*. PhD thesis, Université Joseph Fourier, G2ELab, Grenoble, France, 2009.
- C. Scherer and S. Weiland. *Linear Matrix Inequalities in Control*. Delft University of Technology, Eindhoven University of Technology, 2005.

- C. Scherer, P. Gahinet, and M. Chilali. Multiobjective Output-Feedback Control via LMI Optimization. *IEEE Transactions on Automatic Control*, 42:896–911, 1997.
- K. Sedghisigarchi and A. Feliachi. H-infinity Controller for Solid Oxide Fuel Cells. *IEEE Transactions on Energy Conversion*, 19(2):429–434, June 2004.
- O. Sename and L. Dugard. Robust \mathcal{H}_∞ control of quarter-car semi-active suspensions. In *Proceedings of the European Control Conference*, Cambridge, UK, Sept. 2003.
- A. A. Shah, K. H. Luo, T. R. Ralph, and F. C. Walsh. Recent trends and developments in polymer electrolyte membrane fuel cell modelling. *Electrochimica Acta*, 56:3731–3757, 2011.
- S. Skogestad and I. Postlethwaite. *Multivariable Feedback Control: Analysis and Design*. Jhon Wiley & Sons, New York, USA, 1996.
- R. E. Sonntag, C. Borgnakke, and G. J. Van Wylen. *Fundamentals of Thermodynamics*. Jhon Wiley and Sons, 2003.
- O. Stalter. *Inverter-integrated, sensorless and power-optimized position control of a concentrating photovoltaic dual-axis tracker*. PhD thesis, Institut National Polytechnique de Grenoble, G2ELab, Grenoble, France, 2009.
- K. W. Suh. *Modeling, Analysis and Control of Fuel Cell Hybrid Power Systems*. PhD thesis, Department of Mechanical Engineering, The University of Michigan, 2006.
- Kyung-Won Suh and Anna G. Stefanopoulou. Coordination of converter and fuel cell controllers. *International Journal of Energy Research*, 29(12):1167–1189, 2005.
- E. Takegami, S. Tomioka, K. Watanabe, K. Higuchi, K. Nakano, and T. Kajikawa. Robust control of DC-DC converter by good approximate 2-degree-of-freedom system. In *SICE 2004 Annual Conference*, volume 1, pages 614–619, Aug. 2004.
- R.J. Talj, R. Ortega, and M. Hilairet. A controller tuning methodology for the air supply system of a PEM fuel-cell system with guaranteed stability properties. *International Journal of Control*, 82(9):1706–1719, Sep. 2009.
- M. Tekin, D. Hissel, M-C. Pera, and J-M. Kauffmann. Energy consumption reduction of a PEM fuel cell motor-compressor group thanks to efficient control laws. *Journal of Power Sources*, 156:57–63, July 2006.
- A. Teninge. *Participation aux services systèmes de parcs éoliens mixtes: application en milieu insulaire (in French)*. PhD thesis, Institut National Polytechnique de Grenoble, G2ELab, Grenoble, France, 2009.
- D. Thirumalai and R.E. White. Steady-state operation of a compressor for a proton exchange membrane fuel cell system. *Journal of Applied Electrochemistry*, 30:551–559, 2000.
- P. Thounthong and S. Rael. The benefits of hybridization. *Industrial Electronics Magazine, IEEE*, 3(3):25–37, Sep. 2009.

- P. Thounthong, S. Raël, and B. Davat. Energy management of fuel cell/battery/supercapacitor hybrid power source for vehicle applications. *Journal of Power Sources*, (193):376 – 385, 2009.
- P. Tritschler. Emulation of Fuel Cell Systems. Master’s thesis, Institut National Polytechnique de Grenoble, G2ELab, Grenoble, France, 2007.
- P. Tritschler. *Optimisation de l’architecture électrique et gestion d’énergie pour un système à pile à combustible embarquée dédié à l’application agricole (in French)*. PhD thesis, Université de Grenoble, G2ELab, Grenoble, France, 2010.
- I. Valero. *Interfaçage et contrôle commande de piles à combustible pour applications stationnaires et transport (in French)*. PhD thesis, Institut National Polytechnique de Grenoble, Laboratoire d’Électrotechnique de Grenoble LEG (now G2ELab), Grenoble, France, 2004.
- I. Valero, S. Bacha, and E. Rulliere. Comparison of energy management controls for fuel cell applications. *Journal of Power Sources*, 156(1):50–56, 2006. Selected papers from the 2nd France-Deutschland Fuel Cell Conference.
- P. Van den Hof and R. Schram. Identification and control—Closed loop issues. *Automatica*, 31(12):1751–1770, 1995.
- C. Wang and M. Hashem Nehrir. Load Transient Mitigation for Stand-Alone Fuel Cell Generation Systems. *IEEE Transactions on Energy Conversion*, 22:864–872, Dec. 2007.
- C. Wang, H. Nehrir, and S. R. Shaw. Dynamic Models and Model Validation for PEM Fuel Cells Using Electrical Circuits. *IEEE Transactions on Energy Conversion*, 20(2): 442–451, June 2005.
- Fu-Cheng Wang and Chin-Chun Ko. Multivariable robust pid control for a pemfc system. *International Journal of Hydrogen Energy*, 35(19):10437–10445, 2010. Indo-French Workshop on Biohydrogen: from Basic Concepts to Technology.
- Fu-Cheng Wang, Hsuan-Tsung Chen, Yee-Pien Yang, and Jia-Yush Yen. Multivariable robust control of a proton exchange membrane fuel cell system. *Journal of Power Sources*, 177(2):393–403, 2008.
- X. Yu, M.R. Starke, L.M. Tolbert, and B. Ozpineci. Fuel cell power conditioning for electric power applications: a summary. *IET Electr. Power Appl.*, 1(5):643–656, September 2007.
- F. Zheng, Q. G. Wang, and T. H. Lee. On the design of multivariable PID controllers via LMI approach. *Automatica*, 38:517–526, March 2002.
- Z. Zhi-dan, H. Hai-bo, Z. Xin-jian, C. Guang-yi, and R. Yuan. Adaptive maximum power point tracking control of fuel cell power plants. *Journal of Power Sources*, (176):259–269, 2008.
- K. Zhou, J. Doyle, and K. Glover. *Robust and Optimal Control* participation factor analysis participation factor analysis. Prentice-Hall, Englewood Cliffs, New Jersey, 1996.

- A. Zin. *Robust automotive suspension control toward global chassis control*. PhD thesis, Institut National Polytechnique de Grenoble, Laboratoire d'Automatique de Grenoble LAG (now Gipsa-Lab), Grenoble, France, 2005.

Titre: Commande robuste de générateurs électrochimiques hybrides

Résumé

L'objectif de cette thèse est la conception, dans un premier temps, des différentes stratégies de commande pour un générateur hybride composé par une pile à combustible et une source auxiliaire de stockage d'énergie. L'outil des Inégalités Linéaires Matricielles (LMI) est utilisé dans la thèse pour la solution du problème de la commande robuste et multi-variables. Dans un premier temps la commande se consacre à la gestion de la partie électrique de la pile. Des stratégies de commande sont proposées pour les convertisseurs élévateurs du bus continu mais aussi pour le contrôle d'un onduleur de tension conçu pour une opération en mode isolé du réseau. La validation d'une partie du contrôle sous un banc d'essai a été réalisée. Dans un deuxième temps, la commande de la partie fluide de la pile a été traitée. La gestion de la dynamique de l'air en entrée de la pile est assurée par la commande du débit du compresseur. Le sous-système de compression d'air est régulé pour garantir un certain taux d'excès d'oxygène désiré, ce qui permet d'améliorer les performances de la pile. Une introduction au contrôle des systèmes à paramètres variants (LPV) est aussi présentée. Des études de robustesse des contrôleurs proposés ont été effectuées, et ces caractères robustes sont comparés avec plusieurs méthodes de commande classique, prouvant ainsi l'importance des méthodologies de commande robuste et multi-variables.

Mots clés: Commande robuste, commande multi-variables, pile à combustible, générateur hybride, compresseur d'air, commande LPV.

Title: Robust control of hybrid electro-chemical generators

Abstract

The objective of this thesis is the design of several control strategies for a hybrid power generator composed by a fuel cell and an auxiliary energy storage source. The Linear Matrix Inequalities (LMI) tools are extensively used in this dissertation as a solution to the multivariable robust control problem. As a first approach, the control methodology is consecrated to the electrical power management sub-system of the fuel cell. Different strategies are proposed to control the hybrid boost power converter configuration for DC voltage applications. The methodology is extended to AC islanded applications considering the additional control of a voltage inverter. The validation on a dedicated test-bench, of a part of the proposed control strategies, is presented. In a second approach, the control of the air supply system is addressed. The management of the air dynamic entering the fuel cell is assured by the control of the air flow of a compressor. The air supply sub-system is controlled to keep a desired oxygen excess ratio, this allow to improve the fuel cell performance. An introduction to the control of Linear Varying Parameter (LPV) systems is also presented. Robustness analysis studies are performed, these robust properties are contrasted with several classic control strategies, demonstrating the advantage and the importance of multivariable robust methodologies.

Keywords: Robust control, multivariable control, fuel cells, hybrid power generators, air compressor, LPV control.